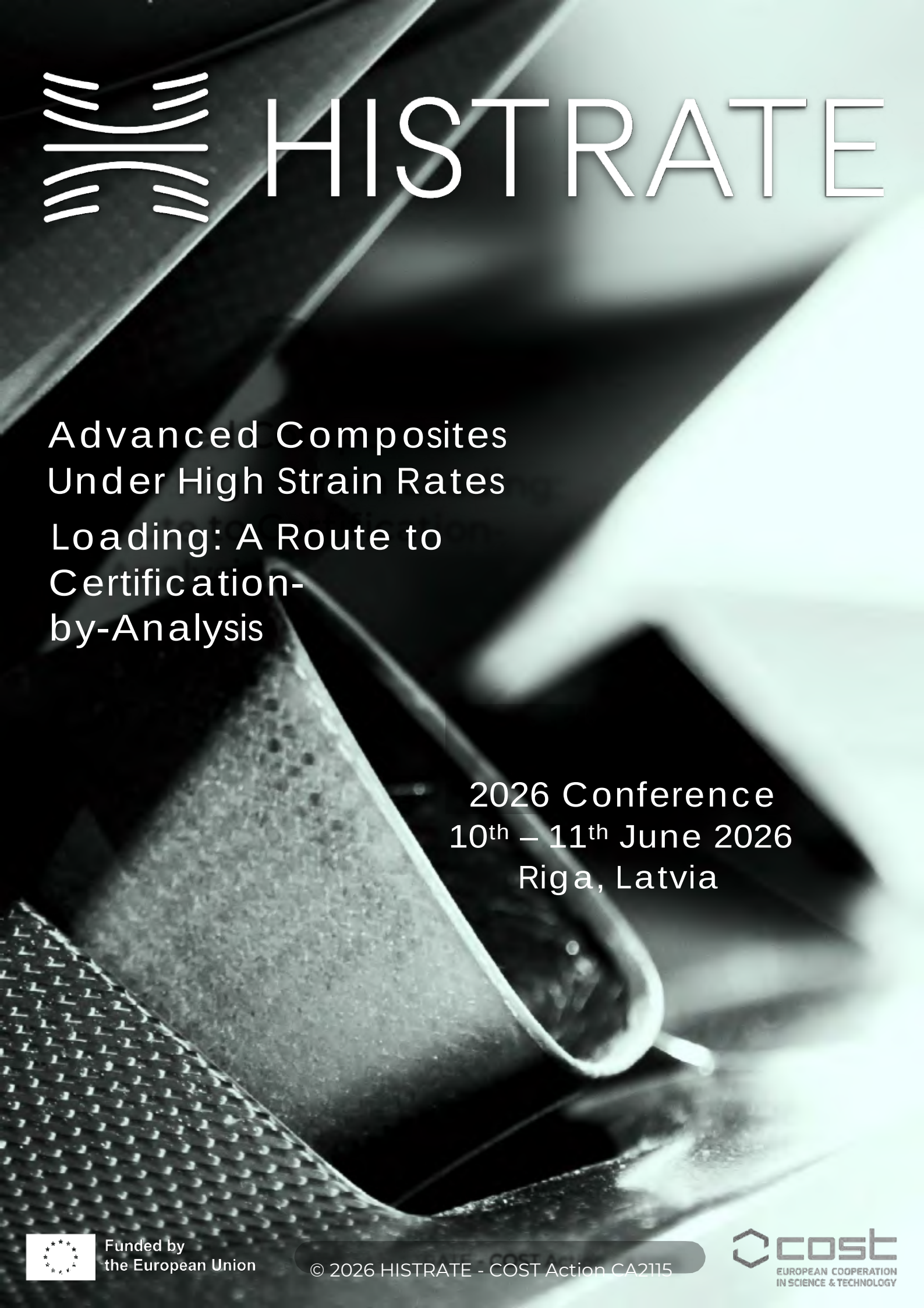

HISTRATE

Advanced Composites Under High Strain Rates Loading: A Route to Certification-by-Analysis

2026 Conference
10th – 11th June 2026
Riga, Latvia

Funded by the European Union

cost
EUROPEAN COOPERATION IN SCIENCE & TECHNOLOGY

PREFACE

We present the **Book of Abstracts** for the 3rd HISTRATE Conference — *Advanced Composites under HIgh STRAin raTEs Loading: A Route to Certification-by-Analysis*, held at the University of Latvia on 10th and 11th June 2026 in Riga, Latvia. Building on the strong positive response to the first two HISTRATE conferences in 2024 and 2025, this year's event continues to serve as a dedicated meeting place for specialists addressing challenges in composite materials, dynamic loading, and computational certification methodologies. Riga, the capital of Latvia, offered a unique blend of historical heritage, modern infrastructure, and a dynamic academic community. Known for its outstanding architecture and vibrant cultural life, the city provided an excellent environment for scientific discussions, networking, and international collaboration. As a major hub in the Baltic region, Riga was a fitting host for bringing together researchers, engineers, and industry professionals involved in the COST Action CA21155.

Advanced composite materials have become indispensable in industries such as aerospace, automotive, defense, marine, and renewable energy, where lightweight, high-performance, and impact-resistant structures are essential. Understanding their response under high strain-rate conditions is therefore a matter of both scientific significance and engineering necessity. In parallel, the growing adoption of certification-by-analysis reflects a shift toward more efficient, reliable, and cost-effective alternatives to traditional qualification procedures. Realizing this vision depends critically on the availability of validated, high-fidelity computational models capable of accurately predicting material and structural behavior under dynamic loading conditions. The HISTRATE conference series realizes knowledge transfer by ideas sharing and discussing both the advances and the hurdles in the domain of composites. The 2026 edition integrates experimental, numerical, and analytical approaches to make possible transition towards certification-by-analysis for composite structures subjected to high strain rate loading.

The conference program features 6 invite lectures by experts from industry, technical sessions with 25 oral presentations and 24 poster presentations following thematically the research conducted by the COST CA21155 Working groups, including research from early-career scientists. The program fostered both formal and informal exchanges, encouraging collaborations and continuation of research in future.

This **Book of Abstracts** offers diversity of methods, depth of analysis, and future trends by compiling contributions from 40 universities, 16 academic research centers, and 8 industrial research centers. A broad spectrum of topics is addressed, including innovative experimental material characterization, recent developments in constitutive modeling and high-strain-rate failure criteria, multiscale simulation methodologies, and advanced composite architectures tailored for enhanced dynamic performance. Particular emphasis is also placed on strategies for integrating numerical predictions into certification processes. Emerging directions such as the application of artificial intelligence and machine learning to material modeling under dynamic loading, together with uncertainty quantification techniques for predictive simulations, constitute important and rapidly evolving areas represented in this volume. The conference united participants from 22 countries, including Belgium (3), Bulgaria (4), Chroatia (1), Cyprus (1), France (1), Georgia (2), Germany (3), India (2), Ireland (1), Italy (6), Kosovo (1), Latvia (8), Lithuania (1), The Netherlands (1), North Macedonia (5), Poland (8), Portugal (3), Romania (1),

Spain (1), Switzerland (1), Tunisia (1), Turkiye (12), UK (2). There are 12 joint papers with authors from two or more of the following countries: Belgium, Bulgaria, Georgia, Germany, Ireland, Italy, Latvia, Lithuania, The Netherlands, North Macedonia, Portugal, Turkiye, UK. .

We wish to thank all the authors for their valuable contributions, the reviewers from the conference program committee for their thorough evaluations and their tireless efforts in shaping this conference. Special recognition is also due to our host from University of Latvia for their organizing work and generous support.

We believe this collection of abstracts will serve not only as a useful reference but also as a lasting record of the ongoing efforts to push the boundaries of composite material technology and certification practices under dynamic loading conditions.

The HISTRATE 2026 Organizing Committee

HISTRATE

Advanced Composites under High Strain Rate Loading
A Route to Certification-by-Analysis

2026 Conference

PROGRAMME

10TH - 11TH JUNE 2026

DAY 1 10 June

WEDNESDAY

09:00 – 09:30	**Registration**	
09:30 – 09:45	**Welcome by Local Organizer and Opening Speech** *University of Latvia*	**Tatjana Glaskova-Kuzmina** **Guntars Kitenbergs**
09:45 – 10:00	**Introduction by Action Chair** ***HISTRATE*** *- A Route to Certification-by-analysis for Impact-loaded Aeronautical Composite Structures*	**Patricia Verleysen**
10:00 - 10:30	*Neural Network Based Composite Failure Prediction for Accelerated Explicit Finite Element Simulations*	**Jens Wiegand** *(Invited Speaker)*
10:30 - 11:00	Novel Simulation Methods and Best Practices for Composites Under High Strain Rates	**Cristiano Veloso** *(Invited Speaker)*
11:00 – 11:30	***COFFEE BREAK***	
11:30 – 12:45	**Session 1 - Novel composite materials for high strain applications (WG3)**	**Chair:** **Vineta Srebrenkoska** **Mauro Zarrelli**
11:30 – 11:45	*Evaluating Thermal Reconsolidation Efficiency in CF/PEKK Composites Subjected to Single and Multiple Low-Velocity Impacts*	Hatice S. Sas
11:45 – 12:00	*Structural Performance of Voided RC slab under Blast Loading*	Ashish Kumar Chaudhary - *ONLINE*
12:00 – 12:15	*New Epoxy/ESO Composite Systems Produced by Pultrusion and Their High Strain Rate Compressive Performance*	Ivan Vasileski
12:15 – 12:30	*Explosion Fabrication of High Entropy Composites for High Strain Rate Applications*	Nikoloz Chikhradze
12:15 - 12:30	*Enhanced Mechanical Performance of MXene-Coated Basalt Fiber-Reinforced Composites Impregnated with Star-Like Polymer-Modified Epoxy Matrix*	*Tatjana Glaskova-Kuzmina*

LUNCH BREAK

UNIVERSITY OF LATVIA, RIGA

Tatjana Glaskova-Kuzmina @

cost EUROPEAN COOPERATION IN SCIENCE & TECHNOLOGY

Funded by the European Union

This conference programme is within the scope of COST Action HISTRATE, CA-21155, supported by COST (European Cooperation in Science and Technology).

HISTRATE

Advanced Composites under High Strain Rate Loading
A Route to Certification-by-Analysis

2026 Conference

PROGRAMME

10TH - 11TH JUNE 2026

DAY 1 10 June

WEDNESDAY

13:45 – 14:45	**Poster session with 3 minute pitches**	**Chair: Hatice Sinem Şaş Çaycı**
14:45 – 15:45	***COFFEE BREAK with POSTER SESSION***	
15:45 – 17:15	**Session 2 - Novel simulation methods and best practices for composites under high strain rates (WG4)**	**Chair: Andreas Hornig**
15:45 – 16:00	*Modelling and simulation of the mechanical response and damage of carbon fibre-reinforced polymer (CFRP) laminates for aero-structures subjected to simulated lightning strike*	*Albertino Arteiro*
16:00 – 16:15	*Incubation-time-based failure criterion to predict delamination due to spalling and through-thickness impact loading*	*Andreas Hornig*
16:15 – 16:30	*Fracture modeling of the interface for composites: stick-slip behaviors – a dynamic process*	*Dayou Ma*
16:30 – 16:45	*High-Velocity Impact Behaviour of CFRP–PET Foam Sandwich Panels: Experimental Characterisation, Tomography and Numerical Modelling*	*Filipe Ribeiro*
16:45 – 17:00	*Numerical Modelling of the Additively Manufactured Continuous Fibre Reinforced Composites*	*Fran Ušurić*
17:00 – 17:15	*Advanced 3D Modeling of Functionally Graded Sandwich Plates under High Strain Rate Loading*	*Volkan Kahya*
19:30	***CONFERENCE DINNER***	

UNIVERSITY OF LATVIA, RIGA

Tatjana Glaskova-Kuzmina @

cost EUROPEAN COOPERATION IN SCIENCE & TECHNOLOGY

Funded by the European Union

This conference programme is within the scope of COST Action HISTRATE, CA-21155, supported by COST (European Cooperation in Science and Technology).

HISTRATE

Advanced Composites under High Strain Rate Loading
A Route to Certification-by-Analysis

2026 Conference

PROGRAMME

10TH - 11TH JUNE 2026

DAY 2 11 June

THURSDAY

08:45 – 09:00	**Registration**	
09:00 - 10:30	**Industry Session on Certification of Composite Products**	**Intro by Michele Meo & Jens Wiegand**
09:00 - 09:30	*Image-based High Strain Rate Testing of Composites: beyond Hopkinson's bar*	**Fabrice Pierron- ONLINE** *(Invited Speaker)*
09:30 – 10:00	*The Use of Multiscale Modeling & Machine Learning for Certification by Analysis in Composite Materials*	**David Dumas** *(Invited Speaker)*
10:00 - 10:30	***Keynote speech:*** *Quo vadis Certification by Analysis?*	**André Haufe**
10:30 – 11:00	***COFFEE BREAK***	
11:00 – 12:30	**Session 3 - Multi-modal sensing for impact detection and damage characterisation (WG5)**	**Chair: Rohan Soman**
11:00 – 11:15	*Ultrasound Array Signal Reconstruction for Porosity and Defect Characterization in Complex Composite Structures Subjected To High Strain*	*Krzysztof Dragan*
11:15 – 11:30	*Impact Detection in Composite Structures in Aircraft and Space Systems*	*Michele Meo*
11:30 – 11:45	*Impact Damage Influence on the Local Wavenumber of Guided Ultrasonic Waves in Thermoplastic Composites*	*Pawel Malinowski*
11:45 – 12:00	*MWCNT-Modified Cellulose Interleaved Multifunctional CARALL Composites for Real-Time Impact Detection and EMI Shielding*	*Volkan Eskizeybek*
12:00 - 12:15	*Local Wavenumber Imaging of Thin-walled Structures for Damage Detection*	*Lukasz Pieczonka*
12:15 - 12:30	*Detection of Impact Events Using Optical Fiber Sensors*	*Rohan Soman*
12:30 – 12:45	***COFFEE BREAK***	

UNIVERSITY OF LATVIA, RIGA

Tatjana Glaskova-Kuzmina @

cost EUROPEAN COOPERATION IN SCIENCE & TECHNOLOGY

Funded by the European Union

This conference programme is within the scope of COST Action HISTRATE, CA-21155, supported by COST (European Cooperation in Science and Technology).

HISTRATE

Advanced Composites under High Strain Rate Loading
A Route to Certification-by-Analysis

2026 Conference

PROGRAMME

10TH - 11TH JUNE 2026

DAY 2 11 June

THURSDAY

12:45– 13:30	**Session 4 - Advanced testing and instrumentation for composites under high strain rates (WG6)**	**Chair: Andrei Anisimov**
12:45 – 13:00	*In-Situ Liquid Resin Healing of Elium/Glass Fibre Composites for Wind Turbine Blades under Elevated Mode I Loading Rates*	*Mohamad Alsaadi*
13:00 – 13:15	*Temperature-Dependent Impact Behavior of Carbon Fiber/PEKK Composite Laminates*	*Ceren Yıldırım*
13:15 – 13:30	*Multiaxial Characterisation of Polymers and Composites from Quasi-Static to High Strain Rates*	*Naveen Chakravarthi Petchiappan*
13:30 – 14:30	***LUNCH***	
14:30 – 15:00	**Session 4 - Advanced testing and instrumentation for composites under high strain rates (WG6) - continued**	**Chair: Tatjana Glaskova-Kuzmina**
14:30 – 14:45	*Design of A Round-robin Exercise on the High Strain-rate Tensile Properties of Commercial Structural Composites*	*Marco Peroni*
14:45 – 15:00	*HISTRATE: Progress Towards a Roadmap for Standardisation of High Strain Rate Testing of Composite Materials*	*Andrei Anisimov*
15:00 - 15:45	***COFFEE BREAK with POSTER SESSION***	

UNIVERSITY OF LATVIA, RIGA

Tatjana Glaskova-Kuzmina @

cost EUROPEAN COOPERATION IN SCIENCE & TECHNOLOGY

Funded by the European Union

This conference programme is within the scope of COST Action HISTRATE, CA-21155, supported by COST (European Cooperation in Science and Technology).

HISTRATE

Advanced Composites under High Strain Rate Loading
A Route to Certification-by-Analysis

2026 Conference

PROGRAMME

10TH - 11TH JUNE 2026

DAY 2 11 June

THURSDAY

15:45 - 16:15	**Invited speaker:** Route to Certification-by-Analysis of Thick Walled Single Loadpath Flight Critical Composite Landing Gear Components	**Tjaard Sijpkes** *Intro by Andrei Anisimov*
16:15 – 17:00	**Session 5 - Novel simulation methods and best practices for composites under high strain rates (WG4) - continued**	**Chair: Andreas Hornig**
16:15 - 16:30	*Coupling Proper Generalized Decomposition with Domain Decomposition for 2D ElasticWave Simulation*	*Toufik Boubehziz*
16:30 – 16:45	*Numerical Investigation of the Effect of Adhesives Used in Honeycomb Composite Structures Subjected to High-Velocity Ballistic Impact on Impact Resistance and Its Prediction Using the Fuzzy Logic Method*	*Yunus Emre Togar*
16:45 - 17:00	*High Strain Rate Deformation of Nanocomposites: A Molecular Dynamics Simulation*	*Murat Şen*
17:00 - 17:15	**SUMMARY AND FAREWELL**	*Elena Stoykova Tatjana Glaskova-Kuzmina*

UNIVERSITY OF LATVIA, RIGA

Tatjana Glaskova-Kuzmina @

cost EUROPEAN COOPERATION IN SCIENCE & TECHNOLOGY

Funded by the European Union

This conference programme is within the scope of COST Action HISTRATE, CA-21155, supported by COST (European Cooperation in Science and Technology).

HISTRATE

Advanced Composites under High Strain Rate Loading
A Route to Certification-by-Analysis

2026 Conference

PROGRAMME

10TH - 11TH JUNE 2026

Poster Presentations

Maciej Radzienski	Multipoint Excitation-Based S0 Mode Conversion Mapping for BVID Detection in Complex Composite Laminates
Elena Stoykova	Numerical Simulation of a Shearographic System with a Pixelated Polarization Camera
Alicja Szostak	Microring Resonators for Impact Sensing in Plates
Yang Zhang	Frequency-Wavenumber Domain Guided Wave Mode Superposition Imaging for Surface Damage Characterization of Composite Materials
Vito Pagliarulo	Non-destructive investigation of basalt-based laminates by shearography and ESPI
Amine Haj Taieb	Textile-Fiber-Based Metamaterial Structures for Impact Detection and Damage Characterisation: A Review of Multi-Modal Sensing Approaches
Violeta Madjarova	Laser Speckle Photometry of Composites under Tensile Loading
Patrycja Pyzik	Lamb wave dispersion for material characterisation of short fiber-reinforced polymer composite plates
Çağatay Yılmaz	A Numerical Study on the Usage of Lamb Waves for Damage Detection in Fiber Reinforced Polymers
Ana-Teodora Untariu	Dynamic Mechanical Analysis of neat PK and two PK-GF30 Batches
Kaleeswaran Balasubramaniam	EMAT-Based Detection of Interfacial Disbonds in Composites for Dynamic and High-Strain-Rate Applications
Ezio Cadoni	High strain rate characterisation of natural fiber composites for drones (HISTRAND)
Özgen Çolak Çakır	Microstructure-Driven Design of Strain-Rate Sensitive Nanocomposites
Svetlana Risteska	Damage and Delamination Behavior of Thermoset Composites under Impact and Medium to High-Strain-Rate Compression
Aldobenedetto Zotti, Mauro Zarrelli	High Strain Rate Behavior of Silica Loaded Epoxy Nanocomposites
Sara Srebrenkoska	Effect of ATL Processing Parameters on the Flexural Behavior and High Strain Rate Response of Carbon Fiber/PPS Thermoplastic Laminates
Svetlana Risteska	Defect Evolution and High-Strain Rate Mechanical Performance of Thermoset and Thermoplastic Fiber-Reinforced Composites

UNIVERSITY
OF LATVIA, RIGA

Tatjana Glaskova-Kuzmina

cost
EUROPEAN COOPERATION
IN SCIENCE & TECHNOLOGY

Funded by
the European Union

This conference programme is within the scope of COST Action HISTRATE, CA-21155, supported by COST (European Cooperation in Science and Technology).

HISTRATE

Advanced Composites under High Strain Rate Loading
A Route to Certification-by-Analysis

2026 Conference

PROGRAMME

10TH - 11TH JUNE 2026

Poster Presentations

Abdülkadir Sezai Saraç	Magneto-Mechanical Response of Electrospun Polyacrylonitrile/Magnetic Nanoparticle Composite Nanofibers for Dynamic Sensing
Sabri Can Ekerer	Additively manufactured PETG - PLA hybrid composites: Effect of high strain rates on tensile properties
Shunqi Zhang	Stochastic Effects of Interlayer Matrix Non-Uniformity on Impact Response of TPU Thermoplastic Composites
Vineta Srebrenkoska	Predictive Modeling of Ballistic Limit and Trauma Response in Aramid Fiber Reinforced Phenolic Composites
Brikena Duga	Parameters Optimization of the Gurson–Johnson–Cook Damage Model for Dual Phase Steel
Burak Bal	Molecular Dynamics Investigation of Dislocation-Mediated Mechanical Behavior and Hydrogen Embrittlement in Metal-Matrix Composites Under High Strain Rate Loading
Yüksel Çakır	Multi-Layer Perceptron Neural Network Based Prediction of Dynamic Stress–Strain Response of Polyethylene

UNIVERSITY OF LATVIA, RIGA

Tatjana Glaskova-Kuzmina @

cost EUROPEAN COOPERATION IN SCIENCE & TECHNOLOGY

Funded by the European Union

This conference programme is within the scope of COST Action HISTRATE, CA-21155, supported by COST (European Cooperation in Science and Technology).

HISTRATE

Advanced Composites under High Strain Rate Loading
A Route to Certification-by-Analysis

2026 Conference

PROGRAMME

10TH - 11TH JUNE 2026

Speakers*

NAME	ORGANISATION
Tatjana Glaskova-Kuzmina	University of Latvia
Guntars Kitenbergs	University of Latvia
Patricia Verleysen	Ghent University
Jens Wiegand	Compact Engineering Ltd. Cyprus
Cristiano Veloso	Beyond Composite, Portugal
Hatice Sinem Sas	University of Sheffield
Ashish Kumar Chaudhary	Indian Institute of Technology, Ropar
Ivan Vasileski	Goce Delcev University, North Macedonia
Nikoloz Chikhradze	Grigol Tsulukidze Mining Institute, Georgia
Albertino Arteiro	INEGI, Faculty of Engineering, University of Porto
Andreas Hornig	TUD Dresden University of Technology
Dayou Ma	Politecnico di Milano, Italy
Filipe Ribeiro	Instituto de Soldadura e Qualidade, Portugal
Fran Ušurić	University of Zagreb, Croatia
Volkan Kahya	Karadeniz Technical University, Türkiye
Fabrice Pierron	MatchID nv, Belgium
David Dumas	Cenaero ASBL, Belgium

NAME	ORGANISATION
André Haufe	Ansys (part of Synopsis) Germany
Krzystof Dragan	Air Force Institute of Technology, Poland
Mıchele Meo	University of Southampton
Pawel Malinowski	Polish Academy of Science,Poland
Volkan Eskizeybek	Çanakkale Onsekiz Mart University, Türkiye
Lukasz Pieczonka	University of Krakow, Poland
Rohan Soman	Polish Academy of Science,Poland
Mohammad Alsaadi	University College Dublin, Ireland
Ceren Yıldırım	Thermoplastics Composite Research Centre, The Netherlands
Naveen Chakravarthi Petchiappan	Ghent University, Belgium
Marco Peroni	European Commission, Italy
Andrei Anisimov	TUDelft, The Netherlands
Toufik Boubehziz	ENSAM France
Yunus Emre Togar	Yıldız Technical University, Türkiye
Murat Şen	Fırat University, Türkiye
Elena Stoykova	Bulgarian Academy of Science
Tjarad Sijpkes	TUDelft, The Netherlands
Mauro Zarrelli	CNR IPCB Italy

** listed per order of talks*

Tatjana Glaskova-Kuzmina @

UNIVERSITY OF LATVIA, RIGA

cost EUROPEAN COOPERATION IN SCIENCE & TECHNOLOGY

Funded by the European Union

This conference programme is within the scope of COST Action HISTRATE, CA-21155, supported by COST (European Cooperation in Science and Technology).

HISTRATE

Advanced Composites under High Strain Rate Loading
A Route to Certification-by-Analysis

2026 Conference

PROGRAMME

10TH - 11TH JUNE 2026

Poster Presenters

NAME	ORGANISATION
Maciej Radzienski	Institute of Fluid Flow Machinery, Polish Academy of Science Poland
Elena Stoykova	Institue of Optical Materials and Technologies, Bulgarian Academy of Science
Alicja Szostak	Gdansk University of Technology, Poland
Yang Zhang	Institute of Fluid Flow Machinery, Polish Academy of Science Poland
Vito Pagliarulo	CNR - National Research Council of Italy
Amine Haj Taieb	ISAMS University of Sfax, Tunisia
Violeta Madjarova	Institue of Optical Materials and Technologies, Bulgarian Academy of Science
Patrycja Pyzik	AGH University of Krakow, Poland
Çağatay Yılmaz	Abdullah Gül University, Türkiye
Ana-Teadora Untariu	Politehnica University of Timisoara, România
Kaleeswaran Balasubramaniam	Innerspec Technologies, Spain
Ezio Cadoni	University of Applied Sciences and Arts of Southern Switzerland

NAME	ORGANISATION
Sabri Can Ekerer	Çukurova University, Türkiye
Shunqi Zhang	Politecnico di Milano, Italy
Vineta Srebrenkoska	Goce Delcev University, North Macedonia
Brikena Duga	University of Applied Sciences in Ferizaj, Kosovo
Burak Bal	Abdullah Gül University, Türkiye
Yüksel Çakır	İstanbul Technical University, Türkiye
Abdülkadir Sezai Saraç	İstanbul Technical University, Türkiye
Sara Srebrenkoska	Goce Delcev University, North Macedonia
Aldobenedetto Zotti	CNR - IPCB Italy
Svetlana Risteska	Goce Delcev University, North Macedonia
Özgen Çolak Çakır	İstanbul Technical University, Türkiye

Tatjana Glaskova-Kuzmina @

UNIVERSITY OF LATVIA, RIGA

cost EUROPEAN COOPERATION IN SCIENCE & TECHNOLOGY

Funded by the European Union

This conference programme is within the scope of COST Action HISTRATE, CA-21155, supported by COST (European Cooperation in Science and Technology).

Neural network based composite failure prediction for accelerated explicit finite element simulations

Jens Wiegand[1*] and Giuseppe Zumpano[2]

[1] *COMPACT Composite Impact Engineering LTD, 12 Gateway Mews, London N11 2UT, UK*

[2] *Rolls Royce PLC, Moor Lane, Derby DE24 8BJ, UK*

[*] *jens@compact-engineering.co.uk*

Summary: Explicit FEA for composite materials is computationally hindered by complex failure theories and tensor rotations. This study introduces a Depp Neural Network based surrogate model integrated into LS-DYNA to accelerate simulations. The framework employs a hybrid approach: computationally efficient neural networks predict damage onset in elastic regions, switching to high-fidelity constitutive models only when failure is imminent. Validated against impact simulations, the method achieved a 50% reduction in constitutive subroutine runtime and a 25% overall speedup. This strategy significantly optimizes resource allocation, enabling faster large-scale structural integrity assessments without sacrificing predictive accuracy.

Abstract

Finite Element Analysis (FEA) is a cornerstone in engineering simulations, particularly for assessing the structural integrity of composite materials. However, explicit FEA methods are often computationally intensive, especially when modelling the intricate failure mechanisms inherent in composites. Over the years, failure theories have evolved in sophistication, leading to constitutive models that, while more accurate, further exacerbate computational demands. This challenge is magnified in large-scale engineering applications where extensive meshes are employed, despite the reality that failure typically occurs in localized regions, leaving vast portions of the mesh elastic but still subject to complex computations.

To address this inefficiency, it is imperative to strategically allocate computational resources, concentrating efforts on critical areas prone to failure while minimising costs in regions where failure is unlikely. The rapid advancement of data-driven methodologies offers promising avenues in this context [1,2]. Deep neural networks (DNNs), renowned for their exceptional function approximation capabilities [3], have demonstrated potential in capturing complex patterns within data. By integrating DNNs into FEA frameworks, one can develop surrogate models that predict failure responses with high fidelity, thereby reducing the reliance on computationally expensive simulations in non-critical mesh areas.

The simulation environment inherent in FEA provides a rich repository of data, facilitating the training of DNNs to achieve high accuracy. By leveraging this data, DNN-based models can be trained to recognise and predict failure behaviours, enabling a more efficient allocation of computational resources. This approach enhances the efficiency of simulations involving composite materials.

A homogenised constitutive model is used in this study for the prediction of the onset of damage in composite laminates. Local orientation-based damage algorithms then calculate material degradation once the onset of damage is detected. The constitutive model allows for the representation of up to eight fibre orientations in a single finite element, hence allowing for manageable mesh sizes for large, component-level, finite element models, and is implemented as a user-defined subroutine (UMAT) in the finite element solver LS-DYNA. Evaluating various stress-based failure criteria in this UMAT requires multiple tensor rotations to obtain the stress state in coordinate systems which are aligned with the various material orientations in each element. These rotations and the local evaluation of the failure criteria are computationally intensive and were identified as significant drivers of the computational cost of the constitutive model.

A surrogate model was developed that allows for the rapid evaluation of the failure criteria without performing the failure analysis in all present fibre orientations. Once any orientations inside an element indicate that the material nears the onset of damage, the model switches from the surrogate model back to the expensive but accurate orientation-based constitutive model for evaluating any potential damage for the remainder of the simulation. Consequently, all finite elements that remain elastic during the simulation only use the computationally efficient surrogate model, which results in significant time savings.

The proposed surrogate model was selected by comparing the computational efficiency and accuracy of DNNs of varying sizes and activation functions. Optimised synthetic data generation strategies were developed and assessed based on the observed network accuracy after training. In addition, a computationally efficient

algorithm for fast inference on large parallel architectures was developed and implemented in the finite element software LS-DYNA.

The comparison of the runtime of the accelerated surrogate-based constitutive model and the original constitutive model allowed for the measurement of the resulting computational time savings. It was demonstrated that a significant reduction in the required computational time could be achieved. The time savings depend on the finite element model (e.g., the presence of additional expensive features such as contacts). The application to simple ball-bearing impacts on composite laminates demonstrated a 50% reduction in time spent in the constitutive model subroutine and a 25% reduction in overall required computational time (see Figures 1 and 2).

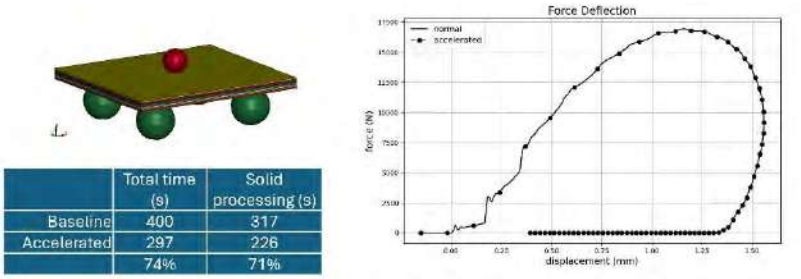

	Total time (s)	Solid processing (s)
Baseline	400	317
Accelerated	297	226
	74%	71%

Fig. 1. Acceleration of a plate impact simulation.

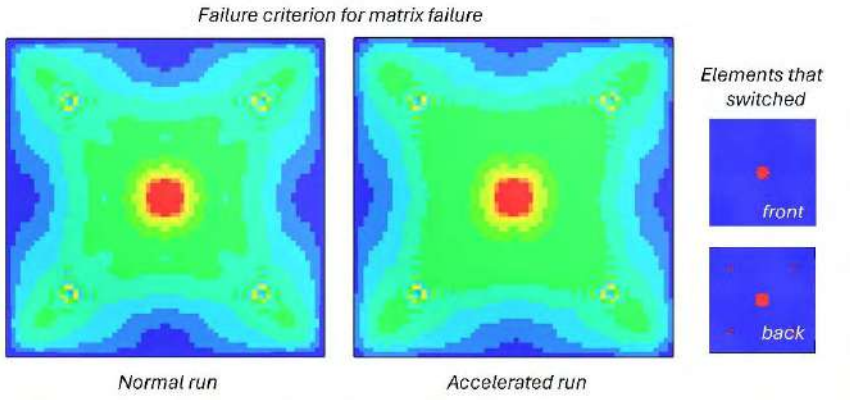

Fig. 2. Comparison of accelerated and baseline failure prediction.

1. References

[1] Ge, W., and Tagarielli, V. L., 2021, "A Computational Framework to Establish Data-Driven Constitutive Models for Time- or Path-Dependent Heterogeneous Solids," Sci Rep, **11**(1), p. 15916. https://doi.org/10.1038/s41598-021-94957-0.

[2] Furtado, C., Pereira, L. F., Tavares, R. P., Salgado, M., Otero, F., Catalanotti, G., Arteiro, A., Bessa, M. A., and Camanho, P. P., 2021, "A Methodology to Generate Design Allowables of Composite Laminates Using Machine Learning," International Journal of Solids and Structures, **233**, p. 111095. https://doi.org/10.1016/j.ijsolstr.2021.111095.

[3] Cheng, L., Knoop, H.-B., and Zhou, X., 2012, "Neural Networks for Optimal Approximation of Continuous Functions on the Unit Sphere," Results. Math., **62**(3), pp. 227–233. https://doi.org/10.1007/s00025-012-0278-2.

HISTRATE

Advanced Composites under High Strain Rate Loading A Route to Certification-by-Analysis

2026 Conference

10th – 11th JUNE 2026

Session 1 - Novel composite materials for high strain applications (WG3)

cost EUROPEAN COOPERATION IN SCIENCE & TECHNOLOGY

Funded by the European Union

Evaluating Thermal Reconsolidation Efficiency in CF/PEKK Composites Subjected to Single and Multiple Low-Velocity Impacts

Mahsa Seyednourani[1,2], Sinem Elmas[1,2], Hasan Ulus[1,3], Mehmet Yıldız[1,2], Hatice S. Sas[4*]

[1]*Sabanci University Integrated Manufacturing Technologies Research and Application Center, Tuzla, Istanbul 34956, Türkiye*
[2]*Faculty of Engineering and Natural Sciences, Sabanci University, Tuzla, Istanbul 34956, Türkiye*
[3]*Selcuk University, Huglu Vocational School, Konya 42700, Türkiye*
[4]*School of Mechanical, Aerospace and Civil Engineering, The University of Sheffield, S1 3JD, UK*
** h.s.sas@sheffield.ac.uk*

Abstract: This study investigates the efficiency of thermal reconsolidation as a repair strategy for carbon-fiber-reinforced polyether ketone ketone (CF/PEKK) laminates subjected to single and repeated low-velocity impacts. Laminates were impacted at 2.5, 5, and 10 J and then repaired by hot-press reconsolidation. Residual behavior was assessed using repeated impact tests, compression after impact (CAI), charpy impact, and dynamic mechanical analysis (DMA). Reconsolidation markedly recovered compressive strength and local impact resistance after low to moderate damage, whereas its effectiveness decreased with increasing cumulative damage. The results clarify both the potential and the limitations of reconsolidation for sustainable life extension of aerospace-grade thermoplastic composites.

Introduction

Thermoplastic composites are increasingly attractive for aerospace structures because they combine low density, high toughness, weldability, and repairability. Among them, CF/PEKK has received growing attention due to its thermal stability and damage tolerance. However, low-velocity impact events such as tool drops and service-induced contacts still generate matrix cracking, delamination, and local fiber damage, which reduce residual load-bearing capacity. Thermal reconsolidation offers a promising repair route because the thermoplastic matrix can be reheated and reflowed to close cracks, rebond interfaces, and partially restore structural continuity [1-3]. While earlier studies have mainly examined single-impact damage, the influence of repeated impact and repeated healing on repair efficiency remains insufficiently understood. This work therefore investigates the effectiveness of reconsolidation for CF/PEKK laminates exposed to both single and cumulative impact histories, with emphasis on residual compressive response and impact resistance.

Material and Methods

CF/PEKK laminates were manufactured from Toray Cetex TC1320 unidirectional slit tapes using automated fiber placement followed by autoclave consolidation. Panels with nominal dimensions of 600 × 600 × 3.15 mm³ were manufactured and subsequently cut into test coupons. Low-velocity impact tests were performed according to ASTM D7136 using impact energies of 2.5, 5, and 10 J to represent different damage severities. In addition to single-impact configurations, repeated-impact scenarios were introduced by striking the same region multiple times, either with or without an intermediate reconsolidation cycle. Reconsolidation was carried out in a hydraulic hot press at 380 °C under pressure, followed by controlled cooling. The repaired laminates were evaluated through repeated low-velocity impact testing, Charpy impact, DMA, and CAI testing. This combined approach enabled assessment of both residual structural performance and thermo-mechanical changes induced by damage and repair.

Results and Discussion

The results show that reconsolidation is most effective when applied after low to moderate damage. For the reference condition, reconsolidated specimens reached a peak CAI stress of about 276 MPa compared with 263 MPa for the as-manufactured laminate, indicating that the thermal cycle itself did not degrade the material. For 2.5 J impacted laminates, the peak compressive stress increased from about 220 MPa in the damaged state to about 265 MPa after reconsolidation, corresponding to a substantial recovery of residual load-bearing capacity. At 5 J, the peak stress increased from about 180 MPa to about 261 MPa after healing, confirming that reconsolidation can still recover significant strength after more severe damage. By contrast, for the 10 J condition, only limited recovery was possible because the damage approached a catastrophic threshold [2,3].

Repeated impact results further demonstrated the limitation of the repair process under cumulative damage. At 2.5 J, a single-impact laminate absorbed about 91% of the applied impact energy, whereas a double-impacted unrepaired specimen absorbed only about 40%. When reconsolidation was introduced between impacts, the absorbed energy recovered to about 79%, showing a clear restoration of stiffness and impact tolerance. Charpy testing also confirmed the benefit of healing, with reconsolidated specimens exhibiting higher absorbed energy than the damaged state and, in some cases, even exceeding the reference condition. DMA results indicated partial recovery of thermal stability after reconsolidation, although the repaired material did not fully return to its original microstructural state. Overall,

the findings suggest that reconsolidation is more successful in restoring compressive strength than in fully recovering ductility once damage becomes repeated or extensive.

Table 1. Summary of absorbed energy and CAI performance for damaged and reconsolidated CF/PEKK laminates under repeated impact conditions.

Sample Type	Absorbed Energy (J)	CAI Stress (MPa)	Interpretation
2.5J Impact	2.274	220	Baseline toughness
2.5J-Reconsolidated-2.5J	1.967	264	Strength recovery and improved resistance
Double Strike 2.5J (2.5JX)	0.944	289	Brittle failure, higher residual strength
2.5JX2-Reconsolidated-2.5J	1.953	267	Improved resistance, slightly higher strength
5J Impact	3.297	261	Higher impact energy absorbed
5J-Reconsolidated-5J	3.282	278	Slight decrease in dissipation after reconsolidation

Conclusion

Thermal reconsolidation is a promising repair strategy for aerospace-grade CF/PEKK laminates after low-velocity impact damage. The method significantly restores residual compressive strength and improves impact resistance when applied after early-stage or moderate damage. However, its efficiency decreases as impact severity and cumulative damage increase. These results highlight the potential of reconsolidation for maintenance and life extension of thermoplastic composite structures, while also defining the practical limits of the process under repeated damage conditions. Future work should focus on multi-cycle healing strategies and localized repair approaches to improve performance retention under realistic service histories.

References

[1] Tarpani, J.R., Canto, R.B., Saracura, R.G.M., Ibarra-Castanedo, C., and Maldague, X.P.V. "Compression after impact and fatigue of reconsolidated fiber-reinforced thermoplastic matrix solid composite laminate." Procedia Materials Science, 3 (2014): 485-492.

[2] Conejo, L. dos S., Santos, L.F. de P., Ribeiro, B., Kok, W., Warnet, L., Costa, M.L., and Botelho, E.C. "Reconsolidation effect on impact, compression after impact and thermal properties of poly(aryl ether ketone) composites for aeronautical applications." Journal of Thermoplastic Composite Materials, 36 (2023): 2562-2581.

[3] Liu, A., Zou, Y., Chen, Y., Hu, J., and Wang, B. "Experimental investigation of impact resistance and compression behavior of CF/PEEK laminates after hot-press fusion repair with different stacking sequences." Polymer Composites, 44 (2023): 6467-6481.

[4] Elmas, S., Atac, B., Senol, C.O., Topal, S., Yildiz, M., and Sas, H.S. "Annealing impact on mechanical performance and failure analysis assisted with acoustic inspection of carbon fiber reinforced poly-ether-ketone-ketone composites under flexural and compressive loads." Polymer Composites (2024).

Structural Performance of Voided RC slab under Blast Loading

Ashish Kumar Chaudhary,[1] Muthulingam Subramaniyan,[1*]

[1] *Indian Institute of Technology Ropar, Rupnagar, Punjab, India 140001*

[*] *ashish.19cez0001@iitrpr.ac.in*

Abstract: Developing blast-resistant concrete systems is essential to overcome the limitations of traditional reinforced concrete slabs and enhance structural resilience under extreme impulsive loads. This research conducts an experimental analysis of the blast response in biaxially voided reinforced concrete slabs subjected to air-blast loading. Spherical void formers were carefully placed within two-way reinforced slabs and exposed to a 1 kg TNT explosion at a scaled distance of 0.5 m/kg$^{1/3}$. The slabs' dynamic behavior was tracked using strain gauges and pressure transducers to record strain–time histories and incident overpressure, while post-blast structural integrity was assessed through non-destructive testing, including rebound hammer and ultrasonic pulse velocity (UPV) measurements. Results showed a clear two-peak compressive strain pattern linked to incident and reflected stress waves propagating through the slab. Localized strain enhancements appeared around the void edges due to stress-wave interactions and geometric discontinuities caused by the voids. Despite these localized stress concentrations, the slabs avoided full perforation or structural failure. Damage evaluation revealed mainly localized, uneven cracking, primarily in the slab's central area. Non-destructive tests indicated a moderate decrease in surface hardness and up to a 50% reduction in UPV values in the damaged zones, suggesting localized material degradation. Nonetheless, damage indices suggest the slabs maintained sufficient residual load capacity after blast exposure. Overall, the findings show that internal voids significantly alter stress-wave propagation and promote energy dissipation within the slab, reducing the risk of catastrophic failure and enabling lighter structural designs. Biaxially voided reinforced concrete slabs, therefore, hold promise as a lightweight, blast-resistant solution for advanced structural systems.

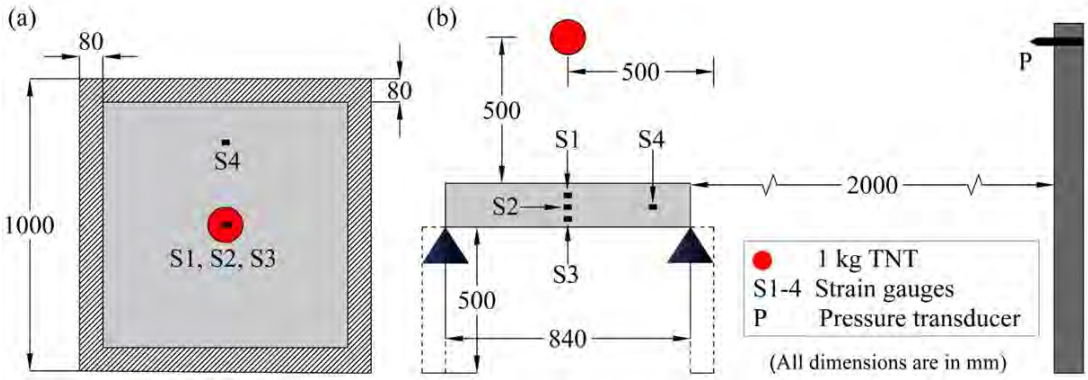

Fig. 1. Schematic of instrumentation: (a) top view; and (b) sectional-view.

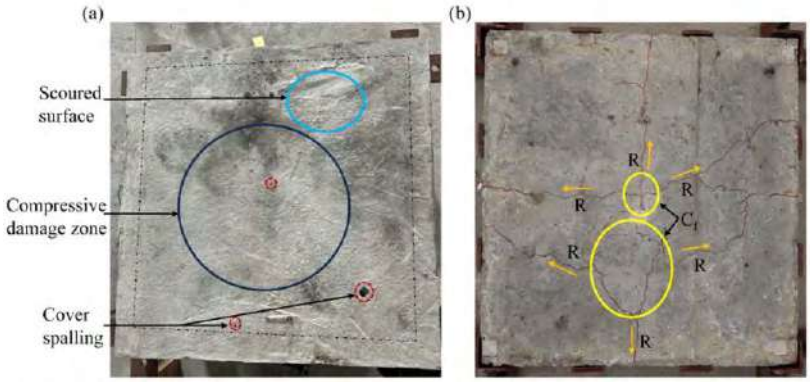

Fig. 2. Damage analysis of BVRCS: (a) top view; and (b) bottom view.

References

[1] Sagadevan, R., and Rao, B. N., 2020, “Flexural Behavior of Reinforced Concrete Biaxial Voided Square Slabs,” ACI Structural Journal, 117(5), pp. 3–14.

[2] Yao, S., Zhang, D., Chen, X., Lu, F., and Wang, W., 2016, “Experimental and Numerical Study on the Dynamic Response of RC Slabs under Blast Loading,” Engineering Failure Analysis, 66, pp. 120–129.

[3] Hao, H., Hao, Y., Li, J., and Chen, W., 2016, “Review of the Current Practices in Blast-Resistant Analysis and Design of Concrete Structures,” Advances in Structural Engineering, 19, pp. 1193–1223.

New Epoxy/ESO Composite Systems Produced by Pultrusion and Their High Strain Rate Compressive Performance

Ivan Vasileski[1*], Svetlana Risteska[1,2**], Sara Srebrenkoska [3], Evgenija Gjorgjieska Angelovska [1], Aleksandar Pižov[1] and Vineta Srebrenkoska[2]

[1] *Laminati Kom D.O.O., Aleksandar Makedonski 122, 7500 Prilep, Republic of North Macedonia.*

[2] *Faculty of Technology, Goce Delcev University, Krste Misirkov, No. 10-A Stip, Republic of North Macedonia.*

[3] *Faculty of Mechanical Engineering, Goce Delcev University, Krste Misirkov, No. 10-A Stip, Republic of North Macedonia.*

** ivan.v@laminati.com.mk*

***svetlana.r@laminati.com.mk, svetlana.risteska@ugd.edu.mk*

Abstract: The increasing demand for sustainable high-performance materials has driven the development of bio-based composite systems suitable for high strain rate applications. This study investigates fiber-reinforced laminates based on epoxy resin modified with epoxidized soybean oil (ESO) as a renewable toughening agent. The incorporation of ESO improves matrix ductility, energy dissipation capacity, and crack propagation resistance without significantly compromising stiffness. Glass-fiber-reinforced laminates were manufactured and subjected to dynamic compression loading at elevated strain rates to evaluate their mechanical response. The results demonstrate enhanced strain-rate sensitivity and improved impact resistance compared to conventional brittle thermoset systems. Failure analysis indicates reduced matrix cracking and delayed interlaminar delamination due to improved matrix–fiber interfacial behavior. The study confirms that bio-based epoxy/ESO pultruded composites exhibit promising mechanical stability and enhanced dynamic performance, making them suitable for structural applications subjected to impact and high-rate compressive loading.

1. Experiment

The production of thermosetting fiber-reinforced polymer composites by pultrusion generally takes much less time due to their short consolidation cycles [1-5]. Several resin systems were used for the pultrusion experiments, some of which also contained bio-modified resin with different % in the resin system.

1.1. Production of new composites

Pultrusion represents an efficient and highly controlled manufacturing process for continuous fiber-reinforced composites based on thermosetting matrices. In epoxy systems modified with epoxidized soybean oil (ESO), the process offers a promising route for producing sustainable structural profiles with enhanced toughness and strain-rate sensitivity.

In the pultrusion process, continuous glass or carbon fibers are impregnated with a reactive epoxy resin system, typically based on DGEBA modified with ESO as a bio-based toughening agent and reactive diluent. The incorporation of ESO reduces resin viscosity, improving fiber wet-out during impregnation, while simultaneously increasing matrix ductility and fracture resistance after curing. The impregnated fiber bundle is then pulled through a heated die, where polymerization and crosslinking occur under controlled thermal conditions. Optimization of die temperature profile and pulling speed is essential to achieve complete curing while maintaining dimensional stability and minimizing residual stresses.

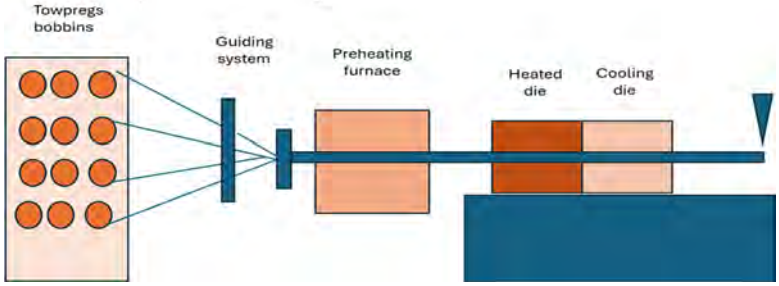

Fig. 1 Schematic layout of designed laboratory pultrusion

From a mechanical perspective, ESO-modified epoxy ma[1,6]. trices significantly influence the compressive behavior of pultruded composites under high strain rate loading. The increased flexibility introduced by ESO enhances energy absorption capacity and delays catastrophic brittle failure typically observed in conventional epoxy systems. Under elevated strain rates, pultruded laminates often exhibit increased compressive strength and stiffness due to strain-rate sensitivity of the polymer matrix. The presence of ESO can further improve damage tolerance by promoting microplastic deformation within the matrix and improving fiber–matrix interfacial stress transfer. Failure mechanisms under dynamic compression commonly include fiber microbuckling, matrix cracking, and interlaminar shear failure. However, ESO-modified systems tend to show reduced crack propagation speed and improved resistance to delamination compared to unmodified epoxy composites. These characteristics make bio-based epoxy/ESO pultruded composites attractive for applications subjected to impact,

crash loading, and other high-rate mechanical events. [7-11]. Overall, the combination of pultrusion technology and bio-modified epoxy systems provides a sustainable and mechanically efficient solution for structural components requiring reliable performance under high strain rate compressive loading.
However, these processes require careful management of key parameters, including temperature, fiber tension, speed and resin flow, to ensure optimal consolidation and part performance. Optimizing these parameters ensures high-quality composite parts with superior mechanical properties. These technologies offer significant benefits across a variety of industries, automotive and energy, by providing high-performance composite materials with tailored properties.

2. Results and Discussion

In this study, several thermosetting composite laminates with different matrix formulations were manufactured and systematically tested under both quasi-static and high-strain-rate compressive loading conditions, as well as under impact. The composite matrices included conventional epoxy systems and bio-based epoxy modified with varying contents of epoxidized soybean oil (ESO) as a toughening agent. Pultrusion and hand lay-up techniques were employed to produce laminates with consistent fiber volume fractions and controlled thicknesses. Mechanical testing involved low, intermediate and high-speed compression and impact tests following standards. Selected samples were analyzed using optical and scanning electron microscopy to characterize damage evolution, including matrix cracking, fiber micro-buckling, delamination, and interfacial failure.

The results show that increasing ESO content enhances impact resistance, improves energy absorption, and provides greater stability under high-strain-rate compression. Microscopic analysis indicates that ESO-modified matrices promote more uniform stress distribution and delay crack propagation, leading to improved damage tolerance compared to unmodified epoxy composites. These findings demonstrate that bio-based ESO-modified thermosetting composites offer superior mechanical performance under dynamic loading conditions, highlighting their potential for structural applications requiring high impact resistance and high-rate compressive stability.
Failure mechanisms transitioned from progressive matrix cracking and fiber micro-buckling under quasi-static loading to more localized and confined damage under dynamic impact conditions.

3. Summary

Bio-modified thermosetting composites exhibit improved impact resistance and enhanced stability under high-strain-rate compression. The incorporation of ESO contributes to increased energy absorption capacity, delayed crack initiation and propagation, and mitigation of typical brittle failure mechanisms. However, these improvements are observed only up to an optimal ESO concentration. Beyond this threshold, further addition of ESO leads to a gradual deterioration of mechanical properties, primarily due to plasticization effects and a reduction in crosslink density within the epoxy network. Therefore, ESO-based bio-composites represent promising candidates for structural applications subjected to dynamic loading conditions, provided that the ESO content is carefully optimized.

References

1. Risteska, S.; Vasileski, I.; Gjorgjieska Angelovska, E.; Pižov, A. Epoxy and Bio-Based Epoxy Glass Fiber Composites: Taguchi Design of Experiments and Future Applications. J. Compos. Sci. 2025, 9, 513. https://doi.org/10.3390/jcs9100513.
2. Fombuena, V.; Bernardi, L.; Fenollar, O.; Boronat, T.; Balart, R. Characterization of green composites from biobased epoxy matrices and bio-fillers derived from seashell wastes. Mater. Des. 2014, 57, 168–174. [CrossRef]
3. Chen, Y.; Liting, Y.;Wu, J.; Ma, L.; Finlow, D.E.; Lin, S.; Song, K. Thermal and mechanical properties of epoxy resin toughened with epoxidized soybean oil. J. Therm. Anal. Calorim. 2013, 113, 939–945. [CrossRef]
4. Senthilkumar, K.; Ungtrakul, T.; Chandrasekar, M.; Kumar, T.S.M.; Rajini, N.; Siengchin, S.; Pulikkalparambil, H.; Parameswaran pillai, J.; Ayrilmis, N. Performance of Sisal/Hemp Bio-based Epoxy Composites Under Accelerated Weathering. J. Polym. Environ.2021, 29, 624–636. [CrossRef]
5. Altuna, F.; Esposito, L.; Ruseckaite, R.; Stefani, P. Thermal and Mechanical Properties of Anhydride-Cured Epoxy Resins with Different Contents of Biobased Epoxidized Soybean Oil. J. Appl. Polym. Sci. 2011, 120, 789–798. [
6. Samper, M.; Fombuena, V.; Boronat, T.; Garcia-Sanoguera, D.; Balart, R. Thermal and Mechanical Characterization of Epoxy Resins (ELO and ESO) Cured with Anhydrides. J. Am. Oil Chem. Soc. 2012, 89, 1521–1528. [CrossRef]
7. Wang, Z.; Cao, N.; He, J.; Du, R.; Liu, Y.; Zhao, G. Mechanical and anticorrosion properties of furan/epoxy-based basalt f iber-reinforced composites. J. Appl. Polym. Sci. 2017, 134, 44799.
8. Wu, M.S.; Jin, B.C.; Li, X.; Nutt, S. A recyclable epoxy for composite wind turbine blades. Adv. Manuf. Polym. Compos. Sci. 2019, 5,114– 127.
9. Liu, G.; Jin, C.; Huo, S.; Kong, Z.; Chu, F. Preparation and properties of novel bio-based epoxy resin thermosets from lignin oligomers and cardanol. Int. J. Biol. Macromol. 2021, 193, 1400–1408.
10. Mattar, N.; de Anda, A.R.; Vahabi, H.; Renard, E.; Langlois, V. Resorcinol-Based Epoxy Resins Hardened with Limonene and Eugenol Derivatives: From the Synthesis of Renewable Diamines to the Mechanical Properties of Biobased Thermosets. ACS Sustain. Chem. Eng. 2020, 8, 13064–13075.
11. Capretti, M.; Giammaria, V.; Santulli, C.; Boria, S.; Del Bianco, G. Use of Bio-Epoxies and Their Effect on the Performance of Polymer Composites: A Critical Review. Polymers 2023, 15, 4733.

Explosion Fabrication of High Entropy Composites for High Strain Rate Applications

N. Chikhradze,[1,2,*] D. Tsverava,[1] and M. Chikhradze[2]

[1] *Department of Explosion Technologies, LEPL Grigol Tsulukidze Mining Institute, 7, E. Mindeli Str., 0186, Tbilisi, Georgia*

[2] *Department of Engineering Physics, Georgian Technical University, 77, Kostava Str., 0160, Tbilisi, Georgia*

[*] *e-mail: chikhradze@mining.org.ge*

Summary: High-Entropy Alloys (HEAs) are alloys that contain at least 5 principal metallic elements with equimolar concentration, or where the presence of principal elements varies between 5-35%. Four core effects: high configurational entropy, sluggish diffusion, lattice distortion and cocktail effects provide to HEA's the unique complex of properties, in particular: shock resistance, high hardness, wear-resistance, high strength, good corrosion/oxidation-resistance etc. [1-5].
The Fe-W-Al-Ti-Ni system was selected to fabricate HEA. Mechanical Alloying was applied to obtain ultrafine/nanostructured powder mixture. The explosion compaction was used for consolidation of ultradisperse powders. The technological regimes of fabrication of HEA's and structure-properties are discussed in the paper.

1. Motivation and Experimental set-up

1.1. Motivation

The Fe-W-Al-Ti-Ni–B-C composition is very attractive for both, fundamental investigations and for practical point of view (advanced materials for ballistics, energy sector, defense, machine building, chemical industries, anti-corrosion coatings, electronics, nuclear power plant etc.).

1.2. Fabrication of HEA Nanopowders

Crystalline Fe, W, Al, Ti, Ni coarse elementary pure (at list 96%) powders were used as precursors and subjected to "incoming control", which includes following operations: Sieve analyses, sorting by fraction in vibratory sieve; granulometric analyses; x-ray phase and fluorescence analyses. Purity of principal metallic components was: ≥96%; main impurities: Si, Mn, C. Blend of 15%Fe-45%W7%Al-12%Ti-15%Ni-3%C-3%B (by mass) composition was prepared for mechanical alloying (MA). The MA of the HEA powder blend performed in the high energetic "Fritsch" Planetary Mill PULVERISETTE 7 (Fig 1). Mill was equipped with WC Balls and jars. Conditions of milling: ratio: balls to blend mass ratio 10:1; Diameter of balls: 5mm; The time of MA varied and was: 2h; 6h; 10h; 14h; 28h; 36h; 48h; 72h; Rotation speed of the jar was 500 rpm in reverse regime with delay 30min; The phase composition and particle sizes of the powders were controlled by X-ray diffraction system, nano-sizer and SEM investigations.

Fig.1. MA of 15%Fe-45%W7%Al-12%Ti-15%Ni-3%C-3%B: a) Ball mill view; b) Blend view Charged in jar.

1.3. Fabrication of Bulk High Entropy Alloys

The cylindrical container was fabricated from a low carbon steel tube, closed from one side. Pre-alloyed ultrafine blend was charged in powder container. Charging of powder performed step by step in little portions of powder, followed by pressing on static press-installation for pre-densification (intensity of loading P=500-1000 kg/cm^2). After filling the containers were closed on both sides. Explosion consolidation of pre-alloyed HEA powder (HEAP) performed by well-known [6] axis-symmetric explosion loading scheme (Fig.2). For this purpose, cylindrical containers for explosives, from polymer tube (with increased diameter) were prepared. The steel container charged by HEAP was in polymer box axis-symmetrically, filled with the powdered explosive (ANFO, ammonite or RDX) and was detonated. The stress-deformed condition of the reaction mixture generated under explosive loadings, were determined according to solutions of mathematical physics and elasticity theory and by the computer program created by authors [7].

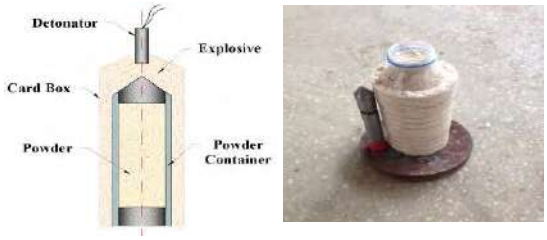

Fig.2 Axis-Symmetric Cylindrical Set-up for explosion consolidation of HEAP.

2. Experimental Results

The pictures of Bulk HEA composite samples fabricated by explosion compaction technology are presented on Fig. 3.

Fig. 3. View of Bulk composite samples obtained by explosive consolidation of FeWAlTiNi: a) steel container after explosion loading; b) Bulk sample by mechanical treatment for removal of steel jucket; c) FeWAlTiNi Bulk composite.

Investigations of microstructural transformations of pre-alloyed powders and Bulk HEA's matrix composites consolidated by explosion consolidation technology carried out by JEOL JSM-6510LV scanning microscopes.
The Bulk HEA composites fabricated by explosion consolidation are characterized by ultrafine grained structure. By SEM and XRD investigations confirmed formation of nanostructure in composites obtained from blend, MA in 72h.
At the same time the radial cracks are observed in cross-section of bulk samples. It is an indicator of the necessity to change the explosion load parameters, to reduce peak pressure and increase the impulse duration.

Conclusions:

- Mechanical Alloying of preliminary prepared precursors mixture was performed in planetary ball mill and technological parameters for pre-alloyed powder fabrication are determined.
- Pre-alloyed ultrafine blend was consolidated by explosion generated high pressure and bulk HEA composites are fabricated.
- The possibilities of formation bulk Alloys by considered technological route are confirmed.
- The radial cracks in cross section of FeWAlTiNiBC HEA bulk samples were observed.
- The necessity of future works for optimization of explosion consolidation parameters of FeWAlTiNiBC pre alloyed powder is established.

References

[1] Yeh J. et al, Nanostructured high entropy alloys with multiple principal elements: novel alloy design concepts and outcomes, Adv. Eng. Mater. V. 6., #5, 2004
[2] Cantor B. et al., Materials Science and Engineering: A, 375-377, 213-218, 2004
[3] He Q. F. et al, Design of High-Entropy Alloy: A Perspective from Nonideal Mixing, JOM, v.69., # 11, p. 2092-2098, 2017
[4] Miracle D.B. et al, Exploration and Development of High Entropy Alloys for Structural Applications, Entropy, v.16. #1, p.494-525, 2014, http://www.mdpi.com/1099-4300/16/1/494
[5] Kumar A., Singh A., Suhane A, Mechanically alloyed high entropy alloys: existing challenges and opportunities, Journal of Materials Research and Technology, v. 17, March-April 2022, pp. 2431-2456
[6] L. E. Murr. K. P. Staudhammer, M. A. Meyers, Metallurgical and Materials Application of Shock-Wave High-Strain-Rate Phenomena, Ed. by Section 1. Dynamic Consolidation of Materials, 1995
[7] N. Chikhradze, K. Staudhammer, F. Marquis, I. Lomidze, A. Peikrishvili, Calculation of the stress Tensor under symmetric cylindrical shock wave loading, Book: "Powder Materials: Current research and industrial practice",Edited by F.D. S. Marquis, N.N.Thadhani, E.V. Barrera, Indianapolis, Indiana, USA, 2001, pp. 243-256

Enhanced Mechanical Performance of MXene-Coated Basalt Fiber-Reinforced Composites Impregnated with Star-Like Polymer-Modified Epoxy Matrix

Tatjana Glaskova-Kuzmina,[1, 2*] Gediminas Monastyreckis,[1] Kristina Zukiene,[1] Vladimir Spacek,[3] and DaivaZeleniakiene[1]

[1] *Department of Mechanical Engineering, Kaunas University of Technology, Studentų g. 56, 51424 Kaunas, Lithuania*

[2] *Faculty of Science and Technology, University of Latvia, Jelgavas 3, LV-1004, Riga, Latvia*

[3] *SYNPO a.s., S. K. Neumanna 1316, 530 02 Pardubice, Czech Republic*

[*] *tatjana.glaskova-kuzmina@lu.lv*

Summary: This study aimed to investigate the effect of MXene surface coating on the impact, interlaminar fracture toughness, and fatigue properties of basalt fiber-reinforced composites (BFRC) impregnated with a star-like polymer (SLP)-modified epoxy matrix. The matrix modification, i.e., addition of 0.5 wt.% SLP in epoxy resin for BFRC impregnation led to the highest impact and interlaminar fracture properties, but an antagonistic effect was observed with dual modification strategies. However, fatigue test results showed that combining bulk matrix modification with interfacial treatment was the most effective approach for improving the fatigue behavior of BFRC.

1. Introduction

Basalt fibers (BF) are a cost-effective alternative to glass fibers in fiber-reinforced composites [1]. With high tensile strength (~2.8 GPa), excellent thermal stability, and strong chemical resistance, BFRC are suitable for automotive, electrical, wind energy, insulation, and fire-protection applications [2]. A key limitation of BFRC is poor interfacial bonding between the BF and the epoxy matrix. The inert, smooth fiber surface restricts mechanical interlocking and chemical adhesion, reducing overall composite performance [3]. Surface modification methods, including low-temperature plasma treatment (air or oxygen) and chemical sizing, enhance fiber wettability and interfacial adhesion, thereby improving interlaminar shear strength and toughness [4].

MXenes, particularly $Ti_3C_2T_x$, are emerging two-dimensional materials that are widely explored as coatings or nanofillers in polymer composites [5]. Their incorporation improves interfacial bonding, mechanical strength, and multifunctionality by enhancing electrical and thermal conductivity. Combining plasma-based surface activation with MXene nanocoatings may reduce fiber–matrix debonding and introduce multifunctionality. Additionally, modifying the epoxy matrix with SLP improves wettability and adhesion due to its branched structure and reduced surface tension [6]. Previous studies revealed significant improvements in interlaminar fracture properties of SLP-modified BFRC, highlighting the potential of multiscale modification approaches for advanced composite design [2,6].

2. Materials and methods

The reference material was BFRC, made from BAS UNI 350 BF (Basaltex, Belgium), and a bio-based epoxy system consisting of SR Greenpoxy 33 resin (Sicomin, France) and LITE 2401 hardener (Cardolite, Belgium) mixed at a 100:34 ratio. The epoxy matrix was modified with 0.5 wt.% SLP, i.e., poly(n-butyl methacrylate)-block-(glycidyl methacrylate), developed by SYNPO a.s. (Czech Republic). This concentration was selected based on previous results showing optimal improvements in wettability, mechanical, and thermophysical properties of SLP-modified BFRC [6].

Oxygen plasma treatment was carried out for 2 min using a radio-frequency capacitive plasma unit (JSC Kvartz Plasma-600T, Quvasoy, Uzbekistan) operating at 13.56 MHz and 0.3 W/cm². Subsequently, the BF samples underwent three cycles of dip-coating in a 0.67 mg/mL aqueous MXene suspension, with each dipping step followed by drying at 70 °C.

Specimens for low-velocity impact testing were prepared in accordance with ISO 14125, with dimensions of 60 × 60 × 1 mm (±0.2). Laminates were fabricated by manual lay-up using five plies of basalt fiber fabric to achieve the required thickness. After fabrication, the samples were vacuum bagged for 12 hours and cured according to the previously described protocol. At least five specimens were produced and tested for each experimental group. Low-velocity impact tests were performed in accordance with ISO 6603-02 using an instrumented drop-weight system (Coesfeld GmbH & Co. KG, Germany). Specimens were clamped between two steel plates with a 40 mm circular opening for striker access. A hemispherical striker (20 mm diameter, 5.185 kg) was dropped from 1.0 m, producing an impact velocity of approximately 2.80 m/s.

Double cantilever beam (DCB) specimens were prepared from BFRC laminate plates in accordance with ASTM D5528, with nominal dimensions of 125 × 25 × 3 mm (±0.2), consistent with our previous research [2]. The laminates were made by stacking 12 layers of basalt fiber fabric, each manually impregnated with resin in a custom mold. For plasma-treated and MXene-coated samples, the two central plies were modified accordingly. Laminates were pressed at 20 kPa for 24 hours at room temperature, then post-cured at 80 °C and 120 °C for 2 hours each, and finally cut along the fiber direction. Mode I interlaminar fracture toughness tests were performed on a Zwick 2.5 universal machine at a crosshead speed of 2 mm/min. Crack growth was visually monitored on one specimen face using reference marks at 1- and 2-mm intervals. A total of 20 crack-length measurements per specimen were recorded to calculate Mode I interlaminar fracture toughness by using modified beam theory.

Flexural fatigue specimens were prepared according to ISO 14125 with nominal dimensions of 50 × 15 × 1.2 ± 0.2 mm. Prior to testing, specimens were conditioned for at least 48 hours at 23 ± 2 °C and 50 ± 5% relative humidity in accordance with ISO 291. Fatigue tests were performed in three-point bending in accordance with ISO 14125 and ASTM D7774. The span was 40 mm (~20× specimen thickness), with 5 mm-radius cylindrical loading and support noses. Tests were conducted on an Instron E10000 machine (1–10 kN load cell) under force-controlled sinusoidal loading at 5 Hz and a stress ratio of R = 0.1. Maximum stress levels were set between 0.9 and 0.5 of the static flexural strength (determined per ISO 14125), with at least 5 specimens tested at each level. Failure was defined as a complete fracture; specimens surviving 10^7 cycles were classified as run-outs.

3. Main results and conclusions

Due to different dominant fracture modes in impact and bending fatigue, distinct effects were observed for the SLP and MXene treatments. For impact results, the dual modification of BFRC was ineffective because the dominant mode was shear stress, and MXenes could reduce interfacial shear strength. Thus, the highest impact resistance, with 38% and 78% improvements over BFRC in maximum force and absorbed energy, respectively, was achieved with BFRC modified with 0.5 wt.% SLP, due to improved interfacial bonding.

The most improved fatigue behavior, with the number of cycles improved by 191% compared with the reference BFRC, was observed for the hybrid system combining SLP modification and plasma/MXene treatment. It also showed that the highest resistance to cyclic failure, indicating a clear synergistic effect between matrix toughening and interfacial reinforcement. Thus, it can be concluded that SLP improved matrix ductility and energy dissipation, while the plasma/MXene-treated interphase enhanced the overall resistance of BFRC to normal stress, which dominates in bending.

For interlaminar fracture properties, a 45% increase in Mode I interlaminar fracture toughness (ILFT) for BFRC containing 0.5 wt.% SLP, attributed to higher epoxy crosslink density and improved fiber–matrix bonding. For oxygen plasma and MXene-treated BFRC, critical load and ILFT increased by 18.8% and 28.8%, respectively, owing to enhanced interfacial adhesion, surface functionalization, roughness, and nano-reinforcing crack-deflection mechanisms. However, similarly to impact properties, dual modification did not yield further improvement and slightly reduced performance.

The enhanced performance of BFRC modified with SLP and coated by MXenes highlights the importance of multiscale design approaches in developing next-generation fiber-reinforced composites for long-term and cyclic loading applications.

Acknowledgements

This research is funded by the Research Council of Lithuania (LMTLT) under agreement No. S-MIP-23-134.

References

[1] Chen, D., Sun, G., Meng, M., Jin, X., Li, Q., 2019, “Flexural performance and cost efficiency of carbon/basalt/glass hybrid FRP composite laminates,” Thin-Walled Struct., 142, pp. 516–31. https://doi.org/10.1016/j.tws.2019.03.056.
[2] Glaskova-Kuzmina, T., Pinto, R., Zukiene, K., Monastyreckis, G., Spacek, V., Zeleniakiene, D., 2025, “Hydrothermal ageing of basalt fibre-reinforced epoxy composites modified with star-like polymer,” Polymer Composites, 2026, 47, pp. 2666–2677. https://doi.org/10.1002/pc.70315
[3] Wei, Y., Zhao, J., Zhuang, J., Zhang, P., Han, Zh., 2024, “Optimization mechanism of mechanical properties of basalt fiber-epoxy resin composites by interfacially enriched distribution of nano-starch crystals,” Chin. J. Mech. Eng., 37, 44. https://doi.org/10.1186/s10033-024-01031-7.
[4] Li, Y., Sun, Sh., Zhou, Y., Xu, X., Zhan, J., 2023, “Influence of air plasma modification power on surface properties of basalt fibers and basalt/poly(butylene succinate) adhesion,” Applied Surface Science, 630, 157416, https://doi.org/10.1016/j.apsusc.2023.157416.
[5] Monastyreckis, G., Mishnaevsky, L., Hatter, C.B., Aniskevich, A., Gogotsi, Y., Zeleniakiene, D., 2020, “Micromechanical modeling of MXene-polymer composites,” Carbon, 162, 2020, pp. 402-409, https://doi.org/10.1016/j.carbon.2020.02.070.
[6] Zukiene, K., Pinto, R., Monastyreckis, G., Spacek, V., Glaskova-Kuzmina, T., Zeleniakiene, D, 2025, “Enhanced adhesion of epoxy resin to basalt fibres using a segregating star-like copolymer additive,” Composites Communications, 57, 102497. https://doi.org/10.1016/j.coco.2025.102497

HISTRATE

Advanced Composites under High Strain Rate Loading A Route to Certification-by-Analysis

2026 Conference

10th – 11th JUNE 2026

Session 2 - Novel simulation methods and best practices for composites under high strain rates (WG4)

cost EUROPEAN COOPERATION IN SCIENCE & TECHNOLOGY

Funded by the European Union

Modelling and simulation of the mechanical response and damage of carbon fibre-reinforced polymer (CFRP) laminates for aero-structures subjected to simulated lightning strike

Albertino Arteiro,[1,*] João Pedro,[2] Paulo T. Gonçalves,[2] and Christian Karch[3]

[1] *INEGI, Faculdade de Engenharia, Universidade do Porto, Rua Dr. Roberto Frias, s/n, 4200-465 Porto, Portugal*

[2] *INEGI, Universidade do Porto, Rua Dr. Roberto Frias, 400, 4200-465 Porto, Portugal*

[3] *Airbus Defence and Space GmbH, Manching 85077, Germany*

[*] *aarteiro@fe.up.pt*

Summary: In protected CFRP subjected to lightning strike, while thermal effects mostly affect the topmost UD plies, damage in the bulk, where temperatures can be far from the ablation temperatures of the composite constituents, is mainly the result of the pressure generated by the explosion of the lightning protection layer, supersonic plasma expansion and magnetic forces. In this work, a 3D intralaminar damage model and cohesive zone interlaminar damage models are applied to study the effects of stacking sequence, paint layer thickness and artificial lightning parameters on the mechanical damage induced by the direct effects of lightning strikes on carbon/epoxy multi-directional laminates protected by expanded copper foil. The models show an influence of stacking sequence not only on the orientation of the damage projected area, but also on its size. In addition, no effect on the damage depth is observed, in agreement with available experimental observations. The models also show that laminates with thicker ply blocks have larger damage projected areas. The effect of paint layer thickness is then predicted, showing that thicker paint layers lead to larger damage extent, as observed experimentally. Finally, it is shown that varying the peak current and deposited energy changes the extent of damage, with the proposed models following the trends observed in experiments. Ultimately, this study demonstrates that the progress and development of reliable models that accurately predict the main effects of lightning strikes is key to simulation-based product development and certification-by-analysis of protected composite aero-structures.

1. Introduction

In this work, the physically-based models proposed by Karch et al. [1] for the mechanical loads induced by lightning strikes are implemented into a 3D structural finite element model and combined with a modified continuum damage mechanics (CDM) model for CFRPs [2] and an interlaminar cohesive zone model for delamination to predict the mechanical response of protected, painted composite laminates subjected to simulated lightning strike. This model, after experimental validation [3], is employed in the prediction of the influence of (i) stacking sequence, lay-up and effective ply thickness, (ii) paint thickness and (iii) lightning parameters (covering the application domain of the SAE aerospace recommended practice for lightning strike testing of aeronautical structures) on the mechanical response of CFRP laminates subjected to simulated lightning strike.

2. Mechanical lightning loads

Experimental observations show that, in protected CFRP, “thermal” damage to the CFRP is mostly restricted to the first or second topmost UD plies [4, 5]. Thus, in a first approximation, the thermal and thermal-mechanical effects can be neglected when predicting (bulk) mechanical damage on protected CFRP samples.

Following Karch et al. [1], the mechanical pressures from the near-surface explosion of the lightning protection layer are computed numerically based on a one-dimensional shock peening model [6], the supersonic plasma expansion is accounted using a shock wave model based on Lin’s approach [7], and the magnetic field caused by the impressed current flow in the electrically conducting structures is determined analytically [1]. The associated pressure distributions are implemented in the finite element solver Abaqus/Explicit [8] using the user-defined subroutine VDLOAD, since the adoption of an explicit dynamics solution is compatible with the highly transient lightning strike problem considered in this study.

3. Finite element model

A finite element model with solid elements is used together with a CDM model [2] and a cohesive zone model [8] to represent mechanical damage to the composite plies. An energy regularisation approach based on the fracture energy associated with each failure mechanism and based on the characteristic length of the finite elements (l^*) is used to ensure mesh independent results after damage onset [9]. Each composite ply is modelled as a homogeneous orthotropic material, assuming transverse isotropy. To account for ply thickness effects, *in situ* strengths are defined as a function of ply thickness and position in the laminate [2, 10]. The CDM model is

implemented in a user-defined subroutine VUMAT for Abaqus/Explicit [8]. Delamination between plies is modelled using volumetric elements and a cohesive zone model implemented in a VUMAT or using cohesive surface interactions [8]. The lightning protection layers, consisting of copper mesh embedded in epoxy matrix, are assumed homogeneous orthotropic linear-elastic solids [1]. The paint layer on the surface of the laminates is not explicitly modelled, but it is accounted for in the computation of the mechanical pressures from the near-surface explosion of the lightning protection layer [1].

4. Results

4.1. Laminate stacking sequence effects

In agreement with experimental observations [11, 12], the models reveal that the stacking sequence and lay-up have an influence on the surface damage distribution, not only on its orientation, but also on its size; it has, however, no effect on the damage depth. In addition, the models predict that laminates with thicker ply blocks have larger damage projected areas, again in agreement with the available experimental observations [11, 13].

4.2. Paint thickness effects

The models proposed in this work predict the increase of damage extent with the increase of paint thickness, so far observed experimentally [4, 14, 15]. Moreover, they satisfactorily capture the effect of paint thickness on different lightning protection layers, following experimentally observed trends reported in literature [4, 14, 15].

4.3. Lightning parameters effects

Compared with the nominal values of peak current and action integral proposed by the SAE aerospace recommended practice for lightning strike testing of aeronautical structures [16], a ±10% variation of the peak current (admissible bounds set in the standard) creates non-negligible changes of the pressure, force and impulse magnitudes, with higher peak currents producing higher deflections and more mechanical damage. Likewise, the waveforms with higher action integral also induce more damage than the waveforms with lower action integral (considering the admissible bounds of ±20% as set in the standard [16]).

5. Conclusions

As the aerospace industry moves towards hybrid experimental/numerical design and certification processes, the development of reliable models that accurately predict the main transient effects of lightning strikes becomes crucial. This study is one demonstration of application of such models.

References

[1] Karch, C., Arteiro, A. and Camanho, P. P., 2019, “Modelling mechanical lightning loads in carbon fibre-reinforced polymers,” Int. J. Solids Struct., 162, pp. 217-243.
[2] Furtado, C., Catalanotti, G., Arteiro, A., Gray, P. J., Wardle, B. L. and Camanho, P. P., 2019, “Simulation of failure in laminated polymer composites: Building-block validation,” Compos. Struct., 226, 111168.
[3] Pedro, J., Gonçalves, P. T., Soares, G., Arteiro, A., Honke, R. and Karch, C., 2025, “Mechanical loads from simulated lightning strike on protected carbon fibre-reinforced polymers revisited: implementation and experimental validation,” Aeronaut. J., 129, pp. 3569-3601.
[4] Murillo, R., Flourens, F., Garcia, V., Duval, Y. and Cavaliere F., 2017, “Lightning strike protection of carbon composite skin. Kinetic and signature of the damage,” In Proceedings of ICOLSE 2017, Nagoya, pp. 1-7.
[5] Abdelal, G. and Murphy, A., 2014, “Nonlinear numerical modelling of lightning strike effect on composite panels with temperature dependent material properties,” Compos. Struct., 109, pp. 268-278.
[6] Fabbro, R., Fournier, J., Ballard, P., Devaux, D. and Virmot, J., 1990, “Physical study of laser-produced plasma in confined geometry,” J. Appl. Phys., 68, pp. 775-784.
[7] Lin, S. C., 1954, “Cylindrical shock waves produced by instantaneous energy release,” J. Appl. Phys., 25(1), pp. 54-57.
[8] Dassault Systèmes Simulia Corp., 2014, “Abaqus 6.14 Documentation”, Providence, USA.
[9] Bažant, Z. P. and Oh, B. H, 1983, “Crack band theory for fracture of concrete,” Mater. Struct., 16(93), pp. 155-177.
[10] Camanho, P. P., Dávila, C. G., Pinho, S. T., Iannucci, L. and Robinson, P., 2006, “Prediction of in situ strengths and matrix cracking in composites under transverse tension and in-plane shear,” Compos. Part A-Appl. S., 37, pp. 165-176.
[11] Kawakami, H., 2011, “Lightning Strike Induced Damage Mechanisms of Carbon Fiber Composites,” PhD thesis, University of Washington.
[12] Li, Y., Li, R., Lu, L. and Huang, X., 2015, “Experimental study of damage characteristics of carbon woven fabric/epoxy laminates subjected to lightning strike,” Compos. Part A-Appl. S., 79, pp. 164-175.
[13] Yamashita, S., Sonehara, T., Takahashi, J., Kawabe, K. and Murakami, T., 2017, “Effect of thin-ply on damage behaviour of continuous and discontinuous carbon fibre reinforced thermoplastics subjected to simulated lightning strike,” Compos. Part A-Appl. S, 95, pp. 132-140.
[14] Bigand, A. and Duval, Y., 2017, “Quantification of the mechanical impact of lightning strike protection explosion confined by thick paint,” In Proceedings of ICOLSE 2017, Nagoya, pp. 1-7.
[15] Lepetit, B., Escure, C., Guinard, S., Revel, I., Peres, G. and Duval, Y., 2011, “Thermomechanical effects induced by lightning on carbon fiber composite materials,” In Proceedings of ICOLSE 2011, Oxford, pp. 1-8.
[16] ARP5412, 2013, “Aircraft Lightning Environment and Related Test Waveforms,” Society of Automotive Engineers.

Incubation-time-based failure criterion to predict delamination due to spalling and through-thickness impact loading

Andreas Hornig[1,2,3,*], Maik Gude[1]

[1] *Institute of Lightweight Engineering and Polymer Technology (ILK), TUD Dresden University of Technology, Holbeinstrasse 3, Dresden, 01307, Germany*

[2] *Department of Engineering Science, Solid Mechanics and Materials Engineering, University of Oxford, Oxford, OX1 3PJ, United Kingdom*

[3] *Center for Scalable Data Analytics and Artificial Intelligence Dresden/Leipzig (ScaDS.AI), TUD Dresden University of Technology, Strehlener Straße 12-14, Dresden, 01069, Germany*

[*] *andreas.hornig@tu-dresden.de*

Summary

In the reflection zones of impact-induced elastic waves, the time-strain response is highly nonlinear, preventing the identification of representative strain-rate states with corresponding strength parameters. Moreover, the observed strain rates are exceptionally high. Conventional strain-rate dependent failure criteria for composite materials usually fail to predict failure under these conditions. Therefore, an improved failure criterion for through-thickness failure in composites, along with a corresponding experimental parameter identification methodology, is proposed to enable more accurate prediction of delamination due to spalling.

1. Conventional rate dependent failure criteria

To describe rate-dependent failure, strain-rate-based formulations can be employed. Although the general applicability of criteria originally proposed by Johnson and Cook [1] has already been demonstrated for fiber-reinforced thermoplastic composites at low strain rates [2], this approach allows the increase in material parameters with rising strain rate to be captured. These parameters are determined under constant strain-rate conditions, assuming a constant reference strain rate for evaluating strength. Logarithmic approaches may yield unrealistic or even physically meaningless results. Therefore, the use of a power-law formulation is proposed:

$$\sigma_3^{fail} = R_3^+ \left(\frac{\dot{\varepsilon}_3}{\dot{\varepsilon}_3^{(ref)}} \right)^p \qquad \text{(strain-rate approach)} \qquad (1)$$

with σ_3^{fail} representing the stress at failure at the current train rate $\dot{\varepsilon}_3$, R_3^+ the strength at reference strain rate $\dot{\varepsilon}_3^{(ref)}$ in laminate through thickness direction 3 and p the slope exponent.

However, in real deformation scenarios, and particularly during wave propagation processes, strain rates vary continuously and significantly. Constant strain-rate conditions, to which the corresponding failure parameters could be associated, are therefore absent as a reference, limiting the applicability of this criterion. In contrast, the temporal-spacial failure criterion proposed by Petrov and Utkin [3] is based on averaged impulse loads acting on the structure. For undamaged materials and under the assumption of brittle failure behavior, the spatial dependence can be neglected and a purely incubation-time based-approach can be used. Failure is initiated, when

$$\int_{t-\tau_c}^{t} \sigma_3 dt \geq R_3^+ \tau_c \qquad \text{(incubation-time approach)} \qquad (2)$$

with t denoting the time and τ_c the incubation time. It becomes evident that, in this approach, the instantaneous state of the material is not considered for evaluating the stress condition; instead, the loading history is incorporated into the failure assessment.

2. Incubation-time-based spalling criterion

The incubation time-approach (2) is well-suited for calculating failure under nonlinear stress-time histories. However, this formulation tends to predict unrealistically high failure thresholds at high strain rates. In contrast, the strain-rate-based approach (1) does not account for variations in stress rate during loading, but it provides realistic predictions for composite materials. Therefore, a combined criterion is proposed here. In this approach, the conceptual idea of an incubation time τ_c - an associated duration of a stress or strain leading to failure - is transferred to the mean incubation stress-rate $\dot{\sigma}_3^{\tau_c}$ acting within this period and used for linearization. Considering the power-law formulation from (1), the combined criterion for tensile loading can be expressed as

$$\sigma_3^{fail} = R_3^+ \cdot \left(\frac{\left|\dot{\sigma}_3^{\tau_c}\right|}{\dot{\sigma}_3^{(ref)}} \right)^p \quad \text{with} \quad \dot{\sigma}_3^{\tau_c} = \frac{\sigma_3(t) - \sigma_3(t-\tau_c)}{\tau_c} \quad \text{(incubation-time-based failure criterion)} \quad (3)$$

With this formulation, the conventional strain-rate approach can also be applied to loading histories with varying stress or strain rates, since the domain for determining the mean reference stress rate is precisely defined. Fig. 1 illustrates the relevant model parameters using a nonlinear stress-time response as an example.

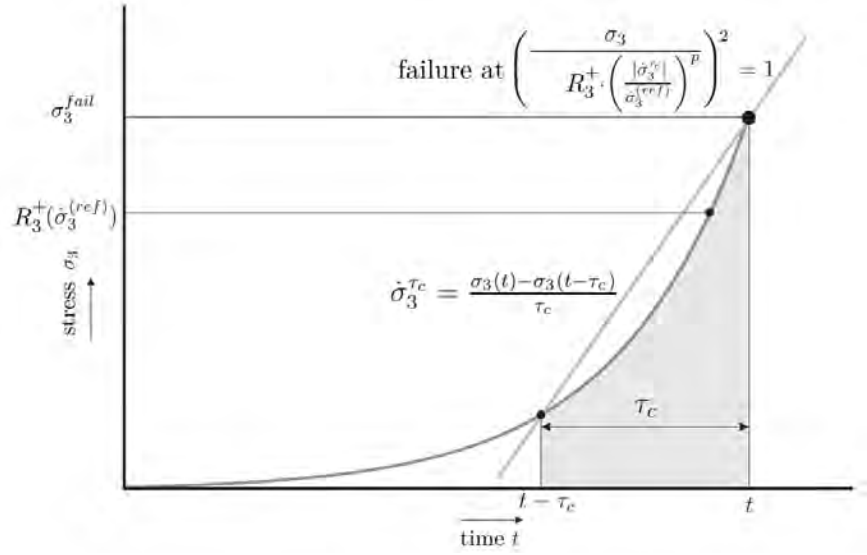

Fig. 1. Model parameters of the incubation-time-based failure criterion.

3. Experimental characterisation

For the delamination criterion according to (3), in addition to the failure parameters (reference tensile strength R_3^+ at the respective reference rate $\sigma_3^{(\dot{ref})}$), the incubation time τ_c and the slope parameter p must be determined. Using these parameters, the current incubation stress-rates $\sigma_3^{\dot{\tau_c}}$, and subsequently the through-thickness failure stresses σ_3^{fail} at the current time t, can be calculated. For this purpose, stress-time histories are obtained from highly dynamic tests, and the corresponding failure stresses and their mean values are derived, as illustrated in Fig. 2. The associated incubation stress rates are determined by linear regression, whereby the lowest identified rate in each case is selected as the reference rate. The incubation time τ_c is determined for the highest test velocity. Finally, the slope parameter p and the reference strength are obtained by curve fitting.

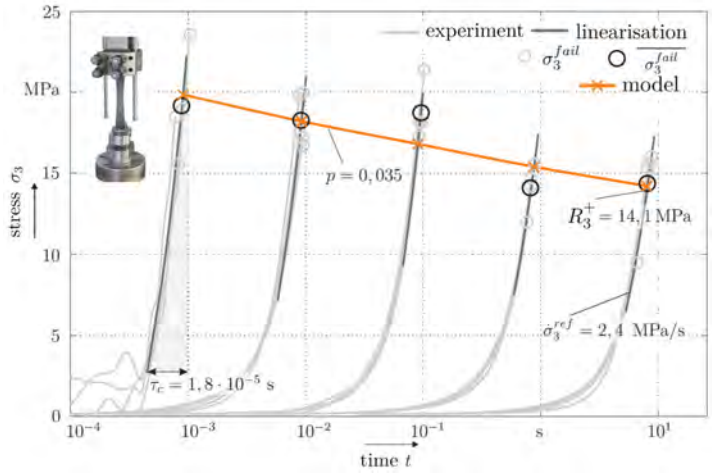

Fig. 2. Exemplary experimental evaluation for the identification of the model parameters.

References

[Q1] Johnson, G. R., & Cook, W. H. (1985). Fracture characteristics of three metals subjected to various strains, strain rates, temperatures and pressures. Eng. Frac. Mech., 21(1), 31-48. https://doi.org/10.1016/0013-7944(85)90052-9
[Q2] Gerritzen, J., Gude, M. & Hornig, A. (2025). Strain rate dependent 3D shear characteristics of thermoplastic FRC – Experiments, modelling and analysis by machine learning. in 2nd HISTRATE Conference, 04.-05.06.2025, San Sebastian (Spain). https://10.5281/zenodo.16962743
[Q3] Petrov, Y.V. & Utkin, A.A. (2017). Structural-temporal approach and geometry of the fracture zone in spalling. Proc. Struc. Integ. 6, 134-139 https://doi.org/10.1016/j.prostr.2017.11.021

Fracture modeling of the interface for composites: stick-slip behaviors – a dynamic process

Dayou Ma[1,*]

[1] *Politecnico di Milano, Department of Mechanical Engineering, via la Masa, 1, Milan 20156, Italy*

Summary: Laminate composites may exhibit discontinuous fracture during mode-I cracking, which is known as stick–slip fracture. Such behavior complicates the fracture of composite interfaces as a dynamic fracture even under static conditions. This study models such behaviors using a novel cohesive model. Relationships between crack length and opening displacement during double cantilever tests were developed based on fracture mechanics to identify key parameters. As validation, two experimental datasets were applied. Results show that the model accurately predicts stick–slip fracture, suggesting that mode-I crack propagation should be considered as a dynamic process even initiated under static conditions.

1. Main Text

The variation in energy release rate during crack initiation and propagation is believed to be the main mechanism for stick-slip behavior. To account for the reduced energy release rate for crack propagation compared to crack initiation, an adapted cohesive model was proposed, depicted as a "chopped" triangle in Figure 1. The profile-triangle behavior indicates crack initiation within the cohesive model, consistent with the present work's CZM. After initiation, the model shifts to a degrading behavior to simulate a slip-stick fracture. The model introduces two new zones: energy accumulation and rapid cracking, as found in Figure 1. The energy accumulation zone allows for the buildup of energy needed for both crack initiation and propagation. Once sufficient energy is accumulated, rapid crack propagation occurs immediately after initiation in the rapid-cracking zone, often marked by white bands, as indicated in Figure 1, which represents energy stored during microcrack nucleation. The white striation correlates with stick-slip fracture, visible as roughness on the fracture surface under microscopy [1,2], indicating greater energy absorption here. Parameters δ_a and δ_f, shown in the figure, denote the crack-opening displacements for the DCB samples, defining the lengths of the energy-accumulation and rapid-cracking zones. Numerically, these are derived from the separation of the CZM, based on the energy release rate difference at crack initiation and propagation (ΔG in Figure 1), obtained from R-curves. Adjusting δ_a and δ_f tunes the evolution of damage to match the material's nonlinear behavior. After rapid cracking, a new crack cycle begins until the next initiation. The shape of the cohesive model depends on δ_a relative to the original critical separation, δ_0: Figure 1a shows $\delta_a < \delta_0$, while Figure 1b shows $\delta_0 > \delta_a$.

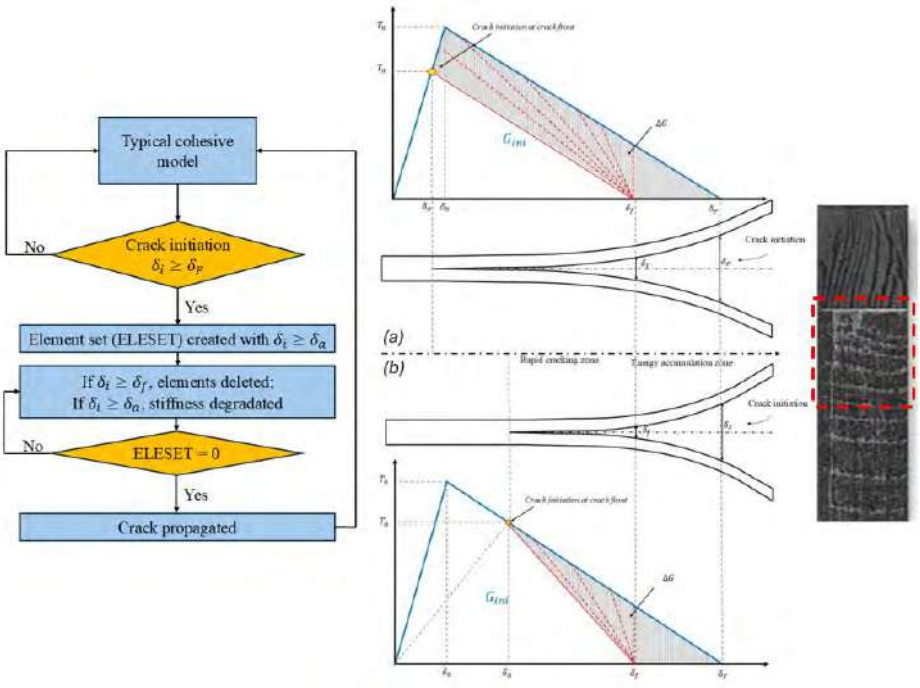

Figure 1 Proposed cohesive model for stick-slip fracture and schematic for theoretical basis (a&b).

With experimental data on stick-slip fracture during mode-I cracking, the proposed cohesive model can be validated using a user subroutine in LS-DYNA. Figure 2 shows that the FE model closely replicates the load-displacement history, particularly the decline in stiffness after each crack-propagation cycle and the stair-like increase in crack length. The initial peak in load for Sample-1 (Figure 2b) is disregarded because it arises from a rich resin region at the crack tip prior to pre-cracking, as noted by Li et al. [3]. For all results, the load-displacement curves from FE modeling display how stiffness decreases after each rapid crack growth. The fluctuations in the FE load are caused by damping effects in the detached composite beam following crack propagation. These oscillations in load and crack progression correspond to the variations seen in the experimental R-curve. Overall, the proposed cohesive model effectively simulates stick-slip behavior, i.e., crack growth and arrest, as observed in DCB test experiments.

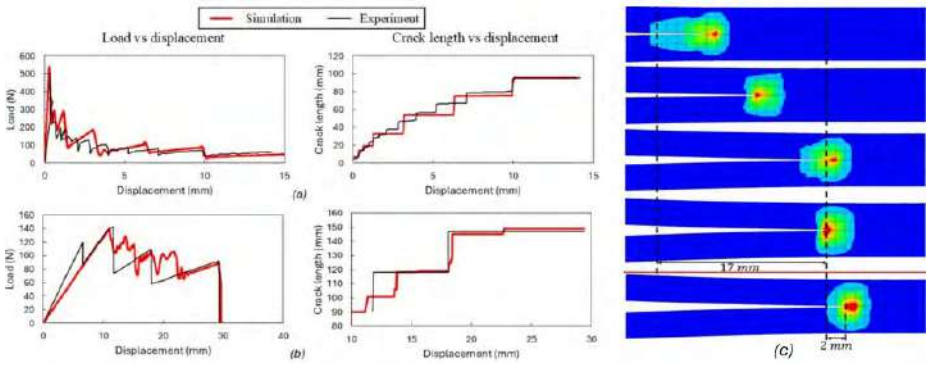

Figure 2 Model validation with experimental data (a&b), and FE model for propagation (c).

With model validation complete, a detailed analysis of the cracking process at the crack front of the DCBs can be performed using Figure 2c. In the current crack cycle, the crack length increases by 17 mm, accompanied by a 0.3 mm increase in crack opening displacement. Subsequently, energy is stored over the next 3 mm of loading displacement, with the crack length remaining constant until the next crack initiation. When the new crack begins, another 2 mm zone is added, representing energy accumulation. Considering DCB tests with a constant displacement loading rate, crack initiation and growth occur in less than 10% of the time needed for energy accumulation (assuming a steady loading speed). This behavior results from stick-slip fracture, where the crack rapidly advances and then arrests. A more detailed analysis [4] can be achieved using the proposed cohesive model for stick-slip fracture behavior.

References

[1] A. Chudnovsky, Slow crack growth, its modeling and crack-layer approach: a review, *Int. J. Eng. Sci.*, 83 (2014), pp. 6-41.

[2] Y. Zhou, Y. Xiao, Q. Wu, Y. Xue, A multi-state progressive cohesive law for the prediction of unstable propagation and arrest of Mode-I delamination cracks in composite laminates, *Eng. Fract. Mech.*, 248 (2021), Article 107684.

[3] X. Li, F. Monticeli, J.-A. Pascoe, Y. Mosleh, Interlaminar fracture behaviour of emerging laminated-pultruded CFRP plates for wind turbine blades, *Eng. Fract. Mech.*, 308 (2024), Article 110353.

[4] D. Ma, A cohesive model for stick–slip behavior in mode-I fracture during double cantilever beam tests: A dynamic process with static loading, *International Journal of Solids and Structures* 321 (2025): 113553.

High-Velocity Impact Behaviour of CFRP–PET Foam Sandwich Panels: Experimental Characterisation, Tomography and Numerical Modelling

Filipe Ribeiro[1*], Luís Correia[2], and Mário Rui Arruda[3]

[1] *Instituto de Soldadura e Qualidade (ISQ), R&D and Innovation, 2740-120 Porto Salvo, Portugal*

[2] *University of Minho, ISISE, ARISE, Department of Civil Engineering, Guimarães, Portugal*

[3] *Assistant Researcher, LNEC – National Laboratory of Civil Engineering, Department of Structures, Structural Behaviour Unit, Lisbon - Portugal. marruda@lnec.pt*

**fjribeiro@isq.pt*

Summary: High-velocity impacts pose a critical threat to lightweight composite structures used in aerospace applications. This work investigates the impact behaviour of CFRP sandwich panels with PET foam cores subjected to steel projectile impacts at velocities between 56 and 198 m/s using a pneumatic gas gun. Post-impact damage was characterised through computed tomography to evaluate internal failure mechanisms. Experimental results show complete perforation across all velocities, with increasing delamination and core crushing as velocity rises. Finite element simulations in Abaqus/Explicit were developed to reproduce the impact response. The numerical model captured the general damage trends, although limitations were observed due to uncertainties in foam properties and numerical instabilities.

1. Introduction

Composite sandwich structures are widely used in aerospace structures due to their high stiffness-to-weight ratio and structural efficiency. However, their vulnerability to high-velocity impacts remains a critical concern, particularly for aircraft leading edges, UAV structures, and control surfaces exposed to foreign object impacts such as hail or debris. While high-velocity impact behaviour has been widely investigated for honeycomb sandwich structures and fibre–metal laminates, comparatively fewer studies have focused on CFRP sandwich panels with polymeric foam cores. Among these, PET foam cores are gaining interest due to their recyclability, low density, and cost-efficient manufacturing. The objective of this work is to investigate the impact response of CFRP–PET foam sandwich panels subjected to projectile impacts across a range of velocities representative of aerospace impact scenarios. The study combines:

- experimental impact testing using a pneumatic gas gun,
- computed tomography (CT) for post-impact damage evaluation,
- finite element modelling (Abaqus/Explicit) to simulate damage progression and energy absorption mechanisms.

2. Experimental Methodology

2.1. Materials and Sandwich Configuration

The investigation structure consists of CFRP skins bonded to a PET foam core. The skins were manufactured using plain weave and ±45° carbon fibre fabrics, while the core material is a recyclable PET foam. Table 1 summarises the main properties of the constituent materials. The layup sequence of the sandwich panel is: Plain weave CFRP / ±45° CFRP / PET foam core / ±45° CFRP / Plain weave CFRP. The panels were manufactured by vacuum infusion and cut into square specimens. The panels were manufactured by vacuum infusion and cut into square specimens with average size dimensions of 308 mm and a total thickness of 6.02 mm. These dimensions ensured sufficient panel area to avoid edge effects during the impact tests while allowing rigid clamping in the experimental fixture.

Table 1. Nominal material properties of sandwich constituents

Material	Density (g/cm³)	Tensile Strength (MPa)	Tens. Modulus (GPa)	Flexural Str. (MPa)	Flex. Mod. (GPa)	In-plane Shear Str. (MPa)	Shear Mod. (GPa)	Orie-nt-ation	Areal Wt. (g/m²)
Plain CFRP	~1.77	~480	~42	~486	~766	~74	~4.8	0/90°	195
+-45 CFRP	~1.77	~156	~7	~164	~154	62	~7.5	±45°	100
PET foam	0.06	1.5	0.085	-	-	0.55	0.015	–	–

2.2. High-Velocity Impact Testing

Impact experiments were conducted using a single-stage pneumatic gas gun equipped with a 4 m launch barrel. Hardened AISI 4340 steel spherical projectiles (19.05 mm diameter) were used as impactors. Impact tests were conducted at four nominal velocity levels of approximately 56 m/s, 80 m/s, 136 m/s, and 198 m/s. Projectile velocity was measured using infrared photogates Post-impact damage was analysed using computed tomography (CT) to evaluate internal damage mechanisms including delamination in CFRP skins, fibre fracture and matrix cracking, and PET foam crushing and perforation (Fig. 1). CT analysis enabled quantification of delamination area as a function of impact velocity, providing insight into damage propagation within the sandwich structure.

3. Numerical Modelling

Finite element simulations were performed using Abaqus/Explicit to reproduce the impact behaviour observed experimentally (Fig 1). The model includes: CFRP skins represented using composite shell elements; PET foam core modelled with 3D solid elements using a crushable foam model, a deformable steel projectile. The composite plies were defined using a Hashin damage model to simulate fibre and matrix failure. A refined mesh was implemented in the impact region to capture local damage evolution. The shell elements are deleted once a given damage threshold is surpassed.

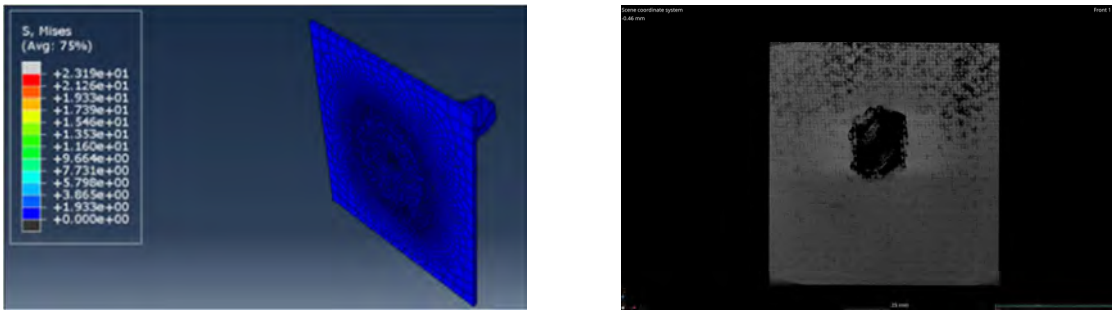

a) b)

Fig. 1. a) Impact simulation discrete rigid 19mm projectile on PET foam core at 60 m/s; b) Tomographic scans of a post-impact panel subjected to 136.3 m/s

4. Results and Discussion

Experimental observations showed that the investigated sandwich configuration exhibited complete perforation at all tested velocities. CT analysis revealed that the delamination area decreases with increasing impact velocity. The largest delaminated area was observed at the lowest velocity (≈56 m/s), while the highest velocity (≈198 m/s) produced a more localized damage zone. This behaviour suggests that at higher velocities the projectile perforates the panel rapidly, limiting the time available for damage to propagate laterally. The numerical simulations reproduced the general impact response and stress distribution, although numerical instabilities were observed at the highest velocity. These limitations are attributed mainly to the scarcity of reliable dynamic material data for PET foams.

5. Conclusions

This work investigated the high-velocity impact behaviour of CFRP–PET foam sandwich panels through a combined experimental and numerical approach. The main conclusions can be summarised as follows:

- The tested CFRP–PET sandwich configuration exhibited limited impact resistance, with complete perforation occurring at all investigated velocities between approximately 56 m/s and 198 m/s.
- Damage morphology varied with impact velocity, with larger delamination areas observed at lower velocities and more localized penetration damage at higher velocities.
- Finite element simulations in Abaqus/Explicit reproduced the general impact response and stress wave propagation, although numerical instabilities were observed at the highest velocity.

Numerical Modelling of the Additively Manufactured Continuous Fibre Reinforced Composites

Fran Ušurić[1], Ivica Smojver[1, *] and Darko Ivančević[1]

[1] *University of Zagreb, Faculty of Mechanical Engineering and Naval Architecture, Department of Aeronautical Engineering, Zagreb, Croatia*

[*] *ivica.smojver@fsb.unizg.hr*

Summary: Additively manufactured continuous fibre reinforced composites enable lightweight structures with tailored mechanical properties but exhibit microstructural defects that influence their mechanical response. This study combines experimental testing and numerical modelling to investigate their behaviour under quasi-static and dynamic loading. Tensile, flexural, and drop-tower impact tests were performed on printed composite specimens. Microstructural features, including porosity, were characterized using X-ray computed tomography and incorporated into representative volume elements for homogenisation-based numerical modelling. The homogenised material properties were implemented in finite element simulations. Good agreement between simulations and experiments demonstrates that the proposed homogenisation framework can effectively predict the mechanical response of additively manufactured continuous fibre composites.

1. Main Text

Additive manufacturing (AM) of continuous fibre reinforced polymer composites enables the production of lightweight structures with tailored mechanical properties and complex geometries. The ability to place continuous fibres along prescribed load paths offers significant potential for aerospace applications. However, the layer-wise deposition process introduces microstructural heterogeneity, including voids, imperfect fibre–matrix bonding, and interlayer defects, which significantly influence the mechanical response and complicate predictive numerical modelling.

This work presents a combined experimental and numerical investigation of additively manufactured continuous fibre reinforced composites with the objective of predicting their mechanical behaviour under quasi-static and dynamic loading conditions. Composite specimens reinforced with continuous fibres were fabricated using a continuous fibre additive manufacturing system based on the co-extrusion of fibre bundles and a polyamide thermoplastic matrix. Mechanical characterisation included quasi-static tensile and three-point bending tests as well as dynamic impact testing. The tensile tests on unidirectional specimens aligned with the fibre direction showed a predominantly linear elastic response up to failure, with an average Young's modulus of approximately 37.8 GPa and an ultimate tensile strength of about 236 MPa. Flexural testing revealed an average flexural modulus of approximately 26.4 GPa and a flexural strength of about 184 MPa, with progressive damage behaviour observed during loading.

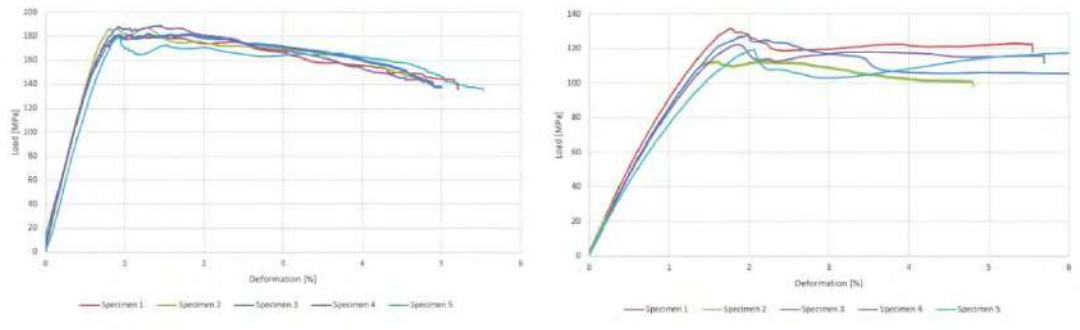

Figure 1 Results for the three point bending tests for carbon (left) and basalt (right) fibre specimens.

Dynamic behaviour was investigated using instrumented drop-tower impact tests under different impact velocities. The experiments demonstrated a stable response characterised by rapid force increase followed by gradual load reduction associated with progressive damage mechanisms such as fibre cracking and interlayer debonding. The experimental force–time histories and absorbed energy values provided a basis for validating the numerical simulations of the dynamic response.

To capture the influence of additive manufacturing-induced microstructural features, X-ray computed tomography (CT) was used to characterise the internal architecture of the printed composites, including fibre distribution and void morphology. Quantitative analysis revealed a measurable void content within the printed

material, with average porosity levels of approximately 15% and local porosity within fibre bundles due to incomplete impregnation. These microstructural observations highlight the importance of incorporating process-induced defects into predictive numerical models.

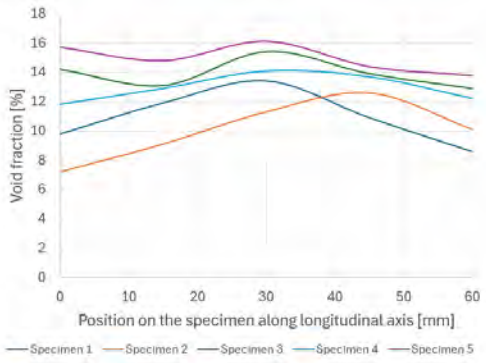

Figure 2 Void fraction for specimens manufactured using different printing parameters at different positions.

A numerical modelling framework based on micromechanical homogenisation was developed to predict the effective material properties of the additively manufactured composites. Representative volume elements (RVEs) derived from CT data were used to capture fibre architecture, matrix regions, and void distribution. Two homogenisation approaches were employed: finite-element-based numerical homogenisation and the high-fidelity generalized method of cells. The homogenised anisotropic material properties obtained from the RVE analysis were implemented in explicit finite element simulations to model structural response under quasi-static and dynamic loading conditions.

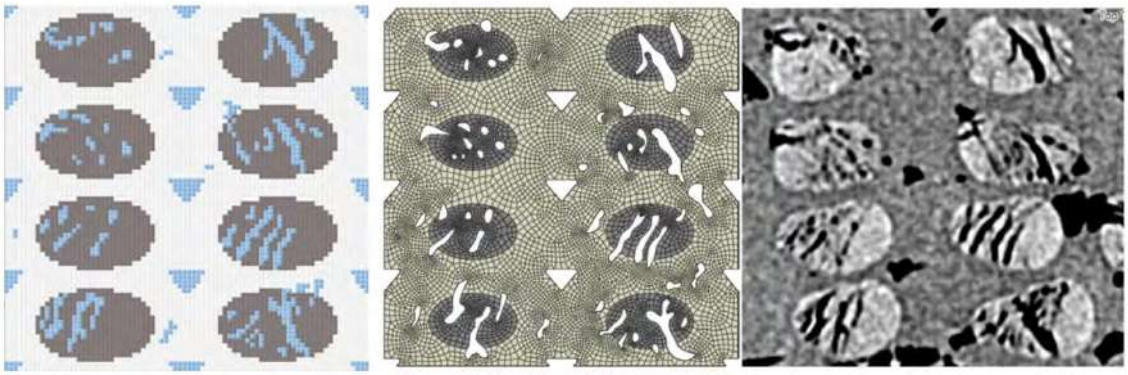

Figure 3 RVE geometry used for HFGMC (left) and FEM (middle) homogenization. Reference microstructure used for RVE modelling (right) representing 15% void content.

Comparison between experimental results and numerical predictions demonstrates that the homogenisation-based modelling approach is capable of reproducing the measured mechanical behaviour of additively manufactured continuous fibre composites with satisfactory accuracy. The developed framework provides an efficient multiscale methodology for linking microstructural characteristics with structural-level performance and offers a useful tool for the design and optimisation of additively manufactured composite structures.

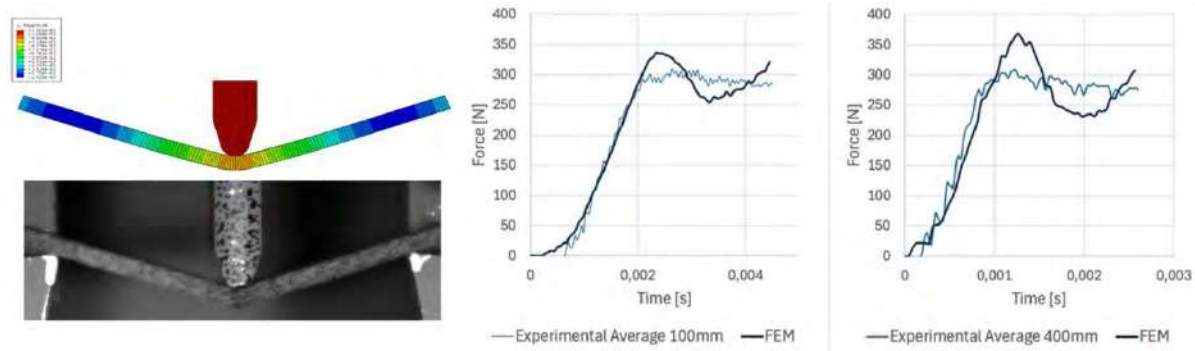

Figure 4 Comparison of numerical results and experiment for the drop height of 100 mm for carbon fibre specimen (left) and comparison of numerical and experimental results for reaction force for 100 mm (middle) and 400 mm (right) height.

Advanced 3D Modeling of Functionally Graded Sandwich Plates under High Strain Rate Loading

Sebahat Şimşek[1], Magd Abdel Wahab[2], and Volkan Kahya[1, *]

[1] *Karadeniz Technical University, Faculty of Engineering, Department of Civil Engineering, Trabzon, Türkiye*

[2] *Soete Laboratory, Department of Electrical Energy, Metals, Mechanical Constructions, and Systems, Faculty of Engineering and Architecture, Ghent University, Belgium*

[*] volkan@ktu.edu.tr

Summary: Composite structures subjected to high-strain-rate loading require reliable predictive models to support certification-by-analysis approaches. This study develops a three-dimensional elasticity-based numerical framework for the dynamic analysis of functionally graded sandwich plates. The governing equations are discretized using the Differential Quadrature Method, enabling accurate high-order spatial approximation while retaining the full three-dimensional stress representation. The ongoing study focuses on implementing the numerical model and performing parametric investigations of material gradation and core configurations.

1. Introduction

Composite materials are increasingly used in aerospace, automotive, and civil engineering structures due to their high strength-to-weight ratio and superior energy absorption capacity [1]. In many practical applications, these structures may be subjected to impact or high-strain-rate loading conditions, which can significantly influence their dynamic behavior and damage mechanisms. Accurate modelling of such responses is therefore essential for reliable structural assessment and for developing certification-by-analysis approaches for advanced composite structures.

Functionally graded (FG) sandwich configurations represent a promising class of composite structures in which material properties vary continuously across the thickness to enhance stiffness, stability, and damage tolerance. These structures have attracted significant attention in applications requiring improved resistance to dynamic loading. However, many existing analyses rely on classical or higher-order plate theories that introduce simplifying assumptions on the displacement field and may not accurately capture the three-dimensional stress state, particularly for thick or heterogeneous sandwich configurations [2–4].

To address these limitations, the present work develops a three-dimensional (3D) elasticity-based formulation for the dynamic analysis of FG sandwich plates subjected to high-rate loading. The governing equations are discretized using the Differential Quadrature Method (DQM), enabling efficient high-order spatial approximation and improved predictive modelling capability for advanced composite structures.

2. Methodology

The considered sandwich configuration consists of two face sheets and a core layer whose effective material properties vary continuously through the thickness according to a predefined grading function (see Fig. 1). The elastic constants can be expressed as

$$C_{ij}(z) = C_{ij}^{(m)} + (C_{ij}^{(c)} - C_{ij}^{(m)})f(z)$$

where $C_{ij}^{(m)}$ and $C_{ij}^{(c)}$ denote the material properties of the constituent phases, and $f(z)$ represents the material gradation function along the thickness coordinate.

The governing equations are obtained from the 3D equations of motion

$$\sigma_{ij,j} = \rho \ddot{u}_i$$

where σ_{ij} are the stress components, u_i are the displacement components, and ρ is the mass density. The strain–displacement relations follow the classical small-strain formulation

$$\varepsilon_{ij} = \frac{1}{2}(u_{i,j} + u_{j,i})$$

To obtain a numerical solution, the DQM is employed to discretize spatial derivatives. In this approach, the derivative of a function at a grid point is approximated as a weighted linear sum of function values at all grid points,

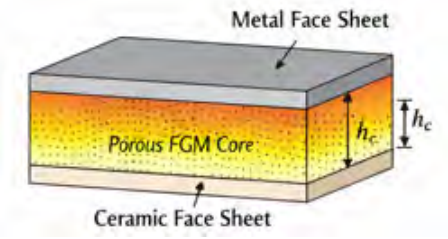

Fig. 1. FGM sandwich plate structure.

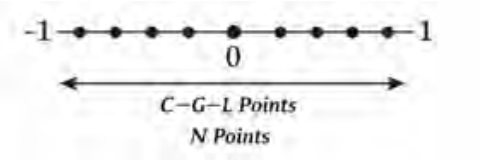

Fig. 2. Chebyshev-Gauss-Lobatto points.

$$\frac{\partial^n w(x)}{\partial x^n}\Big|_{x_i} = \sum_{j=1}^{N} a_{ij}^{(n)}\, w(x_j)$$

where $a_{ij}^{(n)}$ are the weighting coefficients associated with the n-th derivative. Chebyshev–Gauss–Lobatto points are adopted for spatial discretization to enhance numerical stability and accuracy.

3. Numerical Framework

The proposed formulation provides a numerical framework for investigating the dynamic response of FG sandwich plates subjected to high-rate loading conditions. The computational domain is discretized along the in-plane and thickness directions using Chebyshev–Gauss–Lobatto grid points (see Fig. 2), which improve numerical stability and convergence in DQ implementations.

Within this framework, the displacement components are evaluated at discrete grid points and assembled into a global algebraic system incorporating the effects of material gradation, geometric parameters, and inertia. The developed model enables efficient evaluation of the structural response while maintaining full 3D stress representation.

Ongoing work focuses on investigating the influence of parameters such as material gradation profiles, core-to-face sheet thickness ratios, and geometric aspect ratios. These parametric studies will help assess the dynamic characteristics of FG sandwich structures and their suitability for applications involving high-rate loading.

4. Conclusions

This study presents a 3D numerical framework for analyzing FG sandwich plates subjected to high-rate loading conditions. The formulation is based on elasticity theory and discretized using the DQM. The ongoing implementation will enable systematic parametric investigations of material gradation and geometric characteristics. The developed framework aims to improve predictive modelling and support certification-by-analysis approaches for advanced composite structures.

References

[1] Reddy, J. N., 2004, *Mechanics of Laminated Composite Plates and Shells*, CRC Press, Boca Raton.
[2] Mohamed, I., Kahya, V., and Şimşek, S., 2024, “Finite element static analysis of functionally graded sandwich beams with porous core resting on a two-parameter elastic foundation based on quasi-3D theory,” *Proc. IMechE Part C: Journal of Mechanical Engineering Science*.
[3] Mohamed, I., Kahya, V., Şimşek, S., and Lanc, D., 2024, “Computational modeling of functionally graded sandwich beams with porous core using an ANSYS APDL-based approach,” *Mechanics Based Design of Structures and Machines*.
[4] Mohamed, I., Kahya, V., and Şimşek, S., 2024, “Ritz-type quasi-3D solution for free vibration and buckling of functionally graded sandwich beams with porous core resting on a two-parameter elastic foundation,” *Arabian Journal for Science and Engineering*.

Quo vadis Certification by Analysis?
A discussion of possible routes in the automotive industry

André Haufe[1*]

[1] *ANSYS Germany GmbH, Industriestrasse 2, D-70565 Stuttgart, Germany*

[*] *andre.haufe@synopsys.com*

Summary

In recent years, the predictive capabilities of finite element models in crash and impact simulation have undoubtedly reached new heights. There is no question that rigorous model setup, by employing sub-modeling techniques supported by stringent verification and validation steps based on the modular building-block principle, is the key factor for unprecedented reliability, robustness and predictiveness. Moreover, the credibility such models can add to technical statements and design decisions is invaluable and enables engineers to replace a good percentage of hardware testing.

This will add value to the product development chain that will, of course, be used to reduce costs in downstream development steps: certification of products for specific technical applications, legal approval of products for specific target markets, or virtual testing to ensure conformity with hardware test scenarios and even continuously reducing the hardware testing regime in consumer goods testing. Furthermore, it should be noted that at present different industries are making separate efforts to achieve these goals. Therefore, a certain degree of harmonization of regulations will be desirable in the future.

This presentation illuminates the nomenclature of CAE models used in certification, approval, and virtual testing. The need for harmonized qualification requirements for virtual testing is discussed. The necessity of virtual measuring instruments, such as virtual ATDs or even human body models, is explained. Against this backdrop, subsystems intended for the evaluation of parts or components in the development process like impactors, barriers, test sleds and such, must also be evaluated and qualified for this task. This leads to higher requirements and increased effort on the modelling side before such measuring instruments can finally be used in certification processes. And finally, the traceability of models becomes the last and probably most important element to ensure that the models submitted to regulatory authorities actually delivered the requested results and that the integrity of such models was not infringed. This puts additional pressure on software companies to implement traceable model setup and result generation.

HISTRATE

Advanced Composites under High Strain Rate Loading A Route to Certification-by-Analysis

2026 Conference

10th – 11th JUNE 2026

Session 3 - Multi-modal sensing for impact detection and damage characterisation (WG5)

cost EUROPEAN COOPERATION IN SCIENCE & TECHNOLOGY

Funded by the European Union

Ultrasound Array Signal Reconstruction for Porosity and Defect Characterization in Complex Composite Structures Subjected To High Strain

Krzysztof Dragan[2,*] Marcin Lewandowski[1] and Piotr Karwat[1]

[1]US4US Sp.z.o,,, 111A Puławska Str. / apt. U2, 02-707 Warsaw, Poland
[2]ITWL,ul. Ks. Boleslawa 6, 01-494 Warsaw, Poland
[*]*Corresponding author, E-Mail: krzysztof.dragan@itwl.pl*

Summary: The advancement of Non-Destructive Evaluation (NDE) systems necessitates programmable, high-performance ultrasonic solutions capable of real-time data processing and seamless integration with Artificial Intelligence and Machine Learning (AI/ML) methods[1]. Composite materials, widely utilized in aerospace present unique inspection challenges due to their complex geometries including volumetric failure modes, particularly porosity and delamination [2]. Traditional ultrasonic or Phased Array Ultrasonic Testing (PAUT) struggles with the limitations of processing capabilities required for detailed tomographic imaging [3]. This paper introduces a novel, programmable ultrasonic scanner featuring embedded high-performance GPU processing and advanced ultrasonic understanding. Paper demonstrate the platform's utility in developing advanced real-time tomographic reconstruction algorithms specifically tailored for diagnosing manufacturing defects, such as porosity, within composite elements of complex geometry.

1. PROBLEM INTRODUCTION

1.1. Data acquisition

The implementation of Full Matrix Capture (FMC) data acquisition, combined with the Total Focusing Method (TFM) image reconstruction, represents a powerful step toward high-resolution composite inspection [4]. FMC/TFM provides superior defect mapping and allows for extensive post-processing analysis using the recorded raw RF data. Studies confirm the effectiveness of TFM in quantifying damage, such as low-velocity impact (LVI) damage in thin CFRP plates, with relative errors in defect length characterization reported below 10% [5,6]. The ability to perform 3D reconstruction and data fusion further enhances detailed defect characterization. However, for the complex geometries and anisotropic materials, the simple TFM model must be extended. The proposed solution encompasses traditional limitations connected with relatively low speed of data processing as well as constraints connected with closed architecture.

1.2. Proposed solution

The inspection of composite structures presents several critical challenges that necessitate advanced tomographic approaches for data visualization [7]. Manufacturing defects like porosity and internal voids occur due to the improper manufacturing cycle which imposes a diagnostic challenge because its presence causes high attenuation and significant scattering of acoustic waves. This leads to an acoustic shadowing effect, resulting in the loss of information about defects situated deeper within the material, potentially causing imaging artifacts [8]. Effective ultrasonic tomography is required to accurately localize and characterize these volumetric defects, especially in complex geometries (as corners and thickness gradients) [2]. Consequently, robust tomographic solutions must incorporate complex geometry constraints to determine the propagation path and accurately perform signal reconstruction. Additional challenge relates to necessity of inspection automatization and data visualization and analysis [4]. The massive data throughput of FMC acquisition, while enhancing image quality, presents the challenge of data overload. Therefore, the solution must embed real-time processing and automated evaluation capabilities directly into the scanner to streamline flaw detection and sizing. The us4NDT platform solves the processing bottleneck by integrating embedded high-performance GPU processing using the NVIDIA Jetson AGX Origin [4]. This high-end edge-computing capability supports the implementation of highly demanding, parallel processing algorithms, making real-time Software-Defined Beamforming and TFM processing feasible. The most crucial element for automated defect characterization is the integration of AI/ML frameworks. The

us4NDT's architecture supports open-source AI/ML frameworks/libraries. Semantic segmentation allows for labeling each pixel in the image to provide an in-depth understanding, enabling automatic detection, localization, and sizing of defects (e.g., porosity, delamination) [9]. The platform has successfully demonstrated real-time automated detection and sizing of simulated defects, classifying them as "acceptable" or "unacceptable" based on size criteria. This automation is essential for transitioning from manual data interpretation to autonomous, reliable NDE system.

2. References

[1]. M. Lewandowski, P. Karwat, et.al. “Challenging the multimodal ultrasound with GPU-based research ultrasound platforms”, August 2023, Research and Review Journal of Nondestructive Testing, 10.58286/28163;

[2]. Wronkowicz A., Dragan K., Dziendzikowski M., Chalimoniuk M. and Sbarufatti C. (2016): 3D Reconstruction of Ultrasonic B-Scans for Nondestructive Testing of Bibliography 129 Composites. In: Proc. of the International Conference on Computer Vision and Graphics, L. J. Chmielewski;

[3]. Lewandowski, Marcin & Walczak, Mateusz & Witek, Beata & Rozbicki, Jakub & Steifer, Tomasz. (2018). A GPU-Based Portable Phased-Array System with Full-Matrix Capture. 1-3. 10.1109/ULTSYM.2018.8579964.

[4]. Lewandowski, Marcin & Karwat, Piotr & Jarosik, Piotr & Rozbicki, Jakub & Walczak, Mateusz & Smach, Hanna. (2023). A High-Speed Ultrasound Full-Matrix Capture Acquisition System for Robotic Weld Inspection. Research and Review Journal of Nondestructive Testing. 1. 10.58286/28163.

[5]. Caminero MA, García-Moreno I, Rodríguez GP, Chac´on JM. Internal damage evaluation of composite structures using phased array ultrasonic technique: impact damage assessment in CFRP and 3D printed reinforced composites. Compos B Eng 2019;165:131–42.

[6]. Wronkowicz A., Mihaylov G., Dragan K. and Timofiejczuk A. (2019): Uncertainty estimation for ultrasonic inspection of composite aerial structures. Journal of Nondestructive Evaluation (2019) 38:82 https://doi.org/10.1007/s10921-019-0622-5

[7]. Bai, Z.; Chen, S.; Xiao, Q.; Jia, L.; Zhao, Y.; Zeng, Z. Compressive sensing of phased array ultrasonic signal in defect detection: Simulation study and experimental verification. Struct. Health Monit. 2017, 17, 434–449.

[8]. Felice MV, Fan Z. Sizing of flaws using ultrasonic bulk wave testing: a review. Ultrasonics 2018;88:26–42. https://doi.org/10.1016/j.ultras.2018.03.003.

[9]. Sen Zhang, Yansong Zhang, Automated weld defect segmentation from phased array ultrasonic data based on U-net architecture, NDT & E International, Vol.146, 2024, https://doi.org/10.1016/j.ndteint.2024.103165.

Impact detection in composite structures in aircraft and space systems

Michele Meo,[1]

[1] *Department of Aero and Astro, University of Southampton, UK*

[*] *m.meo@soton.ac.uk*

Summary: Reliable impact detection is essential for composite structures used in aircraft components and spacecraft exposed to debris strikes. This work presents a review of our work on acoustic-emission-based methods for impact localisation and force reconstruction in aeronautical composite panels and for impact localisation, trajectory estimation, and velocity measurement in a smart carbon-fibre-reinforced polymer orbital-debris detector. The methods combine time-reversal processing, hierarchical radial-basis-function interpolation, and arrival-time analysis using sparse piezoelectric sensor networks. Experiments showed accurate impact identification, supporting structural-health-monitoring and in-situ debris-sensing applications.

1. Introduction

Composite structures are widely used in aerospace because they combine low weight with high stiffness and strength, but they remain vulnerable to impact events that can generate internal damage and barely visible damage states. In aircraft structures, low-velocity impacts from tools, runway debris, or hail can degrade performance and complicate maintenance decisions, which motivates structural health monitoring methods capable of identifying both impact location and force history. In spacecraft, small debris particles are not always trackable by existing monitoring systems, yet they can still damage orbiting platforms, so in-situ impact sensing is attractive for improving spacecraft awareness and survivability. This paper unifies three related developments into a common impact-detection framework for aerospace composites. The first strand concerns impact source localisation in aerospace composite structures using acoustic-emission measurements and time-reversal processing. The second develops a hierarchical method for reconstructing impact force histories in composite components from experimentally measured transfer functions and sparse sensor data. The third extends the same acoustic-wave philosophy to a smart composite orbital-debris detector able to estimate impact position, trajectory direction, and particle velocity from two instrumented CFRP plates.

2. Methodology

The common basis of the proposed approach is the use of sparse piezoelectric sensor networks to record elastic waves generated by impact events in composite structures. For localisation, the method uses time reversal, where calibration impacts are first recorded over a predefined grid and the unknown event is then identified by cross-correlation with the stored responses. The impact position is finally estimated within the identified cell by a centre-of-gravity procedure based on correlation coefficients.

For force reconstruction in aeronautical composite structures, the localised impact point is combined with experimentally derived transfer functions rather than numerical models. A hierarchical radial-basis-function interpolation is then used to estimate the transfer function at the unknown impact point and reconstruct the impact force history, which reduces dependence on dense calibration data and on detailed mechanical-property knowledge. This feature is important for real structures where geometry is complex and operating conditions make full modelling difficult.

For orbital-debris sensing, the detector consists of two thin parallel CFRP plates, each instrumented with three embedded piezoelectric transducers. Time reversal is used to localise the impact on each plate, while the arrival times are estimated with an Akaike Information Criterion picker and combined with calibrated wave-speed information to determine debris direction and velocity. The embedded-sensor concept is especially attractive for space applications because the transducers are protected within the laminate rather than exposed on the surfaceMargins and type size will be as set by the abstract template.

3. Results and discussion

The impact-force-reconstruction method was validated experimentally on a composite plate-like specimen and on a wing stringer-skin panel representative of real aircraft structure. The studies used sparse receiving sensors and MATLAB-based processing to assess whether transfer-function interpolation could recover force histories with useful accuracy even when calibration information near the impact point was limited. The reported comparisons

showed that the hierarchical radial-basis-function method could exploit information from points farther from the impact location better than simpler interpolation approaches.

The orbital-debris detector was validated on two CFRP plates of about 200 mm by 200 mm and about 1.3 mm thickness, manufactured from T800/M21 prepreg with embedded PZT transducers. The plates were separated by 190 mm, and low-velocity impact tests were carried out with a roughly 2.7 kg sharp-tip impactor dropped from 1000 mm, producing a representative mean speed between the plates of about 4.2 m/s for the proof-of-concept tests. Although these were not hypervelocity tests, the papers justify the approach by noting that elastic modes from low-velocity impacts resemble the standard elastic waves that remain after hypervelocity shock-wave conversion.

For the force-reconstruction problem, the proposed hierarchical method was reported to reconstruct impact force histories with high accuracy on both a composite plate and a wing stringer-skin panel, while avoiding the need for numerical models of the monitored component. The paper also states that the method could extrapolate information from points far from the impact location, which is valuable when dense calibration is unavailable in full-scale aircraft structures. These results suggest that sparse experimental calibration can still support practical impact monitoring in aerostructures.

For the debris-detector problem, the time-reversal localisation method achieved sub-millimetre errors in the reported tests, with one perpendicular-impact case showing localisation errors of 0.13 mm and 0.14 mm on the two plates. In that same case, the average estimated particle speed was about 4.35 m/s, close to the test mean velocity of 4.2 m/s. In the skewed-impact cases, the direction parameters were also estimated accurately, with percent errors below 1 percent according to the reported results.

Taken together, the three papers show a consistent research direction: acoustic-emission-based impact sensing can be used not only to locate impacts in composite structures, but also to reconstruct their severity and, in dual-plate space systems, to infer the trajectory and velocity of impacting objects. This combined capability is relevant to aircraft structural health monitoring, where maintenance decisions depend on rapid damage assessment, and to spacecraft protection, where onboard sensing can complement external surveillance systems. The work therefore supports the development of lightweight, sensor-integrated composite structures with built-in impact-awareness functions.

4. Conclusions

The presented body of work demonstrates that sparse piezoelectric sensing, time-reversal localisation, radial-basis-function interpolation, and arrival-time analysis can be integrated into a practical impact-identification framework for composite aerospace structures. In aeronautical applications, the framework enables localisation and force-history reconstruction without relying on detailed numerical models. In space applications, it enables proof-of-concept localisation, direction estimation, and velocity measurement of debris impacts using a lightweight smart composite detector.

5. References

[1] De Simone, M. E., Andreades, C., Hilmi, A. M., Meo, M., and Ciampa, F., 2019, “Proof of concept for a smart composite orbital debris detector,” Acta Astronautica, 160, pp. 499–508.
[2] De Simone, M. E., Ciampa, F., and Meo, M., 2019, “A hierarchical method for the impact force reconstruction in composite structures,” Smart Materials and Structures, 28, 085022.
[3] De Simone, M. E., Andreades, C., Meo, M., and Ciampa, F., 2021, “Smart composite detector of orbital debris and micrometeoroids particles,” Materials Today: Proceedings, 34, pp. 202–209.Collaborative Writing in Industry: Investigations in Theory and Practice, 1991, Baywood Publishing Co., Amityville, NY.

Impact damage influence on the local wavenumber of guided ultrasonic waves in thermoplastic composites

Paweł H. Malinowski[1,*], Luigi Sorrentino[2]

[1] Institute of Fluid Flow Machinery, Polish Academy of Sciences, 14 Fiszera Street, 80-231 Gdańsk, Poland

[2] Istituto per i Polimeri, Compositi e Biomateriali, Consiglio Nazionale delle Ricerche, P.le E. Fermi 1, 80055, Portici (NA), Italy

[*] pmalinowski@imp.gda.pl

Summary: A set of thermoplastic composites fabricated from poly(lactic acid) matrix and woven basalt fibers was investigated. Within the set there were undamaged sample, samples with single and multiple damage and repaired samples. Wave propagation was studied by exciting the waves with surface-bonded piezoelectric sensor and sensing with scanning laser Doppler vibrometer (SLDV). The whole samples area was scanned in dense grid of points. In order to study the wave interaction with damage the grid of points was divided into smaller windows and wavenumber was calculated. The local changes of the wavenumber was used in order to detect and localize damage.

1. Introduction

The research towards developing effective nondestructive evaluation and structural health monitoring methods is ongoing in many research groups. One of the promising method is based on ultrasonic guided wave propagation. These wave propagate in thin-walled plate-like structures and are characterizes by multimodal nature. In the lower frequencies and for lower thickness fundamental symmetric and antisymmetric modes propagate, while for higher frequency ranges and thicker plates more modes appear [1]. In this work the non-contact SLDV-based sensing was employed to register the propagating waves. Due to measurements in many points it was possible to calculate the wavenumbers of the propagating waves [2]. This allows to filter the modes and track the changes caused by obstacles on wave propagation path such as damage. The local changes of the wavenumber [3] were used as damage indicator that allowed to distinguish the damaged samples from the referential one.

2. Measurements

The investigated samples were made of polylactic acid - PLA (Luminy L175, Total/Corbion NV, the Netherlands) used as matrix and plain weave fabric of basalt fibres (BAS 220.1270.P, Basaltex-Flocart NV, Belgium). The composites sample plate were prepared using the film stacking process. Laminates of 10 fabric layer 0/90 were symmetrically arranged $[(0/90)_5]s$ resulting in 1.8 mm thick plates with 45% volume content of fibres. The elastic waves were excited in the samples with surface bonded piezoelectric sensor disc (10-mm diameter and 0.5-mm thickness). It was bonded to the front face (Fig. 1a). The acquisition was made with an 3D SLDV (PSV-400, Polytec, Germany) using its single head. The signals were measured on the back face (Fig. 1b) at 3723 spaced by 2.2 mm in horizontal and vertical directions.

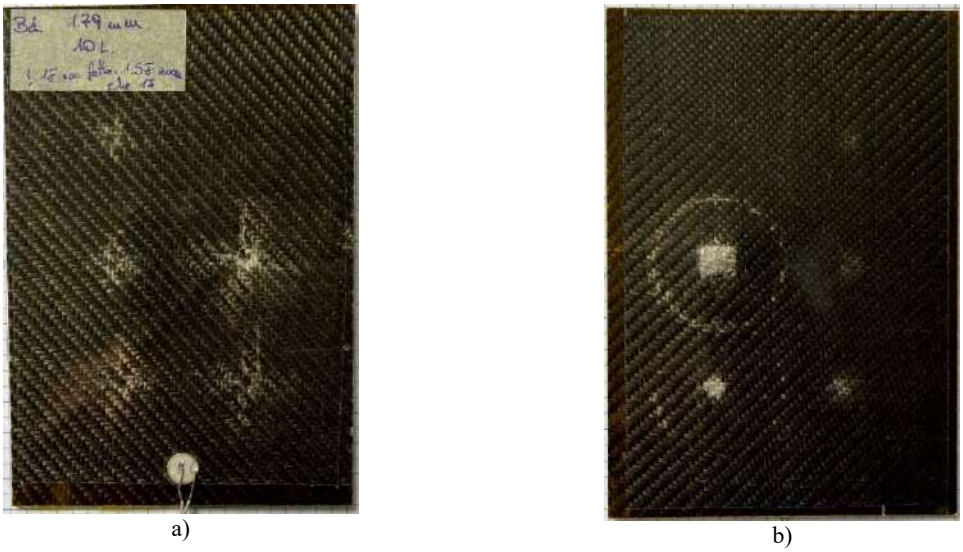

a) b)

Fig. 1. Photo of one of the impacted samples at 5 locations; a) front face, b) back face

3. Results

Out of the measured points a square window of side length 17.6 mm was selected. In this window a three dimensional fast Fourier transformation was calculated on the time signals. This resulted in transition from space-time domain [x,y,t] into wave vector-frequency domain [k_x,k_y,f]. At the selected frequency the dominant wavenumber was calculated and assigned to the coordinates of the window center. The window was then moved to cover all the points. The procedure result for the referential sample is shown in Fig. 2a (the color scale corresponds to the wavenumber value). The zero value at the edges is the result of the windowing procedure. So the approach would not work for damage localization near the edge of the sample. The depicted colors show what wavenumber values can be expected when there is not damage present. Next, the same data processing procedure was applied to a sample with 5 impacts made with 1.5J, 2J, 4J, 8J and 16J projectile energy. The result is depicted in Fig. 2b. The increase in wavenumber values indicate the damage locations. In this way the location of the four impact damage can be indicated. Only the impact made at 1.5J did not resulted in noticeable wavenumber change. Taking the referential sample result (Fig. 2a) as a thresholding value it can be deduced that the damage impacts made with the highest energy were localized because the k value exceeds 2.83 that is the maximal value extracted from Fig. 2a result. Explicitly, the damage made with 8J and 16J was indicated in this way.

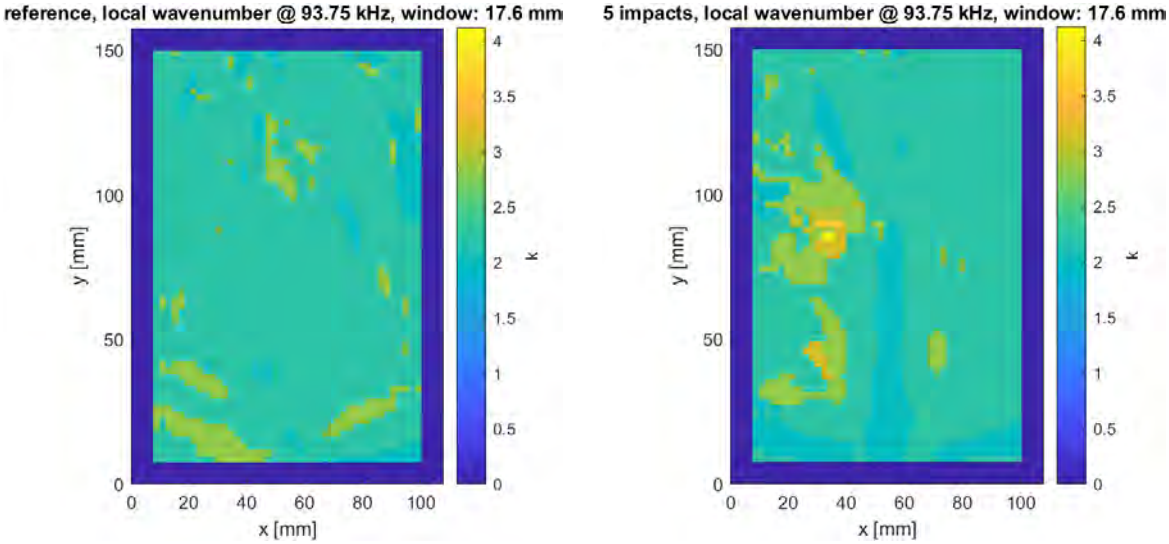

a) b)

Fig. 2. Local wavenumber visualization for a) referential sample, b) sample with 5 impacts made with 1.5J, 2J, 4J, 8J and 16J projectile energy.

4. Conclusions

The local wavenumber-based visualization allows for single damage localization (not shown in this short abstract) as well as multiple damage indication. The use of the referential data obtained for undamaged sample allows for setting an universal threshold for damage detection and localization in damaged samples.

5. Acknowledgments

This study has been carried out within the bilateral collaboration project “Non-destructive evaluations on repaired fibre reinforced composites (REPCOM)” – Biennium Program 2020-2021 between IPCB-CNR and IMP-PAN. The authors would like to thank Mr Fabio Docimo for his contribution to the preparation of all tested samples.

References

[1] Giurgiutiu, V., 2015, "Structural health monitoring of aerospace composites", Academic Press.
[2] Michaels, T. E., Michaels, J. E., & Ruzzene, M.,2011, “Frequency–wavenumber domain analysis of guided wavefields”. Ultrasonics, 51(4), pp. 452-466.
[3] Zhenhua, Tian et al., 2015, “Guided wave imaging for detection and evaluation of impact-induced delamination in composites”, Smart Materials and Structures 24, 105019.

MWCNT-Modified Cellulose Interleaved Multifunctional CARALL Composites for Real-Time Impact Detection and EMI Shielding

Tugay Üstün[1], Ebru Saraloğlu Güler[2], Volkan Eskizeybek[3*], Ferhat Yıldırım[4]

[1] *Kahramankazan Vocational School, Başkent University, Ankara, Türkiye*

[2] *Department of Mechanical Engineering, Başkent University, Ankara, Türkiye*

[3] *Department of Material Science and Engineering, Çanakkale Onsekiz Mart University, Çanakkale, Türkiye*

[4] *Biga Vocational School, Çanakkale Onsekiz Mart University, Çanakkale, Türkiye*

[*] *veskizeybek@comu.edu.tr*

Summary: Carbon reinforced aluminum laminates (CARALL) can experience low-velocity impacts (LVI) during service, creating barely visible damage that degrades both structural integrity and electromagnetic interference (EMI) shielding. This study proposes a bio-based, conductive interleaf for simultaneous structural health monitoring (SHM) and post-impact EMI shielding. Cellulose sensing papers were fabricated via conventional papermaking with two areal densities (160 and 210 g/m²) and three MWCNT loadings (5, 7, and 9 wt.%). These papers were inserted at the Al/CFRP interface in CARALL laminates manufactured by hand lay-up and vacuum bagging. LVI tests (ASTM D7136) were performed and resistance change (ΔR/R) was recorded in real time using an Arduino-based circuit. EMI shielding effectiveness (X-band, 8.2–12.4 GHz) was measured after impact. Among all designs, 210 g/m² + 9 wt.% MWCNT preserved sensing sensitivity beyond the first impact and maintained ~60 dB total shielding, while increasing the reflection component markedly compared with lower CNT contents. The results show that interleaf areal density and CNT content govern the balance between interfacial compliance (impact response) and conductive network resilience (SHM + EMI).

1. Introduction

Fiber-metal laminates (FMLs) are used in weight-critical structures due to favorable metal/FRP synergy, while CARALL is attractive for aerospace-grade stiffness/strength with improved damage tolerance. However, LVI events (hail, debris, tool drop) can trigger internal cracking/delamination with limited surface evidence, motivating embedded SHM solutions. CNT-based conductive networks enable resistance-based self-sensing and have been leveraged for damage detection in composites. In parallel, electrically conductive architectures are needed for EMI shielding, which is closely tied to conductivity and conductive pathway continuity [1].

Cellulose is a sustainable platform for functional papers; when combined with CNTs it can form flexible, conductive interleaves. Here, we integrate MWCNT-modified cellulose papers into CARALL as an interlaminar multifunctional layer and evaluate (i) impact response, (ii) real-time damage sensing, and (iii) post-impact EMI shielding [2].

2. Materials and Methods

2.1. Materials

Functionalized MWCNTs (purity >96%, diameter 48–78 nm, length 10–25 μm) were used as conductive fillers. Aluminum sheets and twill weave carbon/epoxy prepregs were employed with an epoxy system for hand lay-up impregnation.

2.2. Fabrication of MWCNT-Modified Cellulose Papers

MWCNTs were dispersed in deionized water and tip-sonicated (ice bath) to promote stable dispersion and minimize damage. Shredded cellulose was blended into the dispersion to form a slurry and then filtered and oven-dried to obtain conductive papers. Two areal densities (160 and 210 g/m²) corresponding to ~0.15 and ~0.25 mm thickness were produced. SEM verification confirmed preserved fiber morphology and CNT presence on fiber surfaces, with more continuous networks at higher CNT loadings.

2.3. CARALL Manufacturing and Specimen Set

Al surfaces were prepared following standard adhesive-bonding surface treatment practices to enhance interfacial adhesion. Conductive papers were placed between Al and CFRP plies, edge electrodes were connected using conductive paste to preserve laminate integrity. A vacuum bagging step reduced voids and excess resin, and laminates were cured under vacuum. Six reinforced variants plus a neat control were produced.

2.4. LVI Testing and SHM Acquisition

LVI tests were conducted per ASTM D7136 with a hemispherical impactor tip; 75 J was selected for detailed comparison based on preliminary damage observations. ΔR/R was recorded during impact using a microcontroller and current sensor, enabling real-time resistance tracking (Figure 1).

Figure 1. Schematic illustration of the damage monitoring configuration for CARALL composites

2.5. EMI Shielding Measurements

EMI shielding was measured in the X-band using a vector network analyzer (two-port calibration). SETot, SER, and SEA were determined from S-parameters; multiple internal reflections were neglected when SETot exceeded ~10 dB.

3. Results and Discussion

The electrical response of the embedded MWCNT-modified cellulose paper sensors under low-velocity impact is strongly correlated with the damage mechanisms activated within the CARALL composite. Upon impact, the abrupt increase in electrical resistance observed in Figures 2a and 2b coincides with the initiation of back-surface fiber breakage and interfacial damage, which induces in-plane tensile stresses within the cellulose paper interlayer. These stresses promote separation within the percolated MWCNT network, leading to a sudden reduction in CNT–CNT contact points and, consequently, an increase in resistance. Although partial recovery of the ΔR/R signal is observed during unloading, the permanent offset in resistance indicates irreversible microstructural rearrangement of the conductive network, consistent with damage-induced disruption of electrical pathways. Notably, the sustained sensitivity observed in the 9K8 specimen during subsequent impacts highlights the critical role of cellulose paper areal density and MWCNT content in preserving network connectivity. The higher filler loading and thicker paper layer provide a degree of redundancy in conductive pathways, enabling continued strain sensitivity even after the initial impact event [3]. These findings demonstrate that the SHM performance of CARALL composites is governed not only by the magnitude of mechanical damage but also by the resilience of the embedded conductive network, underscoring the importance of interlayer design for reliable post-impact sensing.

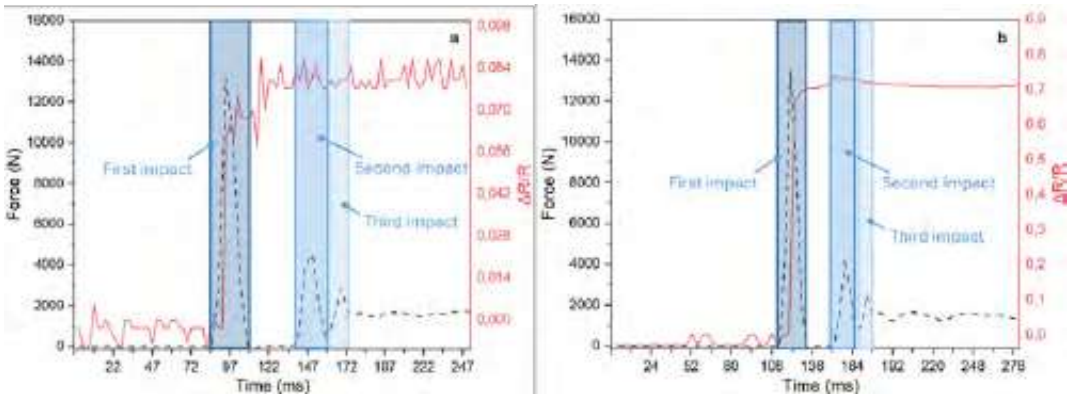

Figure 2. Force–time and normalized resistance change (ΔR/R)–time responses of (a) 9K6 and (b) 9K8-CARALL composite specimens subjected to LVI

References

[1] T. Üstün, E. S. Güler, and V. Eskizeybek, "Enhanced cellulose paper interfaces with MWCNT/Graphene for improved structural health monitoring and mechanical performance in CARALL," Engineering Fracture Mechanics, p. 111857, 2026.
[2] Y. Chen, J. Yang, X. Qiu, C. Ji, and B. Wang, "DIC-based constant amplitude and two-block loading fatigue life prediction of open hole GLARE laminate," *Engineering Fracture Mechanics,* vol. 278, p. 109016, 2023.
[3] S. Han, P. Wang, Y. Zhou, Q. Meng, M. Aakyiir, and J. Ma, "Flexible, mechanically robust, multifunctional and sustainable cellulose/graphene nanocomposite films for wearable human-motion monitoring," Composites Science and Technology, vol. 230, p. 109451, 2022.

Local wavenumber imaging of thin-walled structures for damage detection

Jakub Spytek,[1] Łukasz Pieczonka[1,*]

[1] AGH University of Krakow, Krakow, Poland

[*] *lukasz.pieczonka@agh.edu.pl*

Full-field imaging of Lamb waves is an emerging nondestructive testing technique that allows for detection and localization of damages. This technique can be effectively applied to the inspection of both homogeneous and multilayered thin-walled components to detect defects such as corrosion and delaminations. The quality of imaging often depends on the selection of a proper signal processing algorithm, which makes detection and evaluation of defects feasible. One of the most effective algorithms of full-field imaging data is known as local wavenumber estimation (LWE) [1] which enables damage detection based on local wavenumbers of Lamb waves propagating in thin-walled components. Due to the dependence of Lamb waves on plate thickness, the wavenumbers vary in locations where damages are present, corresponding to effective thickness reduction. Therefore, the LWE can be used to clearly visualize defects such as corrosion or delaminations in different types of structures. Despite its effectiveness, the original algorithm proposed by Flynn et al. [1] had some limitations that hindered its practical applicability. Firstly, the LWE is based on a complex filtration procedure in the frequency-wavenumber domain, which results in relatively high computational cost and high memory requirements. Secondly, the inspection of structures with complex shapes or significant anisotropy, such as carbon-fiber reinforced polymer (CFRP) composites, may be challenging due to high attenuation and direction-dependent wave velocity. The latter challenge significantly influences the wavenumber maps, resulting in non-uniform values of local wavenumbers, which are difficult to interpret and may mask the presence of damage in the structure.

Therefore, in this work, we would like to discuss several improvements to the LWE algorithm that are meant to overcome some of its shortcomings and increase its applicability as a nondestructive testing method. Firstly, we proposed a method to apply LWE imaging to structures with complex non-planar shapes using nonuniform Fourier transform [2]. Secondly, we devised a more efficient implementation of the signal processing techniques required for the use of LWE, which significantly decreased its computational cost and memory requirements [3]. Thirdly, we devised an improved version of the LWE algorithm in the form of Anisotropic LWE (ALWE) [4]. The proposed algorithm introduced an improved filtering scheme in the wavenumber domain to adapt the wavenumber estimation procedure to the anisotropy of the structure. These modifications significantly improved the quality of wavenumber maps for damage detection. An exemplary result of ALWE compared to LWE for an anisotropic composite sample is presented in Figure 1. Both results were obtained from full-field Lamb wave simulations of an anisotropic plate with artificial defects. ALWE compensates for direction-dependent wavenumber and produces a more uniform background, significantly improving the visibility of defects (regions with increased wavenu

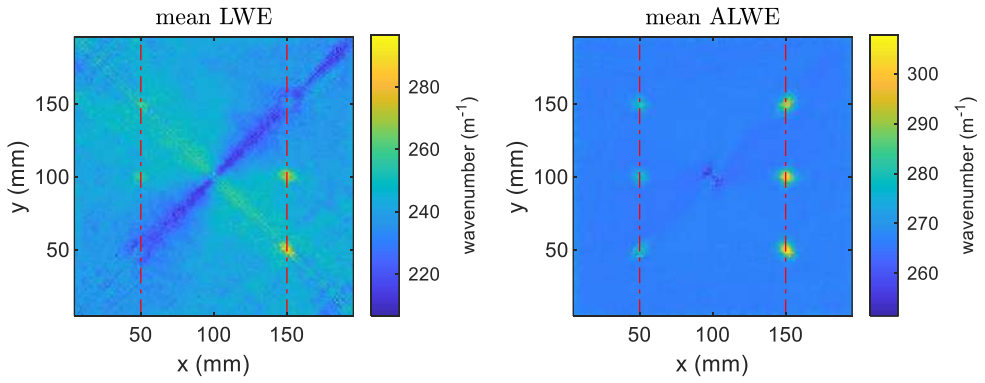

Fig. 1. Local wavenumber maps of Lamb waves obtained with the LWE (left) and ALWE (right) algorithms.

References

[1] Flynn, E. B., Chong, S. Y., Jarmer, G. J., & Lee, J.-R. (2013). Structural imaging through local wavenumber estimation of guided waves. NDT & E International, 59, 1–10. https://doi.org/10.1016/j.ndteint.2013.04.003

[2] Spytek, J., Mrowka, J., Pieczonka, L., & Ambrozinski, L. (2020). Multi-resolution non-contact damage detection in complex-shaped composite laminates using ultrasound. *NDT & E International*, *116*(September), 102366. https://doi.org/10.1016/j.ndteint.2020.102366

[3] Spytek, J., Dziedziech, K., & Pieczonka, L. (2023). Improving efficiency of local wavenumber estimation for damage detection in thin-walled structures. *Mechanical Systems and Signal Processing*, *199*(May), 110470. https://doi.org/10.1016/j.ymssp.2023.110470

[4] Spytek, J., & Pieczonka, L. (2025). Local wavenumber imaging in anisotropic structures. *Mechanical Systems and Signal Processing*, *224*, 112102. https://doi.org/10.1016/j.ymssp.2024.112102

Detection of impact events using optical fiber sensors

Alicja Szostak[1,2], Rohan Soman,[2,*]

[1] *Faculty of Applied Physics and Mathematics, Gdansk University of Technology,Gdansk, Poland*

[2] *Institute of Fluid Flow Machinery, Polish Academy of Sciences, Gdansk, Poland*

[*] *rsoman@imp.gda.pl*

Summary: Impact detection and localization remain very important aspects of a structural health monitoring (SHM) system. Composite structures typically have low damage tolerance and an impact may lead to barely visible or internal damage not visible in ordinary visual inspections. Hence a system that is able to detect and localize impact is invaluable for non-destructive testing inspectors. Furthermore, if a sensor system is capable of determining the impact energy, real-time decision-making may be possible. Several techniques have been developed for impact detection. The problem with the localization is that most techniques depend on the time of arrival of the impact-induced waves. Furthermore, the impact characterization remains a challenge as well due to the limitations of sensor systems and signal processing algorithms.

Several different sensor systems have been developed in the past, the optical fiber sensor based systems bring several advantages such as light weight, ability to be embedded and multiplexed as well as electromagnetic neutrality. Some work to study the utilization of the FBG sensors has been carried out in the past. In the current work the impact of the size of sensor on the performance of the impact detection is determined and compared with a new class of optical fiber sensors based on the micro ring resonator. Response of the FBG sensors of different sizes are studied for the spatial effects, time of arrival estimation and compared to that of MRR.

1. Introduction

Structural health monitoring (SHM) is of significant interest to infrastructure owners as it reduces the lifecycle cost of structures. Several different sensors have been developed trying to address the challenges of developing reliable, accurate and sensitive sensor systems. Optical fibers sensors (OFS) are a new and upcoming sensing technology. The OFS based sensors particularly on the fiber Bragg grating (FBG) sensors are considered mature for static and quasi-static strain measurements. But for dynamic measurements, including those for impact characterization they are still in their infancy. The FBG sensors in the conventional wavelength based interrogation are typically not capable of capturing the impact events on very small time scales. For this purpose the application of the FBG sensors in the edge filtering configuration is necessary [1]. In order to further develop the sensors for impact sensing as well as other high-strain rate events (such as in split-Hopkinson bar set up) a thorough understanding of the sensor response to high strain events is necessary.

Traditionally, FBGs are treated as point sensors; however, when the impact-induced elastic wave (typically a Lamb wave) possesses a wavelength comparable to or shorter than the grating length, the sensor no longer acts as a simple strain gauge. Instead, it functions as a spatial integrator. This study employs a numerical approach to analyse FBGs of varying lengths (ranging from 1 mm to 20 mm) bonded to a structure. Two cases are studied, in first impact on a plate and the resultant spectral response is analysed, and the in the second the response in a split Hopkinson Bar experiment is studied. The analysis shows that a trade-off is necessary to ensure appropriate length and reliable FBG sensor response. It also indicates the use of micro-ring resonator (MRR) which improves the performance event further. The performance of the sensors in terms of aperture effect (spatial averaging) and time of arrival computation is analyzed.

2. Methodology and scope of study

The core of this research centers on the spectral power density and the distortion of the FBG's Bragg peak. Under the influence of a high-frequency impact wave, the strain field across the grating becomes highly non-uniform. Our results demonstrate that for "long" sensors, the spectral response undergoes significant broadening and chirping, often resulting in multi-peak splitting. This phenomenon, while providing a richer data set regarding the wave gradient, significantly complicates the signal demodulation process and reduces the Signal-to-Noise Ratio (SNR) for standard peak-tracking algorithms. Conversely, "short" sensors (1 mm) maintain a consistent spectral shape, behaving as quasi-point sensors that capture the temporal frequency of the impact with higher fidelity. However, smaller FBGs exhibit lower absolute reflectivity, necessitating higher-gain interrogation systems.

In order to compare the performance, FBGs of different length are compared under same impact loading occurring 5cm away from the middle point of the sensor. In order to achieve the accurate response of the FBG spectrum the transfer matrix method (TMM) able to capture the non-uniform strain effects is utilized [2]. Similar to the FBG spectrum the MRR spectrum too is simulated using the transfer matrix method.

3. Results

In the edge filtering approach, it is known that the sensitivity of the sensor is proportional to the reflectivity of the FBG spectrum, and the slope of the spectrum. In order to ensure comparability the reflectivity of the sensor is kept constant (around 70%).

As can be seen in Figure 1, the shape of the impact event changes as the length of the FBG increases. This is due to spatial averaging that the sensor does. Also the maximum amplitude changes quite significantly first it increases upto 8mm FBG and then reduces. This is due to combination of 2 effects, where the as the FBG length increases, the slope of the edge becomes steeper leading to better sensitivity but spectral distortion due to spatial averaging. It can be also seen that the MRR sensor is the fastest to react. This is due to the point nature (considerably smaller size) which has minimal spatial sampling effects. The TOA was determined using a standard threshold technique commonly used in the literature. For an assumed 1% limit (common across all sensors) the MRR gave the TOA closest to the theoretical TOA. The figure 2 shows that the 1mm FBG undergoes a shift due to the impact load but the longer FBG due to the non-uniform strain over the 20 mm FBG length undergoes spectrum distortion which might be tricky to demodulate without specialized equipment.

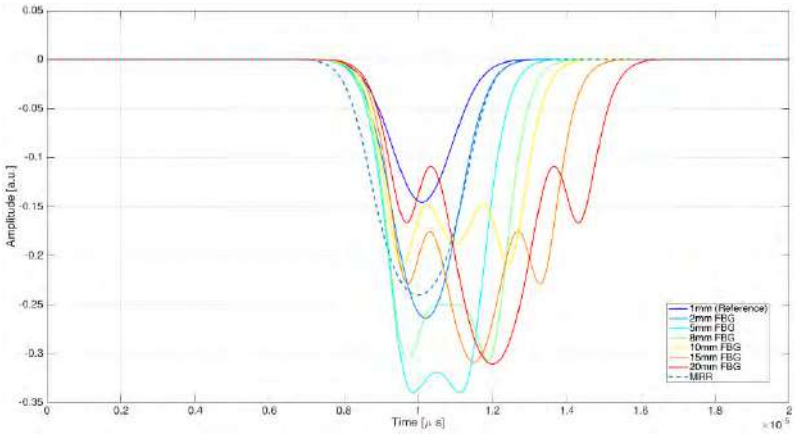

Figure 1: Response of FBGs of different length to impact

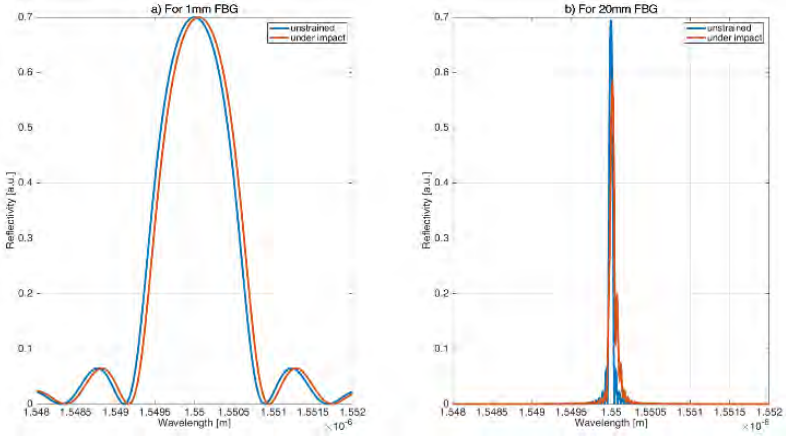

Figure 2: FBG spectrums under impact a) 1mm b) 20mm

4. Conclusions

The results indicate that smaller the sensor the better it is for impact localization, and characterization. In case of the FBG sensors, the smaller FBGs have lesser sensitivity but this issue is overcome through use of MRR sensors which will be investigated experimentally in the future.

References

[1] Wu, Q., Okabe, Y., & Yu, F. (2018). Ultrasonic structural health monitoring using FBG. Sensors, 18(10), 3395.
[2] Wee, J., Hackney, D. A., Bradford, P. D., & Peters, K. J. (2017). Simulating increased Lamb wave detection sensitivity of surface bonded fiber Bragg grating. Smart Materials and Structures, 26(4), 045034.

Acknowledgements

Dr Rohan Soman acknowledges the funding support of National Science Center, Poland, grant number: 2024/55/B/ST8/00272.

HISTRATE

Advanced Composites under High Strain Rate Loading A Route to Certification-by-Analysis

2026 Conference

10th – 11th JUNE 2026

Session 4 - Advanced testing and instrumentation for composites under high strain rates (WG6)

cost EUROPEAN COOPERATION IN SCIENCE & TECHNOLOGY

Funded by the European Union

In-Situ Liquid Resin Healing of Elium/Glass Fibre Composites for Wind Turbine Blades under Elevated Mode I Loading Rates

Mohamad Alsaadi,[1,2,3 *], Andreas Hornig[4], Moritz Kuhtz[3], Dipa Ray[5], Tomas Flanagan[3] and Declan Devine[1]

[1]*PRISM Research Institute, Technological University of the Shannon, Athlone, Ireland, * mohamad.alsaadi@tus.ie*

[2]*Materials Engineering Department, University of Technology, Baghdad 10066, Iraq*

[3]*Éire Composites Teo., An Choill Rua, Indreabhán, H91 Y923 Galway, Ireland*

[4]*TUD Dresden University of Technology, ILK, Germany*

[5]*School of Engineering, Institute for Materials and Processes, The University of Edinburgh, EH9 3FB, Scotland, United Kingdom*

Abstract: This study investigates an in-situ resin-injection welding method to enhance Mode I delamination resistance in thermoplastic composite structures. Composite panels manufactured using Elium® resin and triaxial glass fibres were repaired via liquid resin injection, promoting semi-interpenetrating polymer network formation at the crack interface. Mode I fracture behaviour was evaluated using double-cantilever beam (DCB) tests at standard and elevated loading rates. The repaired composites exhibited up to 42% higher crack initiation loads and improved fracture toughness compared with virgin specimens. These results demonstrate a scalable, sustainable repair strategy for large composite structures, supporting extended service life and reduced environmental impact in wind energy applications.

1. Introduction

Wind energy has become a cornerstone of the global renewable energy transition, providing a sustainable alternative to fossil fuels and playing a key role in reducing greenhouse gas emissions in line with net-zero targets for 2050 [1]. It is among the fastest-growing renewable technologies worldwide. In wind turbine blade (WTB) manufacturing, advanced composites, such as sustainable liquid acrylic resins (e.g., Elium®, developed by Arkema, France), offer significant environmental advantages. These resins combine the low viscosity and room-temperature processability of thermosets with the recyclability of thermoplastics. Based on methyl methacrylate monomers, they are infused into fibre reinforcements and polymerised in situ, thereby reducing the carbon footprint. To improve efficiency and ensure stable power generation, modern wind turbines increasingly use longer, larger rotor blades. However, the increased size and flexibility of these blades make them more susceptible to structural damage under varying operational and environmental conditions. Wind farms are often located in remote and harsh environments, including offshore, mountainous, and desert regions, where blades are exposed to strong winds, salt spray, rain, and lightning, significantly increasing the likelihood of damage. Consequently, damage detection and maintenance planning are complex and costly. Previous studies report that operation and maintenance costs for offshore wind turbines account for 15–35% of total lifecycle costs, with up to 80% attributed to unplanned failures [2].

Delamination is a critical damage mechanism in wind turbine blades, significantly reducing structural integrity and service life. Delamination occurs when the layers of the composite material separate, often due to manufacturing defects, impact damage, or environmental factors (Figure 1a), severely compromising structural integrity [3]. For instance, impacts from birds or other flying bodies can cause delamination in the WTB. Another reason is that while leading-edge erosion primarily affects surface integrity, it can also induce local tensile stresses and interface weakening, which trigger Mode I delamination [4]. Composite healing extends component lifespan, reduces material waste, and minimises the carbon footprint associated with new manufacturing, making it a key driver of sustainability and lower CO_2 emissions. To the best of the authors' knowledge, no prior studies have investigated resin-injection healing in the Triaxial glass fabric-reinforced Elium® 191 XO/SA (Three parts resin) composite. This study investigates the repair of Mode I delamination using resin-injection welding and examines the delamination resistance of virgin and healed composites at elevated opening rates, providing direct probing of composite deformation mechanisms under extreme loading conditions.

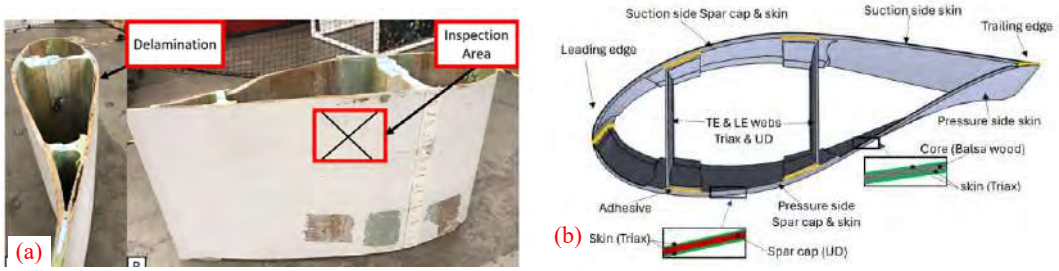

Fig. 1. (a) Delamination in WTB [5]; (b) Cross-sectional view of the WTB [6].

2. Materials and Testing

The Triaxial glass fabric (Cristex, U-E-1182 g/m^2-1270mm, often used for the outer surface and web of the WTBs, Figure 1b), four layers (+45/0/-45) are used to reinforce Elium® 191 XO/SA (comprising three components: 191 XO acrylic resin (50% w/w), 191 SA accelerator (50% w/w), and methyl ethyl ketone peroxide (MEKP) initiator (2% w/w)). The DCB test (Figure 2a) is used to evaluate Mode I fracture toughness in accordance with ASTM D5528. The DCB test specimens (eight plies) were cut to dimensions of 165 mm × 20 mm. Aluminium loading blocks are placed on the front and back sides of the DCB specimens. A Polytetrafluorethylen (PTFE) film be inserted to generate a crack length a_o of 50 mm. Constant extension rates of 3, 6, and 9 mm/min are applied to separate the specimens. Load, crosshead displacement, and delamination length are continuously recorded. A video extensometer (DIC) enabled the automatic detection of crack initiation and real-time tracking of delamination length as the specimens gradually opened. Each test continued until a minimum delamination length of 50 mm was achieved, measured from the pre-crack tip. Five samples are tested at each loading rate, and the average results are recorded.

3. Results, Discussion, and Conclusion

As shown in the Figure 2b, the delamination resistance load (P) versus crack opining displacement (COD), the healed samples were notably higher than those of the virgin samples, not only at the standard crack-opening rate (3 mm/min) but also at elevating loading rates (6 and 9 mm/min), thanks to a novel resin injection repair technique due to the formation of a semi-interpenetrating polymer network (semi-IPN) at the bonding interface. The resin injection repair developed in this study is based on a University of Edinburgh patent [7]. Notably, the repaired coupons exhibited higher delamination loads and, consequently, improved fracture toughness at both crack initiation and during crack propagation compared to the literature.

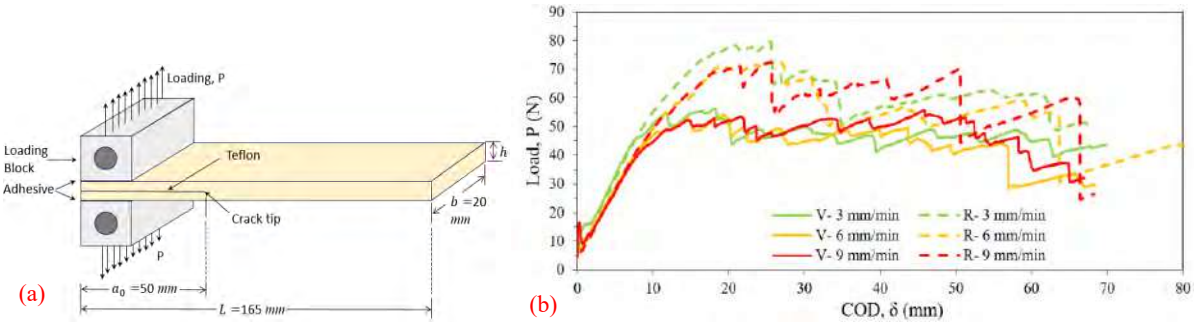

Fig. 2. (a) Schematic of the DCB test, and (b) Delamination load versus crack opening displacement.

The liquid resin injection repair significantly increases the crack initiation load by 36–42% compared with virgin samples across all tested loading rates (3, 6, and 9 mm/min), due to semi-IPN formation, reflecting robust performance under elevated loading rates. Using the same novel liquid thermoplastic resin for both manufacturing and repair enables an efficient, scalable in-situ repair strategy for large composite structures, such as WTB, reducing downtime and maintenance costs. The proposed healing approach extends component service life, reduces material waste, and lowers CO_2 emissions associated with replacement manufacturing, supporting more sustainable composite utilisation in renewable energy infrastructure.

4. References

1. Long, Y.; Chen, Y.; Xu, C.; Li, Z.; Liu, Y.; Wang, H. The Role of Global Installed Wind Energy in Mitigating CO2 Emission and Temperature Rising. *J. Clean. Prod.* **2023**, *423*, 138778. https://doi:10.1016/j.jclepro.2023.138778.
2. Tong, Y.; Liu, W.; Liu, X.; Wang, P.; Sheng, Z.; Li, S.; Zhang, H.; Meng, Y.; Zhu, Y.; Lei, X.; et al. Materials Design and Structural Health Monitoring of Horizontal Axis Offshore Wind Turbines: A State-of-the-Art Review. *Materials (Basel).* **2025**, *18*, 329. https://doi:10.3390/ma18020329.
3. Boopathi, K.; Mishnaevsky, L.; Sumantraa, B.; Premkumar, S.A.; Thamodharan, K.; Balaraman, K. Failure Mechanisms of Wind Turbine Blades in India: Climatic, Regional, and Seasonal Variability. *Wind Energy* **2022**, *25*, 968–979. https://doi:10.1002/we.2706.
4. Li, H.; Xin, W.; Xu, B.; Bao, H. Delamination Failure Analysis of Wind Turbine Blades Based on Equivalent Fatigue Load. *Ocean Eng.* **2024**, *310*, 118642. https://doi:10.1016/j.oceaneng.2024.118642.
5. 5 Common Wind Turbine Blade Failures and Repair Processes, VIVABLAST, Https://Vivablast.Com/ (Assesed on 18/02/2026).
6. Carallo, G.A.; Casa, M.; Kelly, C.; Alsaadi, M. Comparative Life Cycle Assessment (LCA) of Traditional and New Sustainable Wind Blade Construction. *Sustainability* **2025**, *17*, 2026. https://doi:10.3390/su17052026.
7. Bolluk, A.; Devine, M.; Quinn, J.A.; Ray, D. Repair of Acrylic/Glass Composites by Liquid Resin Injection and Press Moulding. *Compos. Part B Eng.* **2024**, *281*, 111513. https://doi:10.1016/j.compositesb.2024.111513.

Funding: This work is funded by the HISTRATE Conference 2026 and Short-Term Scientific Mission (STSM).

Temperature-Dependent Impact Behavior of Carbon Fiber/PEKK Composite Laminates

Ceren Yildirim [a,b*], Hasan Ulus [a,c], Hatice S. Sas [a,b,d], Mehmet Yildiz [a,b *]

[a] *Sabanci University Integrated Manufacturing Technologies Research and Application Center & Composite Technologies Center of Excellence, Manufacturing Technologies, Istanbul 34906, Turkiye*

[b] *Faculty of Engineering and Natural Sciences, Sabanci University, Tuzla, Istanbul 34956, Turkiye*

[c] *Selcuk University, Huglu Vocational School, Konya 42700, Turkiye*

[d] *School or Mechanical, Aerospace and Civil Engineering, The University of Sheffield, S1 3JD, UK*

** Corresponding author e-mail: yildirimceren@sabanciuniv.edu*

Abstract:

Aerospace structures are increasingly transitioning from thermoset to thermoplastic composites to enable higher-rate manufacturing, improved reparability, and enhanced recyclability, while maintaining sufficient damage tolerance. This study experimentally investigates the coupled effects of impact temperature on the low-velocity impact (LVI) response of unidirectional carbon fiber/poly(ether ketone ketone) (CF/PEKK) laminates. The laminates are manufactured from UD CF/PEKK tapes using vacuum bagging followed by oven consolidation, demonstrating a viable out-of-autoclave processing route for aerospace-grade thermoplastic composites. The consolidation cycle employs a two-step thermal profile with dwell temperatures of 340 °C and 380 °C, followed by controlled cooling. A symmetric stacking sequence, $[(0/90°)\backslash_7/0°]_s$, is adopted, resulting in laminates with an average thickness of 4.5 mm. Differential scanning calorimetry (DSC) is used to quantify the degree of crystallinity of the PEKK matrix, while void content analysis indicates a void fraction of 3.60%. LVI tests are conducted at low, room, and elevated temperatures. The force–time and force–displacement responses exhibit a pronounced temperature dependence: elevated-temperature impacts show reduced stiffness and larger displacements, whereas low-temperature impacts produce higher peak forces and a stiffer response, consistent with more localized damage development.

1. Introduction

Carbon fiber-reinforced thermoplastic (CFRTP) composites have been extensively studied as an alternative to traditional thermoset composites, particularly in the aerospace industry [1,2]. These materials offer a combination of high toughness, damage tolerance, impact resistance along with excellent solvent resistance. Additionally, their as recyclability, ease of handling, and cost-effective storage provide further advantages over thermoset counterparts [3,4]. Due to these benefits, CFRTPs have been successfully utilized in the production of helicopter canopies and various aerospace subcomponents, including clips and frames [5,6].

During the assembly or service life of composite structures, low-velocity impact (LVI) is common occurrence. Although the resulting damage may not always be visually apparent, it can significantly compromise structural integrity, similar to damage caused by high-velocity impacts. This is primarily due to the anisotropic nature of composites, which affects the way impact energy is absorbed and distributed. To maintain structural integrity, damage-tolerant designs must retain sufficient load-bearing capacity even when affected by barely visible impact damage. Thus, understanding of LVI-induced damage and impact response is essential for maximizing the potential of CFRTPs in lightweight structural applications [7,8].

Aircraft structural components operate under diverse environmental conditions, where exposure to fluctuating temperatures can alter the damage mechanisms and mechanical behavior of composites. These temperature variations, experienced throughout the service life of an aircraft, play a critical role in damage formation and propagation [9]. To address this challenge, the present study systematically investigates the LVI response of CFRTP laminates with cross-ply orientations under room temperature (RT), high temperature (HT), and low temperature (LT).

2. Experimental Procedure

2.1. Materials and specimen preparation

The unidirectional carbon fiber/poly-ether-ketone-ketone (CF/PEKK) tape, which purchased from Toray Cetex® with the commercial code of TC1320, is used to fabricate thermoplastic composite laminates. The tape used for hand lay-up have a nominal thickness of 0.15 mm and a width of 305 mm. Each ply is cut to the desired dimensions

(305mm x 305mm) using a digital cutting machine (ZÜND G3-L3200) as shown in Figure 1a. The laminates are manufactured using a vacuum-assisted hand lay-up process with the lay-up sequence of $[(0/90°)\backslash_7/0°]_s$ as shown in Figure 1b-c. After lay-up, the laminates are held under 1 atm pressure using vacuum bagging for 1 hour at room temperature, followed by oven consolidation. The consolidation process consists of two steps: first, the temperature is increased to 340 °C at a rate of 3 °C/min and maintained for 90 minutes. In the second step, the temperature is further increased to 380 °C at the same rate and held for 120 minutes before cooling to room temperature at 3 °C/min. The cured thermoplastic composite laminates have final dimensions of 305 mm × 305 mm, with an average thickness of 4.5 mm, measured at three different points.

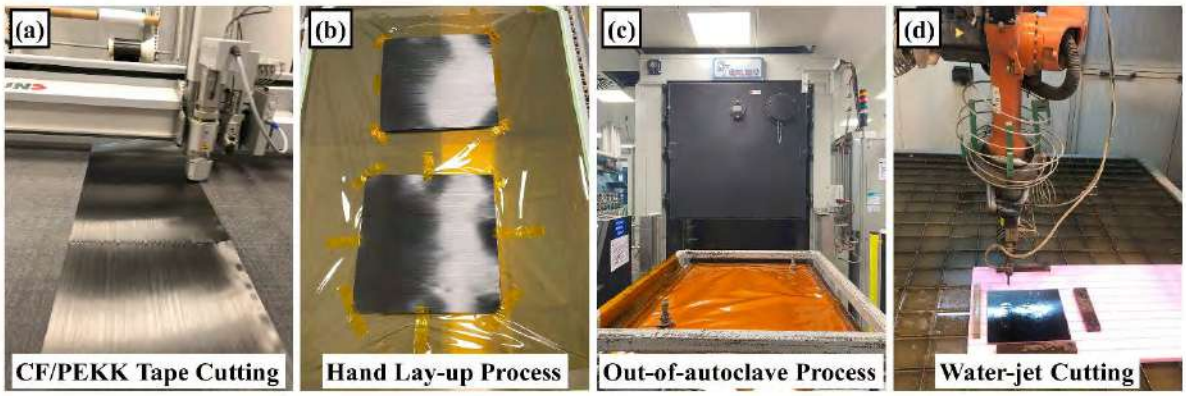

Figure 1. Manufacturing stages of CF/PEKK composite plates.

2.2. Impact Tests

LVI test specimens are then cut to 100 mm × 150 mm, following ASTM D7136 [10], using a robotic water jet system (Kuka KR16 Ultra F robot equipped with a high-performance water jet pump). The specimens are subsequently subjected to LVI testing, with the impactor positioned at the center of each sample as shown in Figure 2. LVI tests are conducted at an energy level of 30 J to analyze the structural behavior under barely visible impact damage conditions. Room-temperature (RT) tests are performed at 25 °C. To investigate the effect of high temperature (HT) on the thermoplastic composites, the specimens are conditioned at 75 °C in a climatic chamber for 60 minutes to ensure uniform temperature distribution before LVI testing. After being placed in the impact chamber, the temperature is continuously monitored using a non-contact digital laser infrared thermometer. Once the temperature reaches 70 °C, the impact test is conducted.

Figure 2. Drop tower test setup with specimen positioning and temperature monitoring for HT-conditioned specimen.

3. Results and Discussion

Figure 3(a) and 3(b) depict the force-time and force-displacement curves, respectively, obtained from LVI tests performed on composite laminates conditioned at RT, HT, and LT. The data reveal significant variations in impact response attributable to thermal conditioning. The LT-conditioned specimen demonstrates the highest peak force, reaching approximately 8300 N. This value is 5.1% greater than that observed at RT (7900 N) and 10.8% higher than at HT (7500 N). This increase suggests enhanced stiffness and resistance to deformation at low temperatures, likely due to reduced matrix ductility [11]. In the initial loading phase, the LT-conditioned specimen exhibits the steepest slope in its force-displacement curve, further indicating increased stiffness. However, the unloading phase is more abrupt compared to RT and HT specimens, implying a more brittle failure mode with limited plastic deformation. Notably, the area under the LT curve, representing absorbed impact energy, is smaller than that of RT and HT specimens, confirming reduced energy dissipation. Conversely, the HT-conditioned specimen displays the lowest peak force and the most extended displacement. This behavior is indicative of matrix softening at elevated temperatures, which facilitates increased plastic deformation and higher energy absorption. The broader hysteresis loop observed in the HT specimen further corroborates enhanced energy dissipation. The RT specimen exhibits an intermediate response, balancing stiffness, peak force, and energy dissipation. This balanced behavior underscores the influence of thermal conditioning on the mechanical performance of composite materials under impact loading. These findings align with previous studies highlighting the critical role of temperature in influencing the impact damage resistance and tolerance of carbon-fiber-reinforced epoxy laminates. For instance, research has demonstrated that thermal aging can significantly alter the impact behavior of such composites, affecting both damage initiation and progression [12].

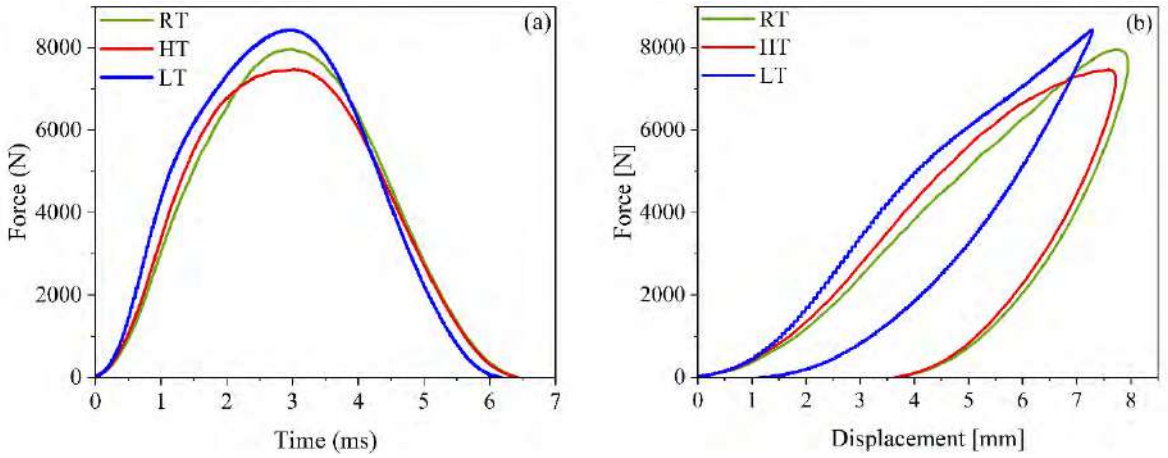

Figure 3. Force-time (a) and force-displacement (b) curves obtained from LVI tests conducted RT, HT, and LT

References:

[1] El-Dessouky HM, Lawrence CA. Ultra-lightweight carbon fibre/thermoplastic composite material using spread tow technology. Compos Part B Eng 2013;50:91–7. https://doi.org/10.1016/j.compositesb.2013.01.026.

[2] Favaloro M. A comparison of the environmental attributes of thermoplastic vs. thermoset composites. Int SAMPE Tech Conf 2009.

[3] Yildirim C, Tabrizi IE, Al-Nadhari A, Topal S, Beylergil B, Yildiz M. Characterizing damage evolution of CF/PEKK composites under tensile loading through multi-instrument structural health monitoring techniques. Compos Part A Appl Sci Manuf 2023;175:107817. https://doi.org/https://doi.org/10.1016/j.compositesa.2023.107817.

[4] Yildirim C, Ulus H, Beylergil B, Al-Nadhari A, Topal S, Yildiz M. Effect of atmospheric plasma treatment on Mode-I and Mode-II fracture toughness properties of adhesively bonded carbon fiber/PEKK composite joints. Eng Fract Mech 2023;289:109463. https://doi.org/https://doi.org/10.1016/j.engfracmech.2023.109463.

[5] Pantelakis SG, Katsiropoulos C V., Labeas GN, Sibois H. A concept to optimize quality and cost in thermoplastic composite components applied to the production of helicopter canopies. Compos Part A Appl Sci Manuf 2009;40:595–606. https://doi.org/10.1016/j.compositesa.2009.02.012.

[6] Hoang VT, Kwon BS, Sung JW, Choe HS, Oh SW, Lee SM, et al. Postprocessing method-induced mechanical properties of carbon fiber-reinforced thermoplastic composites. J Thermoplast Compos Mater 2023;36:432–47. https://doi.org/10.1177/0892705720945376.

[7] Seyyednourani M, Akgun S, Ulus H, Yildiz M, Sas HS. Experimental investigation on Compression-After-Impact (CAI) response of aerospace grade thermoset composites under low-temperature conditions assisted with acoustic emission monitoring. Compos Struct 2023;321:117260. https://doi.org/10.1016/j.compstruct.2023.117260.

[8] Körbelin J, Derra M, Fiedler B. Influence of temperature and impact energy on low velocity impact damage severity in CFRP. Compos Part A Appl Sci Manuf 2018;115:76–87. https://doi.org/10.1016/j.compositesa.2018.09.010.

[9] Yildirim C, Ulus H, Sas HS, Topal S, Yildiz M. Assessing the fracture and dynamic mechanical performance of CF/PEKK joints bonded with epoxy-based adhesive film for aerospace applications: Impact of thermal and cycling hygrothermal conditions. Compos Part A Appl Sci Manuf 2025;190:108659. https://doi.org/10.1016/J.COMPOSITESA.2024.108659.

[10] ASTM D7136/D7136M-Standard Test Method for Measuring the Damage Resistance of a Fiber-Reinforced Polymer Matrix Composite to a Drop-Weight Impact Event. ASTM Int 2011;i:4–6. https://doi.org/10.1520/D7136.

[11] Benli S, Sayman O. The effects of temperature and thermal stresses on impact damage in laminated composites. Math Comput Appl 2011;16:392–403. https://doi.org/10.3390/mca16020392.

[12] García-Moreno I, Caminero MÁ, Rodríguez GP, López-Cela JJ. Effect of thermal ageing on the impact damage resistance and tolerance of carbon-fibre-reinforced epoxy laminates. Polymers (Basel) 2019;11. https://doi.org/10.3390/polym11010160.

Multiaxial Characterisation of Polymers and Composites from Quasi-Static to High Strain Rates

Naveen Petchiappan[1*] , Georg Ganzenmüller[2,3] , and Patricia Verleysen[1]

[1] *Materials Science and Technology-DyMaLab, EMSME Department, Ghent University, Technologiepark 46, 9052 Ghent, Belgium*

[2] *Fraunhofer Institute for High-Speed Dynamics, Ernst-Mach-Institut, EMI, Ernst-Zermelo Str. 4, Freiburg, 79104, Germany*

[3] *Institute for Sustainable Systems Engineering, INATECH, Albert-Ludwigs Universität Freiburg, Emmy-Noether-Str.2, Freiburg im Breisgau, 79110, Germany*

[*] *naveenchakravarthi.petchiappan@ugent.be*

Abstract: Advanced polymers and composite materials are widely employed in engineering applications that require high impact resistance and energy absorption capacity. Reliable prediction of their mechanical response during impact-loading requires accurate experimental characterization under the often complex, multiaxial deformation states and large strains occurring in real loading scenarios. However, most conventional material testing techniques primarily impose uniaxial stress states and therefore do not fully represent the multiaxial loading conditions encountered in real applications. Among alternative techniques, the bulge test is particularly promising, as it enables controlled multiaxial deformation up to large strains. For metals, established procedures are available for both testing and data processing to extract constitutive behaviour. However, the assumptions underlying these standardised procedures for metals are not necessarily valid for other material classes. For polymers, especially the assumption of volume conservation might not necessarily be valid, while for composites, additional limitations arise from the limited accuracy of result processing procedures in the critical low-deformation regime. To address these challenges, the application of a new generation of identification techniques offers a promising solution. By using full-field deformation data alongside conventional measurements, inverse identification methods or data-driven techniques can be employed to obtain calibrated material models. In this work, both quasi-static (QS) and dynamic bulge tests are performed on polycarbonate and composite samples. Full-field deformation maps are obtained using static and high-speed imaging in combination with stereo digital image correlation (DIC). The experimental results provide insights into the deformation behaviour of the materials under biaxial stress conditions and establish a framework for improved material modelling under complex loading states.

1. Experiments

In the present work, hydraulic bulge tests were performed on circular specimens machined from polycarbonate (PC) sheets with a thickness of 2.85 mm, and composite plates with thicknesses of 1 mm and 2 mm. The composite plates consist of an RTM6 matrix reinforced with woven basalt fabric. The specimens were clamped at the boundary, and upon application of pressure, the samples deform through a die opening with a diameter of 60 mm. The experiments were conducted under both QS and dynamic loading regimes.

For the QS bulge tests, the applied pressure was directly measured using a pressure transducer connected to the hydraulic chamber (Fig. 1a). The dynamic bulge configuration follows the split Hopkinson bar principle, and the pressure inside the chamber was determined from the stress wave transmitted to the output bar [1]. A distinguishing feature of the DyMaLab dynamic bulge setup (Fig. 1b) is that the specimen remains fully optically accessible during testing, enabling the use of high-speed imaging. In both cases, the deformation of the specimen was continuously recorded using a stereo camera system, and the captured images were processed using DIC to obtain full-field displacement and strain distributions.

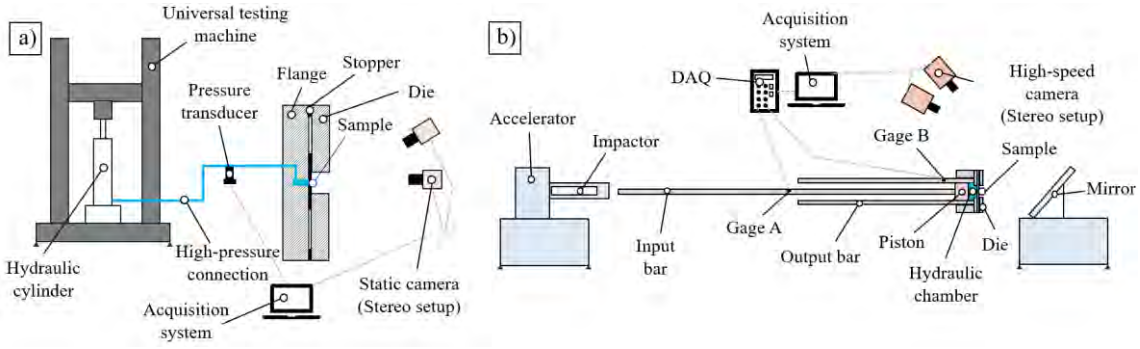

Fig. 1. Schematic representation of (a) Quasi-static bulge setup and (b) dynamic bulge setup

By combining the measured pressure with the DIC-based reconstruction of the dome surface, additional quantities describing the deformation behaviour can be obtained. In particular, for the PC samples, the radius of curvature at the dome apex is evaluated from the reconstructed surface. Assuming membrane behaviour and volume conservation, this enables a first-order estimation of the biaxial stress during deformation. However, for polycarbonate, the assumption of volume conservation may not always hold [2]. Moreover, due to the constraints imposed on the dimensions of the specimen in the dynamic tests, membrane theory does not apply to the relatively thick PC specimens either. Although the composite samples satisfy the assumptions required for the application of membrane theory due to their small thickness, the level of deformation is insufficient to obtain reliable values for the apex radius. Consequently, more advanced test processing procedures are needed for both materials.

2. Results and Discussion

The results and discussion focus on polycarbonate, which exhibits the highest deformation levels. The PC tests have a much richer information content and still allow meaningful interpretation using simplified analysis procedures. The apex displacement response obtained from the hydraulic bulge tests (Fig. 2a and 2b) based on the rate of applied pressure, describes the global mechanical behaviour and the strain rate dependence of the material under biaxial deformation. Together with the full-field strain measurements obtained from DIC, these results provide a comprehensive experimental characterization of the deformation behaviour of polycarbonate sheets and offer a rich dataset for calibrating advanced material models.

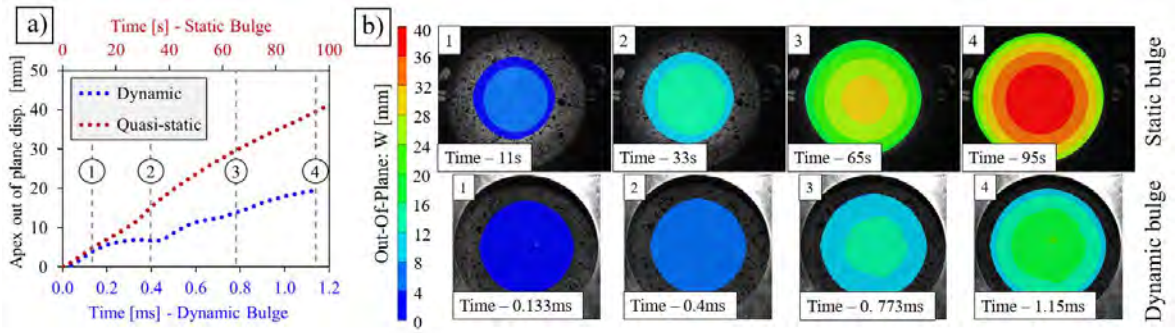

Fig. 2. (a) Apex out of plane displacement of PC samples tested at static and dynamic rates and (b) corresponding DIC out-of-plane displacement fields at different time steps

The maximum pressure applied to the samples during QS and dynamic tests was 9.3 MPa and 8.2 MPa, respectively (Fig. 3a). The maximum in-plane strains ε_x and ε_y at the apex reached approximately 0.75 under QS conditions (Fig. 3b). This high value demonstrates the potential of bulge tests to deform materials to significantly larger strain levels compared to the uniaxial tests and biaxial tests performed on cruciform specimens. Especially the latter involve complex design and optimization procedures to achieve a uniform biaxial stress or strain state in the targeted test region of the specimen [3].

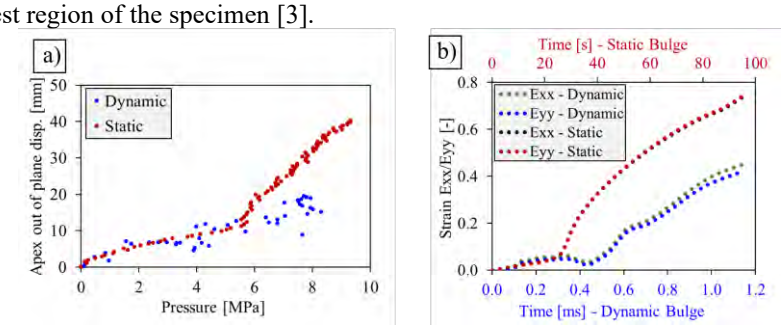

Fig. 3. a) Evolution of pressure and b) evolution of strain under static and dynamic bulge test

3. References

[1] Corallo, L., Mirone, G., and Verleysen, P., 2023, "A Novel High-Speed Bulge Test to Identify the Large Deformation Behavior of Sheet Metals," Exp Mech, 63(4), pp. 593–607. https://doi.org/10.1007/s11340-022-00936-5.

[2] Siviour, C. R., Walley, S. M., Proud, W. G., and Field, J. E., 2005, "The High Strain Rate Compressive Behaviour of Polycarbonate and Polyvinylidene Difluoride," Polymer, 46(26), pp. 12546–12555. https://doi.org/10.1016/j.polymer.2005.10.109.

[3] Horta Muñoz, S., and Serna Moreno, M. D. C., 2022, "Advances in Cruciform Biaxial Testing of Fibre-Reinforced Polymers.," Polymers, 14(4), p. 686. https://doi.org/10.3390/polym14040686.

Design of a round-robin exercise on the high strain-rate tensile properties of commercial structural composites

Marco Peroni[1*], Andrei G. Anisimov[2], Patricia Verleysen[3], Tatjana Glaskova-Kuzmina[4] and Michele Meo[5]

[1] *European Commission, Joint Research Centre (JRC), Via E. Fermi, 2749, 21027 Ispra, Italy*

[2] *Department of Aerospace Structures and Materials, Delft University of Technology, Kluyverweg 1, 2629 HS, Delft, the Netherlands*

[3] *Materials Science and Technology-DyMaLab Research Group, Faculty of Engineering and Architecture, Ghent University, Technologiepark 46, 9052 Zwijnaarde, Belgium*

[4] *Institute for Mechanics of Materials, University of Latvia, Jelgavas 3, LV-1004, Riga, Latvia*

[5] *Department of Aeronautics and Astronautics, University of Southampton, Southampton SO17 1BJ, UK*

[*] *e-mail of the corresponding author*

Summary: This paper presents the design of a round-robin exercise primarily intended for HISTRATE members, but extendable to other research institutions, focusing on the high strain-rate properties of commercial structural composites. The objectives of this exercise are to: (i) compare experimental data obtained from benchmark or reference material tests in order to assess the influence of different testing and data-processing procedures across participating laboratories; (ii) improve best-practice guidelines for split Hopkinson bar testing; (iii) share practical insights and operational details related to the selected tests; and (iv) lay the groundwork for the standardization of high strain-rate testing methods for composite materials.

1. Introduction

High strain-rate testing is widely employed in the design of structures subjected to impacts and explosions; however, it is still not governed by comprehensive standards for either conventional materials (e.g., metals and plastics) or advanced materials (e.g., composites, foams, and additively manufactured/3D-printed materials). The split Hopkinson bar remains the primary experimental apparatus (used mainly for tension, compression, and torsion tests) operating within a strain-rate range of approximately 10^2 to 10^4 s^{-1}. Nevertheless, as its use has been largely confined to the scientific community, the associated standards are often incomplete or not updated to reflect recent advances in measurement techniques [1]. Only a limited number of round-robin studies have been conducted in the past to address this gap. These efforts have predominantly focused on compression testing of metallic specimens and involved a relatively small number of participating research institutes [2-4]. Studies on tensile testing are even fewer [5], partly because numerous specimen geometries have been proposed over the years, with limited systematic evaluation of their performance. Critical assessments of the challenges associated with high strain-rate tensile testing of composite materials are rarer still [6]. The HISTRATE COST Action aims to promote a round-robin exercise, primarily involving HISTRATE members, but open to other research institutions, focusing on the high strain-rate behavior of commercial structural composites. The objectives of this initiative are to: (i) compare experimental data obtained from benchmark material tests to evaluate the influence of different testing and data-processing procedures across laboratories; (ii) refine best-practice guidelines for split Hopkinson bar testing; (iii) share practical insights and operational recommendations related to the selected tests; and (iv) establish a foundation for the standardization of high strain-rate testing methods for composite materials.

2. Practical Implementation

This section summarizes the outcomes of an ad hoc WG6 HISTRATE meeting focused on the design of the aforementioned round-robin exercise. In particular, it addresses the key aspects of the initiative, including the preparatory phase, test execution, data collection and processing, and, finally, data analysis and exploitation.

2.1. Preparatory work

The HISTRATE round-robin exercise will focus on the high strain-rate tensile characterization of a limited number of commercially available composite materials. Candidate materials may include glass, carbon or basalt fiber reinforced polymers (GFRP, CFRP or BFRP respectively), with a maximum of three materials considered in the study. Given this limitation, it would be beneficial to select materials representing different classes (i.e. thermoplastic composites, a quasi-isotropic fabric and unidirectional fiber reinforcement) in order to capture a broad range of material behaviors. The use of certified materials may further enhance material availability and ensure data consistency across participants. Selected materials will be procured by the Joint Research Centre (JRC) and distributed to participants following a call for interest open to HISTRATE members and other research institutions. Materials will be supplied in two possible forms, with participants allowed to request one or both options: (i) as-manufactured plates and (ii) specimens machined via CNC under the supervision of JRC. For option

(i), participants will be responsible for machining the specimens according to their preferred methodologies. For option (ii), JRC will collect specimen design specifications from participants and take responsibility for CNC machining the requested geometries. This dual approach will enable the assessment of the influence of specimen manufacturing procedures on test results. In all cases, participants will be responsible for measuring (e.g., mass and geometry) and documenting (via photographs) each specimen, whether received or machined in-house, prior to the testing phase. If feasible, an ultrasound scan on both sample series (produced by JRC and other round-robin partners) could be beneficial to check possible defects before the testing phase.

2.2. Experimental tests

The test campaign will be defined by only two constraints: the target strain rate and the number of repetitions. Specifically, the tests will be conducted at strain rate of about 500 s^{-1} (average strain rate prior to maximum stress), with 5 repetitions for each material. Testing may be performed using either the split Hopkinson bar technique or a high-velocity servo-hydraulic system. No constraints will be imposed on participants regarding specimen geometry, testing procedures, or experimental equipment.

2.3. Data collection

Participants in the round-robin exercise will be required to provide the stress–strain curves obtained from the 5 test repetitions for each material, together with high-speed video recordings of the specimen gauge section (image acquisition frequency ≥ 100,000 fps). In addition to the test data, participants must supply detailed information on the adopted testing setup, to be reported using a standardized template. The required information will include, among others: materials and geometries of bars/striker/equipment; a detailed description of the instrumentation (e.g., strain gauge types and characteristics, Wheatstone bridge configuration, signal conditioning system, sensor locations, etc.). For tests performed using the split Hopkinson bar technique, raw strain signals must also be provided. Any additional information regarding calibration procedures adopted by the participants will be valuable for the data analysis phase. This includes, in particular, calibration methods for force and displacement measurements used to determine specimen stress and strain, as well as procedures related to Digital Image Correlation (DIC), if applied. Participants are also encouraged to share the data-processing methodologies used to derive stress–strain curves from raw sensor data. At the conclusion of the testing phase, all specimens must be returned to the JRC, which will coordinate post-mortem analyses in collaboration with other HISTRATE partners.

2.4. Data elaboration and exploitation

The collected data will be analyzed by a group of researchers (on a voluntary basis) under the supervision of the HISTRATE Core Group. The analysis will be carried out in three progressive phases (Steps 1–3), each characterized by an increasing level of complexity.

Step 1. The initial phase will focus on the evaluation and comparison of processed outputs (i.e., stress–strain curves) to quantify data scatter across different materials and participating laboratories. Key parameters such as Young's modulus and stress–strain response up to failure will be considered. This step will provide a first assessment of the maturity and reliability of current high strain-rate testing methodologies.

Step 2. Following the computation of global statistics, the second phase will investigate whether different testing methodologies (i.e., specimen and equipment design, as well as data processing and calibration procedures) introduce systematic effects or errors in the measured responses (e.g., premature failure induced by clamping systems). This stage may require reprocessing raw signals and high-speed images and/or performing numerical simulations of the experimental setups. The outcome of this analysis is expected to support the identification of optimal testing methodologies.

Step 3. The final objective of the round-robin exercise is the development of a best-practice document for high strain-rate testing of composite materials, which could serve as a basis for future standardization efforts. The document will address both experimental design (including equipment and specimen geometry) and data processing procedures, with particular attention to advanced measurement techniques (e.g., DIC and multiphysics instrumentation). If the results of the round-robin exercise reveal limitations in terms of reliability, additional approaches, such as virtual testing or novel experimental methodologies, may also be considered.

At the conclusion of the project, the results will be disseminated through a peer-reviewed journal publication, and the best-practice guidelines will be made available on the HISTRATE website. This work is expected to contribute to the establishment of standardized methods for high strain-rate testing of composite materials.

References

[1] Peroni, M. et. al., 2025, Proceedings HISTRATE Conference 2025.
[2] Kariem, M. A. et. al., 2019, Int. J. Impact Eng., 126, pp. 62-75.
[3] Kariem, M. A. et. al., 2013, Key Engineering Materials, 535–536, pp.518–521.
[4] Kruszka, L. and Sobczyk, K., 2022, Critical Energy Infrastructure Protection,60, pp.81–95.
[5] Borsutzki, M. et. al., 2005, Report International Iron and Steel Institute.
[6] Elmahdy, A. and Verleysen P., 2018, EPJ Web of Conferences 183.

HISTRATE: progress towards a roadmap for standardisation of high strain rate testing of composite materials

Andrei G. Anisimov,[1*] Marco Peroni,[2] Tatjana Glaskova-Kuzmina,[3] and Patricia Verleysen[4]

[1] *Department of Aerospace Structures and Materials, Delft University of Technology, Kluyverweg 1, 2629 HS, Delft, the Netherlands*

[2] *European Commission, Joint Research Centre (JRC), Via E. Fermi, 2749, 21027 Ispra, Italy*

[3] *Institute for Mechanics of Materials, University of Latvia, Jelgavas 3, LV-1004, Riga, Latvia*

[4] *Materials Science and Technology-DyMaLab Research Group, Faculty of Engineering and Architecture, Ghent University, Technologiepark 46, Zwijnaarde 9052, Belgium*

**a.g.anisimov@tudelft.nl*

Abstract: One objective of the HISTRATE COST Action is to develop a roadmap for the standardisation of high strain rate testing of composite materials. The initial HISTRATE contribution structured this roadmap through (i) a gap analysis, (ii) roadmap objectives and milestones, (iii) proposed actions, and (iv) stakeholder involvement and implementation needs. Key gaps include the limited applicability of existing dynamic testing standards to composite materials at high strain rates (up to 10^3-10^5 s^{-1}) and the need for more realistic loading scenarios, improved testing efficiency, and richer measurement data up to failure. Since then, WG6 has advanced roadmap implementation through (a) a dedicated standards overview on high strain rate testing and (b) a round-robin concept to benchmark inter-laboratory practice for high strain rate tensile characterisation of commercial structural composites. This paper summarises the current status of this roadmap development and identifies what has been achieved, what is in progress, and what remains open before a final roadmap can be completed.

Introduction

The roadmap activity is coordinated in HISTRATE WG6 and targets traceable, comparable high strain rate test data (up to failure) to support reliable modelling and the design of safety-critical structures in overlapping sectors (aerospace, automotive, energy, marine). Earlier COST experience on certification-related topics [1] is relevant because it shows that community practice must be translated into actionable guidance and a credible standardisation pathway. The roadmap elements and their current status are therefore presented in a table below.

Current status of the roadmap development in HISTRATE

Roadmap element	Progress achieved in HISTRATE	Status Next steps
Need for standardisation/ gap analysis	■ Existing dynamic standards identified as insufficient for composites at high strain rates up to 10^3-10^5 s^{-1} (e.g., ISO 26203, ISO 18872, ISO/DIS 18989) ■ Priority technical gaps defined: multiaxial vs uniaxial loading; multidirectional and woven vs unidirectional systems; interlaminar fracture toughness vs strain rate ■ Enabling gaps: testing efficiency (too many parameters/tests); sustainable testing pyramids; richer observations (higher spatial/temporal resolution, full-field methods, multimodal sensor fusion)	**Defined** To reduce the gap to a smaller number of prioritised standardisation topics.
Roadmap structure and objectives	■ The main roadmap components were defined in [2], following general roadmap-development approaches [3-5]) ■ Short-term goals (1–2 years): generalise best practices and in-house procedures; compare/benchmark methods across laboratories ■ Mid-term goals (3–5 years): adapt/modify existing standards; propose new test methods and specimen geometries; integrate advanced monitoring ■ Long-term goals (5+ years): unified methodologies across leading European laboratories; potential inputs to a CEN prestandard (ENV)	**Defined at the concept level** Convert the time-horizon goals into possible deliverables and measurable outcomes that can be tracked across WG6 activities

Overview of available standards	■ Standards overview on high strain rate testing is a dedicated building block of the roadmap [6] ■ The review provides the baseline practices (mostly for metals) and limitations to composites	**Completed** Convert into a prioritised list of standardisation gaps and candidate actions.
Benchmarking and inter-laboratory comparison	■ Round-robin exercise proposed as a short-term mechanism to ensure repeatability and comparability via benchmark tests and reference material/specimen design ■ Round-robin positioned as the key evidence generator for harmonisation decisions	**Designed, but not yet completed** Execute the exercise and compare the experimental datasets.
Good-practice documentation	■ Drafting good-practice documents identified as a short-term action to establish a common technical baseline for test setup, measurement, and reporting ■ Intended to capture transferable procedures beyond single-lab practice	**Identified, but not yet completed** To be compiled based on the outcomes of the round-robin exercise
Reference materials/specimen strategy, testing conditions and required outputs	■ Round-robin exercise targets: ☐ Commercially available composite materials to support reproducibility and availability (incl. thermoplastic composites, quasi-isotropic fabric laminates, unidirectional composites) ☐ Strain rate about 500 s^{-1}; five repetitions; test via split Hopkinson bar (SHB) tests or high-velocity servo-hydraulic systems ■ Defined outputs: stress-strain curves; high-speed video of the gauge section; raw SHB strain signals; complete setup and processing metadata	**Defined round-robin**. Final material selection and commitment of participating laboratories are still needed. Validate the exercise and refine it, by implementing
Advanced instrumentation and multimodal measurements	■ Roadmap emphasises higher spatial/temporal resolution for shock/wave characterisation and failure evolution ■ Full-field techniques explicitly prioritised over single-point-only measurements; multimodal sensor fusion identified as a key need ☐ DIC measurements included in the round-robin	**Identified, but not standardised** Specify measurement recommendations (minimum/advanced/optional) compatible with both lab capability diversity and standardisation goals
Data processing, calibration, and uncertainty awareness	■ The roadmap requires traceability beyond reported "typical curves", implying consistent data reduction and reporting practices ■ Round-robin exercise concept: three-step workflow ☐ (1) compare reported stress-strain outputs ☐ (2) quantify systematic effects of differing setups/data processing ☐ (3) compile best-practice recommendations suitable for standardisation	**Partially addressed** Derive robust calibration and data-reduction practices from the inter-laboratory exercise.
Stakeholders and standardisation pathway	■ HISTRATE community is broad (academia + industry stakeholders, e.g. modelling, instrumentation, materials, applications) ■ Explicit need identified for stronger engagement with certification/standardisation bodies (CEN, SAE, ASTM) to enable adoption	**Still limited** To establish WG6/7-led standardisation plan (named contacts, target committees)
Final integrated roadmap	■ Roadmap development is recognised as more complex than anticipated and not yet complete ■ The main building blocks (all above) defined/initiated	**In progress** Integrate all building blocks into one concise, actionable roadmap

Conclusion

HISTRATE progress toward standardisation of high strain rate testing of composite materials is best described as completion of core roadmap building blocks rather than completion of the final roadmap itself: the gap analysis and time-phased objectives are defined, and the implementation path is developed through a standards overview plus a round-robin exercise intended to generate harmonisation evidence. The remaining task is to integrate these elements into a single actionable roadmap with clear deliverables, evidence gates (from benchmarking), and an explicit engagement path toward CEN/SAE/ASTM to support eventual prestandardisation.

References

[1] Santandrea, F., G. G. Momm, P. Tsokanas, V. Rajcic, D. Skejic, D. Rajnovic, R. Petkovic, and S. Kruse-Strack. "WG6: Review of certification procedures for bonded structures." (2023). https://certbond.eu/wp-content/uploads/CA18120_WG6_D01_Deliverable.pdf
[2] Anisimov, A.G., Peroni, M., Glaskova-Kuzmina, T., Verleysen, P. "Elements for a roadmap for standardisation of high strain rate testing of composite materials", Proceedings HISTRATE Conference 2025, https://doi.org/10.5281/zenodo.16962743
[3] Garcia, M. L., & Bray, O. H. (1997). "Fundamentals of technology roadmapping." Sandia National Laboratories Report, SAND97-0665.
[4] Phaal, R., Farrukh, C. J., & Probert, D. R. (2005, July). Developing a technology roadmapping system. In A Unifying Discipline for Melting the Boundaries Technology Management: (pp. 99-111). IEEE.
[5] Maxwell, J. Research to Standards: Part 2: The Roadmap to Success, https://www.astm.org/news/research-standards-part-2-roadmap-success-ja18?utm_source=chatgpt.com
[6] Peroni, M., Anisimov, A.G., Glaskova-Kuzmina, T., Verleysen, P. "Overview of available standards on high strain rate testing", Proceedings HISTRATE Conference 2025, https://doi.org/10.5281/zenodo.16962743

Coupling Proper Generalized Decomposition with Domain Decomposition for 2D Elastic Wave Simulation

Toufik Boubehziz[1,*], Dimitri Goutaudier[1], Juan-Pablo Marquez Costa[1], Laurent Berthe[1]
[1] PIMM–CNRS, ENSAM, 151 Blvd de l'Hôpital, 75013 Paris, France
[*] Corresponding author: toufik.boubehziz@ensam.eu

Summary: Simulation of laser shock wave propagation in composite laminates requires efficient numerical methods. In this work, we present a new simulation approach coupling the Proper Generalized Decomposition (PGD) with a non-overlapping domain decomposition (DD) strategy for 2D elastic wave simulation. Building on the hybrid PGD–SEM model, the out-of-plane direction is decomposed into non-overlapping subdomains solved locally. Simulation validations confirm accurate wave propagation with DD convergence.

Introduction

Laser shock testing for controlled delamination of composite materials is a challenging problem to simulate numerically since it involves high-frequency wave propagation in heterogeneous media [1]. Several numerical methods can solve wave propagation problems with controlled accuracy and good convergence properties. Yet, even if the spatial domain is as simple as a plate, the computational effort remains prohibitive without appropriate numerical resources. The Proper Generalized Decomposition (PGD) has shown promise for efficient simulation of such problems [2], but its monolithic nature limits scalability. Domain decomposition (DD) methods [3] offer a way to address this limitation efficiently by partitioning the out-of-plane direction into subdomains, allowing for parallel solves and reduced computational cost.

PGD–SEM Framework

The 2D elastodynamic problem seeks $\mathbf{u}(x,z,t)$ over $\Omega = \Omega_x \times \Omega_z$ satisfying

$$\rho \frac{\partial^2 \mathbf{u}}{\partial t^2} - div[\boldsymbol{\sigma}] = \mathbf{f}, \quad \text{for } (x,z,t) \in \Omega \times]0,T], \tag{1}$$

with initial and boundary conditions:

$$\begin{aligned} \frac{\partial \mathbf{u}}{\partial n} &= 0 \quad \text{on } \partial\Omega, \\ \mathbf{u}(x,z,0) &= \mathbf{u}_0(x,z), \quad \text{for } (x,z) \in \Omega, \\ \frac{\partial \mathbf{u}}{\partial t}(x,z,0) &= \frac{\partial \mathbf{u}_0}{\partial t}(x,z), \quad \text{for } (x,z) \in \Omega, \end{aligned}$$

where ρ is the density, $\mathbf{f}$ the applied load, and $\boldsymbol{\sigma} = \mathbf{C} : \boldsymbol{\varepsilon}(\mathbf{u})$ for an anisotropic stiffness tensor $\mathbf{C}(x,z)$. The PGD approximation reads:

$$\mathbf{u}(x,z,t_k) \approx \sum_{j=1}^{M_k} \boldsymbol{\phi}_j(x,t_k)\, \psi_j(z,t_k), \tag{2}$$

where modes are found by alternating fixed-point iterations (in-plane then out-of-plane) until stagnation, with a hybrid explicit/implicit time scheme for stability.

Domain Decomposition Strategy

The out-of-plane domain is partitioned into S non-overlapping subdomains $\Omega_z = \bigcup_{s=1}^{S} \Omega_z^{(s)}$. On each subdomain, the discrete problem reads:

$$\left[\mathbf{L}_z^{(s)} + \mathbf{R}_z^{(s)}\right] \boldsymbol{\psi}^{(s)} = \mathbf{M}_{BZ}^{(s)} \left(\mathbf{M}_{BXY}^{T} \boldsymbol{\phi}\right) + \mathbf{g}_{\Gamma}^{(s)}, \tag{3}$$

where $\mathbf{L}_z^{(s)}$ is the subdomain physics operator, $\mathbf{M}_{BZ}^{(s)}$ the out-of-plane RHS pre-operator, $\mathbf{M}_{BXY}$ the in-plane RHS pre-operator (both concatenating mass, stiffness, and time-scheme contributions), $\mathbf{R}_z^{(s)}$ the Robin impedance matrix, and $\mathbf{g}_{\Gamma}^{(s)}$ the interface data. The Robin condition is given by:

$$\mathbf{g}_{\text{nbr}}^{n+1} = -\mathbf{g}_{\text{own}}^{n} + \left(\boldsymbol{\alpha}_{\text{eff}}^{\text{own}} + \boldsymbol{\alpha}_{\text{eff}}^{\text{nbr}}\right) \odot \boldsymbol{\psi}_{\text{own}}^{n}. \tag{4}$$

where $\boldsymbol{\alpha}_{\text{eff}}^{\text{own}}$ and $\boldsymbol{\alpha}_{\text{eff}}^{\text{nbr}}$ are the effective impedance parameters for the own and neighboring subdomains, respectively, and $\odot$ denotes element-wise multiplication. Global SEM double-counts contributions at shared nodes.

Numerical Results

The model is validated on a multi-layer composite material.

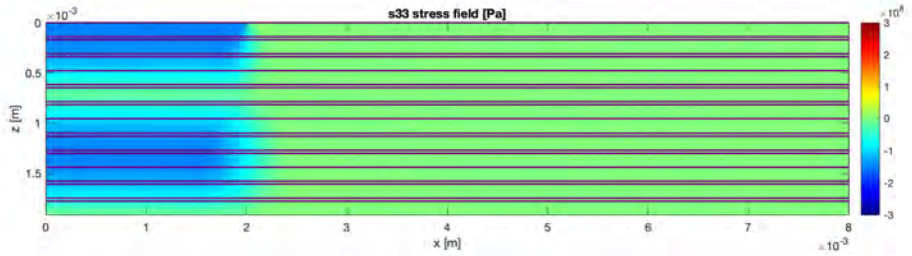

Figure 1: Laser shock simulation with $S = 20$ subdomains. Wave fronts propagate continuously across subdomain interfaces without artificial reflections.

With multiple subdomains $S > 1$, the DD–PGD solver matches the 2D reference model without domain decomposition. It also matches with 3D reference solution at time early time steps where the reflexions are not yet . Figure 1 shows wave fronts crossing interfaces without artefacts.

Conclusions and Perspectives

A domain decomposition strategy for the PGD–SEM hybrid elastodynamic framework has been validated on laser shock configurations. Future work targets incorporating delamination phase and extending to 3D simulations. This approach opens the door to efficient simulation of delamination processes.

References

[1] Romain Ecault, Fabienne Touchard, Michel Boustie, Laurent Berthe, and Nicolas Dominguez. Numerical modeling of laser-induced shock experiments for the development of the adhesion test for bonded composite materials. *Composite Structures*, 152:382–394, 2016.

[2] Dimitri Goutaudier, Laurent Berthe, and Francisco Chinesta. Exploring space separation techniques for 3d elastic waves simulations. *Computational Mechanics*, 69(5):1147–1163, 2022.

[3] Andrea Toselli and Olof Widlund. *Domain decomposition methods-algorithms and theory*, volume 34. Springer Science & Business Media, 2004.

Numerical Investigation of the Effect of Adhesives Used in Honeycomb Composite Structures Subjected to High-Velocity Ballistic Impact on Impact Resistance and Its Prediction Using the Fuzzy Logic Method

Yunus Emre Toğar[1,2*], Halil Özer[2]

[1] *Vocational School, Mechatronics Program, Istanbul Beykent University, Istanbul, 34500, Turkey*

[2] *Mechanical Engineering Department, Faculty of Mechanical Engineering, Yıldız Technical University, Istanbul 34349, Turkey*

[*] *emretogar@beykent.edu.tr*

Summary: Optimization of structures with lightweight properties and high impact resistance is of critical importance in the aerospace and defense industries. In this study, the ballistic impact behavior of honeycomb composite structures was investigated through numerical simulations, and a fuzzy logic-based prediction model was developed. The honeycomb composite structure consists of a 15 mm Al-3003 honeycomb core with GFRP(Woven) face materials, a variable-thickness AL2024-T3 protection plate, and an adhesive layer. The bonding process of the face sheets was analyzed using the Cohesive Zone Model (CZM) with brittle (AV138) and ductile (DP8005) adhesives. A three-input, 27-rule fuzzy logic model produced results in high correlation with the numerical data. The findings revealed that adhesive thickness is a fundamental parameter significantly affecting energy absorption capacity.

METHODS AND RESULTS

1. Numerical Methodology and FEA Setup

The honeycomb composite configuration was developed by bonding a variable-thickness AL2024-T3 face sheet (0.5–2.0 mm) and an adhesive layer (0.1–1 mm) onto a fixed-thickness honeycomb core structure. The core structure comprises a 15 mm Al-3003 honeycomb core sandwiched between two 1 mm GFRP (woven) skins. To optimize computational efficiency, the honeycomb core was modeled as a homogenized orthotropic material based on the Gibson-Ashby cellular solids theory. The schematic drawing of the structure utilized in numerical analysis is presented in Figure 1.

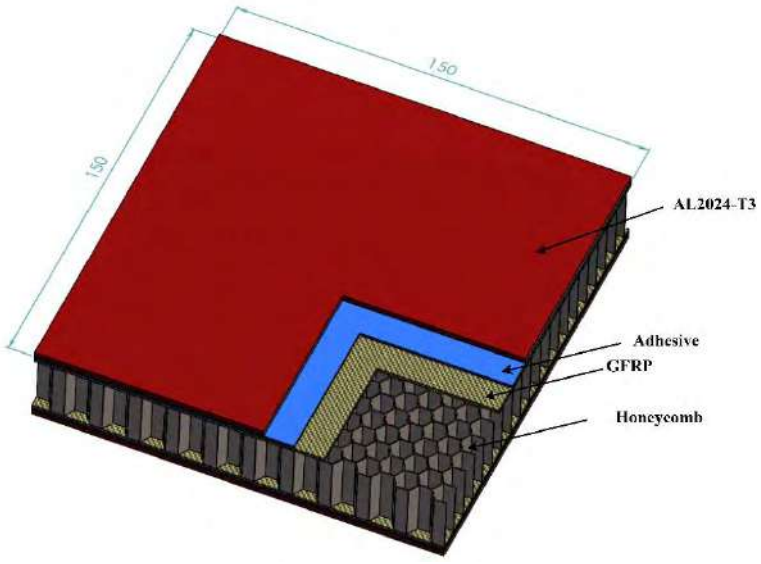

Fig. 1. Schematic drawing of the honeycomb structure.

Numerical analyses were performed using ANSYS Explicit Dynamics. As a result of a comprehensive mesh convergence study, a 3 mm element size was determined to provide a stable balance between accuracy and computational time, utilizing an optimized mesh of 28,450 elements. The projectile was defined as a rigid cylindrical structure with a 20 mm diameter, hemispherical tip, and 40 mm length, with impact velocities varied between 300 and 600 m/s. The time-dependent damage progression in the numerical analyses is illustrated in Figure 2.

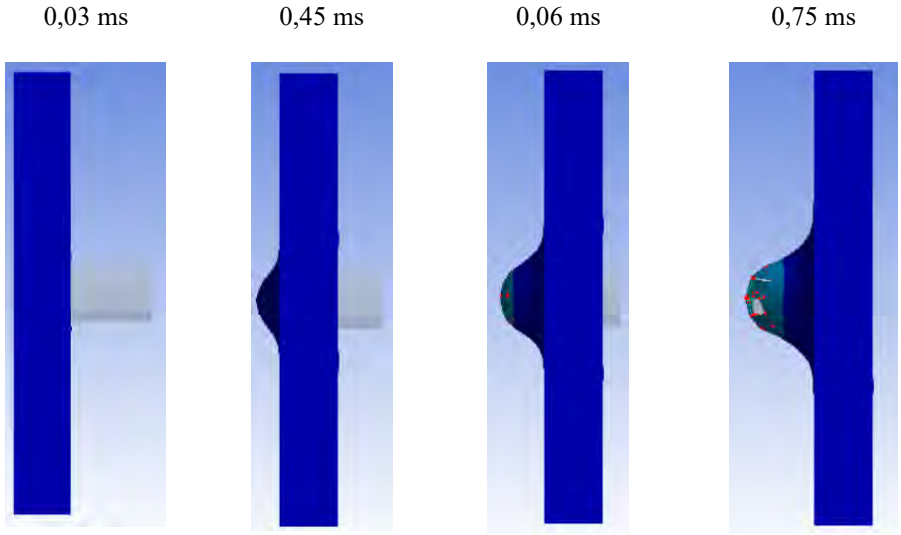

Fig. 2. The time-dependent damage progression.

2. Cohesive Zone Modeling and Material Performance

The adhesive layer providing the connection between the AL2024-T3 face sheet and the GFRP skin was defined using the Cohesive Zone Model (CZM) to capture delamination and debonding physics. Brittle (AV138) and ductile (DP8005) adhesives were analyzed through four different scenarios involving individual and hybrid combinations. It was observed that in high-strain rate ballistic impact analyses, the adhesive layer and its mechanical properties must be considered as critical parameters affecting structural strength.

The combination of a 1.5 mm AL2024-T3 face sheet and a 0.6 mm adhesive layer yielded the optimal parameter values in terms of ballistic impact resistance. Furthermore, it was observed that employing a ductile adhesive on the initial impact side significantly increased total energy absorption.

3. Fuzzy Logic Based Predictive Modeling

The developed fuzzy model predicts optimum structural parameters with an accuracy of over 95%, which is expected to significantly reduce the need for costly and time-consuming experimental trials during the preliminary design phase. The fuzzy logic model architecture and the resulting surface plots are provided in Figure 3.

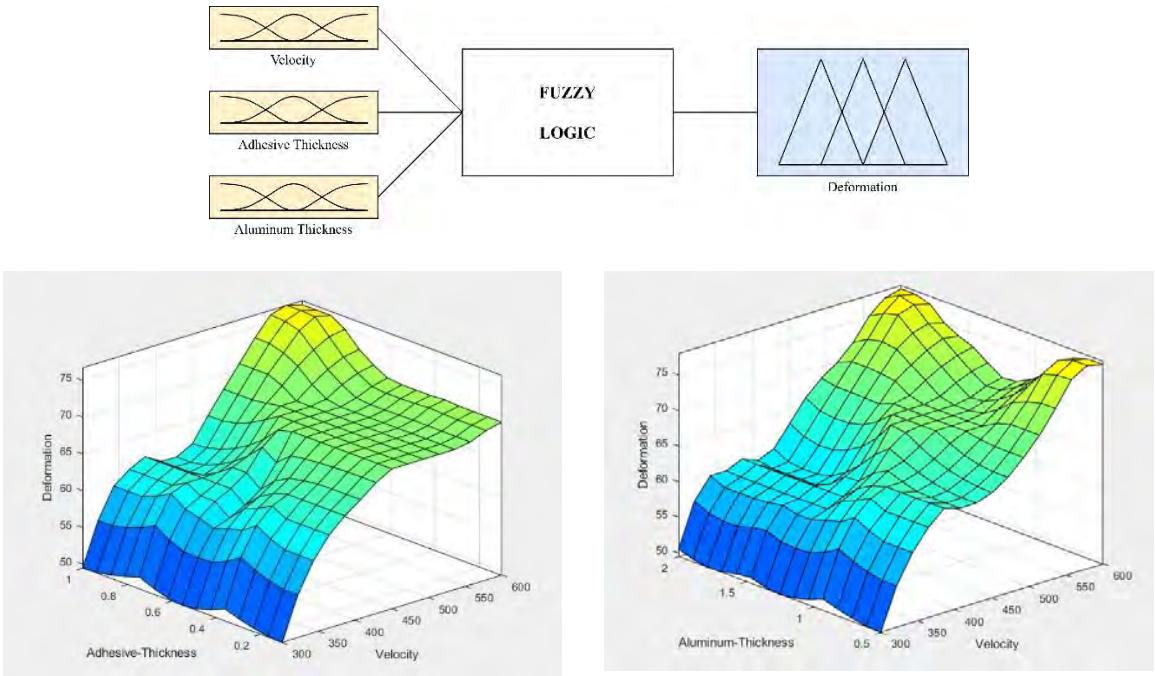

Fig. 3. The fuzzy logic model and surface plots.

High Strain Rate Deformation of Nanocomposites: A Molecular Dynamics Simulation

Yunus Onur Yildiz[1] and Murat Sen[2, *]

[1] *Department of Naval Architecture and Marine Engineering, Maritime Faculty, Bursa Technical University, 16310 Bursa, Türkiye*

[2] *Department of Mechanical Engineering, Faculty of Engineering, Firat University, 23119 Elazig, Türkiye*

[*] *corresponding.author : msen@firat.edu.tr*

Summary: This study establishes a comprehensive molecular dynamics (MD) simulation framework designed to investigate the mechanical response and failure mechanisms of metal-matrix nanocomposites (MMNCs) under extreme dynamic loading. The proposed methodology utilizes LAMMPS to model various metallic matrices reinforced with ceramic or carbon-based nano-inclusions. By systematically varying strain rates from 10^8 to 10^{10} s^{-1}, the framework enables a comparative analysis of yield criteria, strain-rate sensitivity, and atomistic defect evolution. Advanced post-processing via OVITO's aCNA and DXA algorithms allows for the quantification of dislocation densities and interfacial damage, providing a robust tool for the design of impact-resistant nanomaterials.

1. Introduction

Metal-matrix nanocomposites (MMNCs) have attracted significant interest in aerospace, defense, and automotive industries due to their exceptional strength-to-weight ratios and superior hardness. In these systems, the interaction between the metallic matrix and the reinforcing phase - often a ceramic nanoparticle - creates a complex stress field that governs the overall mechanical performance [1,2]. Among various MMNC systems, Cu/SiC nanocomposites represent a prototypical configuration where the significant elastic mismatch between the FCC copper matrix (a = 3.615 Å) and the zinc-blende SiC inclusion (a = 4.36 Å) introduces pronounced coherency strains and a complex stress field at the metal–ceramic interface [3]. Under high strain rate loading conditions—characteristic of plate impact, hypervelocity collision, and laser shock scenarios—the deformation response of such nanocomposites is governed by fundamentally different mechanisms than those operative at quasi-static rates, including homogeneous dislocation nucleation, deformation twinning, and amorphization at interfaces [4].

Molecular dynamics (MD) simulation provides an atomistic framework capable of resolving these nanoscale phenomena with femtosecond temporal resolution. The present work establishes a systematic LAMMPS-based simulation methodology for high strain rate deformation analysis of nanocomposites, integrating hybrid interatomic potentials with advanced post-processing through OVITO's adaptive common neighbor analysis (aCNA) and dislocation extraction algorithm (DXA) [5,6]. Particular attention is given to dislocation–inclusion interaction mechanisms and the strain-rate-dependent evolution of defect populations, building upon the foundational observations of Yildiz et al. [4] who demonstrated that elevated loading rates produce enhanced strength accompanied by complex deformation mechanisms in nanoporous metallic systems.

2. Methods

The simulation cell is constructed as a three-dimensional periodic supercell approach, typically oriented along the primary crystallographic axes (x–[100], y–[010], z–[001]). Using tools such as the Atomsk package, various nano-reinforcement geometries (spherical, cylindrical, or plate-like) are embedded into the single-crystalline or polycrystalline metallic matrix. In order to accurately capture the diverse bonding environments, a hybrid force-field approach is implemented. Embedded-Atom Method (EAM) potentials are used to describe the many-body interactions and electron density effects in the metal. Tersoff or Bond-Order Potentials (BOP) are applied to covalent structures like SiC, Al_2O_3, or carbon nanotubes. Morse or Lennard-Jones potentials are parameterized to define the cross-species interactions at the matrix-filler boundary.

Generally, all molecular dynamic simulations are performed using LAMMPS [7] with a timestep of 1 fs. The protocol follows three sequential stages: (i) conjugate gradient energy minimization (tolerance: 10^{-8} eV/Å); (ii) NPT equilibration at 300 K and zero pressure for 100 ps using a Nosé–Hoover thermostat/barostat; and (iii) uniaxial deformation along the z-axis via the fix deform command at four/five strain rates (such as 10^8, 10^9, 5×10^9, and 10^{10} s^{-1}) with NPT-controlled lateral boundaries to enforce uniaxial stress conditions. The deformation-subtracted temperature is computed using compute temp/deform to prevent thermostat artifacts at extreme loading rates. Atomic configurations are dumped at 5 ps intervals including per-atom stress tensor components computed via the virial formulation. Post-processing employs OVITO [5] with a sequential modifier pipeline: aCNA for structural identification (FCC, HCP, BCC, and disordered), DXA for dislocation network extraction including

Shockley partials (⅙⟨112⟩), perfect dislocations (½⟨110⟩), stair-rod (⅙⟨110⟩), and Frank partials (⅓⟨111⟩), and color-coded von Mises stress mapping for strain localization visualization.

3. Results and Discussion

The studies in the literature consistently predict a strong positive correlation between yield stress and strain rate. As the rate increases, the time available for thermal activation of dislocations decreases, necessitating higher stresses to initiate plastic flow. Interestingly, the elastic modulus remains rate-independent, as it is governed by the inherent bond stiffness of the composite constituents [8].

In metal-matrix nanocomposites (MMNCs), the interface serves a dual purpose: first, it acts as a preferential site for the heterogeneous nucleation of dislocations due to elastic mismatch and coherency strains; and second, once nucleated, the reinforcement phase functions as a barrier that causes dislocation pile-up, leading to significant work hardening, particularly under compressive loading. A critical finding enabled by this framework is the identification of a "regime transition" at extreme strain rates (typically $\geq 5\times10^{9}$ s^{-1}). At these rates, the material transitions from sequential partial dislocation emission to a regime of homogeneous multi-slip activation and deformation twinning, dramatically increasing the total dislocation density [2, 9].

4. Conclusion

The established LAMMPS-based methodology provides a reproducible and high-fidelity approach for exploring the mechanical limits of metal-matrix nanocomposites. By integrating hybrid potential modeling with automated defect analysis, the framework successfully captures the strain-rate-dependent transition of deformation modes and the critical role of interfacial amorphization in damage accumulation. This generalized approach is applicable to a wide range of material systems, facilitating the discovery of next-generation composites for extreme environment applications. The integrated deployment of OVITO's aCNA and DXA analysis modifiers, coupled with automated Python-scripted batch processing, provides a quantitative and reproducible methodology for defect characterization in nanocomposite systems subjected to extreme dynamic loading.

References

[1] Daw, M.S. and Baskes, M.I., 1984, "Embedded-Atom Method: Derivation and Application to Impurities, Surfaces, and Other Defects in Metals," Phys. Rev. B, 29(12), pp. 6443–6453.
[2] C. Cao, A. Killips, and X. Li, 2024, "Advances in the Science and Engineering of Metal Matrix Nanocomposites: A Review," Advanced Engineering Materials, 26: 2400217.
[3] Erhart, P. and Albe, K., 2005, "Analytical Potential for Atomistic Simulations of Silicon, Carbon, and Silicon Carbide," Phys. Rev. B, 71(3), p. 035211.
[4] Yildiz, Y.O., Ahadi, A., and Kirca, M., 2020, "Strain Rate Effects on Tensile and Compression Behavior of Nano-Crystalline Nanoporous Gold: A Molecular Dynamic Study," Mech. Mater., 143, p. 103338.
[5] Stukowski, A., 2010, "Visualization and Analysis of Atomistic Simulation Data with OVITO – The Open Visualization Tool," Modelling Simul. Mater. Sci. Eng., 18, p. 015012.
[6] Stukowski, A., Bulatov, V.V., and Arsenlis, A., 2012, "Automated Identification and Indexing of Dislocations in Crystal Interfaces," Modelling Simul. Mater. Sci. Eng., 20(8), p. 085007.
[7] Thompson, A.P., Aktulga, H.M., Berger, R., et al., 2022, "LAMMPS – A Flexible Simulation Tool for Particle-Based Materials Modeling at the Atomic, Meso, and Continuum Scales," Comput. Phys. Commun., 271, p. 108171.
[8] Fu, S.-Y., Lauke, B., Mäder, E., Yue, C.-Y., and Hu, X., 2000, "Tensile Properties of Short-Glass-Fiber- and Short-Carbon-Fiber-Reinforced Polypropylene Composites," Composites Part A: Applied Science and Manufacturing, 31(10), pp. 1117–1125.
[9] Kardani, A., Montazeri, A., and Urbassek, H. M., 2023, "Strain-rate-dependent plasticity of Ta-Cu nanocomposites for therapeutic implants," Scientific Reports, 13(1), 15788.

Multipoint Excitation-Based S_0 Mode Conversion Mapping for BVID Detection in Complex Composite Laminates

Maciej Radzienski[1*], Kai Zhu[1]

[1] *Institute of Fluid-Flow Machinery, Polish Academy of Sciences (IMP PAN), Gdansk, Poland*

[*] *maciej.radzienski@imp.gda.pl*

Summary: Strong material attenuation in composite structures limits the inspection range of guided waves and hinders reliable damage detection. To address this issue, this study proposes a multi-point excitation approach combined with a time-varying spatial filter for large and complex structures. The filter suppresses source interference, isolates a single wave mode, and compensates for attenuation to extend the inspection area. Experiments on CFRP plates demonstrate rapid imaging, wide-area coverage, and reliable detection of barely visible impact damage, confirming the method's potential for non-destructive testing.

1. Introduction

Composite laminates are widely used in aerospace, automotive, and energy applications because of their high specific strength, high specific stiffness, and excellent fatigue and corrosion resistance. However, these materials are vulnerable to barely visible impact damage (BVID), which can be induced by low-velocity impacts and may significantly degrade the structural integrity while remaining difficult to identify by visual inspection. Guided waves have been widely employed in nondestructive testing and structural health monitoring because of their high sensitivity to defects and capability for long-range inspection. Nevertheless, for large and complex composite structures, strong material attenuation remains a major challenge, as it reduces the effective inspection range and weakens damage-related wave features. In this context, multipoint excitation is desirable because it can enlarge the effective inspection region and enable wide-area inspection within a single measurement.

Among guided-wave-based approaches, full wavefield damage inspection provides richer spatial-temporal information for damage characterization [1]. A variety of imaging methods have been developed, such as root mean square (RMS), adaptive wavenumber analysis [2], local wavenumber analysis [3], and mode-conversion-based methods [4]. Compared with other approaches, mode conversion offers a more direct and efficient way to extract relatively pure damage-sensitive features. Therefore, this study proposes a multipoint-excitation-based mode-conversion mapping method for detecting impact-induced BVID in complex CFRP structures.

2. Multipoint Excitation-Based Mode Conversion

In this study, a multipoint excitation-based S_0 mode-conversion mapping method is proposed. The method generates an S_0 mode tracking mask to automatically capture structural and damage features associated with S_0 mode conversion. Subsequently, the extracted features from different time frames are fused using the RMS operation to produce the final mapping. For mask generation, a semi-analytical method is first used to obtain the envelope of the S_0 mode group velocity, $v(\theta)$, along different propagation directions. As shown in Fig. 1, the procedure includes two parts: an S_0 mode weighting mask, $M_w(x,y,t)$, for tracking the time-evolving S_0 mode envelope generated by different excitations, and a scanned-area removal mask, $M_s(x,y,t)$, for excluding the inspected area and reducing A_0 mode interference. The final mask is obtained by multiplying these two masks.

The final mask is obtained by multiplying these two masks. For the *i*-th excitation source, an annular mask region is defined by the inner and outer anisotropic envelopes, $E_{in}(\theta,t) = v(\theta)t$ and $E_{out}(\theta,t) = v(\theta)\big(t + W/v(\theta_0)\big)$, respectively, where W denotes the mask width for S_0 mode tracking, and θ_0 is the reference direction, taken here as the positive x-axis. The corresponding binary indicator for the weighting mask is defined as:

$$M_i(x,y,t) = \begin{cases} 1 & E_{in} \le r(x,y,t) \le E_{out} \\ 0 & otherwise \end{cases},$$

where $r(x,y,t)$ is the distance from the spatial point (x,y) to the *i*-th excitation source. The overlap number of the three regions is then given by:

$$N(x,y,t) = \sum_{i=1}^{3} M_i(x,y,t)$$

$$M_w(x,y,t) = \begin{cases} 1/N(x,y,t) & N(x,y,t) \ge 1 \\ 0 & N(x,y,t) = 0 \end{cases}.$$

The scanned-area removal mask, $M_s(x,y,t)$, is used to remove the region inside the inner anisotropic envelopes by assigning these pixels a value of 0 and all others a value of 1. The final mask is obtained by multiplying $M_s(x,y,t)$ with the S_0 mode weighting mask. The resulting mask is then applied to the full wavefield data, and RMS processing along the time dimension yields the final mode-conversion mapping.

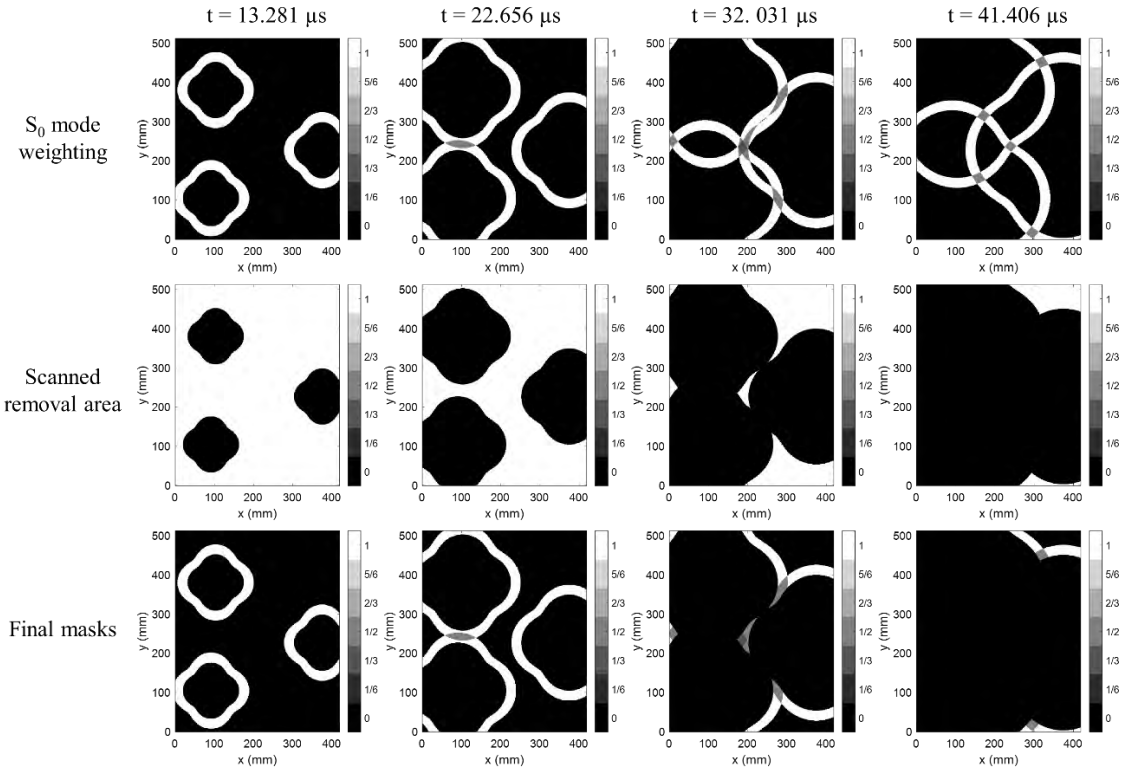

Fig. 1. Anisotropic S_0-mode tracking mask under multipoint excitation.

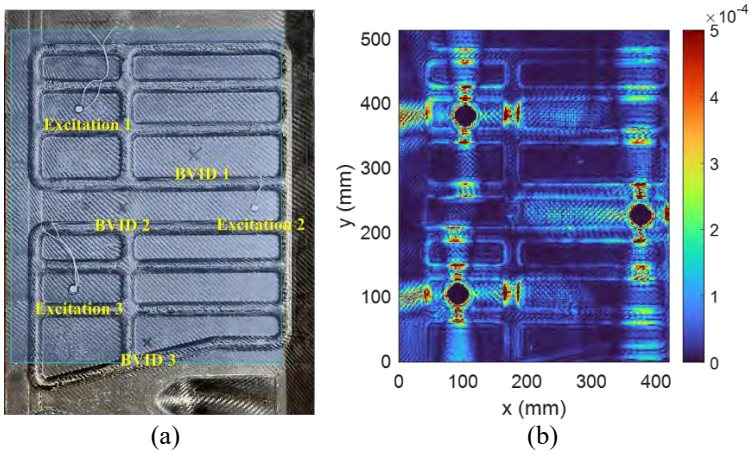

(a) (b)

Fig. 2. BVID detection: (a) specimen with multipoint excitation; (b) multipoint S_0 mode-conversion map.

3. Experimental results

The CFRP specimen contains three excitation sources and three impact-induced damage regions, as shown in Fig. 2(a). All three excitations were applied at 100 kHz, and the scanning area of the full wavefield data is indicated by the light blue region – the scanning has been made from the other side of the specimen which is flat. The final imaging result is presented in Fig. 2(b). The wavefield mapping accurately identifies both the locations and extents of the impact-induced damage regions, even in a complex specimen containing multiple stiffeners. The boundaries of the stiffeners are also clearly highlighted. The highlighted region near the center, corresponding to the three bonded piezoelectric transducer actuators, was excluded from the final mapping for clarity.

References

[1] Radzieński, M., Doliński, Ł., Krawczuk, M., Żak, A., & Ostachowicz, W. (2011, July). Application of RMS for damage detection by guided elastic waves. In Journal of Physics: Conference Series (Vol. 305, No. 1, p. 012085).
[2] Kim, B., Kong, Y., Lee, S., & Park, G. (2026). Adaptive wavenumber variation mapping for full-field ultrasonic wavefield-based damage detection. Structural Health Monitoring, 14759217261428552.
[3] Rogge, M. D., & Leckey, C. A. (2013). Characterization of impact damage in composite laminates using guided wavefield imaging and local wavenumber domain analysis. Ultrasonics, 53(7), 1217-1226.
[4] Wandowski, T., Radzienski, M., & Kudela, P. (2025). Lamb wave S0/A0 mode conversion for imaging the internal structure of composite panel. Composite Structures, 353, 118748.

Numerical Simulation of a Shearographic System with a Pixelated Polarization Camera

Elena Stoykova,[1,2*] Violeta Madjarova,[1,2] and Nataliya Berberova-Buhova[1,2]

[1] *Institute of Optical Material and Technologies, Bulgarian Academy of Sciences, Acad. G. Bonchev Str. 109, 1113 Sofia, Bulgaria*

[2] *National Centre of Excellence "Mechatronics and Clean Technologies", Kliment Ohridski Blvd., Block 8, 1700, Sofia, Bulgaria*

[*] *elena.stoykova@gmail.com*

Summary: Design of optical setups and optimization of algorithms in speckle-based non-destructive testing (NDT) need a simulation tool for numerical modelling of complex speckle measurements. This paper presents a second part of research dedicated to development of such a tool for systems for electronic speckle pattern interferometry (ESPI), shearography and laser speckle photometry. More specifically, options for shearography analysis are described by modelling a system using a polarization camera with an array of linear micro-polarizers enabling single shot four-step phase shifting. The tool facilitates studying the impact of noise and speckle properties, including temporal evolution, on phase retrieval accuracy.

1. Introduction

High sensitivity and full-field measurement capability of speckle-based optical metrology enable rapid contactless inspection, quality control and maintenance of critical components in aerospace, automotive, and manufacturing industries. Design of the measurement setups and optimization of processing algorithms need a simulation tool, which provides numerical modelling of complex speckle patterns for understanding of noise and error sources, and improving accuracy in NDT applications. This work is part II of research conducted in [1] that describes a simulation tool for analysis of speckle-based measurements. Part I [1] was dedicated to modelling an ESPI system. Part II widens the tool's options focusing on shearography analysis by modelling a system using a polarization camera with an array of linear micro-polarizers oriented at 0°, -45°, 45°, 90° that enables four-step phase shifting in a single shot.

2. Simulation tool for a shearographic measurement

The developed simulation tool for ESPI and shearography is based on generation of complex amplitudes for two-beams interferometry and consists of blocks for generation of raw data, extraction of relevant information, and accuracy evaluation. Computer generation of subjective speckle patterns at given properties as size, contrast, evolution of speckles is based on the measurement principle for transforming the sample mechanical change into phase data and introducing speckle evolution in time, environmental and registration noise. The algorithms for phase retrieval, dynamic speckle analysis, filtering and compression form the processing block. Quality assessment of the measurement outputs by means of various metrics is performed in the accuracy block.

We modeled a shearographic system based on a Michelson interferometer [2]. A laser beam reflected from the tested object with a rough surface is divided into two beams, which pass through two linear polarizers with orthogonal polarization and reflect from two mirrors inclined at a small angle to each other for introducing shear. The beams impinge the array of micro-polarizers after passing through a quarter-wave plate with its fast axis oriented at 45° with respect to the linear beam polarizations. This array forms a structure of super-pixels of size $2\Delta \times 2\Delta$ where Δ is the camera pixel pitch. The polarizers provide simultaneously four phase-shifted at $\pi/2$ images i_1, i_2, i_3, i_4 for the interfering two orthogonal circularly polarized beams on the camera's aperture. The set i_1, i_2, i_3, i_4 is formed from the image I of size $N_x \times N_y$, that is recorded at moment $t = s\Delta t$ where Δt is the time interval between two consecutive images and s = 1,2...S. The following relations are valid: $i_1(k,l,s) = I(2m+1,2n+1,s)$, $i_2(k,l,s) = I(2m+1,2n+2,s)$, $i_3(k,l,s) = I(2m+2,2n+1,s)$, $i_4(k,l,s) = I(2m+2,2n+2,s)$, $k,l = 1 \dots N_{x,y}/2$; $m,n = 0 \dots N_{x,y}/2-1$. Intensities in the four images are given by $i_p = E_{x,p}E_{x,p}^* + E_{y,p}E_{y,p}^*, p = 1,2,3,4$ where $E_{x,p}$ and $E_{y,p}$ are the x- and y-components of the electric vector of light passed though the p micro-polarizer. If E_o and E_s are the complex amplitudes of the two circularly polarized beams falling on the array of micro-polarizers, then we have $E_{x,1} = E_o + E_s$ and $E_{y,1} = 0$, $E_{x,2} = 0.5(1+i)E_o + 0.5(1-i)E_s$ and $E_{y,2} = 0.5(1+i)E_o - 0.5(1-i)E_s$, $E_{x,3} = 0.5(1-i)E_o + 0.5(1+i)E_s$ and $E_{y,3} = 0.5(1-i)E_o + 0.5(1+i)E_s$, $E_{x,4} = 0$ and $E_{y,4} = iE_o - iE_s$ .where i is the imaginery unit. The sample is illuminated by a laser light at wavelength λ = 0.6328 μm. The phases φ_o and φ_s, of the complex amplitudes E_o and E_s of the sheared light beams are formed as partially overlapping parts of the phase $\varphi_{total} = \varphi_{sp} + \varphi_d$ composed by the speckle phase, φ_{sp}, uniformly distributed from 0 to 2π, and phase, $\varphi_d = 4\pi d/\lambda$, related in the modeled case to the out of plane object displacement, d, due to the experienced deformation. Both φ_{sp} and φ_d depend on spatial coordinates

and time. Temporal correlation in φ_{sp} is described by the normalized temporal correlation function, $\rho(\tau)$, where the time lag, τ , may vary in space and time. The complex amplitudes E_o and E_s are found from $E_{o,s} = FT^{-1}\left\{H \cdot FT\{E'_{o,s}\}\right\}$ where $E'_{o,s}$ are corresponds to light falling on the camera, $FT\{\cdot\}$ denotes Fourier transform and H is a *circ* function in the Fourier domain with a cut-off frequency equal to $N_x\Delta D/(2\lambda f)$, where D and f are, the diameter and the focal distance of the camera objective and we assume $N_x = N_y$. By varying the parameters of the cut-off frequency, speckle of different size and contrast is generated. The phase estimate at each moment is calculated as $\hat{\varphi} = atan\left(\frac{i_2 - i_3}{i_1 - i_4}\right)$. We used the model of a linearly increasing in time displacement given by $d(x = p\Delta, y = q\Delta, t = s\Delta t) = sf(p,q),\ p,q = 1,2,..,N_{x,y}$, and $f(p,q)$ describes the deformation model. We assume that the displacement is accompanied by correlated in time evolution in speckle described by $\rho(\tau) = exp(-\tau/\tau_{corr})$ at constant temporal correlation radius, τ_{corr} , across the object for the current simulation. As a first object, we modelled a flat plate subjected to out of plane bending only along x-axis with $f(p,q) = -0.09492(p - p_0)^2/p_0^2$ with p = 1,2...1200 and $p_0 = 600$. The other parameters are $N_x = N_x = 1024$ and $S = 300$, shear of 110 pixels along the x-axis is applied. Figure 1 presents variation of the difference $i_2 - i_3$ in time at low ($\tau_{corr} = 500\Delta t$) and high ($\tau_{corr} = 5\Delta t$) speckle evolution at a given pixel and the corresponding filtered unwrapped phase maps calculated as the difference of the 2D phase distributions at the end and the start of the measurement. The sinusoidal profile of the fringes is clearly seen at low speckle evolution while they are rather distorted for the fast-changing speckle. Nevertheless, the phase is correctly restored even in this case.

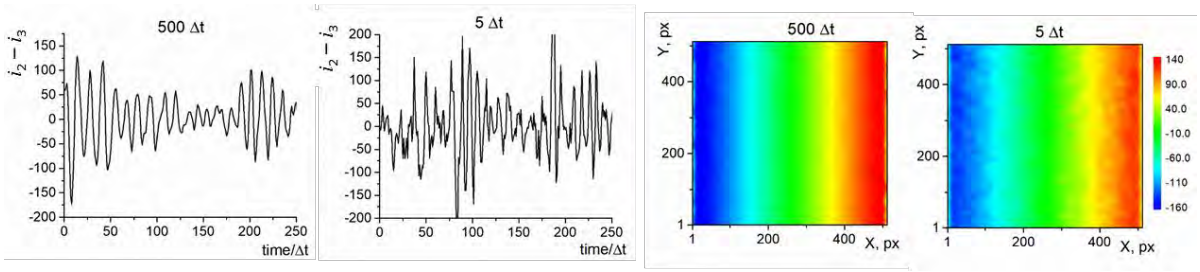

Fig. 1. Intensity fringes at a single pixel (left) and filtered unwrapped phase maps showing the difference between the final and initial states of the flat plate subjected to out-of-plane displacement at low and high speckle evolution.

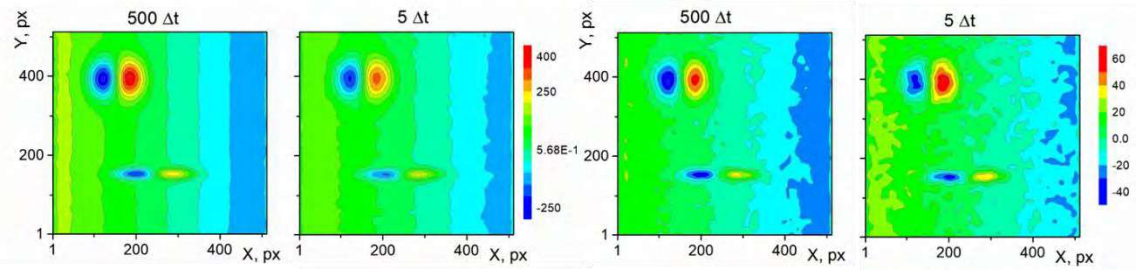

Fig. 2. Filtered unwrapped phase difference of the final and initial states of the flat plate with two local defects subjected to out-of-plane bending at low and high speckle evolution; (a,b) - $f_1(p,q)$, (c,d) -$f_2(p,q)$.

Next, we modeled two plates with local defects for models $f_1(p,q) = 0.09492(p - p_0)^2/p_0^2 + 0.10125exp(-A) + 0.0759exp(-B)$ and $f_2(p,q) = 0.01582(p - p_0)^2/p_0^2 + 0.0169exp(-A) + 0.0189exp(-B)$ where $A(p,q) = 0.0028(p - 0.9p_0)^2 + 0.00008(q - 1.2p_0)^2$ and $B(p,q) = 0.00011(p - 0.6p_0)^2 + 0.00018(q - 0.4p_0)^2$. The same shear was applied. The phase maps in radians are shown in Fig.2 at low and high speckle evolution. We see reliable detection of the defects both for the strong and left deformations and even in the case of high speckle evolution.

This work was supported by the Bulgarian National Science Fund (BNSF) under projects КП-06-КОСТ/14, and the Project BG16RFPR002-1.014-0006 „National Centre of Excellence Mechatronics and Clean Technologies“. Research is conducted in the framework of COST Action CA21155 HISTRATE.

References

[1] Stoykova, E., Madjarova, V., Ivanova, G., Ivanov, B., Berberova-Buhova, N., Numerical simulation tool for speckle-based NDT systems: ESPI, shearography and laser speckle photometry. HISTRATE Conference 2025 - Book of Abstracts, pp. 93-94, 2025, https://doi.org/10.5281/zenodo.16962743.

[2] Yan P, Liu X, Wu S, Sun F, Zhao Q, Wang Y., Pixelated Carrier Phase-Shifting Shearography Using Spatiotemporal Low-Pass Filtering Algorithm. Sensors 19(23): 5185, 2019, https://doi.org/10.3390/s19235185.

Microring Resonators for Impact Sensing in Plates

Alicja Szostak [1, 2], Rohan Soman [2, *]

[1] *Faculty of Applied Physics and Mathematics, Gdansk University of Technology, Gdansk, Poland*

[2] *Institute of Fluid Flow Machinery, Polish Academy of Sciences, Gdansk, Poland*

[*] *rsoman@imp.gda.pl*

Summary:

This study evaluates the application of Microring Resonators (MRRs) for structural health monitoring, focusing on the sensing of impact events across diverse material substrates. A hybrid modeling framework, combining the Finite Element Method (FEM) and Coupled Mode Theory (CMT), was developed to simulate MRR optical responses to signals generated by impact forces in plates, examining how the sensor's position relative to the impact source affects signal acquisition and sensitivity.

1. Introduction

Structural Health Monitoring (SHM) is defined as the continuous monitoring of a structure's condition during operation through integrated sensor systems [1]. Due to its significance and broad range of applications—spanning civil infrastructure, industrial systems, and aerospace—numerous recent studies have evaluated various methodologies for this task. Among these, optical sensors, such as Fiber Bragg Gratings (FBGs), have gained significant attention. Another, less studied approach is integrating MRRs, which offer superior sensitivity and compact dimensions. A typical MRR configuration consists of a straight bus waveguide placed near a closed-loop waveguide (Fig. 1).

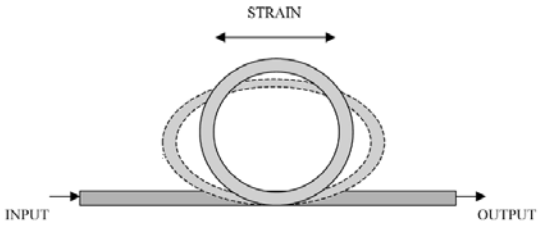

Fig. 1. Schematic representation of the effect of strain on the microring resonator geometry [2]

The interaction between these two structures is governed by the phenomenon of an evanescent field coupling, which allows for the exchange of optical power. Similarly to FBGs, the optical reaction of MRRs to the change in such parameters as the temperature or applied strain is based on the shift in the resonance wavelength. For MRR, the resonance condition can be presented as follows:

$$m\lambda_{res} = n_{eff}L,$$

Where m is an integer, λ_{res} is the resonant wavelength, n_{eff} is the effective refractive index, and L is the circumference of the sensor. The change in resonant wavelength caused by strain and temperature depends on both the change in the length of sensor's waveguide and its effective refractive index [2]:

$$\frac{\Delta\lambda}{\lambda} = \frac{\Delta L}{L} + \frac{\Delta n_{eff}}{n_{eff}}.$$

Combining high sensitivity with a small footprint, MRRs offer a promising approach for impact monitoring through their ability to translate impact-induced elastic Lamb waves into precise optical signals.

2. Methodology

The study utilizes a hybrid modeling approach, combining numerical and analytical methods to simulate the optical response of MRRs to guided waves. The FEM is employed to model the propagation of Lamb waves generated by impact forces in plates. The dynamic strain fields obtained from the numerical simulations are integrated into an analytical model based on CMT. This model accounts for the elasto-optic effect and the geometric deformation of the MRR, translating mechanical vibrations into optical signals.

3. Results

The evaluation of the MRR's performance was based on its sensitivity of response to dynamic strain fields. Numerical simulations (Fig. 2) successfully captured the propagation of Lamb waves across the plate. The integration of these strain fields into the advanced MRR analytical model revealed a high fidelity in translating

mechanical vibrations into optical spectral shifts. Figure 3 illustrates the simulated spectral response of the MRR at three distinct time steps following the impact: before it reaches the sensor and for maximum positive and negative strain amplitudes. This dynamic shift confirms the sensor's capability to track the full wave profile, demonstrating that MRRs can effectively serve as high-resolution detectors for impact-induced vibrations in structural health monitoring. Furthermore, simulations of impact events from various directions were conducted, with results demonstrating the omnidirectional sensitivity of the circular MRR, which allows for effective strain capture and consistent signal acquisition, regardless of the wave propagation direction relative to the sensor.

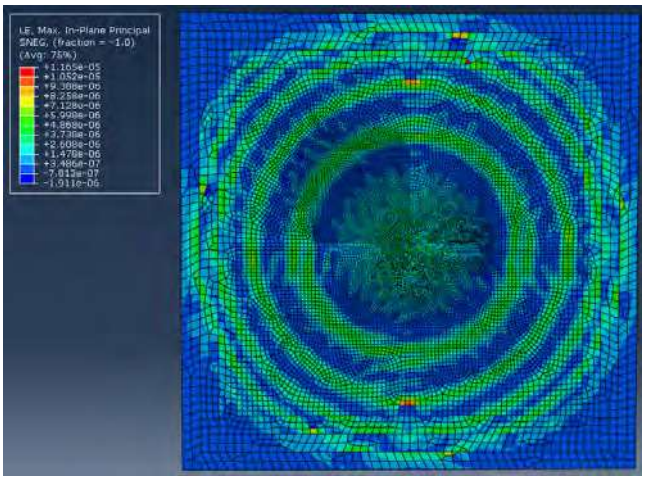

Fig. 2. Numerical simulation of guided wave propagation induced by the impact force

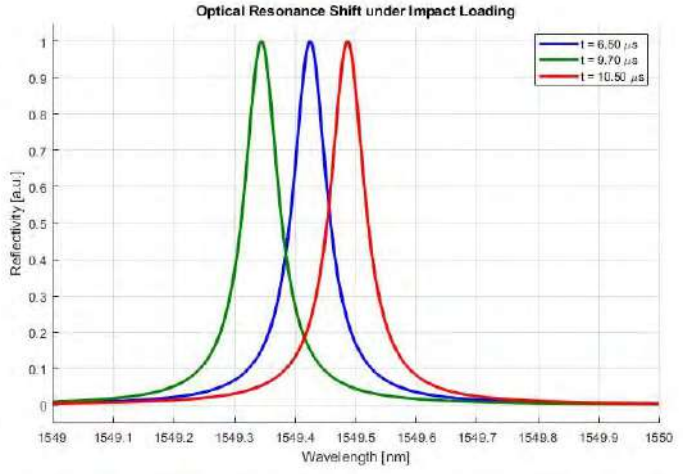

Fig. 3. Simulated MRR optical response under impact loading

4. Conclusion

This study demonstrates the significant potential of MRRs for impact sensing, providing a theoretical framework that invites future experimental validation. Subsequent research could focus on evaluating alternative resonator geometries, such as elliptical or racetrack configurations, to optimize signal acquisition.

References

[1] Kralovec, C., & Schagerl, M. (2020). Review of structural health monitoring methods regarding a multi-sensor approach for damage assessment of metal and composite structures. *Sensors*, *20*(3), 826.
[2] Bhola, B., Song, H.-C., Tazawa, H., & Steier, W. H. (2005). Polymer microresonator strain sensors. *IEEE Photonics Technology Letters*, *17*(4), 867–869.

Acknowledgements

Dr Rohan Soman acknowledges the funding support of National Science Center, Poland, grant number: 2024/55/B/ST8/00272.

Frequency-Wavenumber Domain Guided Wave Mode Superposition Imaging for Surface Damage Characterization of Composite Materials

Yang Zhang[1], Ziping Wang[2], Wieslaw Ostachowicz[1]

[1]Mechanics of Intelligent Structures Department, Institute of Fluid-Flow Machinery, Polish Academy of Science, 80-231 Gdańsk, Poland

[2]Faculty of Civil Engineering and Mechanics, Jiangsu University and National Center for International Research on Structural Health Management of Critical Components, 212013 Zhenjiang, China

Corresponding author: Yang Zhang, yzhang@imp.gda.pl

Abstract

Ultrasonic Lamb wave non-destructive testing technology has a wide application in the damage detection of plate-like structures due to its high detection efficiency, suitability for large-scale detection and the ability to recognize small-scale damages. The frequency wave number (f-k) domain filtering method was adopted. According to the corresponding relationship between the propagation direction of the guided wave and the f-k matrix, combined with the characteristics of the difference in wavenumbers of different modes of guided waves at the same frequency, a three-dimensional (3D) window function was constructed to realize the extraction of different modes and their corresponding damage reflection signals. The Common Source Method (CSM) f-k domain imaging method was used to achieve single-modal damage imaging. Finally, the data fusion imaging method was used to split the modal damage imaging and the accuracy of damage imaging was further improved.

Keywords: Damage detection, composite materials, damage imaging, frequence wavenumber, SHM

I Introduction

In the detection process of the board structure based on Lamb wave, the Lamb wave signal containing the damage feature in the receiving board is generated by the information analysis, extraction time and other information. In addition, detect and identify whether there is damage and location in the structure. Due to the limitations of linear arrays in detection ranges, Rajagopalan et al. **Error! Reference source not found.** chose a circular array with a weak anisotropic Lamb wave mode. Assuming t hat the direction of phase velocity and group velocity of Lamb wave were consistent in local directions, one through-hole damage in a composite laminate was located. Subsequently, Vishnuvardhan et al.[2] also used a ring array to achieve the impact layer damage imaging in a quasi-homogeneous composite laminate. Yu et al. [3,4] determine the value of array spacing by studying the relationship between wave-number curves and array spacing, and design matrix-type phased arrays. Yu's team introduced the SLDV equipment in the experiment. Wang et al. [5] first proposed the use of the Lamb wave combined with sparse sensing arrays to solve the problem of high array costs. Due to the small number of sensors used, it is not possible to obtain enough spatial wave field information, and it is difficult to achieve high-precision imaging of structural damage due to the large influence of the Lamb wave dispersion effect. In view of the above deficiencies, a multimodal damage imaging fusion method is proposed, which can fully consider the multimodal effect of the guide wave and comprehensively weight the damage imaging results of multiple modes in the guide wave, so as to further improve the accuracy of damage imaging

II Experiments

The simulation model shown in Fig. 1 is established in the COMSOL software. The size of the plate in Fig. 1(a) is 200 mm×200 mm×1 mm, the location of the excitation point is selected to be one-third of the length from the lower edge and the left edge, the size of the excitation source is selected as 6 mm in diameter, and the through-hole damage size is selected as 8 mm, its position being set to (68.67 mm, 91.33 mm). The red area is the data acquisition area, and the grid division size is set to 0.35 mm. The specific division details are shown in Fig. 1(b). The grids of the damage area and the signal excitation area are encrypted, and the rest of the area uses a 0.35 mm mesh grid, and sweep along the thickness direction

to set up two layers. The guided wave signal in the scanning area is extracted and imported into the imaging algorithm for post-processing.

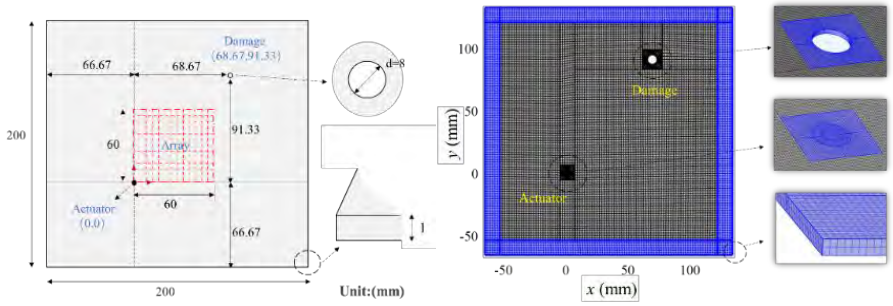

(a) (b)

Fig. 1. (a) Geometric model. (b)Meshing. Schematic diagram of finite element modelling

III Conclusion

Fig. 2 shows the *f-k* domain CSM imaging result, where the black circle in the figure is the actual location of the damage. Fig. 2(a) is the imaging result of a single A_0 mode, and Fig. 2 (b) is the imaging result of a single S_0 mode. Compared with Fig. 2 (a) and (b), the imaging area of the A_0 mode is greater than that of the S_0 mode. The range is relatively small in terms of modalities. At the same time, compared with the results of time-domain single-modality imaging, the imaging area has a smaller width, and the damage area is more concentrated. The 3D imaging results in Fig. 2 (c) and (d) are obtained, where Fig. 2 (c) is the imaging result of the superimposition of the two modal amplitudes, and Fig. 2 (d) is the imaging result of the value superposition method. After comparison, the amplitude full multiplication positioning result basically coincides with the damage, which shows that the superposition of the damage results of the two modes can reduce the damage range and improve the imaging accuracy of the damage. The high-pixel area of damage imaging is more concentrated, and the positioning effect is better, indicating that the *f-k* domain CSM imaging algorithm that considers all frequency components in the frequency band has higher imaging accuracy.

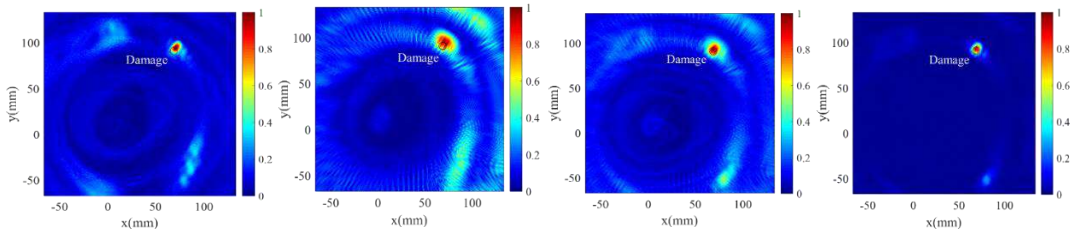

(a) (b) (c) (d)

Fig. 2. (a) A_0 modal imaging. (b) S_0 modal imaging. (c) S_0, A_0 modal amplitude full plus imaging. (d) S_0, A_0 modal amplitude full multiplicative imaging. *f-k* domain imaging results.

References

[1] Ajagopalan J, Multila K, Balasubramaniam K, Krishnamurthy C. “A phase reconstruction algorithm for Lamb wave based structural health monitoring of anisotropic multilayered composite plates,” J*ournal of The Acoustical Society of America,* vol.119, pp. 872–878, Mar. 2006.

[2] Vishnuvardhan J, Muralidharan, A, Krishnamurthy, C V, Balasubramaniam K. “Structural health monitoring of anisotropic plates using ultrasonic guided wave STMR array patches,” *NDT and E Int*. vol. 42, pp. 193–198, Dec. 2009.

[3] Yu L, Tian Z. “Guided wave phased array beamforming and imaging in composite plates,” *Ultrasonics*, vol. 68, pp. 43-53, Nov. 2016.

[4] Tian Z. “Structural health monitoring of power plant structures using ultrasonic guided waves,” *North China Electric Power University,* Jun. 2016.

[5] Gorgin G. Wang Z. “Structural damage identification based on principal curvatures of mode shape,” *International Journal of Acoustics and Vibration*, vol. 25, no. 4, pp. 566-576, Sep. 2020.

Non-destructive investigation of basalt-based laminates by shearography and ESPI

Pietro Russo,[1] Melania Paturzo,[2] and Vito Pagliarulo,[2*]

[1] *Institute for Polymers, Composites and Biomaterials-IPCB, National Research Council, Via Campi Flegrei 34, 80078, Pozzuoli, Naples, Italy*

[2] *Institute of Applied Sciences and Intelligent Systems-ISASI, National Research Council, Via Campi Flegrei 34, 80078, Pozzuoli, Naples, Italy*

[*] *vito.pagliarulo@cnr.it*

Abstract: Recently, growing interest in the use of natural reinforcing fibers has led to the development of new materials that share the same advantages as conventional composite systems while being environmentally friendly. In this work, the use of shearography and ESPI as a non-destructive investigation method in full field and non-contact mode was tested on basalt-based laminates.

1. Introduction

Over recent years, the use of advanced composite materials in aeronautical, automotive and sporting applications has been consolidated. Typical and well-established characteristics of composite materials such as weight reduction, resistance to fatigue and corrosion make them competitive in many cases compared to conventional ones. However, it is unavoidable that these materials, generally reinforced with carbon or glass fibres, require complex, expensive and non-environmentally friendly production processes, and consequently are not in themselves "green". Thus, in recent decades, the use of natural reinforcing fibers has gained increasing attention, allowing the development of new materials that share the same advantages as conventional composite systems while respecting the environment. Promising results have been found for resins, even those of biological origin, loaded with both natural fibres such as jute, linen and hemp, and mineral ones such as basalt. Due to their structural complexity, these materials are not always compatible with the use of standard non-destructive evaluation methods, such as ultrasonic testing. In this work, the use of Electronic Speckle Pattern Interferometry and Shearography as a non-destructive investigation technique in full field and in non-contact mode were considered to test various basalt-based laminates.

2. Materials and methods

In this work, different typologies of specimens and loads have been considered.

1) For the first case, a polypropylene matrix provided by Songhan Plastic Tech. Co. Ltd. (Shangai, China) and a plain wave basalt fabric (areal weight: 210 g/m2) from Incotelogy GmbH (Pulheim, Germany) were used for specimens' preparation. The polymer matrix, either as-is (PP) or pre-modified (PPC) by adding 2% by weight of a coupling agent (Polybond 3000 from Chemtura, USA), was preliminarily melt-filmed. The laminated specimens were obtained by alternating polymer films and basalt fiber fabrics and subsequent hot compaction of the stacked system. Subsequently, impact tests were conducted at various energy levels (U = 3, 8, 15 J) using a drop-weight machine to examine the initiation and progression of damage by shearography on 100x150 mm specimens.
2) 2) In the second case, composites based on polyamide 6 (from BASF) as the matrix and a plain corrugated basalt fabric (weight: 210 g/m2) from (Incotelogy GmbH) as reinforcement were considered. Specimens with dimensions of 100 mm × 12.7 mm were obtained from the hot-compacted laminates and used for three-point bending tests on a universal mechanical testing machine (model Instron 4301). Measurements were carried out according to ASTM-D790 at a crosshead feed rate of 5 mm/min, using a 1 kN load cell and a 70 mm rotation set, regardless of the thickness of the specimens. Flexural damage was analyzed by shearography.
   Finally, non-destructive analyses were performed on reference polypropylene/woven basalt fiber laminates (12 plies) and similar laminates but made up of layers preliminarily stitched at the edges, compacted under the same temperature and pressure conditions. Both samples were cut with a diamond wheel into square 100 mm × 100 mm specimens intended for subsequent low velocity impact tests which damages were evaluated by ESPI.

Shearography and ESPI belong to the speckle-based NDT techniques capable of full field and real time measurements on the displacement (for shearography gradient of the) of the specimens after a perturbation (for example thermal heating) [1].

3. Results and discussion

The following figures show the results obtained by shearography and ESPI.

Fig. 1 shows the wrapped phase of shearogram for specimens belong to case 1) after a low-energy impact (3J). For PPC the impact damage essentially disappears while, for the specimen with polypropylene only, it is clearly visible.

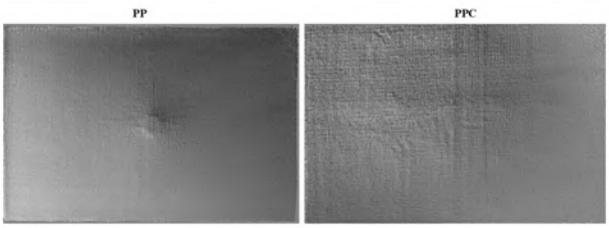

Fig. 1 Shearogram after 3J impact of specimen without coupling agent (left) and with *ca* (right).

For flexural test (2), Fig. 2 highlights the damaged zone revealed by shearography (yellow ring) that can be referred to a delamination.

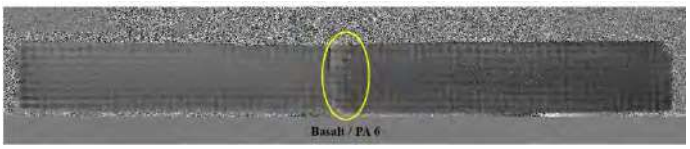

Fig. 2 Shearogram after flexural test of basalt/PA specimen.

The results for last case (3) are shown in Fig. 3. Looking at figure, the damaged area after impact (energy of 40J) is highlighted by yellow ring while cracks propagation is indicated by green arrow. It is also visible the effect of the stitchs (red arrow) which scheme is reported on the left.

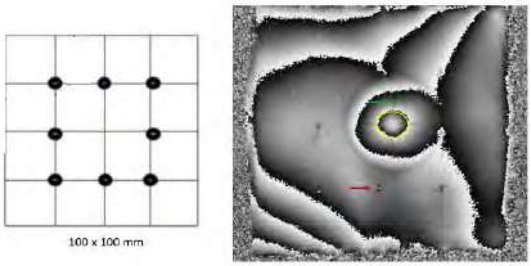

Fig. 3 Stich scheme (left), phase map by ESPI (right).

In summary, the examples shown demonstrate how shearography and ESPI are valid techniques for the non-destructive testing of basalt fiber-based laminates with relevant industrial application potential thanks to their environmental sustainability [2-4].

4. References

[1] Francis, D., Tatam, R.P., and Groves, M.R., “Shearography technology and applications: a review” Meas. Sci. Technol. 21 (2010) 102001 (29pp).
[2] Pagliarulo, V., Saltarelli, C., Paturzo, M., Papa, I., Russo, P. “Defect and Damage Detection in Green Laminates Using Shearography” DRMS 2025. Proceedings in Engineering Mechanics.
[3] Pagliarulo, V., Saltarelli, C., Paturzo, M., Russo, P., “The use of shearography for non-destructive evaluation of damage in “green” composite laminates” Proc. of SPIE Vol. 13436 1343618-6 (2025).
[4] Cigliano, C., Donadio, F., Lopresto, V., Papa, I., Pagliarulo, V., Russo, P., “Stitching Effect on Impact Behaviour of Composite Materials” European Workshop on Structural Health Monitoring. EWSHM 2022. Lecture Notes in Civil Engineering, vol 254. Springer (2022).

Textile-Fiber-Based Metamaterial Structures for Impact Detection and Damage Characterisation: A Review of Multi-Modal Sensing Approaches

Amine Haj Taieb,[1] Souha Koubaa,[2 *]

[1] *ISAMS, University Of Sfax, 2002, Sfax Tunisia*

[2] *ISAMS, University Of Sfax, 2002, Sfax Tunisia*

Summary: Textile-based metamaterial composites are emerging as promising structures for impact mitigation and adaptive structural health monitoring. This paper presents a review survey of recent developments in textile-fiber-based metamaterial architectures designed for high-strain-rate applications and impact detection. Particular attention is given to multi-modal sensing strategies combining acoustic emission, strain sensing, and high-speed imaging to monitor damage initiation and propagation. The review highlights how engineered textile architectures enable tunable mechanical behaviour and improved energy absorption. Integrating sensing technologies within these structures offers new opportunities for advanced composite systems capable of real-time impact detection and damage characterisation.

Main Text

1. Introduction

Advanced composite materials are widely used in aerospace, automotive, and protective structures because of their high strength-to-weight ratio and excellent mechanical performance. However, their vulnerability to **impact damage and high strain-rate loading** remains a critical challenge for structural reliability and safety.

Recent developments in **mechanical metamaterials** have introduced new opportunities for designing composite structures with engineered architectures capable of controlling deformation, energy absorption, and wave propagation. In particular, **textile-fiber-based metamaterial structures,** such as woven, braided, and lattice textile architectures, have demonstrated promising potential for impact mitigation and adaptive structural behaviour.

At the same time, advances in **multi-modal sensing technologies** are transforming structural health monitoring approaches for composite structures. By integrating different sensing modalities, it becomes possible to capture multiple physical signatures of damage events, improving detection accuracy and enabling real-time monitoring.

This paper presents a **review survey of textile-based metamaterial composite structures and their integration with multi-modal sensing systems for impact detection and damage characterisation**.

2. Textile-Based Metamaterial Architectures

Textile manufacturing techniques offer unique possibilities for creating **hierarchical and architectured composite materials** with tailored mechanical responses. Structures such as 3D woven composites, braided reinforcements, auxetic textile patterns, and lattice-inspired fabrics can act as **metamaterial architectures** capable of modifying stress distribution and impact energy dissipation.

These textile-based metamaterials exhibit several advantages:

- Tunable stiffness and energy absorption properties
- Lightweight and flexible structural configurations
- Enhanced damage tolerance and progressive failure behaviour
- Compatibility with bio-based or hybrid fibre systems

Recent studies demonstrate that textile metamaterials can significantly improve **impact resistance and deformation control under high strain rate conditions**.

3. Multi-Modal Sensing for Impact Detection

Monitoring the dynamic behaviour of metamaterial composite structures requires advanced sensing techniques capable of capturing different physical phenomena during impact events.

Several sensing modalities have been investigated in the literature, including:

- **Acoustic emission sensors**, which detect micro-crack initiation and fibre breakage
- **Strain and deformation sensors**, providing quantitative information on structural response
- **High-speed imaging**, enabling visualisation of damage propagation and deformation mechanisms
- **Embedded fibre-optic sensing systems**, which offer distributed strain monitoring

The combination of these sensing approaches forms a **multi-modal sensing framework** capable of significantly improving the reliability of damage detection and structural health monitoring in composite systems.

4. Discussion and Future Perspectives

The integration of **textile metamaterial architectures with multi-modal sensing technologies** opens new perspectives for advanced composite structures capable of adaptive behaviour and real-time damage detection.
Future research directions include:

- Development of **smart textile metamaterials with embedded sensing capabilities**
- Integration of **data-driven approaches and machine learning** for damage detection
- Investigation of **high strain-rate behaviour using advanced experimental techniques**
- Application of these systems in **lightweight protective structures and sustainable composite materials**

These developments contribute to the advancement of **certification-by-analysis methodologies**, a key objective in the design and validation of next-generation composite structures.

References

[1] Bertoldi, K., Vitelli, V., Christensen, J., and van Hecke, M., 2017, "Flexible mechanical metamaterials," *Nature Reviews Materials*, 2, 17066.
[2] Chen, Y., Scarpa, F., and Farrow, I., 2013, "Composite textile metamaterials for energy absorption," *Composite Structures*, 98, pp. 120–128.
[3] Balageas, D., Fritzen, C., and Güemes, A., 2010, *Structural Health Monitoring*, Wiley.

Laser Speckle Photometry of Composites under Tensile Loading

Violeta Madjarova,[1,2,*] Elena Stoykova,[1,2] Briek Luyten[3]. and Patricia Verleysen[3]

[1] *Institute of Optical Material and Technologies, Bulgarian Academy of Sciences, Acad. G. Bonchev Str. 109. 1113 Sofia, Bulgaria*

[2] *National Centre of Excellence "Mechatronics and Clean Technologies", Kliment Ohridski Blvd., Block 8, 1700, Sofia, Bulgaria*

[3]*Materials Science and Technology-DyMaLab, EMSME Department, Ghent University, Technologiepark 46, 9052 Ghent, Belgium*

[*] vdmadjarova@gmail.com, vmadjarova@iomt.bas.bg

Summary: This study presents testing of composite materials using tensile loading and laser speckle photometry (LSP). The LSP is an intensity-based method, which enables tracking the processes within the objects at high spatial and temporal resolution. Statistical processing of sequences of laser speckle patterns formed on the surface of the composite materials during the tensile tests provides different correlation-based parameters and reveals the potential of LSP for materials characterization.

1. Introduction

LSP is a single-beam coherent optical technique exploiting high sensitivity of speckle to micro-changes of topography and/or refractive index due to various processes as e.g. deformation or heating [1-2]. Digital image processing of time-varying speckle patterns extracts reliable statistical parameters for materials characterization and damage inspection. We used LSP for observing the behaviour of different composite materials subjected to tensile loading. Two composite materials were used: a plain-weave basalt-fibre reinforced epoxy, denoted as CM-1, and a satin-weave E-glass-fibre reinforced epoxy, denoted as CM-2. For both materials, off-axis shear samples were used, inclined by 45° relative to the warp direction, each with 10 plies.

2. Laser speckle photometry in tensile testing

We conducted the experiment using the optical set-up illustrated in Fig. 1. The light from the He-Ne laser (LASOS Lasertechnik at λ = 633 nm) passes through a half-wave plate (HWP) with a fast axis at 45º to the horizontal axis, and a quarter wave plate (QWP) with its fast axis oriented at 0º to the horizontal axis, to become left circularly polarized (LCP). Both the HWP and the QWP have λ/10 surface accuracy. Next, the beam is expanded to a beam with cross-section diameter of 40 mm by the beam expander (BE) to illuminate the specimen. The resultant speckle patterns were captured sequentially by a camera (BASLER acA4096-30um) positioned at a small angle to the optical axis. The acquisition rate was set to 96 fps for both samples. The tested samples, CM-1 and CM-2, were subjected to tensile loading at a constant crosshead speed using an AMETEK Lloyd Instruments LRX Plus tensile machine, with a capacity of 5 kN. For CM-1, the tensile speed was set to 5 mm/min, while for CM-2 it was set to 2.5 mm/min. For both samples, the loading limit was set to 4850 N. Time-dependent loading curves for CM-1 and CM-2 are presented in Fig. 1. The curve for CM-1 exhibits a sudden drop in the load, indicating that the sample fractures at a load of 3402.9 N. In contrast, the curve for CM-2 indicates that the sample did not fracture before the testing machine reached its load limit.

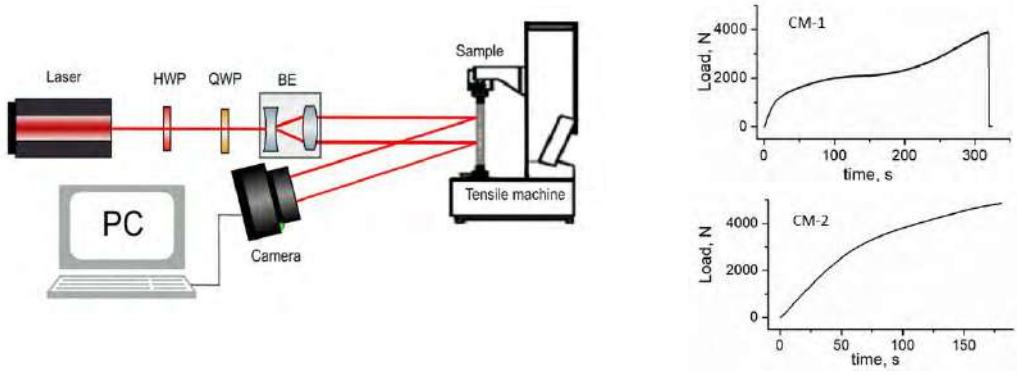

Fig. 1. Optical set-up for tensile laser speckle photometry (HWP and QWP – half-and quarter wave plates, BE – beam expander) and loading curves for the tested composite materials CM-1 and CM-2.

Data processing included pixelwise calculation of the estimates of the mean, $\bar{I}_{x,y} = \frac{1}{N}\sum_{n=0}^{N} I_{x,y;n}$, , and the variance, $\hat{v}_{x,y} = \frac{1}{N}\sum_{n=0}^{N}(I_{x,y;n} - \bar{I}_{x,y;n})^2$, of intensity, $I_{x,y;n}$, at point $(x\Delta, y\Delta)$ and time instant $n\Delta t$ for a sequence of N = 400 images of size $N_y \times N_x$ pixels at pixel period Δ = 3.45 μm and the sampling period between two

successively acquired images Δt . We applied a normalized processing due to the signal-dependent nature of the speckle intensity fluctuations, estimating the normalized temporal correlation function (NTCF) $\Gamma(x,y;m) = \frac{1}{(N-m+1)\hat{v}_{x,z}}\sum_{n=0}^{N-m}\left(I_{x,y;n} - \bar{I}_{x,y}\right) \times \left(I_{x,y;n+m} - \bar{I}_{x,y}\right)$ at time lag $m\Delta$t. The NTCF contour maps at 50 s after the start of the test are presented in Fig. 2 for time lags corresponding to m = 1, 10, 20, 30 and 40 in the case of CM-1. Each of the presented activity maps shows the same mean value and spread of the estimate fluctuations across the map. The mean value falls with the time lag. To characterize the tested material, we chose a region of 500 by 500 pixels and found the average value of the NTCF at a given time lag. Figure 3 gives the variation of the average NTCF-value during the test for CM-1 and CM-2; the plotted curves correspond to m = 1, 10, 20, 30 and 40. The results are completely different for both tested materials. After some short transient interval, the NTCF for CM-1 falls from 1 to levels less than 0.5 becoming narrower until the break of the material. The NTCF level of 0.5, which may be regarded as a threshold for substantial correlation, is observed at time lags decreasing from $40\Delta t$ to $10\Delta t$ during the test. On the contrary, the NTCF of CM-2 remains the same for the whole period of tension and the NTCF level 0.5 corresponds to a time lag close to $40\Delta t$.

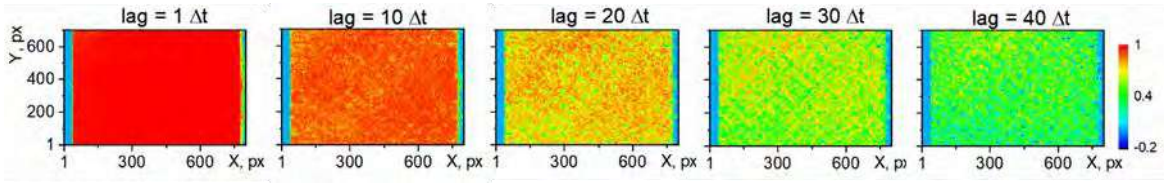

Fig. 2. Activity maps as 2D distributions of NTCF estimate at increasing time lags 50 s after the start of the tension for the composite CM-1.

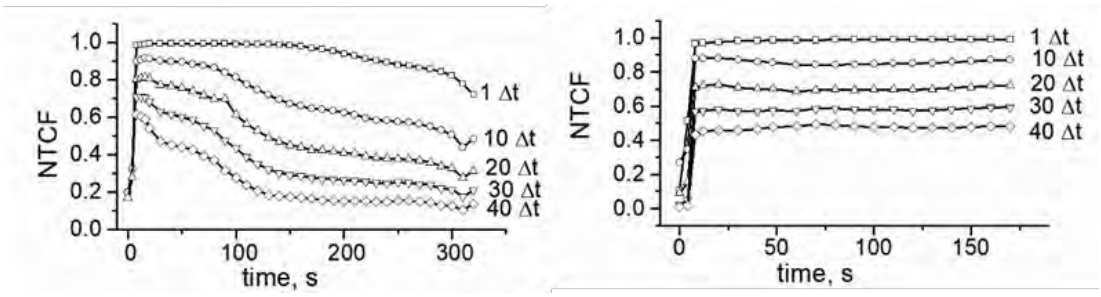

Fig. 3. Average NTCF value during the test at increasing time lags; left – CM-1, right – CM-2.

In summary, we confirmed the efficiency of laser speckle photometry for the characterization of composite materials during tensile testing, by correlation-based dynamic speckle analysis. Building an activity map as a 2D spatial distribution of a statistical parameter for an object subjected to tensile loading provides an instant picture of the speed of temporal changes across the object surface and reveals the presence of defects. A pointwise or average temporal correlation radius gives a quantitative basis for comparison of the tested materials.

Acknowledgements

This research is conducted in the framework of COST Action CA21155 HISTRATE. The work is financially supported by the Bulgarian National Science Fund under projects КП-06-КОСТ/14 and the European Regional Development Fund under „Research Innovation and Digitization for Smart Transformation“, program 2021-2027 under the Project BG16RFPR002-1.014-0006 „National Centre of Excellence Mechatronics and Clean Technologies“.

References

[1] Dang, D., Weingarten, S., Frost, F., Bendjus, B., and Scheithauer, U., 2021, “Laser Speckle Photometry investigation of the thermal conductivity of 3D printed ceramic green bodies using Multi Material Jetting,” Open Ceramics 8, art. no. 100193, https://doi.org/10.1016/j.oceram.2021.100193.
[2] Stoykova, E., Ivanov, B., and Nikova, T., 2014, “Correlation-based pointwise processing of dynamic speckle patterns,” Optics Letters 39(1), pp. 115-118, https://doi.org/10.1364/AO.52.007564.

Lamb wave dispersion for material characterization of short fiber-reinforced polymer composite plates

Patrycja Pyzik,[1,*] Jakub Spytek,[1] Łukasz Ambroziński[1] and Łukasz Pieczonka[1]

[1] *AGH University of Krakow, Faculty of Mechanical Engineering and Robotics, Department of Robotics and Mechatronics, al. Mickiewicza 30, 30-059, Krakow, Poland*

[*] *pyzikp@agh.edu.pl*

Summary: Lamb waves are widely used in structural health monitoring for damage detection in composite structures; however, their propagation is also strongly influenced by material anisotropy. This study investigates Lamb wave dispersion in short glass fiber-reinforced polymer composite plates with different fiber content (PA6-GF35 and PA6-GF50). Plate specimens were excited using a piezoelectric transducer with a chirp signal (80-800 kHz), and dispersion curves were obtained via frequency-wavenumber analysis. The results reveal noticeable differences in wave velocities and dispersion behavior, as well as pronounced anisotropy in the measured wavefields. This work highlights the potential of ultrasonic methods for material characterization and implications for reliable damage detection.

1. Introduction

Short fiber-reinforced polymer composites are widely used in engineering applications due to their favorable mechanical properties and manufacturing efficiency. However, their performance strongly depends on the underlying microstructure, in particular the distribution and orientation of fibers, which introduce significant material anisotropy. Recent studies have shown that fiber orientation plays a key role in determining the effective properties of injection-molded components, and its accurate characterization remains an active research topic [1,2].

Currently, fiber orientation and microstructural features are most commonly assessed using destructive or laboratory-based techniques, such as microscopic cross-section analysis and X-ray micro-computed tomography (μCT) [1–3]. While these methods provide high-resolution insight into internal structure, they are time-consuming, costly, and not suitable for rapid or in-situ evaluation. As a result, there is a growing need for fast and non-destructive approaches capable of capturing material anisotropy in short fiber-reinforced composites.

Ultrasonic methods, and in particular guided waves, offer a promising alternative due to their sensitivity to elastic properties and directional behavior of materials. Lamb wave propagation is directly influenced by material stiffness and anisotropy, which affect both wave velocities and dispersion characteristics. In addition, advanced signal processing approaches based on local wavenumber estimation have been successfully applied in guided wave-based damage detection in thin-walled structures [4]. Despite extensive use of Lamb waves in structural health monitoring (SHM) and non-destructive testing (NDT), their potential for material characterization in short fiber-reinforced thermoplastic composites remains relatively unexplored.

In this study, Lamb wave dispersion in short glass fiber-reinforced PA6 composite plates is investigated with the aim of assessing sensitivity to material anisotropy and fiber content. Frequency–wavenumber analysis is used to extract dispersion characteristics and compare wave propagation behavior for materials with different reinforcement levels. The results provide insight into the role of microstructure in guided wave propagation and highlight its implications for reliable damage detection in composite structures.

2. Materials and methods

Short glass fiber-reinforced polyamide (PA6) composite plates with nominal fiber contents of 35% (PA6-GF35) and 50% (PA6-GF50) were investigated. The specimens had dimensions of 100 × 100 mm and a thickness of 3 mm. The difference in fiber content was expected to result in distinct guided wave propagation characteristics, reflected in variations in dispersion behavior and anisotropy.

Lamb waves were excited using a piezoelectric transducer and a broadband chirp signal in the frequency range of 80–800 kHz. The wavefield was measured over a predefined spatial grid on the plate surface, enabling acquisition of space–time data for further analysis. Frequency–wavenumber (f–k) representations were obtained by applying a two-dimensional Fourier transform (2DFT) to the measured signals, allowing extraction of dispersion characteristics.

The dispersion curves corresponding to different propagation modes were identified from the f–k spectra and compared between the two materials. In addition, the spatial wavefields were analyzed to assess directional dependence of wave propagation and identify anisotropic effects.

3. Results

The measured wavefields revealed pronounced anisotropy in wave propagation (Fig. 1a), manifested as direction-dependent wavefront shapes and propagation characteristics. These effects are attributed to preferential fiber orientation resulting from the manufacturing process, leading to anisotropic effective material properties.

The corresponding frequency–wavenumber representations exhibited clear dispersion patterns for both investigated materials, enabling identification of dominant Lamb wave modes in the analyzed frequency range (Fig. 1b). A comparison between PA6-GF35 and PA6-GF50 showed noticeable differences in dispersion curves, particularly in terms of phase velocities of selected modes. As shown in Fig. 1c, PA6-GF50 exhibits lower wavenumbers for a given frequency, corresponding to higher wave velocities, consistent with its increased stiffness due to higher fiber content.

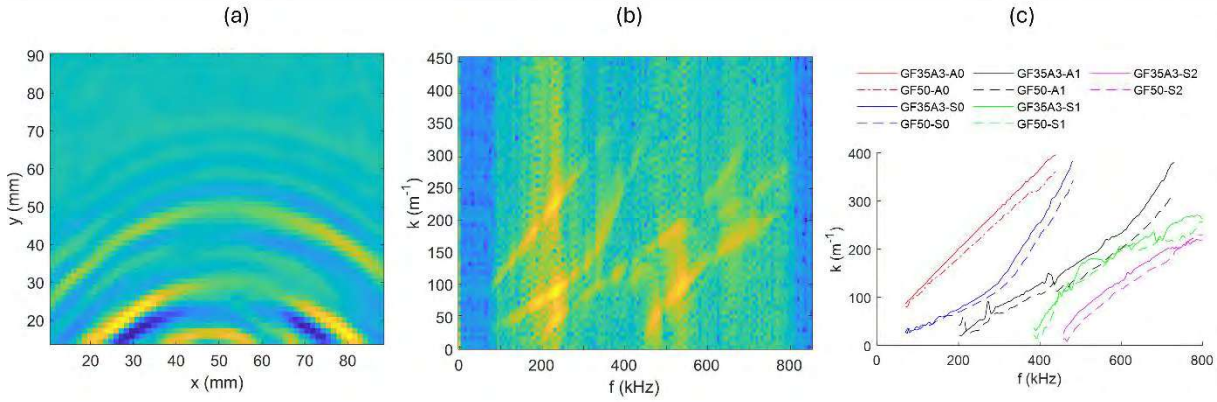

Fig. 1.(a) Example wavefield measured on a short glass fiber-reinforced PA6 composite plate, showing pronounced anisotropy in wave propagation. (b) Corresponding frequency–wavenumber (f–k) representation with clearly visible Lamb wave modes. (c) Comparison of selected dispersion curves for PA6-GF35 and PA6-GF50, with lower wavenumbers observed for PA6-GF50, indicating higher wave velocities.

4. Conclusions

The study demonstrates that Lamb wave dispersion in short fiber-reinforced polymer composites is strongly influenced by material microstructure, including fiber content and orientation-induced anisotropy. The observed differences in dispersion behavior and wavefield patterns confirm that Lamb wave dispersion analysis is sensitive to microstructure-related anisotropy in such materials.

These preliminary results indicate that ultrasonic methods are a promising tool for non-destructive material characterization of short fiber-reinforced composites. From a SHM and NDT perspective, the findings suggest that material anisotropy should be considered when interpreting guided wave signals, as it may affect damage detection performance. This opens the path towards incorporating material characterization into more reliable and robust damage detection strategies.

References

[1] Oubellaouch, A., et al., 2024, “Assessment of Fiber Orientation Models Predictability by Comparison with X-ray µCT Data in Injection-Molded Short Glass Fiber-Reinforced Polyamide,” Int. J. Adv. Manuf. Technol., 130(9–10), pp. 4479–4492.
[2] Auenhammer, F., et al., 2024, “Fibre Orientation Distribution Function Mapping for Short Fibre Polymer Composite Components from Low Resolution/Large Volume X-ray Computed Tomography,” Compos. Part B Eng., 275, p. 111313.
[3] Żurawik, R., Volke, J., Zarges, J.-C., and Heim, H.-P., 2022, “Comparison of Real and Simulated Fiber Orientations in Injection Molded Short Glass Fiber Reinforced Polyamide by X-ray Microtomography,” Polymers, 14.
[4] Spytek, J., Dziedziech, K., and Pieczonka, L., 2023, “Improving Efficiency of Local Wavenumber Estimation for Damage Detection in Thin-Walled Structures,” Mech. Syst. Signal Process., 199, p. 110470.

A Numerical Study on the Usage of Lamb Waves for Damage Detection in Fiber Reinforced Polymers

Çağatay Yilmaz,[1]

[1] *Department of Mechanical Engineering, Abdullah Gül University, Kayseri/Türkiye*

Summary: This study presents a numerical investigation into Lamb wave interaction with damage zones in composite materials, specifically tailored for high-strain-rate applications. Using high-fidelity finite element modeling, we examine how dynamic stress waves interact with localized defects, such as delamination. The research focuses on identifying wave-field perturbations and energy-scattering patterns that occur during the interaction of a Lamb wave with damage. Our results characterize the sensitivity of specific modes to impact-induced damage, providing a theoretical foundation for real-time structural health monitoring in environments where high-speed deformation and wave-to-damage coupling are critical.

1. Introduction

The rapidly increasing reliance on Fiber Reinforced Polymers (FRP) in the aerospace and automotive sectors has catalyzed a critical need for robust Structural Health Monitoring (SHM) protocols that maintain diagnostic integrity under extreme operational loading. Within the current landscape of non-destructive evaluation, Lamb waves have emerged as a premier diagnostic modality; these ultrasonic guided waves leverage low attenuation and high sensitivity to internal discontinuities to facilitate long-range inspection of thin-walled geometries. However, while Lamb waves are highly effective for initial flaw detection, transitioning to comprehensive post-damage characterization introduces significant complexity. The physical interaction of these wave modes with multifaceted damage architecture, specifically the concurrent presence of interlaminar delamination, matrix cracking, and fiber breakage, results in intricate scattering and mode conversion phenomena that challenge existing analytical frameworks and necessitate more sophisticated signal interpretation strategies.

In composite laminates, damage typically manifests as a combination of interlaminar delamination, matrix cracking, and fiber rupture. Unlike isotropic materials, the anisotropic nature of composites causes the Lamb wave velocity to be directionally dependent[1]A0 mode of the lamb wave is used to detect impact-induced damage in aircraft composite parts[2]. With the lamb wave approach, the low-velocity impact damage within composite structures can be detected [3]. When an incident Lamb wave encounters a damaged region, energy scattering occurs. This involves redistributing the wave's mechanical energy into reflected, transmitted, and converted components. The type of damage can be identified by its scattering coefficient [4]. With the scatter matrix, the size, shape, and orientation of damage can be characterized. In high-fidelity numerical models, delamination acts as a waveguide filter. A portion of the energy is "trapped" within the delaminated sub-laminates, leading to localized resonance, while another portion undergoes mode conversion. For instance, an incident S0 mode striking an asymmetric delamination will partially convert into an A0 mode, a signature that is vital for identifying the depth of the damage.

Recent studies demonstrate that numerical simulations can effectively map the Wave Damage Interaction Coefficients (WDIC), allowing researchers to predict how impact-induced damage, such as delamination, will scatter energy before a physical prototype is even built. By focusing purely on a numerical approach, this research isolates the variables damage type and damage geometry, providing a theoretical roadmap for "smart" composites capable of self-diagnosis for damage extent detection.

2. Methodology

To simulate Lamb wave propagation in laminated composites, a high-fidelity Finite Element Method (FEM) approach is employed, typically utilizing dynamic explicit integration to capture the transient nature of wave-structure interactions. The composite laminate is modeled using specialized shell or 3D continuum elements, where the stacking sequence and anisotropic material properties—defined by the stiffness matrix C_{ij}—are strictly assigned to represent the directional dependency of wave velocities. To ensure numerical stability and avoid spatial aliasing, the mesh density is refined such that at least ten elements exist per shortest wavelength (λ_{min}), while the temporal resolution is governed by the CFL (Courant-Friedrichs-Lewy) condition, ensuring the time step Δt is smaller than the time required for the wave to traverse a single element. Actuation is often modeled as a concentrated Hanning-windowed tone burst applied to specific nodes to suppress sidebands, and the resulting displacement or strain histories are extracted from "sensor" nodes to analyze mode conversion and scattering caused by embedded delamination or fiber discontinuities. Initiation of an S0-mode wave under the above-mentioned FEM presetting is shown in Figure 1.

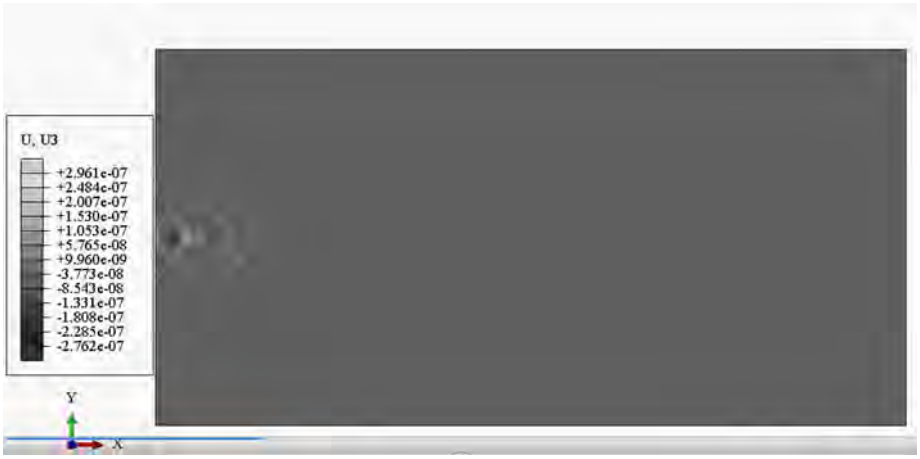

Figure 1:Initation of a symmetric Lamb wave

3. References

[1] S. Pant, J. Laliberte, M. Martinez, B. Rocha, and D. Ancrum, “Effects of composite lamina properties on fundamental Lamb wave mode dispersion characteristics,” *Compos. Struct.*, vol. 124, pp. 236–252, 2015, doi: https://doi.org/10.1016/j.compstruct.2015.01.017.

[2] H. Kaczmarek, “Lamb wave interaction with impact-induced damage in aircraft composite: use of the A0 mode excited by air-coupled transducer,” *J. Compos. Mater.*, vol. 37, no. 3, pp. 217–232, 2003.

[3] K. Zheng, Z. Li, Z. Ma, J. Chen, J. Zhou, and X. Su, “Damage detection method based on Lamb waves for stiffened composite panels,” *Compos. Struct.*, vol. 225, p. 111137, 2019, doi: https://doi.org/10.1016/j.compstruct.2019.111137.

[4] J. Zhang, B. W. Drinkwater, and P. D. Wilcox, “Defect characterization using an ultrasonic array to measure the scattering coefficient matrix,” *IEEE Trans. Ultrason. Ferroelectr. Freq. Control*, vol. 55, no. 10, pp. 2254–2265, 2008, doi: 10.1109/TUFFC.924.

Dynamic Mechanical Analysis of neat PK and two PK-GF30 Batches

Ana-Teodora Untariu [1], Denis Mădroane [1], Sergiu-Valentin Galatanu [1] and Liviu Marsavina [1]

[1] *Department of Mechanics and Strength of Materials, Politehnica University of Timisoara, Mihai Viteazu Bd., Timisoara, 300222, Timis, Romania.*

[*] *Correspondence: sergiu.galatanu@upt.ro*

Summary: This work compares the dynamic mechanical behavior of neat polyketone (PK) and two batches of glass-fiber-reinforced polyketone (PK-GF30) using flexural DMA at 0.1–40 Hz. The three samples show distinct E′, E″, and tan δ responses across the tested temperature range. Both PK-GF30 batches exhibit higher stiffness and lower damping than PK, although the two reinforced batches form separate modulus groups. The α-relaxation (Tg) is visible in all datasets through changes in E′, E″, and tan δ. Differences between the PK-GF30 batches arise from skin-core orientation effects. Only these three datasets are referenced in this abstract.

1. Introduction

Polyketone (PK) is a semicrystalline engineering polymer used in components requiring mechanical stability and chemical resistance. Reinforcement with short glass fibers (PK-GF30) significantly increases stiffness and improves the material's response under vibration and cyclic loading. Because injection-molded short-fiber composites develop an inhomogeneous skin-core microstructure, their flexural and dynamic mechanical properties depend strongly on the fiber orientation in near-surface layers. [1]

Dynamic Mechanical Analysis (DMA) is essential for characterizing stiffness, viscoelastic losses and relaxation behavior as functions of temperature and frequency. These properties are critical for numerical modelling, product design and understanding the thermomechanical stability of composites.

Although several PK-GF30 specimens were tested during the broader campaign, only the three datasets included in the DMA plots (PK-GF30 batch A, PK-GF30 batch B and neat PK) are presented and referenced in this abstract.

The purpose of this study is to evaluate the evolution of E′, E″ and tan δ with temperature and frequency, identify Tg and relaxation mechanisms, and explain the differences between materials.

2. Methodology / Experimental

DMA measurements were carried out in three-point bending, a mode strongly influenced by the outer layers of the specimen due to the linear stress distribution:

$$\sigma(y) = \frac{M\,y}{I},$$

which places maximum tension and compression at ±h/2 from the neutral axis. Consequently, DMA flexure is dominated by the skin layer, where fibers are strongly aligned. [2]

Short-fiber injection-molded composites exhibit a three-layer microstructure:

- Skin: thin external layer with highly aligned fibers in the flow direction
- Sub-skin: transitional region with moderate alignment
- Core: central region with random fiber orientation [3]

DMA tests were performed at 0.1, 0.4, 1, 4, 10 and 40 Hz, over a temperature range of approximately 25-185 °C. The following viscoelastic properties were recorded:E′ - storage modulus, E″ - loss modulus and tan δ = E″/E′ - damping factor.

E′ represents the elastic portion of the viscoelastic response under oscillatory loading. As temperature increases, E′ generally decreases due to enhanced molecular mobility. Higher frequencies restrict molecular relaxation processes, leading to higher recorded stiffness. All conclusions in this study are derived strictly from the provided E′-versus-temperature curves.

3. Results

The DMA results show a clear separation between PK-GF30 batch A, PK-GF30 batch B, and neat PK across all viscoelastic functions. The storage modulus E′ places batch A consistently at the highest stiffness level, batch B slightly lower, and neat PK significantly lower. All materials exhibit a smooth temperature-induced decrease in E′, and higher frequencies raise the modulus. The two reinforced batches follow nearly identical temperature-frequency trends, differing only in their absolute modulus values.

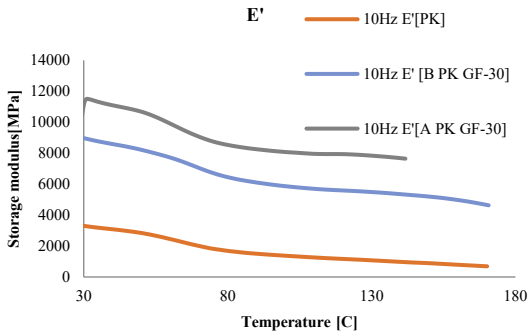

Fig. 1. E’ for all three samples at 10Hz

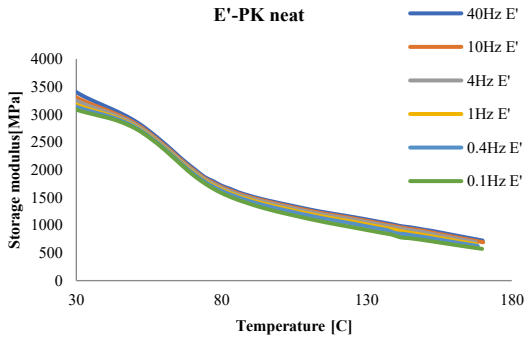

Fig. 2. E’ at all frequencies for PK neat

The loss modulus E″ follows the same hierarchy. Each material shows a low-temperature decrease leading to a minimum near 60-80 °C, followed by a rise characteristic of the α-relaxation. Batch A consistently reaches higher E″ values than batch B at elevated temperatures, while neat PK shows the lowest loss modulus due to its higher molecular mobility.

The tan δ curves confirm these trends. Neat PK displays the highest damping, whereas the reinforced materials show lower values because fiber reinforcement restricts segmental relaxation. Batch A has slightly lower tan δ than batch B, indicating more efficient stress transfer. The similar shapes and Tg positions for both reinforced batches demonstrate that their polymer-matrix relaxation behavior is the same, differing only in reinforcement effectiveness.

The Tg is identifiable in all datasets through the softening of E′, the rise in E″, and the increase in tan δ, occurring in the same temperature range for all three materials. At temperatures above roughly 150-180 °C, the frequency-dependent differences diminish, particularly for neat PK. The reinforced materials also converge, though batch A maintains higher stiffness than batch B across the entire temperature range.

The persistent separation between the two PK-GF30 batches originates from differences in fiber-orientation efficiency in the skin layer formed during injection molding. Because flexural DMA is dominated by the highly stressed surface regions, small variations in skin-layer fiber alignment or thickness lead to measurable differences in E′, E″ and tan δ. Batch A appears to have a more efficiently oriented surface region, explaining its higher stiffness, higher high-temperature E″, and lower damping compared with batch B.

4. Discussion and conclusions

The DMA results show that glass-fiber reinforcement markedly increases stiffness and reduces damping compared with neat PK. PK-GF30 batches A and B display nearly identical temperature (and frequency) dependent trends in E′, E″ and tan δ, indicating the same matrix relaxation behavior and a common Tg. Their difference lies only in reinforcement efficiency: batch A is consistently stiffer and less dissipative than batch B due to more effective fiber alignment in the skin layer, which dominates the flexural response of injection-molded short-fiber composites. Although frequency-dependent effects diminish at higher temperatures, the stiffness hierarchy PK-GF30 A > PK-GF30 B > PK remains throughout the tested range, underscoring the strong influence of microstructural orientation on dynamic mechanical performance.

5. References

[1] AKRO-PLASTIC GmbH, AKROTEK® PK-VM GF 30 (8) HU Natural 8895, Technical Datasheet, accessed March 2026.
Available at: https://akro-plastic.com/en/product/akrotek-pk-vm-gf-30-8-hu-natural-8895-en
[2] TA Instruments, Introduction to Dynamic Mechanical Analysis, TA441, New Castle, DE, USA, n.d.
Available at: https://www.tainstruments.com/pdf/literature/TA441.pdf
[3] Zhao, J., Guo, C., Zuo, X., Román, A. J., Nie, Y., Su, D.-X., Turng, L.-S., Osswald, T. A., Cheng, G., and Chen, W., 2022, Effective Mechanical Properties of Injection-Molded Short Fiber Reinforced PEEK Composites Using Periodic Homogenization, Advanced Composites and Hybrid Materials, 5, pp. 2964–2976.

EMAT-Based Detection of Interfacial Disbonds in Composites for Dynamic and High-Strain-Rate Applications

Kaleeswaran Balasubramaniam*, Borja Nuevo Ortiz, and Álvaro Pallarés Bejarano

Innerspec Technologies, Calle Sanglas 13, Madrid, Spain

* *kbalasubramaniam@innerspec.com*

Summary:

This work presents an advanced EMAT-based non-contact inspection methodology for detecting interfacial disbonds in GFRP composites subjected to dynamic and high-strain-rate conditions. Shear horizontal waves were generated and optimized through systematic coil and frequency selection to enhance defect sensitivity. Signal differentiation between bonded and unbonded regions enabled reliable identification of adhesion loss. The study demonstrates the potential of EMAT as a rapid, reusable, and robust testing tool for in-situ monitoring of composite joints in demanding loading environments.

1. Introduction

Composite materials such as Glass Fiber Reinforced Polymers (GFRP) are widely used in aerospace, automotive, and energy sectors due to their high specific strength and stiffness. Under dynamic and high-strain-rate loading, bonded interfaces may develop interfacial disbonds, delamination, or adhesion failure, making reliable defect detection essential for structural integrity. The studied specimens include a surface layer with a cross-pattern fibre orientation and internal unidirectional plies, introducing anisotropy that influences ultrasonic wave propagation.

Conventional ultrasonic methods, such as Phased Array Ultrasonic Testing (PAUT), require couplants and direct contact, limiting their use in harsh environments. In contrast, Electromagnetic Acoustic Transducers (EMATs) enable non-contact ultrasonic inspection. For GFRP materials, a magnetostrictive tape is externally applied to enable wave generation and enhance the Signal-to-Noise Ratio (SNR), while avoiding permanent adhesion to the specimen surface.

Shear Horizontal (SH) waves are particularly suitable for detecting interfacial defects due to their sensitivity to bonding conditions and minimal mode conversion. While EMAT inspection has been widely demonstrated in metallic structures [1–2], fewer studies address bonded composite interfaces [3-4] under dynamic loading.

This work investigates coil geometry and excitation frequency optimisation to improve defect sensitivity in GFRP composite joints, aiming to develop a rapid and production-compatible inspection approach for detecting interfacial disbonds.

2. Development and Results

The EMAT inspection of GFRP composite I-beams demonstrated a good distinction between bonded and unbonded regions. Variations in received signal amplitude and waveform characteristics were observed in locations corresponding to disbonded areas. The pitch–catch inspection approach proved effective for continuous monitoring along the beam structure.

The influence of coil size on inspection performance was also investigated. Smaller EMAT coils (0.1″– 0.2″) provided higher spatial resolution and improved sensitivity to localized defects. Larger coils (0.3″– 0.5″) produced wider coverage but resulted in reduced defect sensitivity due to spatial averaging of the ultrasonic field.

Among the tested configurations, the 0.2″ EMAT coil demonstrated the best compromise between inspection coverage and defect detectability. Additionally, the pitch-catch method on the tested inspection showed the most consistent ability to differentiate between bonded and unbonded regions.

The plate experiments further indicated that material characteristics within the composite structure influence the EMAT signal response. Variations in signal amplitude and waveform stability were observed across different plate samples, highlighting the sensitivity of EMAT measurements to changes in internal structure and bonding conditions. Some variations in signal amplitude are also attributed to the anisotropic fibre architecture of the composite, where the surface cross-pattern reinforcement and the internal unidirectional fibres affect shear horizontal wave propagation.

Comparison with PAUT inspection results showed good agreement in several inspected regions, confirming the capability of the EMAT approach to identify potential defect locations within the composite structure.

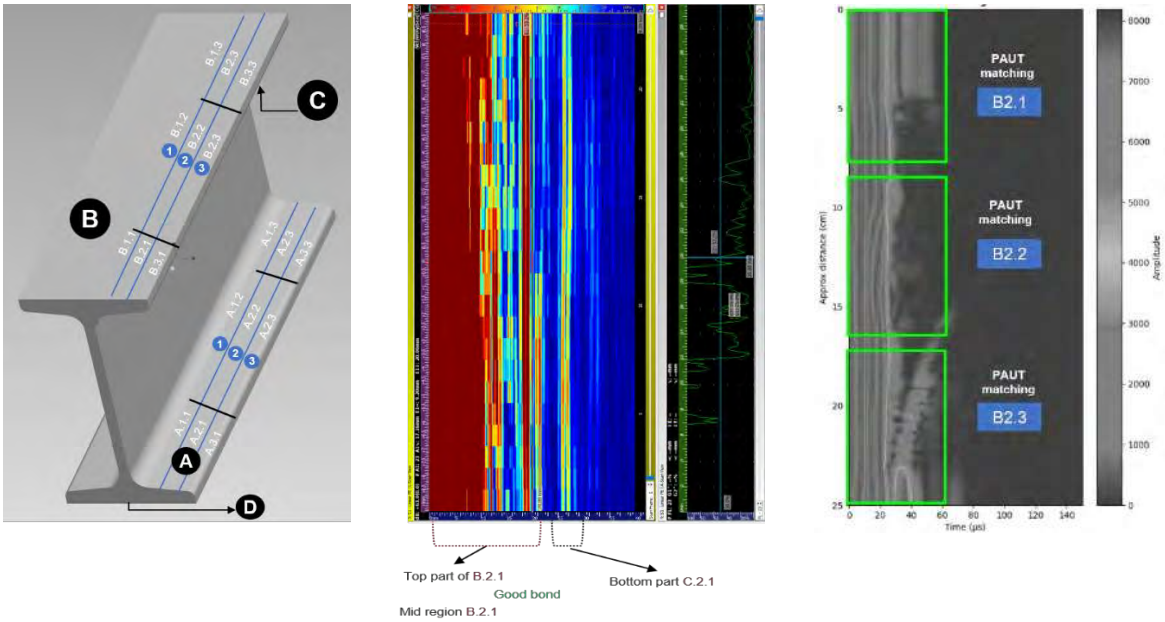

(a) Schematic (b) B 1.1. (c) B region all.

Fig 1. (a) GFRP I-beam aircraft wing assembly, (b) PAUT result, (c) EMAT result.

3. Conclusion

- EMAT-based pitch–catch inspection successfully identified interfacial disbond regions in GFRP composite structures through noticeable variations in transmitted signal amplitude and waveform characteristics.
- Evaluation of multiple coil geometries showed that smaller coils enhance defect sensitivity due to higher spatial resolution, while larger coils provide broader inspection coverage. A 0.2″ EMAT coil offered the most effective balance between spatial resolution and inspection range.
- Comparative experiments on composite plates indicated that material characteristics within the composite influence EMAT signal amplitude and stability, affecting ultrasonic wave generation and overall signal response.
- Inspection results showed good agreement with PAUT in several regions, confirming the reliability of the EMAT-based approach for identifying potential disbonded areas.
- The non-contact and couplant-free nature of EMAT inspection enables rapid and repeatable evaluation of bonded composite structures without the need for surface preparation.
- These characteristics make the proposed EMAT methodology suitable for inspection and quality control of composite components used in dynamic and high-strain-rate structural applications, where hidden interfacial defects may compromise structural integrity.

References

[1] Thompson, R. B., 1990, “Physical Principles of Ultrasonic Measurement,” *Physical Acoustics*, **19**.
[2] Hirao, M., and Ogi, H., 2003, *EMATs for Science and Industry: Noncontacting Ultrasonic Measurements*, Kluwer Academic Publishers, Dordrecht, The Netherlands.
[3] Dixon, S., Edwards, C., and Palmer, S. B., 2018, “Non-Contact Ultrasonic Inspection of Composite Materials,” *NDT & E International*, **99**, pp. 1–10.
[4] Ma, J., Chen, J., Bai, X., Song, J., and Guo, R., 2024, “Debonding Inspection With an Enhanced Miniature EMAT Based on Multiple Pulse Echoes,” *International Journal of Adhesion and Adhesives*, **134**, p. 103797.

High strain rate characterisation of natural fiber composites for drones (HISTRAND)

Ezio Cadoni,[1,*] and Dirk Mohr,[2]

[1] *University of Applied Sciences and Arts of Southern Switzerland, Via Flora Ruchat-Roncati 15, 6850 Mendrisio, Switzerland*

[2] *ETH Zürich, Department of Mechanical and Process Engineering, Tannenstrasse 3, 8092 Zurich*

[*] *ezio.cadoni@supsi.ch*

Summary:

The increasing demand for lightweight, high-performance, and environmentally sustainable materials in aerospace applications has driven growing interest in natural fibre reinforced composites (NFRCs). However, their adoption in safety-critical structures, such as unmanned aerial vehicles (UAVs), is still limited by the lack of reliable data and standardized methodologies for their behaviour under high strain rate (HSR) loading conditions.

Within the framework of COST Action CA21155 (HISTRATE), the HISTRAND project aims to address these gaps by investigating the dynamic response of NFRCs across multiple scales, from material constituents to structural components. The project will focus on the experimental characterisation of NFRCs under tensile, compressive, and shear loading using Split Hopkinson Bar (SHB) systems available at SUPSI and ETH Zurich. Particular attention will be devoted to understanding strain rate sensitivity, failure mechanisms, and fibre–matrix interactions, through testing of both composite materials and their individual constituents.

A key objective of the project will be the cross-comparison of experimental results obtained from different SHB configurations, with the goal of identifying critical parameters influencing measurement accuracy and repeatability, and contributing to the development of harmonised testing protocols (Fig. 1). In parallel, structural-level validation will be performed through impact and crash tests on UAV-representative components at the Joint Research Centre (JRC), enabling the correlation between material behaviour and real-world performance.

The experimental results will support the development and validation of strain-rate dependent material models, contributing to certification-by-analysis approaches. Ultimately, the project aims to demonstrate the feasibility of NFRCs as sustainable alternatives to conventional composites in aerospace applications, while supporting standardisation efforts and advancing the scientific framework for high strain rate testing within HISTRATE.

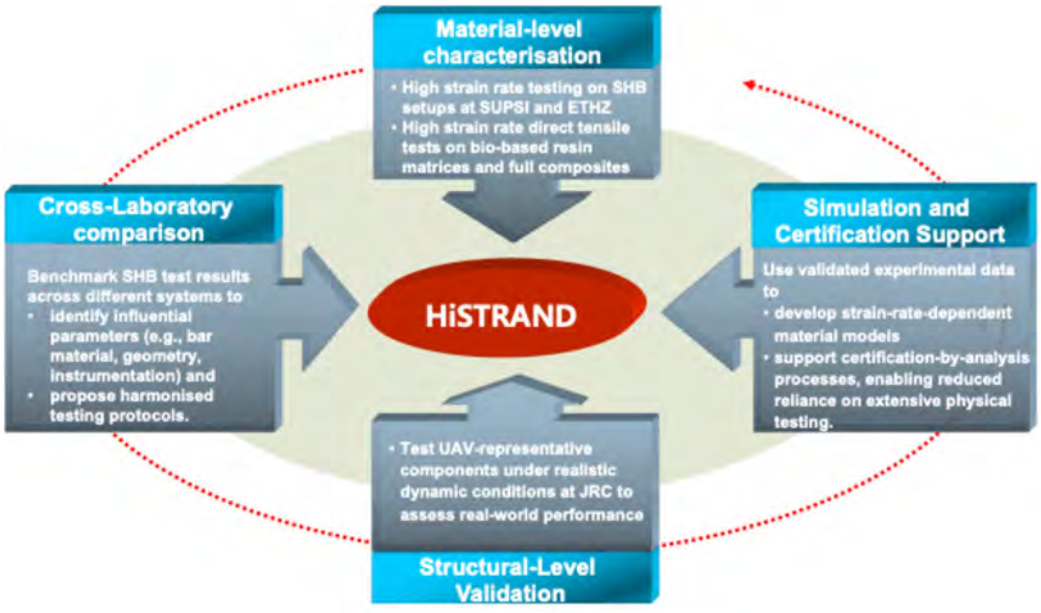

Fig. 1. Sample figure.

Microstructure-Driven Design of Strain-Rate Sensitive Nanocomposites

Ozgen Colak[1, *], Yuksel Cakir[2] and Okan Bakbak[3]

[1]*Istanbul Technical University, Department of Mechanical Engineering*
[2]*Istanbul Technical University, Department of Electronics and Communication Engineering*
[3]*Yıldız Technical University, Department of Mechanical Engineering*
[*] *e-mail: cakirou@itu.edu.tr*

Summary: In this study, graphene oxide (GO) reinforced epoxy nanocomposites are fabricated using an electric-field-assisted alignment technique prior to curing. A high-voltage electric field is applied to orient graphene sheets within the polymer matrix, aiming to induce anisotropic pathway. Quasi-static compression tests are conducted to evaluate orientation-dependent mechanical behavior. The results reveal significant improvements in stiffness and strength along the alignment direction compared to randomly dispersed systems. Although high strain rate experiments are not conducted in this phase, the observed microstructural features suggest strong potential for strain-rate-sensitive performance. The study provides a microstructure-driven framework for the future development of impact-resistant graphene/epoxy nanocomposites

1. Introduction

Graphene-reinforced nanocomposites have attracted considerable attention because of their exceptional stiffness, high aspect ratio, and large specific surface area. Previous studies have demonstrated that uniform dispersion improves mechanical performance; however, random orientation limits efficient stress transfer under directional loading. Microstructural control via external fields offers a promising route to enhance anisotropic reinforcement efficiency, [1, 2].

Electric-field-assisted alignment enables graphene sheets to orient along the applied field direction prior to matrix curing, forming preferential load-bearing pathways. While several studies have reported improvements in quasi-static properties, the implications of such alignment for high strain rate performance remain largely unexplored. This study investigates the microstructure–property relationship of electrically aligned graphene/epoxy nanocomposites and discusses their potential relevance for dynamic loading applications.

2. Materials and Methods

Graphene oxide (GO) is incorporated into a thermoset epoxy matrix using a three-roll milling process to ensure homogeneous dispersion. Prior to curing, a high-voltage electric field (up to 2.5 kV, 50 Hz) is applied across the mold to induce alignment of graphene sheets, (Fig. 1). The electric field is maintained during the pre-curing stage to stabilize orientation within the viscous matrix. Specimens are fabricated for compression testing. Quasi-static mechanical tests are performed at room temperature under displacement-controlled loading conditions.

a) three-roll milling process to ensure homogeneous dispersion

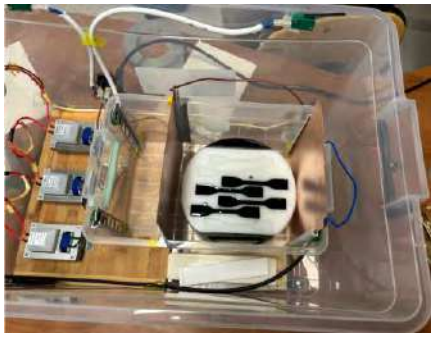

b) Application of a high-voltage electric field

Fig. 1 Manufacturing of nanocomposites

3. Results and Discussion

3.1 Microstructural Observations

Scanning electron microscopy (SEM) analysis confirmed partial alignment of graphene sheets along the applied electric field direction as seen in Fig. 2b. Compared to randomly dispersed nanocomposites, the aligned samples exhibited a more continuous platelet network, suggesting improved stress transfer efficiency.

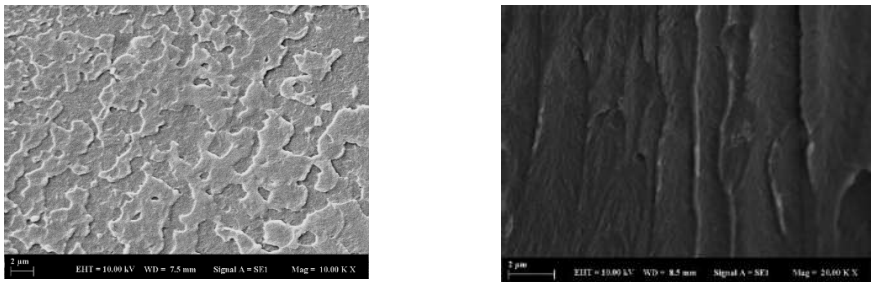

a) without electric field application b) with electric field application

Fig. 2. SEM images of GO/epoxy nanocomposites

3.2 Quasi-Static Mechanical Behavior

Specimens loaded parallel to the alignment direction showed higher elastic modulus, ultimate strength and energy absorption capacity compared to the behavior of nanocomposite without electric field, (Fig. 3). Aligned samples exhibited increased strain energy density, suggesting improved resistance to crack propagation and damage evolution.

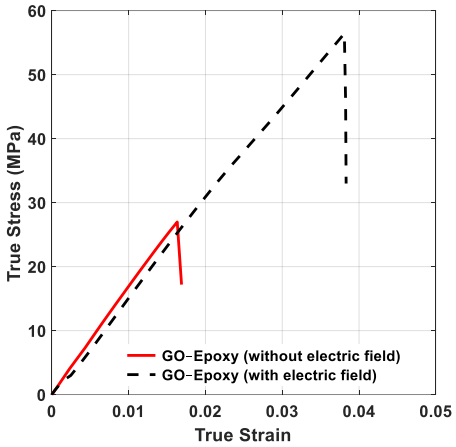

Fig. 3. Comparison of the effect of electric-field-induced GO alignment in GO–epoxy nanocomposites

.

3.3 Implications for High Strain Rate Loading

Although dynamic experiments are not conducted in this study, the observed microstructural features provide important insights into potential high strain rate behavior. Under rapid loading, polymer chain mobility becomes restricted, resulting in increased apparent stiffness. The presence of aligned graphene sheets is expected to further constrain molecular motion, thereby amplifying strain-rate sensitivity.

4. Conclusions

Electric-field-assisted alignment of graphene oxide within an epoxy matrix exhibited improved stiffness, strength, and strain energy density along the field direction. Although limited to quasi-static testing, the results strongly suggest that microstructural orientation control may significantly influence high strain rate response.

5.References

[1] Banda, S. and Ounaies, Z., 2007, “Electric field tailoring of single wall carbon nanotube and carbon nanofiber polymer composites”, Society of Plastics Engineers Annual Technical Conference, Cincinnati, OH, United States
[2] Khan, S.U., Pothnis, JR. and Kim, K., 2013, “Effects of carbon nanotube alignment on electrical and mechanical properties of epoxy nanocomposites,” Composites Part A: Applied Science and Manufacturing, 49:26–34.

Damage and Delamination Behavior of Thermoset Composites under Impact and Medium to High-Strain-Rate Compression

Sara Srebrenkoska[1], **Aleksandar Pizov[2*]**, **Svetlana Risteska[2,3**]**, Ivan Vasileski [2] and Vineta Srebrenkoska[3]

[1] *Faculty of Mechanical Engineering, Goce Delcev University, Krste Misirkov, No. 10-A Stip, Republic of North Macedonia.*

[2] *Laminati Kom D.O.O., Aleksandar Makedonski 122, 7500 Prilep, Republic of North Macedonia.*

[3] *Faculty of Technology, Goce Delcev University, Krste Misirkov, No. 10-A Stip, Republic of North Macedonia.*

Corresponding author*: *aleksandar.p@laminati.com.mk,** svetlana.risteska@ugd.edu.mk*

Abstract:

Composite materials are increasingly used in engineering structures where they may be exposed to dynamic and impact loading conditions. Under high strain rate loading, complex damage mechanisms such as matrix cracking, fiber breakage, and interlaminar delamination can occur, significantly influencing the structural integrity and mechanical performance of the material. In this study, the damage behavior of composite materials subjected to high strain rate conditions was investigated using impact and compression testing methods. Slow deformation under standard laboratory conditions, Charpy impact tests were performed to evaluate energy absorption and impact resistance, while medium and high strain rate compression tests were conducted using the UTM machine and Split Hopkinson Pressure Bar (SHPB) technique to characterize the dynamic mechanical response of the composites. The obtained results enabled identification of dominant damage mechanisms, including crack initiation, propagation, and delamination between composite layers. The experimental observations provide insight into the relationship between loading rate and damage evolution in composite materials. The findings contribute to a better understanding of failure mechanisms in composites subjected to dynamic loading and may support the design of more reliable composite structures for high-performance applications the other investigated systems.

Experiment

This study investigates the effect of a newly developed impregnation process on various material types exhibiting different flow behaviors after curing. The proposed design significantly reduces pore content in the resulting laminates, enhancing structural integrity and mechanical performance. High-quality prepregs with low void content enable fast, automated processing of high-performance composites, whereas tapes with higher porosity require longer consolidation cycles [1–10].

Cotton–phenolic, glass epoxy laminates, with moderate mechanical strength, excellent dielectric properties, and high compressive strain tolerance, are widely used in electrical insulation (e.g., circuit substrates, insulating panels), mechanical components (e.g., bushings, structural panels), and protective barriers. Their performance under impact and high-strain, high-speed compressive loading is therefore critical. Experimental testing focuses on energy absorption, deformation behavior, and failure mechanisms under dynamic compression. For the first impact test, specimens with dimensions 10x10x55mm were used. Compression tests were performed on specimens approximately 15 × 15 × ~16 mm at slow, medium, and high strain rates (Table 1). Split Hopkinson Pressure Bar (SHPB) tests will also be conducted, if feasible, to evaluate matrix cracking, fiber breakage, and interlaminar delamination mechanisms, enabling comparison across strain rates. Typical strain rate ranges for common mechanical tests are summarized below in Table 1 and Fig.1

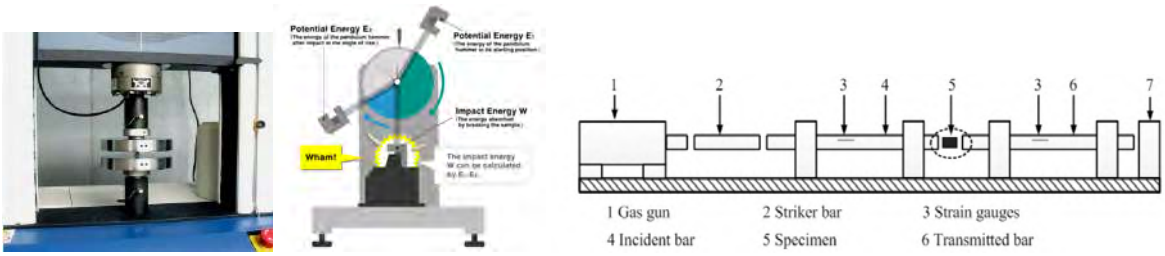

Fig.1 UTM compression test, Impact Test and SHSB compression test of cotton–phenolic laminates

Following the experiments, the damage and fracture morphologies of the composite specimens were analyzed using optical microscopy and scanning electron microscopy (SEM). This study focuses on the high strain rate behavior of composite plates under impact and compression, with particular attention to the evolution of damage and failure mechanisms. Fracture surfaces and affected zones were examined to identify key features such as crack initiation, fiber breakage, and interlaminar delamination. The impact tests were performed with an initial impact

energy of 7.5 J, a side inclination angle of 150°, and an impact velocity of 3.5 m/s. The measured impact strength of these composites was approximately 14 kJ/m². Compressive stress was observed to increase with testing speed, ranging from 1 mm/min to 300 mm/min. It is anticipated that even higher values could be achieved for SHSB composites, provided that the corresponding tests are successfully conducted.

Table 1. Typical strain rates for compression and impact tests

Test Type	Impact Compression	Strain Rate (s^{-1})		Regime / Notes
Impact Test		$\sim 10^3 – 10^4$		Rapid pendulum impact
UTM Slow Compression	1 mm/min	$10^{-4} – 10^{-1}$	$\sim 9.8 \times 10^{-4}$	Low strain rate
UTM Medium Compression	5 mm/min		$\sim 4.9 \times 10^{-3}$	Medium strain rate
UTM High Compression	20 mm/min		$\sim 1.96 \times 10^{-2}$	High strain rate (quasi-static)
UTM Very High Compression	100 mm/min		9.8×10^{-2}	High quasi-static
UTM Extreme Compression	200 mm/min		1.96×10^{-1}	Upper quasi-static / approaching dynamic
UTM Max Compression	300 mm/min		2.94×10^{-1}	Dynamic
SHPB	~10 m/s	$10^3 – 10^4$	~588/1800?	Dynamic, very high strain rate

Conclusion

The study showed that compressive strength in the composites increases with higher testing speeds, demonstrating a clear strain rate effect. Impact and high strain rate compression tests promoted crack initiation, delamination, and localized damage. Optical microscopy and SEM analyses of the fracture surfaces revealed dominant failure mechanisms, including matrix cracking, fiber breakage, and interfacial debonding, highlighting the complex interaction of damage modes under dynamic loading. Overall, these results provide valuable insight into the evolution of damage and failure in composites under high strain rate conditions, contributing to the design and optimization of structures with enhanced impact and compression resistance. This also summarizes the development and current understanding of composite behavior under impact loading, presenting the main experimental techniques for high strain rate tensile, compressive, and shear testing, along with their advantages and limitations. The findings emphasize the need for further research to improve predictive models and design strategies for composite materials subjected to dynamic loading conditions.

References

[1] Risteska, S.; Peroni, M.;Srebrenkoska, S.; Srebrenkoska, V.;Glaskova-Kuzmina, T.; Hornig, A.The In-Plane Compression Response of Thermoplastic Composites: Effects of High Strain Rate and Type of Thermoplastic Matrix. *J. Compos. Sci.* **2025**, *9*, 293

[2] Stokes-Griffin, C.M., Compston, P., The effect of processing temperature and placement rate on the short beam strength of carbon fibre-PEEK manufactured using a laser tape placement process, Composites: Part A (2015), doi:http://dx.doi.org/10.1016/j.compositesa.2015.08.008C.

[3] F. N. Cogswell, Thermoplastic aromatic polymer composites: a study of the structure, processing, and properties of carbon fibre reinforced poly ether ether ketone and related materials. Oxford [England]; Boston: Butterworth-Heinemann, 1992.

[4] Kaven Croft, Larry Lessard, Damiano Pasini, Mehdi Hojjati, Jihua Chen, Ali Yousefpour, Experimental study of the effect of automated fiber placement induced defects on performance of composite laminates, Composites: Part A 42 (2011) 484–491 Elsevier doi: 10.1016/j.compositesa.2011.01.007

[5] Minh Duc Hoang, Procedure for making flat thermoplastic composite plates by Automated Fiber Placement and their mechanical properties, A Thesis Degree of Master of Applied Science (Mechanical Engineering) at Concordia University Montreal, Quebec, Canada, 2015.

[6] Margaret F, Talbott and George S, Springer, The Effects of Crystallinity on the Mechanical Properties of PEEK Polymer and Graphite Fiber Reinforced PEEK, Journal of Composite Materials 1987 21: 1056, DOI: 10.1177/002199838702101104

[7] Fazil O. Sonmez and H. Thomas Hahn, Modeling of Heat Transfer and Crystallization in Thermoplastic Composite Tape Placement Process, Journal of Thermoplastic Composite Materials 1997, DOI: 10.1177/089270579701000301.\

[8] Shiyu Wang, Lihua Wen, Jinyou Xiao, Ming Lei, Jun Liang Influence of strain rate and temperature on mechanical properties of carbon woven-ply PPS thermoplastic laminates under dynamic compression, Journal Polymer Testing 89 (2020) 106725 ,

[9] Huiran Zou, Weilong Yin, Chaocan Cai, Bing Wang, Ankang Liu, Zhen Yang, Yibin Li and Xiaodong He, The Out-of-Plane Compression Behavior of Cross-Ply AS4/PEEK Thermoplastic Composite Laminates at High Strain Rates, Journal Materials 2018, Vol11, 2312; doi:10.3390/ma11112312

[10] Lisa Feuillerat, Olivier De Almeida a, Jean-Charles Fontanier , Fabrice Schmidt, Effect of poly(ether ether ketone) degradation on commingled fabrics consolidation, Journal Composites Part A 149 (2021) 106482 https://doi.org/10.1016/j.compositesa.2021.106482

High Strain Rate Behavior of Silica Loaded Epoxy Nanocomposites

Aldobenedetto Zotti[1], Ahmed Elmahdy[2], Simona Zuppolini[1], Anna Borriello[1], Mauro Zarrelli[1,*], and Patricia Verleysen[2,*]

[1]CNR - National Research Council, IPCB - Institute of Polymers, Composites and Biomaterials, ,P.le E. Fermi, Granatello, Portici, 80055, Italy

[2]Department EA08, Materials Science and Technology-DyMaLab, Ghent University, Technologiepark 46, 9052 Zwijnaarde, Belgium

[*] mauro.zarrelli@cnr.it; patricia.verleysen@ugent.be.

Summary: This study investigates the compressive behavior of an aeronautical epoxy matrix reinforced with 1 wt% silica nanoparticles (~800 nm) under varying strain rates. Tests were performed under quasi-static (0.0008–0.08 s^{-1}) and high strain rate conditions (up to 1050 s^{-1}) on both neat and filled resins. Results indicate that silica nanoparticles enhance compressive yield strength while reducing maximum strain across all conditions. However, strain rate sensitivity decreases at higher rates in the filled system. The relationship between strain rate and compressive yield strength follows a power law, with a strain rate exponent of approximately 0.0227.

1. Introduction

Epoxy resins are widely employed as matrices in high-performance aeronautical composites due to their highly crosslinked structure after curing, which ensures high stiffness, strength, and thermal resistance [1]. However, they are inherently brittle, exhibiting low fracture toughness and poor crack resistance [2]. To overcome these limitations, researchers have introduced rigid fillers such as silica (SiO_2) nanoparticles [3]. Their addition, typically up to nanoscale dimensions, has been shown to enhance elastic modulus, tensile strength, and fracture toughness, especially when the particles are well dispersed, without remarkable effects on failure strain [4].
Despite these improvements, the response of epoxy nanocomposites at high strain rates remains insufficiently explored, particularly for submicrometric particle sizes. This study investigates the compressive behavior of epoxy reinforced with silica nanoparticles of approximately 800 nm. Both high strain rate tests, using a split Hopkinson pressure bar, and quasi-static experiments were conducted to compare mechanical performance. The influence of nanoparticle addition on compressive yield strength across different strain rates is analyzed.

2. Material and Methods

The material studied was RTM6 epoxy resin, both neat and reinforced with 1 wt% silica nanoparticles. Cylindrical rods were produced by degassing the resin at 90 °C for 30 minutes under vacuum, followed by casting into aluminum molds and curing according to the standard RTM6 cycle (cure at 160°C for 90 mins followed by postcure at 180 °C for 120 mins). The nanoparticles, synthesized via a sol–gel method and without surface functionalization, were carefully dispersed to ensure uniform distribution within the matrix. SEM analysis showed an average particle size of about 800 nm. After curing, the rods were machined into small cylindrical specimens with identical geometry to ensure consistent testing conditions in both quasi-static and high strain rate experiments (see Fig. 1.a).
Quasi-static reference tests were performed using an Instron 5569 universal testing machine at crosshead speeds of 0.2, 2, and 20 mm/min, corresponding to strain rates of 8×10^{-4}, 8×10^{-3}, and 8×10^{-2} s^{-1}. A 50 kN load cell was employed to record the applied load, while displacements were measured using 3 linear variable displacement transducers LVDTs which were fixed on the bars close to the sample. The complete experimental setup for quasi-static testing is illustrated in Figure 1.b.

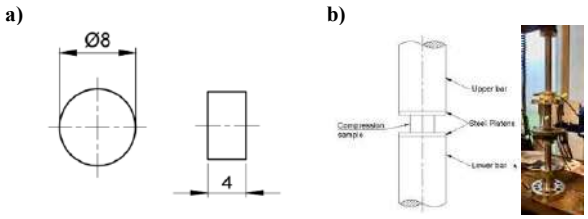

Fig. 1. a) Dimensions of the compression specimen. b) Quasi-static setup.

Dynamic compression tests were performed using a split Hopkinson pressure bar (SHPB) system, where the specimen is positioned between an input and an output bar and loaded by an incident stress wave. Upon interaction with the sample, the wave is partially reflected and transmitted. The bars, made of high-strength aluminum, had diameters of 25 mm and lengths of 6 m (input) and 3 m (output). Stress waves were generated by launching a cylindrical striker at velocities of 8, 11, and 14 m/s. Strain signals (incident, reflected, transmitted) were recorded using strain gauges mounted on the bars. Steel end plates and an alignment device ensured uniform loading

conditions. Sample stress, strain, and strain rate were determined using classical Hopkinson bar equations. Interfaces were lubricated with PTFE to minimize friction.

3. Results and Discussion

Figure 2.a shows the engineering stress–strain behavior of neat epoxy resin under both low and high strain rates, highlighting its strong strain-rate sensitivity due to its viscoelastic nature. For clarity, only the quasi-static strain rate of 0.0008 s^{-1} is reported. The compressive response can be divided into three main regions: (1) an initial linear elastic region followed by a nonlinear stage, (2) a stress plateau where stress remains nearly constant with increasing strain, and (3) a strain-hardening region up to failure. The compressive yield strength is defined as stress at the first point of the plateau region. As strain rate increases, both stiffness and yield strength increase. At intermediate high strain rates (250 and 650 s^{-1}), specimens did not fail, showing stress drop and strain recovery during unloading. Figure 2.b reports the behavior of silica nanoparticle-filled epoxy, which follows the same three-region trend. Yield strength (indicated by arrows) and stiffness also increase with strain rate. However, at high strain rates, the increase in yield strength is less pronounced compared to neat epoxy. At 340 and 670 s^{-1}, samples did not fail, again showing unloading recovery. For tests conducted up to failure (0.0008 and 1000 s^{-1}), the addition of silica nanoparticles led to reduced failure strain.

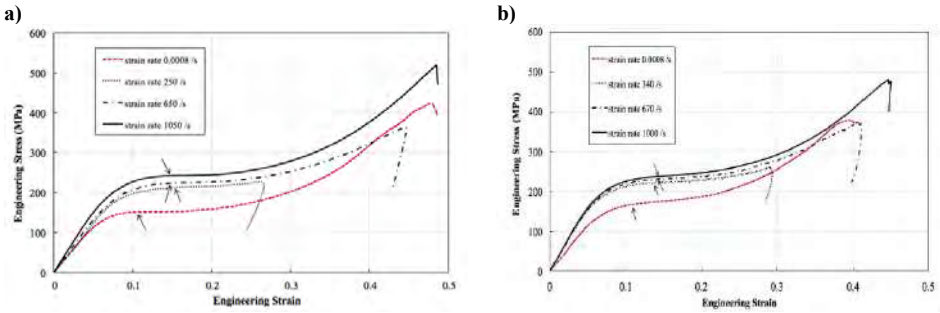

Fig. 2. Engineering stress strain response at different strain rates of a) neat epoxy and b) silica filled nanocomposites.

Figure 3 illustrates the effect of strain rate on compressive yield strength. The nanoparticle-filled system shows significant improvement under quasi-static conditions, while only slight gains are observed at high strain rates. This dependence follows power law:

$$\sigma_y^{comp} = K\dot{\varepsilon}^n$$

with constants K = 181.04 MPa and n = 0.034 for neat epoxy, and K = 195.2 MPa and n = 0.0227 for the filled system. Similar trends were reported by Ying-Gang Miao et al. [5], with differences attributed to nanoparticle size (≈20 nm vs ≈800 nm).

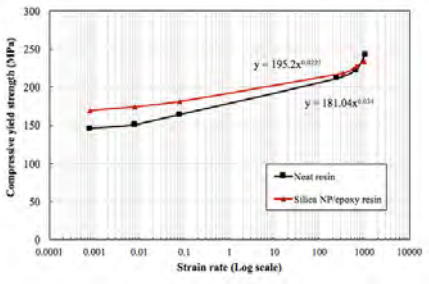

Fig. 3. Effect of strain rate on the compressive yield strength for both neat and silica nanoparticles filled epoxy resins.

References

[1] Hsieh, T. H.; Kinloch, A. J.; Masania, K.; Taylor, A. C.; Sprenger, S.; 2010; "The mechanisms and mechanics of the toughening of epoxy polymers modified with silica nanoparticles", Polymer, 51, pp. 6284–6294.
[2] Domun, N.; Hadavinia, H.; Zhang, T.; Liaghat, G.; Vahid, S.; Spacie, C.; Paton, K.R.; Sainsbury, T.; 2017; "Improving the fracture toughness properties of epoxy using graphene nanoplatelets at low filler content", Nanocomposites, 3, pp. 85–96.
[3] Paluvai, N.R.; Mohanty, S.; Nayak; S. K.; 2014; "Synthesis and Modifications of Epoxy Resins and Their Composites: A Review", Polymer-Plastics Technology and Engineering, 53, pp. 1723–1758.
[4] Jumahat, A.; Soutis, C.; Abdullah, S.A.; Kasolang, S.; 2012; "Tensile Properties of Nanosilica/Epoxy Nanocomposites. Procedia Engineering", 41, pp. 1634–1640.
[5] Miao, Y.-G.; Liu, H.-Y.; Suo, T.; Mai, Y.-W.; Xie, F.-Q.; Li, Y.-L.; 2016; "Effects of strain rate on mechanical properties of nanosilica/epoxy", Composites Part B, 96, pp. 119–124.

Influence of ATL Processing Parameters on the Flexural Strength of Carbon Fiber/PPS Thermoplastic Laminates

Sara Srebrenkoska,[1*] Vladimir Dukovski,[2] Vineta Srebrenkoska,[3] and Svetlana Risteska[4]

[1] *Faculty of Mechanical Engineering, Goce Delcev University, Krste Misirkov, No. 10-A Stip, Republic of North Macedonia.*
[2] *Faculty of Mechanical Engineering,* Ss Cyril and Methodius University,Karpos II bb, 1000 Skopje, Republic of North Macedonia
[3] *Faculty of Technology, Goce Delcev University, Krste Misirkov, No. 10-A Stip, Republic of North Macedonia.*
[4] *Laminati Kom Doo Prilep, Aleksandar Makedonski No. 122, Prilep, Republic of North Macedonia.*
[*] *sara.srebrenkoska@ugd.edu.mk*

Summary: This study examines the in situ manufacturing of high-performance composite laminates from carbon-fiber-reinforced thermoplastic prepregs with PPS matrices using the Automated Tape Laying (ATL) process. A full factorial experimental design was applied to analyze the influence of processing temperature, laser placement angle, and roller compaction pressure on laminate performance. Flexural strength testing and regression analysis showed that processing temperature and compaction pressure significantly affect mechanical properties, while the laser placement angle has a minor influence. Microscopic observations confirmed that higher temperatures and compaction pressures improve interlaminar bonding and reduce porosity, resulting in enhanced flexural strength of the produced laminates.

1. Materials

The thermoplastic unidirectional prepreg material, denoted as **UD1**, was used for the experimental investigations and for the manufacturing of thermoplastic composite laminate plates. The UD1 prepreg consists of unidirectional carbon fibers (HexTow® AS4) combined with a thermoplastic polymer matrix polyphenylene sulfide (PPS). The prepreg tapes were supplied by Suprem (Switzerland). The AS4 carbon fibers are continuous fibers with a tensile modulus of approximately 241 GPa and a tensile strength of about 5419 MPa. These fibers are commonly available in filament bundles of 3K, 6K, and 12K, providing high stiffness and strength suitable for high-performance composite applications.

2. Preparation of Laminated Samples

Composite laminate plates were manufactured using the Automated Tape Laying (ATL) process with laser-assisted heating (LATL). During the process, the prepreg tapes were heated by a laser and consolidated onto a flat tool surface using a compaction roller. The ATL system, developed by Mikrosam (North Macedonia), includes several key components such as a tape transport system, prepreg unwinding unit, edge alignment system, defect detection system, tension control system, cutting system, heating system, and compaction control system. The compaction roller used in the process has an outer diameter of 90 mm.

Prepreg tapes with a width of 25 mm were laid at a constant speed of 9 m/min in the fiber direction (0° orientation). Each laminate plate consisted of eight layers, resulting in a total laminate thickness of approximately 1.5 mm. The produced laminate plates had dimensions of 300 mm × 150 mm, with each layer composed of six prepreg tapes placed side by side. During the lay-up process, several technological parameters were controlled, including processing temperature, laser placement angle, and compaction roller pressure, while other parameters such as laying speed and tool temperature were kept constant. The produced laminates were subsequently analyzed to evaluate their mechanical properties and microstructural characteristics.

2.1. Design of Experiments

To evaluate the influence of key technological parameters on the properties of the produced laminates, a Design of Experiments (DoE) approach was applied. A full factorial experimental design with three factors at two levels (2^3) was used to systematically investigate the process parameters during the Automated Tape Laying (ATL) process. The selected factors were processing temperature, laser placement angle, and compaction roller pressure, as these parameters are reported to have a significant influence on interlaminar bonding and consolidation quality of thermoplastic composite laminates.

Based on this experimental design, eight combinations of processing conditions were defined and laminate plates were produced for each condition. Multiple replications were performed to ensure the reliability of the experimental results. The obtained data were used to develop regression models describing the relationship between the processing parameters and the mechanical performance of the laminates, particularly their flexural strength. Statistical analysis was further conducted to evaluate the significance of the factors and their interactions, as well as to verify the adequacy of the developed regression model.

2.2. Flexural Strength Testing

The flexural strength of the produced laminate plates was evaluated according to the **ASTM D790** standard using the three-point bending method. For each laminate plate, five specimens were cut in the longitudinal direction with dimensions defined by the standard. Prior to testing, the thickness and width of each specimen were measured using a micrometer to ensure accurate stress calculations. The tests were performed using a universal testing machine (Chengde, model Jingmi) with a testing speed of 5 mm/min and a support span of 25 mm. The maximum load recorded before failure was used to calculate the flexural strength of the specimens.

2.3. Microscopic Analysis

The microstructure of the produced laminates was analyzed using optical microscopy and scanning electron microscopy (SEM) to evaluate the quality of interlaminar bonding and the presence of defects such as pores or voids. Cross-sections of the laminate specimens were prepared by cutting samples from different regions of each laminate plate, embedding them in epoxy resin, and polishing them to obtain a smooth surface for observation.

Optical microscopy was used to examine the interlaminar bonding between layers and the distribution of pores within the laminates. The pore content was determined through image analysis using Image J (NIH) software, providing quantitative information about the quality of consolidation of the composite material.

For a more detailed microstructural investigation, selected samples were further analyzed using a **sc**anning electron microscope (SEM) VEGA3 LMU (Tescan**)**. Prior to SEM observation, the samples were polished and coated with a thin layer of gold. SEM analysis enabled detailed observation of fiber–matrix interfaces, interlaminar bonding, and internal defect**s** within the composite structure.

3. Results and Discussion

Flexural strength tests were conducted on laminate plates produced under eight different ATL processing conditions. Five specimens from each laminate plate were tested according to ASTM D790. The flexural strength values ranged from approximately 800 MPa to 1200 MPa, depending on the applied processing parameters.

Higher flexural strength was obtained at higher processing temperatures and compaction roller pressures, which improve consolidation and interlaminar bonding between layers. Lower processing temperature and pressure resulted in weaker bonding and reduced mechanical performance.

Regression analysis based on the factorial design of experiments indicated that processing temperature and compaction pressure have the most significant influence on flexural strength**,** while the laser placement angle has a minor effect**.**

Microscopic observations using optical microscopy and SEM confirmed that laminates produced under optimal conditions exhibit good interlaminar bonding and low porosity (≈2%**)**, whereas samples produced at lower pressure and temperature showed higher porosity (≈4–5%**),** leading to reduced mechanical properties.

4. Summary

In this study, thermoplastic composite laminate plates based on carbon fiber prepreg were manufactured using the Automated Tape Laying (ATL) process with laser-assisted heating. The influence of key processing parameters, including processing temperature, laser placement angle, and compaction roller pressure, was investigated using a factorial design of experiments.

The results showed that processing temperature and compaction pressure have a significant influence on the flexural strength of the laminates, while the laser placement angle has a minor effect. Laminates produced under higher temperature and pressure exhibited improved consolidation, better interlaminar bonding, and lower porosity, resulting in higher flexural strength.

Microscopic analysis confirmed that improved interlaminar bonding and reduced pore content lead to enhanced mechanical performance of the composites. The developed regression model adequately describes the relationship between the processing parameters and the flexural strength of the laminates.

Overall, the results demonstrate that proper control of processing parameters is essential for achieving high-quality thermoplastic composite laminates with improved mechanical properties.

References

[1] Grouve, W. J. B., Warnet, L. L., Rietman, B., and Akkerman, R., 2013, “Optimization of the Tape Placement Process for Thermoplastic Composites,” *Composites Part A: Applied Science and Manufacturing*, 50, pp. 44–53.

[2] Di Francesco, M., Belingardi, G., and Martorana, B., 2018, “Automated Tape Laying Process for Thermoplastic Composites: Influence of Processing Parameters on Mechanical Properties,” *Composite Structures*, 184, pp. 724–732.

[3] Oromiehie, A., Prusty, R. K., and Roy, S., 2016, “Processing and Characterization of Thermoplastic Composite Laminates Manufactured by Automated Tape Laying,” *Journal of Thermoplastic Composite Materials*, 29(6), pp. 769–784.

[4] ASTM International, 2017, *ASTM D790: Standard Test Methods for Flexural Properties of Unreinforced and Reinforced Plastics and Electrical Insulating Materials*, ASTM International, West Conshohocken, PA.

Design and Optimization of Novel Filament-Wound Composites for High Strain Rate Mechanical Performance: Factorial vs Taguchi Approach

Svetlana Risteska[1,2*], Sara Srebrenkoska [3], Ivan Vasileski[1], Evgenija Gjorgjieska Angelovska [1], Aleksandar Pižov[1**] and Vineta Srebrenkoska[2]

[1] *Laminati Kom D.O.O., Aleksandar Makedonski 122, 7500 Prilep, Republic of North Macedonia.*

[2] *Faculty of Technology, Goce Delcev University, Krste Misirkov, No. 10-A Stip, Republic of North Macedonia.*

[3] *Faculty of Mechanical Engineering, Goce Delcev University, Krste Misirkov, No. 10-A Stip, Republic of North Macedonia.*

svetlana.r@laminati.com.mk, svetlana.risteska@ugd.edu.mk

Abstract:
Optimizing processing parameters is crucial for high-quality filament-wound composites. This study compares two statistical approaches—full factorial Design of Experiments (DOE) and the Taguchi L8 method—for evaluating the influence of key processing factors on electrical, mechanical performance and structural quality. Full factorial DOE provided detailed insights into main and interaction effects, while the Taguchi method enabled faster optimization with fewer experiments. Both approaches effectively improved composite performance. The choice of method depends on the desired balance between experimental efficiency and detailed understanding of factor interactions. These results emphasize the value of statistical design in robust filament-wound composite production.

Experiment

For the manufacture of the samples, E-glass fibers and a three-component epoxy resin system were used. The wet filament winding process was carried out on a filament winding machine. Ring-shaped samples were produced according to a factorial Design of Experiments (DOE) with 2^3 permutations, using a combination of key winding parameters specified in Table 1. The selected parameters included winding speed, fiber tension, and resin bath temperature, as these factors significantly influence resin impregnation, fiber alignment, and the resulting mechanical performance of the composites. The DOE approach was selected because it is superior to the traditional one-variable-at-a-time method, which does not account for possible interactions between filament winding parameters.

Table 1. Winding parameters and levels used in the DOE and Taguchi L8 orthogonal array for filament winding experiments.

Experiment	Winding Speed (m/min)	Fiber Tension (N)	Resin Bath Temperature (°C)
1	Low	Low	Low
2	High	Low	Low
3	Low	High	Low
4	High	High	Low
5	Low	Low	High
6	High	Low	High
7	Low	High	High
8	High	High	High

Run	Winding Speed (m/min)	Fiber Tension (N)	Resin Bath Temperature (°C)
1	Low (5)	Low (50)	Low (25)
2	Low (5)	Low (50)	High (40)
3	Low (5)	High (150)	Low (25)
4	Low (5)	High (150)	High (40)
5	High (15)	Low (50)	Low (25)
6	High (15)	Low (50)	High (40)
7	High (15)	High (150)	Low (25)
8	High (15)	High (150)	High (40)

In addition to the full factorial design, the Taguchi L8 orthogonal array was employed. This array can be interpreted as a fractional factorial design $2^{(7-4)}$, enabling the investigation of up to seven two-level factors using only eight experimental runs. In contrast to the full factorial design, some interaction effects may be aliased, meaning that only the main effects can be reliably estimated. Although both the 2^3 factorial design and the Taguchi L8 array require eight experimental runs, the factorial design allows a complete evaluation of interaction effects, whereas the Taguchi method provides a faster optimization approach focused primarily on the main effects.
This combined methodology enables a systematic evaluation of the influence of winding speed, fiber tension, and resin bath temperature on the process–structure–property relationships of filament-wound composites. Understanding these relationships provides valuable insight for optimizing the manufacturing process in order to achieve improved mechanical performance, uniform resin distribution, and enhanced structural integrity.
The low and high levels for each parameter were selected based on experimental constraints and material limitations. In this study, the investigated ranges were: winding speed (10–20 m/min), fiber tension (50–150 N),

and resin bath temperature (25–40 °C). These parameter levels were applied in both the full factorial 2^3 Design of Experiments (DOE) and the Taguchi L8 orthogonal array.

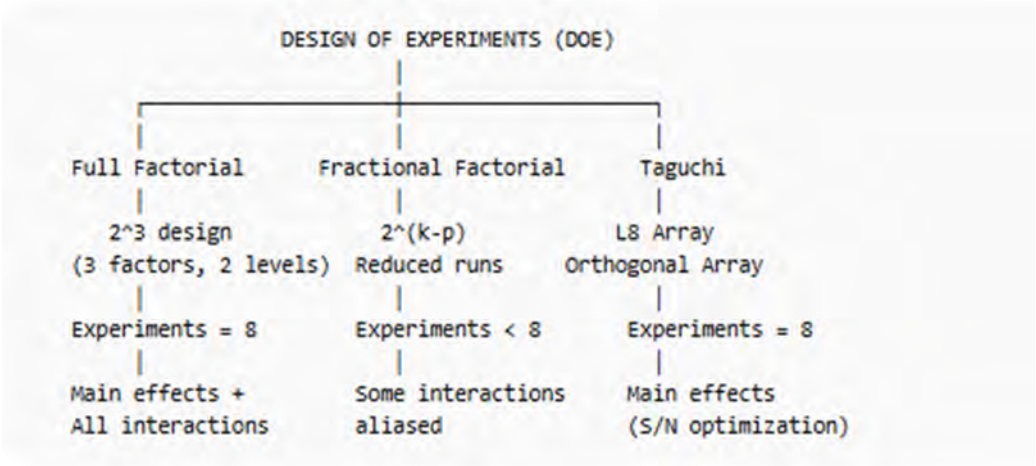

Figure 1. Comparison between full factorial design, fractional factorial design, and the Taguchi orthogonal array used for experimental optimization of composite processing parameters

The factorial DOE approach enables the evaluation of both main effects and interaction effects between the selected parameters. In contrast, the Taguchi L8 method focuses primarily on the estimation of main effects while maintaining experimental efficiency through a reduced number of experimental runs. Although the L8 array allows robust estimation of main effects using only eight experiments, certain interaction effects may be aliased. Therefore, a full factorial analysis is required when detailed interaction effects between parameters must be evaluated.

The experimental results obtained from the designed experiments were analyzed to determine the influence of winding speed, fiber tension, and resin bath temperature on the void content, electrical behavior, and overall structural quality of the filament-wound composites.

Conclusion

A comparative study of full factorial 2^3 and Taguchi L8 experimental designs was conducted to optimize filament-wound composite processing parameters. While the factorial design enabled a detailed evaluation of both main and interaction effects, the Taguchi method provided a faster and more efficient approach for robust parameter optimization with a reduced number of experiments. Both statistical approaches contributed to improving the electrical and mechanical performance, as well as the structural quality of the produced composites. Furthermore, the optimized processing conditions resulted in composite structures with improved resistance to deformation and enhanced structural stability, making the obtained products suitable candidates for high strain rate testing. The selection of the appropriate experimental design therefore depends on whether detailed interaction analysis or experimental efficiency is the primary objective. These findings highlight the importance of statistical design methods in the development of high-quality and reliable filament-wound composite materials.

References

1. Bai, J.; Seeleuthner, P.; Bompard, P. Mechanical Behavior of ±55° Filament-Wound Glass-Fibre/Epoxy-Resin Tubes: I. Microstructural Analyses, Mechanical Behavior and Damage Mechanisms of Composite Tubes Under Pure Tensile Loading, Pure Internal Pressure, and Combined Loading. *Composites Science and Technology*, **1997,** *57*, 141-153. https://doi.org/10.1016/S0266-3538(96)00124-8
2. Mertiny, P.; Ellyin, F.; Hothan, A. An experimental investigation on the effect of multi-angle filament winding on the strength of tubular composite structures. Compos. Sci. Technol. 2004, 64, 1–9. https://doi.org/10.1016/S0266-3538(03)00198-2
3. S. Risteska, B. Samakoski; .Z. Sokoloski, M. Stefanovska," Investigation of influence of carbon fiber delivery system for filament winding process with NOL-Ring specimen tests", ECCM16 - 16TH EUROPEAN CONFERENCE ON COMPOSITE MATERIALS, Seville, Spain, 22-26 June 2014.
4. Lee, S.; Lee, S.G.; Bae, D. ; Kim, B.S. ; Korean J. *Soc. Civ. Eng. Mag.*, **2005**, *25*, 751-760.
5. Sideridis, E.; Papadopoulos, G.A. Short-Beam and Three-Point-Bending Tests for the Study of Shear and Flexural Properties in Unidirectional-Fiber-Reinforced Epoxy Composites. *Journal of Applied Polymer Science*, **2004**, *93*, 63-74.
6. Belingardi, G. ; Cavatorta, M.P. ; Frasca, C. *Compos. Sci. Techol.*, **2006**, *66*, 222–232.
7. Dorigato, A.; Pegoretti, A. *J. Compos. Mat.,* **2014**, *48*, 1121–1130.
8. Kissinger, H.E. Reaction Kinetics in Differential Thermal Analysis. Anal. Chem. 2002, 29, 1702–1706. https://doi.org/10.1021/ac60131a045

9. Srebrenkoska, S.; Kochoski, F.; Srebrenkoska, V.; Risteska, S.; Kotynia, R. Effect of Process Parameters on Thermal and Mechanical Properties of Filament Wound Polymer-Based Composite Pipes. Polymers **2023**, 15, 2829. https://doi.org/10.3390/ polym15132829

Magneto-Thermomechanical Characterization of Electrospun Polyacrylonitrile/Magnetic Nanoparticle Composite Nanofibers

A.Sezai Sarac *

[1] *Istanbul Technical University, Polymer Science & Technology, 34469 Maslak, Istanbul, Turkiye*

[*] *sarac@itu.edu.tr*

Summary: This study addresses the challenge of tailoring mechanical responsiveness in nanofibers for advanced nanotechnological applications. Electrospinning was utilized to fabricate polyacrylonitrile (PAN) composite nanofibers integrated with magnetic metal oxide nanoparticles . Characterization via HRSEM, XRD, and spectroscopy confirmed a homogeneous nanoparticle dispersion. Dynamic Mechanical Analysis (DMA) under magnetic fields revealed significant increases in stiffness and altered glass transition profiles compared to PAN . These results demonstrate that strong interfacial interactions modify polymer chain dynamics, offering a data-driven framework for designing stimuli-responsive materials with precisely controlled thermomechanical properties for sensors and catalysts.

1. Main Text

1.1. Introduction

Electrospinning has emerged as a premier technique for developing micro- and nanofibers characterized by high porosity and vast surface areas. While polymer fibers offer structural utility, there is a growing need for "smart" materials capable of responding to external stimuli. The integration of magnetic nanoparticles into a polymer matrix presents a solution for creating responsive systems, yet the fundamental interactions governing their thermomechanical behavior—especially under active magnetic fields—require deeper investigation to enable precise material design.

2. Experimental Methods

Magnetic metal oxide nanoparticles , specifically Ferrites (e.g., Fe_2O_3, $MnZnFe_2O_4$, $CoFe_2O_4$), were incorporated into the polyacrylonitrile solution prior to electrospinning[1-3]. The electrospinning setup included a grounded collector placed within a syringe,. For the production of nanofibers, the polymer mixtures were electrospun at ambient temperature with driving voltages of 10–15 kV. The electrospinning process was standardized with a constant needle-to-collector distance of 15 cm and a controlled precursor feed rate of 1 mL/h. Thermomechanical properties were evaluated using a PerkinElmer DMA-8000 system. Samples were analyzed in tension mode across a temperature gradient from 300 K to 800 K, utilizing a linear heating rate of 5 K/min. To investigate the frequency-dependent viscoelastic behavior, measurements were recorded under applied sinusoidal forces at frequencies of 0.5 Hz. The morphological characteristics and chemical composition analysis of the produced nanofibers were examined by scanning electron microscopy (SEM) and integrated energy-dispersive X-ray (EDX) analysis, respectively. Surface features were investigated on a Hitachi S-4800 SEM at 2 kV acceleration voltage on samples coated with Au/Pd (5 nm) using secondary electron (SE) mode.

The resulting fibrous mats were subjected to structural analysis by High-resolution scanning electron microscopy (HRSEM) and X-ray diffraction (XRD) and by Chemical Spectroscopy: FTIR, Raman, and XPS to verify molecular bonding and elemental composition. Dynamic Mechanical Analysis (DMA) conducted both in ambient conditions and under applied magnetic fields to observe real-time stiffness shifts.

3. Results and Discussion

The electrospinning process successfully produced uniform nanofibrous structures with consistent nanoparticle distribution, avoiding the common pitfall of agglomeration.

The DMA data provided the most striking insights. When subjected to magnetic fields, the PAN-based composites exhibited a marked enhancement in stiffness, particularly at the glass transition temperature (Tg) compared to PAN . This shift in the transition profile, compared to pristine PAN, suggests that the magnetic fillers do not merely act as passive reinforcements. Instead, strong interfacial interactions between the nanoparticles and the PAN chains fundamentally restrict or modify polymer chain mobility. This research elucidates the critical structure-property relationships necessary for the mechanical characterization of magnetic nanocomposites. By confirming that nanoparticle dispersion and external field application directly dictate thermomechanical response, this study provides a roadmap for tailoring fibers for use in high-performance sensors, energy storage devices, and magnetic catalysts.

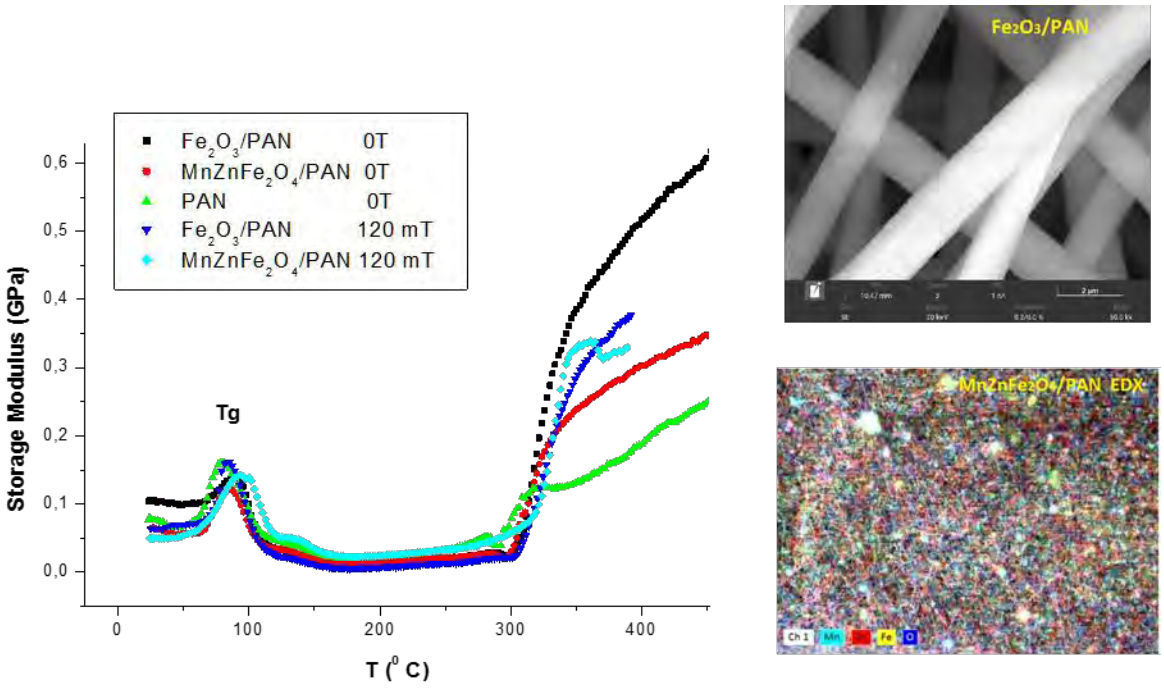

Fig. 1. (a) Dynamic mechanical analysis comparison of the investigated PAN, Fe_2O_3/PAN and MnZnFe2O4 / PAN Nanofibers (for 0 T and 120 mT) at 5 C min^{-1} at 0.5Hz,and SEM of Fe_2O_3/PAN (upper right),EDX of $MnZnFe_2O_4$/PAN Nanofibers (bottom right)

4. References

[1] Sarac, B.,Soprunyuk, V., Herwig, G., Gumrukcu, S., Kaplan, E., Yüce, E., Schranz, W., Eckert, J., Boesel, L., Sarac, A.S.,(2024)" Thermomechanical properties of confined magnetic nanoparticles in electrospun polyacrylonitrile nanofiber matrix exposed to a magnetic environment: structure, morphology, and stabilization (cyclization)",Nanoscale Adv.,6,,6184-6195

[2]B. Sarac, V. Soprunyuk, E. Yüce, S. Gümrükçü, W. Schranz and A. S. Sarac,(2025)" Impact of thermal treatment and magnetic field on the dynamic mechanical behavior of polyacrylonitrile nanofibers with embedded magnetic ferrite nanoparticles" Mater. Adv., 6, 5475-5485

[3]Sarac, B., Sharifikolouei, E., Micusik, M ., Scalia,A., Najmi,Z., Cochis,A., Rimondini,L., Barrera, Coisson,M., Gümrükcü, S., Yüce,E., Sarac,A.S.,(2025) "Development and characterization of (MnZn) ferrite-polyacrylonitrile composite nanofiber membranes for tissue engineering" Emergent Mater. 8, 6635–6652,

Additively manufactured PETG - PLA hybrid composites: Behavior under tensile and compressive loading

Sabri Can Ekerer,[1] * Cem Boğa,[2] and Mirsadegh Seyedzavvar[2]

[1] *Department of Mechanical Engineering, Faculty of Engineering, Adana Alparslan Türkeş Science and Technology University, Adana, Turkey and Department of Motor Vehicles and Transport Technologies, Vocational School of Adana, Çukurova University, Adana, Turkey*

[2] *Department of Mechanical Engineering, Faculty of Engineering, Adana Alparslan Turkes Science and Technology University, Adana, Turkey*

[*] *sekerer@cu.edu.tr*

Summary: In this study additively manufactured PLA – PETG multi material composite was mechanically characterized. PLA is a strong and environmentally friendly material used in additive manufacturing however it is brittle and not suitable for harsh environment applications due to its weak chemical resistance. PETG, well known for its ductile and chemically resistant behavior, was employed as the capsule for the PLA inner structure of the hybrid composite. Tensile and compression tests were carried out to investigate how this novel hybrid shell-core structure affects the mechanical properties. Results show that the composite achieves beneficial characteristics between stiffness and ductility possessing environmental protection.

1. Introduction

Additive manufacturing (AM) gains more attraction day by day thanks to advancements in AM machines and materials used for the method. It enables ease of manufacturing even for very complex geometries which are difficult to fabricate using conventional methods. Fused deposition modelling (FDM) is the most widely used AM method worldwide, generally owing this to its high affordability by hobbyists. Its use in the automotive and aerospace industry is expanding as well [1]. The need for strong, durable and light parts are essential for such industries and the use of novel materials are required to achieve such demands. As the FDM method evolves, the fabrication of multi material composite parts are becoming possible and it becomes possible to compensate the negative aspects of single material parts [2]. PLA has high tensile strength and stiffness compared to PETG whereas PETG is more ductile and has less tensile strength [3]. Though PLA is an eco-friendly and strong material, it is not preferred for outdoor use due to its degradation through environmental exposure, especially due to exposure to chemicals for long durations. It also displays brittle behavior. On the other hand PETG is well known for its chemical resistance [4]. It also has good thermal stability and industries like automotive and aerospace are researching such materials as PETG to be used in their products [5]. This study proposes an architecture with the combination of an environmentally friendly polymers and a chemically resistant polymer aiming to optimize stiffness and ductility which may contribute to the search of materials needed in the mentioned industries especially for the components exposed to harsh environments.

2. Material and Testing

A novel composite which was not investigated before in the literature was studied in this work where PETG was used as an outer shell and PLA was encapsulated in this shell with the help of a dual extruder. This was achieved only with enclosing PLA in the composite for PLA an PETG are chemically incompatible, meaning they show weaker layer adhesion in normal printing operation. Specimens were 3d printed with varying printing parameters which strongly affect the mechanical properties of the material. These printing parameters create the meso-structure of the material such as internal geometry, number of raster lines and infill percentage. Generally, these parameters determine the weight and strength of the specimen. Initial objective of this study is to compare the tensile and compressive behavior of PETG-PLA hybrid composite specimen with the specimens manufactured with only virgin PLA and only with virgin PETG. Specimens with same number of raster lines, same infill geometry and same infill percentage was manufactured. The hybrid composite was 3d printed with raster walls of PETG filament and the inner material was 3d printed with PLA filament. The configuration of the three types of tensile test specimens in the slicer software can be seen in Figure 1. Tensile tests were carried out according to ASTM D638-14 test standard [6]. In order to observe the effect of PLA existence in the PETG envelope in terms of compressive properties compressive test specimens were also manufactured. Compression tests were carried out with respect to ASTM D695-15 test standard [7].

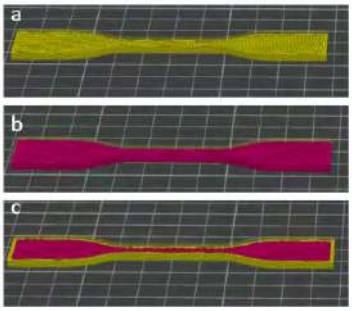

Fig. 1. a) Virgin PETG specimen b) virgin PLA specimen c) PETG-PLA specimen

3. Results and Discussions

When we analyze the tensile test results we see that PLA has a higher ultimate tensile strength (UTS) than PETG which agrees with the literature. PETG-PLA composite has a slightly lower UTS value compared to virgin PETG specimen. On the other hand, PETG-PLA composite shows similar ultimate strain value compared to virgin PETG and this value is much higher than virgin PLA showing an improvement in ductility. When we compare the elastic modulus values we see that virgin PLA specimen has the highest value showing the highest stiffness while virgin PETG specimen has the lowest elastic modulus value. Conversely, we see that PETG-PLA composite specimen has a 16.8 percent higher elastic modulus value compared to virgin PETG. This indicates a balanced mechanical property of stiffness and ultimate strain that might have advantages in some loading scenarios for the PTG-PLA hybrid composite. The tensile test graphs of the three specimens can be seen in Figure 2.

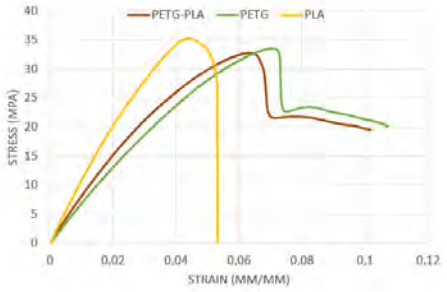

Fig. 2. Tensile test graph for PETG-PLA composite, virgin PETG and virgin PLA specimens

In terms of compression tests we see a similar behavior on compressive modulus and we see that PETG-PLA composite has a value lower than virgin PLA but significantly higher than virgin PETG. The results display a possible improvement in flexural behavior and the future work will include 3-point bending tests and the effect of key printing parameters shaping the shell-core architecture on these mechanical properties will be evaluated.

4. References

[1] V. Mohanavel, K. S. Ashraff Ali, K. Ranganathan, J. Allen Jeffrey, M. M. Ravikumar, and S. Rajkumar, "The roles and applications of additive manufacturing in the aerospace and automobile sector," *Materials Today: Proceedings*, vol. 47, pp. 405–409, Jan. 2021, doi: 10.1016/j.matpr.2021.04.596.

[2] I. Khan, I. Barsoum, M. Abas, A. Al Rashid, M. Koç, and M. Tariq, "A review of extrusion-based additive manufacturing of multi-materials-based polymeric laminated structures," *Composite Structures*, vol. 349–350, p. 118490, Dec. 2024, doi: 10.1016/j.compstruct.2024.118490.

[3] S. Prajapati, J. K. Sharma, S. Kumar, S. Pandey, and M. K. Pandey, "A review on comparison of physical and mechanical properties of PLA, ABS, TPU, and PETG manufactured engineering components by using fused deposition modelling," *Materials Today: Proceedings*, May 2024, doi: 10.1016/j.matpr.2024.05.018.

[4] E. Hozdić and E. Hozdić, "Comparative Analysis of the Influence of Mineral Engine Oil on the Mechanical Parameters of FDM 3D-Printed PLA, PLA+CF, PETG, and PETG+CF Materials," *Materials*, vol. 16, no. 18, p. 6342, Sep. 2023, doi: 10.3390/ma16186342.

[5] A. Kantaros, M. Katsantoni, T. Ganetsos, and N. Petrescu, "The Evolution of Thermoplastic Raw Materials in High-Speed FFF/FDM 3D Printing Era: Challenges and Opportunities," *Materials*, vol. 18, no. 6, p. 1220, Mar. 2025, doi: 10.3390/ma18061220.

[6] D638-14 Standard Test Method for Tensile Properties of Plastics, ASTM International, West Conshohocken. https://doi.org/10.1520/D0638-14

[7] D695-15 Standard Test Method for Compressive Properties of Rigid Plastics, ASTM International, West Conshohocken. https://doi.org/10.1520/D0638-14

Stochastic Effects of Interlayer Matrix Non-Uniformity on Impact Response of TPU Thermoplastic Composites

Shunqi ZHANG,[1,*] Dayou MA,[2] and Andrea MANES[3]

Politecnico di Milano, Department of Mechanical Engineering, Via G. La Masa 1, 20156 Milano, Italy

[*] Shunqi. zhang@polimi.it

Summary: This study investigates the impact of manufacture-induced non-uniform interlayer matrix distribution in thermoplastic polyurethane (TPU) Kevlar-fibre composites on low-velocity impact responses. Laminates with varying TPU contents were fabricated via hot-press forming, and interlaminar matrix thicknesses were characterized by microscopical recognition. A ply-level stochastic finite element model was developed to simulate heterogeneities, compared against experiments and uniform model. Results show such non-uniformity influences laminate's impact stiffness, peak force, and residual deformation, with impact behavior dispersions decreasing with increased matrix content but varying non-monotonically with impact energy. At last, a critical impact-centered 'decisive region' was identified, beyond which non-uniformity exerts negligible influence on response dispersion.

Main Text

Thermoplastics exhibit fluidity and eco-friendly features, offering benefits over thermosets. Thermoplastic composite is therefore regarded as one of promising candidates for advanced composite structures design. Among thermoplastics, thermoplastic polyurethane (TPU) has been widely used as matrix owing to its flexibility and excellent ductility, which contribute to laminate's outstanding resistance against impact loading [1-3]. However, when TPU composites manufactured via hot-press forming [4,5], the matrix exhibits a stochastically non-uniform distribution between adjacent fiber layers, as shown in Fig. 1. This manufacture-induced microstructural uncertainty may influence the overall impact behavior. Prior studies have highlighted the significant role of TPU matrix content in composite's impact resistance performance [3], yet the effects of such spatial heterogeneities remain underexplored. Investigating these stochastic features is crucial for further elucidating the laminates practical production tolerances' contribution to impact responses, thereby informing impact-oriented structural design, engineering applications, and customized fabrication strategies for TPU composites.

Fig. 1. Optical microscopy image of TPU composite in cross-section.

Cross-sectional microscopic recognition across different regions was deployed to extract the probability density distributions of interlayer matrix thicknesses. Building on a validated ply-level macro-homogeneous finite element model developed in previous work [3], where interlayer matrices are constructed as independent sold-element plies, stochastic fields were established and mapped onto the matrix plies to simulate the non-uniform geometric characteristics. Simulations were conducted for various TPU composite configurations and different impact energy levels, with results systematically compared against experimental data and outcomes from conventional uniform model.

The findings demonstrate that under low-velocity impact conditions, the non-uniform interlayer matrix distribution can significantly affect the laminate's impact behavior and cause dispersion on response. Compared

to conventional model, the stochastic model replicated the laminate's behavior with higher accuracy, especially on impact stiffness, peak force, and residual deformation. Further analysis reveals that the dispersions shrink as the TPU matrix content increases, while with elevation of impact energy, exhibiting non-monotonic trend, initially increasing followed by decreasing as reaching high-energy level. For impact-resistant design and practical application, accounting for the probabilistic ranges and extrema of peak forces and maximum displacements is essential. At last, the stochastic fields within FE model were further refined and optimized to investigate the correlations between the response dispersion and the spatial extent of the matrix inhomogeneous distribution area. The outcomes identified a 'decisive region' beyond which the non-uniformity exerts negligible influence on dispersion. This study not only developed a stochastic modeling strategy in macroscale level, but also these insights offer valuable guidance for tailored impact-resistance designs and fabrication optimizations in TPU composites, enhancing their reliability in high-performance applications.

References

[1] Rizzo, F.; D'Agostino, T.; Cuomo, S.; Pinto, F.; Meo, M., 2020, "High-velocity impact investigation on thermoplastic polyurethane/CFRP T-stiffened panel," Mater. Today: Proc., 2214-7853

[2] Russo, P.; Langella, A.; Papa, I.; Simeoli, G.; Lopresto, V., 2016, "Low-velocity impact and flexural properties of thermoplastic polyurethane/woven glass fabric composite laminates," Procedia Eng. 167, pp. 190–196.

[3] Zhang, S.; Silva, Í.A.; Konkan, E.; Ma, D.; Bianchi, O.; Amico, S.C.; Manes, A., 2026, "Investigation on Impact Behavior of Thermoplastic Composites: A Ply-Level Numerical Methodology for Impact-Resistance Design," Polym. Compos., Early View DOI: 10.1002/pc.70721.

[4] Al-Dhaheri, M.A.; Cantwell, W.J., 2024, "Characterization of relaxation behaviour of CF/PEKK aerospace composites using the time-temperature-crystallinity superposition principle," J. Compos. Mater. 58(18), pp. 2061-2077.

[5] Al-Dhaheri, M.A.; Irfan, M.S.; Cantwell, W.J., 2024, "Experimental investigation of warpage in thin CF/PEKK composite laminates consolidated under non-isothermal conditions," J. Thermoplast. Compos. Mater., pp. 1-25.

Predictive Modeling of Ballistic Limit and Trauma Response in Aramid Fiber Reinforced Phenolic Composites

Sara Srebrenkoska,[1] Vineta Srebrenkoska,[2*] and Svetlana Risteska[3,2]

[1] *Faculty of Mechanical Engineering, Goce Delcev University, Krste Misirkov, No. 10-A Stip, Republic of North Macedonia.*

[2] *Faculty of Technology, Goce Delcev University, Krste Misirkov, No. 10-A Stip, Republic of North Macedonia.*

[3] *Laminati Kom Doo Prilep, Aleksandar Makedonski No. 122, Prilep, Republic of North Macedonia.*

[*] *vineta.srebrenkoska@ugd.edu.mk*

Summary: The ballistic behavior of aramid fiber–reinforced phenolic laminates is influenced by fiber volume fraction and molding pressure. This study evaluates the effects of resin content (20% and 50%) and consolidation pressure (2, 6, and 10 MPa) on ballistic limit velocity (V50) and backface deformation. Laminates with areal weights of 2–9 kg/m² were tested according to NIJ 0101.07 standards. Results show a linear increase of V50 with areal weight and up to 18% higher ballistic resistance for laminates containing 80% fiber. Increasing molding pressure reduced trauma depth by approximately 25% with minimal effect on V50. Optimal performance was achieved with high fiber content and 10 MPa consolidation pressure.

1. Materials and experimental procedure

Ballistic laminates were manufactured using ballistic-grade plain woven para-aramid fabric as reinforcement and a modified phenolic resin as matrix. The aramid fabric was a plain weave (1×1) construction with an areal weight of 280 ± 7 g/m² and nominal thickness of 0,43 mm. The yarn linear density was 1260 dtex in both warp and weft directions, with yarn counts of 11,0 ends/cm (warp) and 10,5 picks/cm (weft). The measured tensile strength of the fabric was approximately 10,000 N/5 cm in the warp direction and 9,500 N/5 cm in the weft direction. No surface coupling agent was applied to the fibers.

The matrix system consisted of a resol-type phenolic resin with dry content above 98% and density of approximately 1,1 g/cm³. Because conventional phenolic resins are inherently brittle and unsuitable for dynamic impact applications, the resin was modified with powdered polyvinylbutyral (PVB) to improve toughness and flexibility. The modification aimed to enhance strain accommodation during ballistic loading and to reduce premature interlaminar cracking.

Prepreg sheets were produced using a controlled impregnation process in which resin solution viscosity, temperature, resin pickup, volatile content, and gel time were continuously monitored. Two resin content levels were prepared to investigate the influence of fiber volume fraction: laminates containing approximately 20 wt.% resin (≈80% fiber) and laminates containing 50 wt.% resin (≈50% fiber). After impregnation, prepreg sheets were air-dried to the required volatile content and cut into 400 × 400 mm plies.

Laminates were fabricated by stacking prepreg plies to achieve target areal weights ranging from 2 to 9 kg/m². The stacked assemblies were consolidated in a hydraulic hot press at 160 °C. To evaluate the effect of consolidation pressure on ballistic and trauma behavior, panels were molded under three different pressures: 2 MPa, 6 MPa, and 10 MPa. The pressure time was adjusted according to laminate thickness to ensure complete curing. After molding, panels were cooled under pressure to minimize residual stresses and warpage.

Ballistic performance was evaluated using the V50 ballistic limit method in accordance with NIJ 0101.07 standard procedures. Square panels of 400 × 400 mm were rigidly clamped during testing. A minimum of fourteen projectiles were fired at each configuration to determine the ballistic limit velocity, defined as the arithmetic mean of the highest partial penetration velocities and the lowest complete penetration velocities within the required velocity spread. Projectile velocities were measured using calibrated chronographic instrumentation.

Backface deformation (trauma effect) was assessed on panels with an areal weight of 5 kg/m² molded at different consolidation pressures. After impact, the rear surface deformation was measured by determining both the maximum indentation depth and the effective deformation diameter. The trauma depth was defined as the maximum perpendicular distance from the original rear plane of the panel to the apex of the deformation bulge. The trauma area was calculated from the measured diameter of the affected region. All measurements were performed immediately after impact to avoid elastic recovery effects.

The experimental matrix therefore allowed evaluation of the combined influence of fiber volume fraction, laminate areal weight, and molding pressure on both ballistic resistance and backface deformation behavior.

2. Results and Discussion

Ballistic limit velocity (V50) increased linearly with areal weight for all laminates, confirming that energy absorption scales with the amount of reinforcing material. Laminates containing 20 wt.% resin (higher fiber volume fraction) showed 12–18% higher V50 compared to 50 wt.% resin systems, demonstrating that fibers are

the primary energy-absorbing component. Further increasing fiber content beyond 80% led to insufficient interlaminar bonding and delamination, indicating the need for minimum matrix content to ensure structural integrity.

Molding pressure had a limited effect on V50 but significantly influenced trauma behavior. Increasing pressure from 2 to 10 MPa reduced backface deformation by approximately 20–25%, due to improved laminate densification and interlayer coupling. Higher resin content did not improve trauma performance and slightly increased deformation, likely due to matrix brittleness.

The best overall performance was achieved with 20 wt.% resin and 10 MPa molding pressure, providing high ballistic resistance and reduced trauma. These results confirm that fiber content governs penetration resistance, while consolidation pressure primarily controls rear-face deformation.

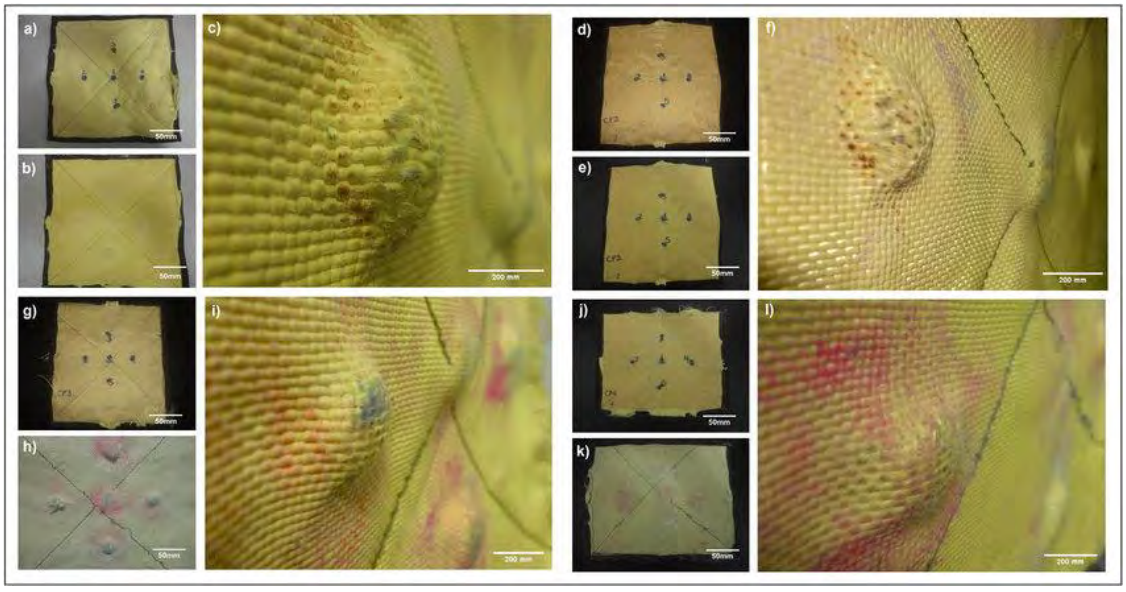

Fig. 1. Post-impact damage patterns and backface deformation of aramid/phenolic laminates at different consolidation pressures and resin contents.

3. Summary

The study demonstrates that ballistic performance of aramid/phenolic laminates is primarily controlled by fiber volume fraction, while trauma behavior is strongly influenced by consolidation pressure. Ballistic limit velocity increases linearly with areal weight and is significantly higher in laminates containing lower resin content (approximately 20 wt.%). Increasing resin content reduces ballistic efficiency due to decreased effective fiber participation. Molding pressure has limited influence on penetration resistance but substantially reduces backface deformation by improving laminate densification and interlaminar bonding. The best overall performance was achieved in laminates with high fiber content molded at 10 MPa, providing both superior ballistic resistance and reduced trauma depth.

These findings confirm that optimized armor design requires maximizing fiber contribution while ensuring sufficient consolidation to control rear-face deformation.

References

[1] Laible, R. C., 1980, *Ballistic Materials and Penetration Mechanics*, Elsevier Scientific Publishing Company, New York.

[2] National Institute of Justice, 2008, *Ballistic Resistance of Body Armor NIJ Standard–0101.06*, U.S. Department of Justice, Washington, DC.

[3] Wendlant, H., 1999, *Manual for Aramid Ballistic Panels*, DSM High Performance Fibers BV, The Netherlands.

[4] Harding, J., and Welsh, L. M., 1983, "A Tensile Testing Technique for Fibre Reinforced Composites at Impact Rates of Strain," *Journal of Materials Science*, 18, pp. 1810–1826.

[6] Cripps, N. P. J., and Cooper, G. J., 1997, "Intestinal Injury Mechanisms After Blunt Abdominal Impact," *Annals of the Royal College of Surgeons of England*, 79, pp. 115–120.

Parameters Optimization of the Gurson–Johnson–Cook Damage Model for Dual Phase Steel

Brikena Duga,[1] Fakije Zejnullahu,[2] Bashkim Çerkini [3] and Labinot Topilla[4, *]

[1,2,3,4] *University of Applied Sciences in Ferizaj. street "Universiteti",70000 FerizajRepublic of Kosovo*

[*] *labinot.topilla@ushaf.net*

Summary: Dual-phase (DP) steels are characterized by a multiphase composition, as well as high strength and ductility. DP600 samples were tested in accordance with ASTM E8 at a strain rate of 0.0083 s^{-1} and simulated using LS-DYNA and LS-OPT. The parameters of the Gurson–Johnson–Cook damage model were optimized to fit the engineering stress–strain curves. The results show good agreement between the experimental results and the numerical simulations in terms of stress-strain curves.

1. Experimental results

In this presentation, a type of dual-phase steel, namely DP600, was investigated. Its chemical composition can be established from [1]. Uniaxial tensile tests were performed on four different samples at room temperature, with a strain rate of 0.0083 s^{-1}, similar to [2]. The tests were conducted to obtain engineering stress–strain curves, as shown in Figure 1. The results in terms of stress and strain may vary depending on the samples, as reported in [3].

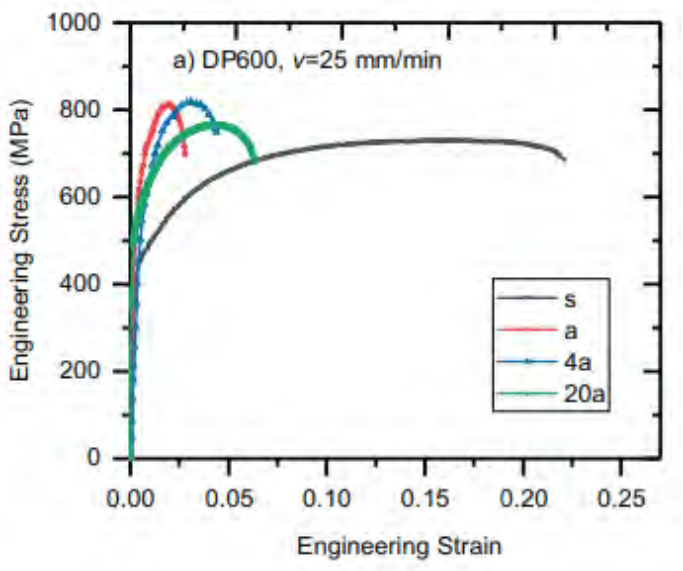

Figure 1. Engineering stress-strain of DP600 steel

2. Experimental and numerical results

The simulations were performed using the LS-Dyna software, while the optimization of the Gurson–Johnson–Cook model parameters was carried out using the LS-Opt software. Through LS-Opt, the parameters for various samples, prepared according to the ASTM E8 standard, were optimized. It is worth noting that the Gurson–Johnson–Cook damage model is the most suitable for samples with different geometries and cross-sections. Figure 2 shows a comparison between the numerical and simulation results for the analyzed samples.

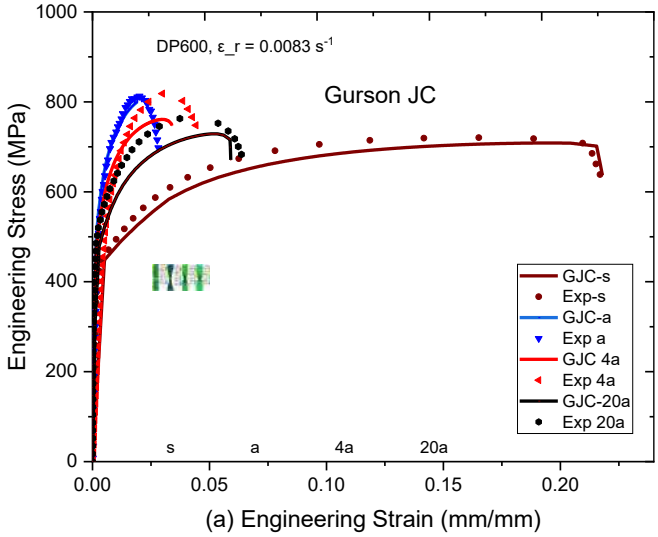

Figure 1. Comparison between experimental and numerical results expressed through engineering stress-strain curves of DP600 steel

In the future, these results for DP600 and DP800 at different strain rates are planned to be published in a scientific journal. This will provide valuable insights for the modeling and optimization of dual-phase steels.

3. References

[1] L. Topilla and S. Toros, “Mechanical Behaviour of Dual Phase Steels under Different Strain Rates,” *Kem. u Ind.*, vol. 72, no. 3–4, pp. 151–159, 2023, doi: 10.15255/kui.2022.044.

[2] S. LabinotTopilla, “GURSON-TVERGAARD-NEEDLEMAN (GTN) PARAMETERS OF DP STEELS WITH DIFFERENT ROLLING DIRECTIONSA WERE DETERMINED AND INVESTIGATED AT DIFFERENT STRAIN RATES,” *Journal*, vol. 3, no. 2, pp. 71–83, 2022.

[3] S. Toros and L. Topilla, “Analysis of the fracture behaviour of dual-phase steels using the Gissmo and Johnson Cook models,” vol. 3, pp. 79–95, 2023.

Molecular Dynamics Investigation of Dislocation-Mediated Mechanical Behavior and Hydrogen Embrittlement in Metal-Matrix Composites Under High Strain Rate Loading

Burak Bal[1, *] and Mehmet Furkan Baltacioglu[1]

[1] *Department of Mechanical Engineering, Abdullah Gül University, 38080, Kayseri, Türkiye*

[*] *burak.bal@agu.edu.tr*

Summary: This study employs molecular dynamics simulations to investigate dislocation-mediated deformation and hydrogen embrittlement in metal matrix composites under tensile loading. The results show that dislocations govern plastic deformation, while reinforcement phases influence their nucleation and mobility. Hydrogen atoms interact strongly with dislocations and lattice defects, altering local stress fields and promoting strain localization. As composite strength increases, hydrogen susceptibility also increases, leading to reduced ductility and earlier crack initiation. The findings provide atomistic insight into the coupling between strengthening mechanisms and hydrogen-assisted failure, supporting the design of high-strength composite systems with improved environmental resistance.

1. Main Text

Hydrogen embrittlement (HE) is a critical degradation phenomenon that severely compromises the mechanical performance and structural integrity of metallic materials exposed to hydrogen-containing environments. It causes reduction in ductility, premature crack initiation, and sudden catastrophic failure, often occurring at stress levels well below the expected strength of the material. Despite decades of research, the underlying mechanisms and molecular/atomic origin of HE remained unclear, including hydrogen transport, trapping at microstructural defects, and interactions with dislocations and crack tips. At the microscale and nanoscale, hydrogen alters local stress fields, reduces cohesive strength, and promotes strain localization, thereby accelerating damage evolution.

Metal matrix composites (MMCs) are advanced structural materials composed of a continuous metallic matrix reinforced with secondary phases such as particles, fibers, or precipitates. The metal matrix provides toughness and ductility, while the reinforcement phase enhances strength, stiffness, and wear resistance. Plastic deformation in the metallic matrix is primarily accommodated by the motion and interaction of dislocations. These line defects enable metals to deform plastically under applied loads by gliding and multiplying within the crystal lattice. The presence of reinforcements modifies dislocation nucleation, motion, and accumulation, leading to strengthening through mechanisms such as friedel cutting, orowan looping, and dislocation pile-up.

However, the same microstructural features that enhance strength can also increase susceptibility to hydrogen embrittlement. Hydrogen atoms diffuse through metallic lattices and tend to accumulate at energetically favorable sites, including dislocations, grain boundaries, interfaces, and other lattice defects (can be octahedral or tehedreh tetrahedral sites). Their interaction with dislocations can either enhance mobility (hydrogen-enhanced localized plasticity) or promote decohesion at interfaces (hydrogen enhanced decohesion), both of which may contribute to premature failure. In MMCs, the complex interplay between dislocations, reinforcement phases, and hydrogen creates localized stress concentrations that can accelerate crack initiation and propagation.

Given that these processes originate from atomistic-scale interactions, a molecular-level understanding is essential for uncovering the fundamental mechanisms governing hydrogen-assisted damage in MMCs. In this work, we employ molecular dynamics simulations to investigate dislocation-mediated deformation and hydrogen embrittlement in metal matrix composites (only the metal part) under tensile loading. By resolving the interactions between hydrogen atoms, dislocations, and reinforcement phases, we provide atomistic insight into the coupling between strengthening mechanisms and hydrogen-assisted failure.

Our simulations reveal that the presence of hydrogen significantly reduces the velocity of dislocations during tensile deformation. In hydrogen-free systems, dislocations glide continuously under the applied stress, enabling homogeneous plastic flow. However, once hydrogen atoms are introduced, dislocation motion becomes progressively hindered. As the hydrogen concentration increases, the reduction in dislocation velocity becomes more pronounced, indicating a concentration-dependent retardation effect.

This behavior can be attributed to the strong interaction between hydrogen atoms and dislocation cores. Hydrogen segregation around dislocations alters the local atomic bonding and stress distribution, increasing resistance to dislocation glide. The effect increases at higher hydrogen contents due to enhanced trapping and accumulation near lattice defects and matrix–reinforcement interfaces.

The observed slowdown in dislocation motion is consistent with the hydrogen-enhanced decohesion (HEDE) mechanism, which reduces cohesive strength along critical regions and facilitates localized damage initiation. Although HEDE is often discussed in the context of monolithic metals, our results demonstrate that it can also be activated in composite systems. In metal matrix composites, hydrogen-assisted decohesion at matrix–reinforcement interfaces further amplifies stress concentration, thereby accelerating the transition from localized plasticity to crack initiation.

In conclusion, our study provides atomistic insight into dislocation-mediated deformation and hydrogen embrittlement in the metal part of the metal matrix composites under tensile loading. Molecular dynamics simulations demonstrate that hydrogen strongly interacts with dislocations and lattice defects, significantly reducing dislocation velocity in a concentration dependent manner. As composite strength increases, hydrogen susceptibility is amplified, promoting strain localization and earlier crack initiation. The results support the activation of hydrogen-enhanced decohesion in composite systems, particularly at matrix–reinforcement interfaces. These findings clarify the coupling between strengthening mechanisms and hydrogen-assisted failure, offering guidance for designing high-strength composites with improved resistance to hydrogen degradation.

Multi-Layer Perceptron Neural Network Based Prediction of Dynamic Stress–Strain Response of Polyethylene

Yuksel Cakir[1,*] and Ozgen Colak[2]

Istanbul Technical University
[1]Department of Electronics and Communication Engineering, Istanbul, Turkiye
[2]Department of Mechanical Engineering, Istanbul, Turkiye
[*] *e-mail: cakiryu@itu.edu.tr*

Summary
This study proposes a data-driven framework to predict the dynamic stress–strain response of polyethylene (PE) in Split Hopkinson Pressure Bar (SHPB) experiments. Strain rate data and stress-strain curves at different strain rates are used as input to a Multi-Layer Perceptron (MLP) neural network, while stress–strain curves derived from classical SHPB analysis served as targets. The model learns the nonlinear relationship between inputs and material response. Results highlight the effectiveness of machine learning for high strain rate material characterization.

Keywords: High strain rate, Polyethylene, Machine learning, Multi-Layer Perceptron

1. Introduction

SHPB technique remains the most widely used experimental method for characterizing material response at strain rates between 10^2 and 10^4 s^{-1}. In a conventional SHPB experiment, incident, reflected, and transmitted strain waves are recorded using strain gauges mounted on elastic pressure bars. Based on one-dimensional elastic wave propagation theory, stress and strain are calculated.

Recent developments in machine learning enable direct identification of nonlinear relationships from experimental data without explicitly solving governing equations. Neural networks, in particular, can approximate complex mappings between measured inputs and target outputs, [1]. The objective of the present study is to develop a Multi-Layer Perceptron (MLP) model capable of predicting the dynamic stress–strain curve of PE. The results demonstrate the potential of machine learning as an alternative computational tool for high strain rate material characterization.

2. Multilayer Perceptron (MLP) Network

MLP is a class of feedforward artificial neural networks widely used for regression, classification, and function approximation tasks. An MLP network consists of an input layer, one or more hidden layers, and an output layer. Each layer contains a set of interconnected nodes (neurons), where each connection is associated with a weight, [2, 3]. MLP structure is given in Fig. 1a. The structure of any neuron is given in Fig.1b.

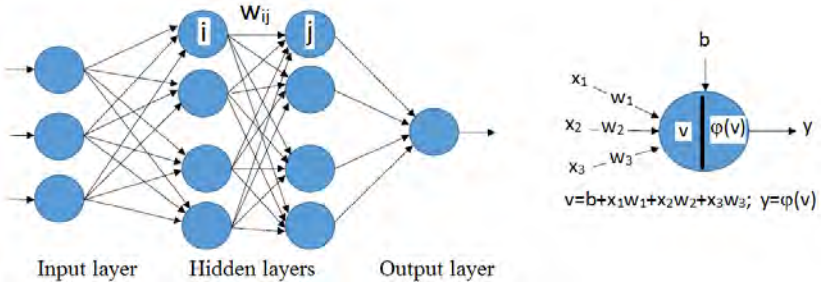

a) b)

Fig. 1. a) Structure of MLP network, b) Structure of any neuron

In an MLP, the input layer receives the predictor variables and forwards them to the hidden layer(s). Each neuron in a hidden layer computes a weighted sum of its inputs and adds a bias term. This linear combination is then passed through a nonlinear activation function, such as the sigmoid or hyperbolic tangent (tanh) to introduce nonlinearity into the model. The output layer performs a similar operation to produce the final prediction.

In this work, a data-driven methodology is proposed to predict the dynamic stress–strain response of PE during SHPB experiment. Limited number of experimental data at multiple strain rates are used for training and validation. Experimentally calculated stress–strain curves and strain rate data obtained using classical SHPB data reduction are employed as input and target outputs during training. Thickness of specimen is 8 mm and experimental results for bar pressures of 1.2, 1.5, and 1.8 are used. Two of the results are used in training stage of network while the remaining is used for testing the performance of the network. The RMSE and R^2 performance metrics are obtained and compared for networks with different number of neurons at hidden layers.

3. Results and Discussion

A machine learning-based framework is developed to predict the dynamic stress–strain behavior of PE directly from SHPB stress-strain curves using a MLP network. The MLP model successfully reconstructed the dynamic stress–strain response of PE across different strain rates. Predicted curves exhibited strong agreement with experimentally calculated references.

Fig. 2a depicts the stress strain curves obtained for 1.2 and 1.8 bar pressure that are used for training the network and Fig. 2b depicts the experimentally obtained stress strain curve for 1.5 bar together with predicted one by network. The network include two hidden layer every consisting of 5 neurons. The performance of network is obtained as RMSE = 9.85726 and R^2 = 0.8297. Increasing the number of neurons in hidden layer gives better results in predicting the training set curves but performance decreased for the test set.

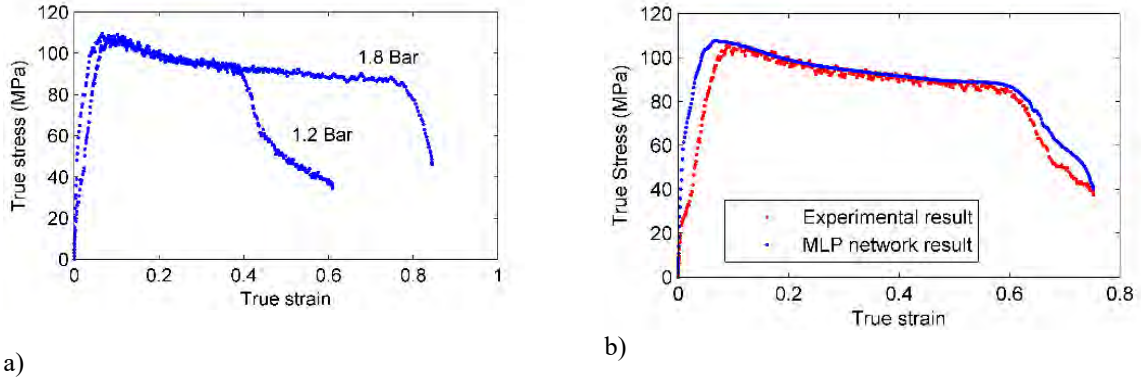

a) b)

Fig. 2.a) Stress strain curves obtained for 1.2 and 1.8 bar pressure, b) experimentally obtained stress strain curve for 1.5 bar together with predicted one by network.

Unlike classical SHPB analysis, the proposed approach does not require explicit knowledge of bar elastic constants, wave speed, or equilibrium verification during prediction. Instead, these relationships are embedded within the trained model parameters. However, generalization capability depends on training data diversity. Expanding the dataset to include additional strain rates, specimen geometries, and different polymer grades would further enhance predictive robustness.

4. Conclusions

In conclusion, the proposed MLP-based framework demonstrates strong potential as an efficient and reliable alternative to conventional SHPB data reduction procedures for predicting the dynamic stress–strain behavior of PE. By directly learning the relationship between input stress–strain signals and the corresponding dynamic response, the model accurately reconstructs material behavior across varying strain rates with high agreement to experimentally calculated references.

References

[1] Cakir, Y. 2025, “Predicting the creep behavior of thermoset polymers using machine learning techniques”, *Polymer Bulletin*, 82 (15), 10341-10358.

[2] Li, W., Chen, P., et al. 2022, “Deep learning modeling strategy for material science: from natural materials to metamaterials,” J. Phys. Mater. 5:014003.

[3] Chan, K. Y., Abu-Salih, B. et al. 2023, “Deep neural networks in the cloud: Review, applications, challenges and research directions,” Neurocomputing, 545: 126327.